Detecting mitophagy in mitochondrial disease: Towards a new type of therapy



Eszter Dombi

Lady Margaret Hall

Thesis submitted for the Degree of Doctor of Philosophy

Michaelmas Term 2019

Abstract

Mitochondrial diseases may result from mutations in the maternally-inherited mitochondrial DNA (mtDNA) or from mutations in nuclear genes encoding mitochondrial proteins. Their bi-genomic nature makes mitochondrial diseases a very heterogeneous group of disorders that can present at any age and can affect any type of tissue. The autophagic-lysosomal degradation pathway plays an important role in clearing dysfunctional and redundant mitochondria through a specific quality control mechanism termed mitophagy. Mitochondria could be targeted for autophagic degradation for a variety of reasons including basal turnover for recycling, starvation induced degradation, and degradation due to damage. While the core autophagic machinery is highly conserved and common to most pathways, the signalling pathways leading to the selective degradation of damaged mitochondria are still not completely understood. The aim of this thesis is to investigate mitophagy in several mitochondrial disease. Additionally, to test potential drug modulators of mitophagy with the view that they may provide an alternative therapy for certain kinds of mitochondrial diseases in the future.

Twenty-nine patient derived fibroblast lines were investigated. Most patient cells had dysregulated mitophagy, where mitochondrial turnover was often higher when compared to control cell lines. Amongst the potential drug modulators, Metformin, AICAR, Chlorodiazepoxide, and Duloxetine were sufficient at inducing mitophagy without a cytotoxic effect.

Altered mitophagy seems to be a hallmark of many mitochondrial diseases and the trigger might be crucial to the phenotype, therefore it offers a potential therapeutic target. Identifying potential drug modulators of mitophagy is the first step towards a novel therapy for not only mitochondrial disease but many neurodegenerative disorders as well. Monitoring mitophagy could also be useful for assessing the efficacy of certain treatments or even supplements on an individual level, as the effect of drugs that benefit patients can manifest in alleviation of the increased mitochondrial turnover.

Acknowledgements

I would like thank Professor Jo Poulton for her never ending support and encouragement. I will be forever grateful for trusting me with this opportunity. A huge thank you to my secondary supervisor, Grant Churchill for his insight and continuous encouragement.

I would like to thank many past and current members of the NDWRH team for cheering me on, technical support but also for delicious sweets and good chats, especially my peers and friends: Helena, Belinda and Sariah.

Janet Carver and Karl Morten for technical as well as moral support.

A huge and very special thanks to Tiff Lodge, who kept me sane in the past few years and encouraged me relentlessly.

Alan Diot who taught me all the basics in lab. I would like to thank him for his never ending patience and support even though he is now countries away.

I would also like to thank Val Millar for technical support as well as the occasional pizza Fridays.

Thanks to Brent Ryan for his useful insights and help with technical bits.

I would like to thank my partner, Norbert for his continuous encouragement and for cheering me up with delicious food on bad days.

And last, but definitely not least I would like to thank my mother (in Hungarian).

Draga Anya! Koszonom hogy minding biztattal, tamogattal es soha nem tartottal vissza. A Te segitseged, tamogatasod es hatartalan szereteted tette lehetove, hogy eljussak ide! Koszonom!

Table of Contents

List of abbreviations 7
List of figures 11
Chapter 1. Introduction 14
1.1 Mitochondrial biology 15
1.1.1 Origin of mitochondria 15
1.1.2 Structure of mitochondria 16
1.1.3 Mitochondrial dynamics 17
1.1.4 The mitochondrial genome 21
1.1.5 Mitochondrial DNA replication 24
1.2 Mitochondrial functions – more than just a 'power house' 26
1.2.1 Mitochondria and ATP synthesis 27
1.2.2 Mitochondria and iron metabolism 30
1.2.3 Mitochondria and calcium signalling 31
1.2.4 Mitochondrial ROS signalling 33
1.2.5 Mitochondria and apoptosis 33
1.3 Mitochondrial quality control 35
1.3.1 Protecting the mitochondrial proteome - Mitochondrial proteases 36
1.3.2 Mitochondrial derived vesicles 37
1.3.3 Mitochondria specific autophagy – mitophagy 38
1.4 Current methods for investigating mitophagy 44
1.5 Mitochondria and human disease 45
1.6 Genetics of mitochondrial disease 46
1.6.1 MtDNA mutations and mitochondrial disease 46
1.6.2 Nuclear DNA mutations and mitochondrial disease 48
1.6.3 Diagnosis of mitochondrial disease 49
1.7 Treatment options for mitochondrial disease 50
1.8 Overall aims of this thesis 51
Chapter 2. Materials and methods 53
2.1 Materials 54
2.1.1 Consumables 54
2.1.2 Chemicals and reagents 54
2.1.3 Solutions 58
2.2 Methods 59

2.2.1 General tissue culture 59
2.2.2 Cell harvesting and counting for experimental set up 59
2.2.3 High-content fluorescent microscopy 60
2.2.4 Western blot analysis 68
2.2.5 Oxygen consumption measurements using the Seahorse XF96 platform 70
2.2.6 Cell growth experiments to determine dependency on glucose 72
2.2.7 Statistical analysis 72
Chapter 3. Characterization of fibroblasts derived from patients with mitochondrial disease resulting from mitochondrial DNA mutations 73
3.1 Introduction 74
3.1.1 An overview of complex I structure and deficiency 76
3.1.2 An overview of complex V structure and deficiency 78
3.2 Aims of chapter 3 80
3.3 Materials and methods 81
3.3.1 Patient and control fibroblasts 81
3.4 Results 82
3.4.1 Characterisation of fibroblasts with complex I mutations 87
3.4.2 Discussion of complex I mutations specific findings (Section 3.4.1) 110
3.4.3 Results continued - Characterisation of fibroblasts with complex V mutations 114
3.4.4 Discussion of complex V mutant specific findings (section 3.4.3) 127
3.5 Overall chapter discussion 129
3.6 Limitations of this study 132
3.7 Future directions 132
Chapter 4. Characterisation of fibroblasts derived from patients with mitochondrial disease resulting from nuclear DNA mutations 133
4.1 Introduction 134
4.2 Aims of chapter 4 135
4.3 Materials and methods 136
4.3.1 Patient and control fibroblasts 136
4.4 Results 137
4.4.1 Patients with *DNM1L* mutation and mitochondrial fission defects 144
4.4.2 Patients with *MFN2* and *OPA1* mutations 159
4.4.3 Patients with mitochondrial encephalopathy due to mutations in FBXL4 171
4.4.4 Patients with mutations in *CHCHD10* 185
4.5 Overall chapter discussion 197
4.6 Limitations of this study 200

4.7 Future directions 200
Chapter 5. Mitochondrial DNA depletion in POLG fibroblasts is rescued by dNTP supplementation 201
5.1 Introduction 202
5.1.1 The mitochondrial replisome 204
5.1.2 The role of POLG in mitochondrial DNA depletion syndromes 207
5.1.3 Nucleotide supplementation therapy as a potential treatment for MDS 208
5.1.4 Proband mutations and clinical presentation 209
5.2 Aims of chapter 5 210
5.3 Materials and methods 211
5.3.1 Fibroblast cultures 211
5.3.2 Nucleotides used for supplementation 211
5.3.3 Cell plating and experimental design 211
5.3.4 Disclaimer 212
5.4 Results 214
5.4.1 *POLG* mutant fibroblasts are depleted of mitochondrial DNA 214
5.4.2 Mitochondrial morphology and mitochondrial content in POLG fibroblasts 216
5.4.3 Bioenergetics of POLG fibroblasts 217
5.4.4 Glucose dependency of POLG fibroblasts 220
5.4.5 Autophagy and mitophagy in POLG and control fibroblasts 221
5.4.6 Nucleoside monophosphate supplementation alleviates mtDNA depletion in POLG fibroblasts 224
5.5 Discussion 227
5.6 Limitations of this study 229
5.7 Future directions 229
Chapter 6. Potential drug modulators of mitophagy 230
6.1 Introduction 231
6.2 Aims 236
6.3 Materials and methods 237
6.3.1 Patient and control fibroblasts used 237
6.3.2 Experimental set up for high-content fluorescent microscopy 238
6.3.3 Measuring mtDNA heteroplasmy of the m.3243A>G mtDNA mutation 239
6.3.4 Statistical analysis 240
6.4 Results 242
6.4.1 Activators of AMPK, metformin and AICAR 244
6.4.2 Chlordiazepoxide (Librium) 249

6.4.3 Duloxetine 251
6.4.4 Mitochondria targeted Doxorubicin (mtDox) 253
6.4.5 KH176 255
6.4.6 3243 heteroplasmy in drug treated patient fibroblasts 258
6.5 Discussion 260
6.6 Limitations of this study 263
6.7 Future directions 263
Chapter 7. General Discussion 265
7.1 General discussion 266
7.2 Measuring mitophagy – High-throughput fluorescent imaging 266
7.3 Does mitophagy contribute to mitochondrial disease pathology? 267
7.4 Can we target mitophagy in mitochondrial disease for therapy? 269
7.5 Can we change the paradigm? - Mitochondrial diseases mechanism and pathogenesis 270
Chapter 8. References 272
Chapter 9. Appendices 298

List of abbreviations

Acetyl-CoA	Acetyl-coenzyme A
ADP	Adenosine diphosphate
AFG3L2	AFG3-like protein 2
ALS	Amyotropic lateral sclerosis
ATG/Atg	Autophagy related
ATP	Adenosine triphosphate
Bcl-2	B cell lymphoma-2
Bcl2-L-13	Bcl-2-like protein 13
BNIP3L	Bcl2-related protein
Ca^{2+}	Calcium ion
CCCP	Carbonyl cyanide m-chlorophenyl hydrazone
CHCHD10	Coiled-Coil-Helix-Coiled-Coil-Helix Domain-Containing Protein 10
CHCHD2	Coiled-Coil-Helix-Coiled-Coil-Helix Domain-Containing Protein 2
CMT2A	Charcot–Marie–Tooth neuropathy type 2A
CPEO	Chronic progressive external ophthalmoplegia
CQ	Chloroquine
cyt c	Cytochrome c
dAMP	Deoxyadennosine monophosphate
dATP	Deoxyadenosine triphosphate
dCK	Deoxycytidine kinase
dCTP	Deoxycytidine triphosphate
dGK	Deoxyguanosine kinase
dGMP	Ddeoxyadenosine triphosphate
dGTP	Deoxyguanosine triphosphate
D-loop	Displacement-loop
DNM1L	Dynamin-like protein 1
dNTP	Deoxynucleotide triphosphate
DRP1	Dynamin-related protein 1
dTTP	Deoxythymidine triphosphate
EMRE	Essential MCU regulator
EP	E64d and Pepstatin A
ER	Endoplasmic reticulum
ERLEC1	Endoplasmic Reticulum Lectin 1
ETC	Electron transport chain
FAD	Flavin adenine dinucleotide
$FADH_2$	Flavin adenine dinucleotide, reduced
FBX	F-box
FBXL4	F-box protein leucine-rich repeat 4
FCCP	Carbonyl cyanide-p-trifluoromethoxyphenylhydrazone
FDA	Food and Drug Administration (USA)
Fe-S clusters	Iron-sulphur clusters

Fis1	Fission protein 1
FTD	Frontotemporal dementia
FUNDC1	FUN14 domain containing protein 1
GFP	Green fluorescent protein
GTP	Guanosine triphosphate
GTPase	GTP hydrolase
H_2O_2	Hydrogen peroxide
HA	Hemagglutinin
HCLX	Ca^{2+}/H^{+} exchanger exchange protein
HIF-1alpha	Hypoxia-inducible factor-1alpha
IMM	Inner mitochondrial membrane
IMP	Inosine monophosphate
IMS	Intermembrane space
Inhibitors	E64d and Pepstatin A (also see EP)
JMJD2	Jumonji Domain Containing 2A
LAMP2	Lysosome-associated membrane protein 2
LC3	Microtubule-associated protein-1 light chain-3
LHON	Leber's Hereditary Optic Neuropathy
LIR	LC3 interacting region
L-OPA1	Long OPA1
LRR	Leucine-rich repeat
LS	Leigh syndrome
MAMs	Mitochondrial associated membranes
MCU	Mitochondrial Ca^{2+} uniporter
MDS	Mitochondrial DNA depletion syndromes
MDV	Mitochondrial derived vesicle
MELAS	Mitochondrial myopathy, encephalopathy, lactic acidosis and stroke-like episodes
MERCs	Mitochondria and endoplasmic reticulum (ER) contact sites
MERRF	Myoclonic epilepsy with ragged red fibres
Mff	Mitochondrial fission factor
Mfn1	Mitofusin 1
Mfn2	Mitofusin 2
MICOS	Mitochondrial contact site and cristae organizing system
MICU1	Mitochondrial calcium uptake protein 1
MICU2	Mitochondrial calcium uptake protein 2
MIDD	Maternally inherited diabetes and deafness
MILS	Maternally inherited Leigh syndrome
MPP+	1-methyl-4-phenylpyridinium
MPV17	Mitochondrial Inner Membrane Protein MPV17
mtDNA	Mitochondrial DNA
mtDox	Mitochondria targeted doxorubicin
mtSSB	Mitochondrial single-strand binding protein

NAD^+	Nicotinamide adenine dinucleotide, oxidised
NADH	Nicotinamide adenine dinucleotide, reduced
NARP	Neuropathy, ataxia, and retinitis pigmentosa
NCLX	Sodium–calcium exchange protein
NDP52	Nuclear dot protein 52kDa
O_2^-	Superoxide
O_H	Mitochondrial DNA origin of replication - heavy chain
O_L	Mitochondrial DNA origin of replication - light chain
OMM	Outer mitochondrial membrane
OPA1	Optic atrophy 1
OPTN	Optineurin
OXPHOS	Oxidative phosphorylation
PE	Phosphatidylethanolamine
PHB2	Prohibitin 2
P_i	Inorganic phosphate
PI3K	Class III phosphatidylinositol kinase
(PI(3)P)	Phosphatidylinositol-3-phosphate
PINK1	PTEN-induced putative kinase 1
POLG	Catalytic subunit of polymerase gamma
POLG2	Accessory subunit of polymerase gamma
poly γ	Mitochondrial polymerase gamma
Q	Ubiquinone
RFP	Red fluorescent protein
RITOLS	**R**ibonucleotides are **I**ncorporated **T**hrough**O**ut the **L**agging **S**trand
RNRs	Ribonucleotide reductases
ROS	Reactive oxygen species
Rot/Ant	Rotenone and Antimycin A
rRNA	Ribosomal RNA
SCF	Skp, Cullin, F-box protein
SLC25A4	Adenine nucleotide translocase type 1
S-OPA1	Short OPA1
SPG7	Spastic paraplegia 7
SUCLA2	Succinyl-CoA synthase α subunit
SUCLG2	Succinyl-CoA synthase β subunit
TCA	Tricarboxylic acid
TFAM	Mitochondrial transcription factor A
TK1	Thymidine kinase 1
TK2	Thymidine kinase 2
TMRM	Tetramethylrhodamine, methyl ester
TOM20	Translocase of the outer membrane subunit 20
tRNA	Transfer RNA
TSPO	Mitochondrial 18-kDa translocator protein
TWINKLE	Mitochondrial 5’-3’ helicase

ULK1	Unc-51-like kinase
UMP	Uridine monophosphate
VDAC	Voltage gated ion channel
VPS34	Vacuolar protein sorting 34

List of figures

Figure 1.1 Current evolutionary models of the endosymbiotic theory....16
Figure 1.2 The structure of mitochondria....17
Figure 1.3 The mitochondrial fission and fusion machineries....20
Figure 1.4 The human mitochondrial genome....22
Figure 1.5 Current models of mitochondrial DNA replication....25
Figure 1.6 Mitochondria are involved in multiple cellular processes....26
Figure 1.7 The TCA cycle....28
Figure 1.8 Oxidative phosphorylation and the generation of ATP through complexes of the electron transport chain....30
Figure 1.9 Calcium import and export through the inner mitochondrial membrane..32
Figure 1.10 Overview of mitochondrial apoptotic signalling....34
Figure 1.11 Mitochondrial quality control proceeds in a step wise manner....35
Figure 1.12 The molecular mechanism of autophagosome formation....39
Figure 1.13 Mitophagy receptor and adaptors....42
Figure 1.14 Heteroplasmy in mitochondrial DNA mutations....48
Figure 2.1 Representative plate layout used for mitophagy and mtDNA/TMRM analyses....61
Figure 2.2 Representative images of DAPI,TOM20 and LC3 labelled control fibroblast....63
Figure 2.3 Representative images of PicoGreen and TMRM labelled control fibroblasts....64
Figure 2.4 Workflow of the image analyses protocol – mitophagy assay....66
Figure 2.5 Comparison of two plates set up, fixed and stained at the same time....68
Figure 2.6 Key parameters of mitochondrial respiration measured during the Seahorse Cell Mito Stress....71
Figure 3.1 Schematic representation of the structure and function of Complex I....77
Figure 3.2 Schematic representation of the structure and function of complex V....79
Figure 3.3 Representative images of control 1 and patient fibroblasts....84
Figure 3.4 Family tree of patients with the 13051G>A mtDNA mutation and relative disease severity of all complex I patients....87
Figure 3.5 Mitophagy in complex I mutant fibroblasts in 25mM glucose....90
Figure 3.6 Representative images of Control 1 and 13051 fibroblasts....91
Figure 3.7 Representative images of Control 2 and 11778 fibroblasts....92
Figure 3.8 Mitophagy in complex I mutant fibroblasts under energetic stress....94
Figure 3.9 Autophagy in complex I mutant fibroblasts in 25mM glucose....96
Figure 3.10 Autophagy in complex I mutant fibroblasts under energetic stress....98
Figure 3.11 Lysosomal content of complex I mutant fibroblasts....100
Figure 3.12 Mitochondrial network properties of complex I mutant fibroblasts....102
Figure 3.13 Oxygen consumption of 13051 mutant fibroblasts....104
Figure 3.14 Protein expressions of OXPHOS complex subunits in 13051 mutant fibroblasts....105
Figure 3.15 Survival of complex I mutant cells cultured galactose media for 9 days 107
Figure 3.16 Analysis of mDNA nucleoid and mitochondrial content in complex I mutant fibroblasts....109

Figure 3.17 Mitophagy and autophagy in complex V mutant fibroblasts in 25mM glucose 116
Figure 3.18 Representative images of Control 1 and 8993 fibroblasts 117
Figure 3.19 Representative images of control and 8993 fibroblasts labelled with Lyso-ID 118
Figure 3.20 Mitophagy and autophagy in complex V mutant fibroblasts under energetic stress 120
Figure 3.21 Mitochondrial network properties of complex V mutant fibroblasts 121
Figure 3.22 Protein expressions of OXPHOS complex subunits in complex V mutant fibroblasts 122
Figure 3.23 Oxygen consumption of 8993 mutant fibroblasts 124
Figure 3.24 Mitochondrial DNA nucleoid and mitochondrial content in complex V mutant fibroblasts 126
Figure 4.1 Representative images of Control 1 and patient fibroblasts with mutations in OXPHOS assembly factors 139
Figure 4.2 Representative images of Control 2 and patient fibroblasts with mutations in OXPHOS structural genes 140
Figure 4.3 Representative images of Control 1 and patient fibroblasts with mutations in genes involved in mitochondrial homestasis-1 141
Figure 4.4 Representative images of Control 2 and patient fibroblasts with mutations in genes involved in mitochondrial homestasis-2 142
Figure 4.5 Mitophagy and autophagy in DNM1L fibroblasts 147
Figure 4.6 Representative images of Control 1 and DNM1L fibroblasts 148
Figure 4.7 Representative images of control and DNM1L fibroblasts labelled with Lyso-ID 149
Figure 4.8 Mitochondrial network properties of DNM1L fibroblasts 151
Figure 4.9 Oxygen consumption and mitochondrial respiration in DNM1L fibroblasts 153
Figure 4.10 Mitochondrial DNA nucleoids in DNM1L fibroblasts 155
Figure 4.11 Mitophagy and autophagy in OPA1 and MFN2 fibroblasts 162
Figure 4.12 Representative images of Control 1, OPA1 and MFN2 fibroblasts 163
Figure 4.13 Representative images of Control and OPA1 fibroblasts labelled with Lyso-ID 164
Figure 4.14 Mitochondrial network properties of OPA1 and MFN2 fibroblasts 165
Figure 4.15 Mitochondrial DNA content in OPA1 and MFN2 fibroblasts 167
Figure 4.16 Representative images of PicoGreen and TMRM labelled OPA1 and MFN2 cells 168
Figure 4.17 Structure of the FBXL4 gene and location of the reported mutations 172
Figure 4.18 Mitophagy and autophagy in FBXL4 fibroblasts 175
Figure 4.19 Representative images of Control 2 and FBXL4 fibroblasts 176
Figure 4.20 Representative images of Control 2 and FBXL4 fibroblasts labelled with Lyso-ID 177
Figure 4.21 Mitochondrial network properties of FBXL4 fibroblasts 178
Figure 4.22 Oxygen consumption rate and mitochondrial respiration in FBXL4 fibroblasts 180
Figure 4.23 Protein expression of OXPHOS complex subunits 181
Figure 4.24 Mitochondrial DNA content in FBXL4 cells 183

Figure 4.25 CHCHD10 gene structure and currently investigated mutations 187
Figure 4.26 Mitophagy and autophagy in CHCHD10 fibroblast.....189
Figure 4.27 Representative images of Control 1 and CHCHD10 fibroblasts.....190
Figure 4.28 Mitochondrial network properties of CHCHD10 fibroblasts 191
Figure 4.29 Oxygen consumption rate and mitochondrial respiration in CHCHD10 fibroblasts 192
Figure 4.30 Mitochondrial content in CHCHD10 fibroblasts 194
Figure 5.1 Mitochondrial DNA replication and nucleotide synthesis.....205
Figure 5.2 *De novo* nucleotide syntheses in the cytosol.....206
Figure 5.3 Increased mitophagy may contribute to mtDNA loss in MDS.....208
Figure 5.4 Structure of the polymerase γ catalytic subunit and its common mutations 209
Figure 5.5 Cell plating and experimental design.....213
Figure 5.6 Mitochondrial DNA analysis of POLG fibroblasts using PicoGreen 215
Figure 5.7 Mitochondrial content and morphology of POLG fibroblasts 216
Figure 5.8 Protein expression of the electron transport chain subunits is reduced in POLG fibroblasts.....217
Figure 5.9 Oxygen consumption and extracellular acidification rates in POLG and control fibroblasts.....219
Figure 5.10 POLG fibroblast growth is heavily dependent on glucose availability....220
Figure 5.11 Autophagy and mitophagy in POLG and control fibroblasts 222
Figure 5.12 Representative images of Control 2 and POLG fibroblasts 223
Figure 5.13 Nucleotide supplementation alleviates mtDNA depletion in POLG fibroblasts 225
Figure 5.14 dNMP supplementation reduces mitophagy in control and POLG fibroblasts 226
Figure 6.1 Chemical modulators of autophagy.....234
Figure 6.2 Representative output of the m.3243 heteroplasmy analysis 240
Figure 6.3 Metformin treatment of control and patient fibroblasts.....246
Figure 6.4 AICAR treatment of control and patient fibroblasts.....248
Figure 6.5 Chlordiazepoxide treatment of control and patient fibroblasts 250
Figure 6.6 Duloxetine treatment of control and patient fibroblasts.....252
Figure 6.7 mtDox treatment of control and patient fibroblasts.....254
Figure 6.8 Mitophagy in KH drug treated control and patient fibroblasts.....256
Figure 6.9 The number of viable cells expressed as the percentage of vehicle treated ones following KH drug treatment 257
Figure 6.10 Heteroplasmy levels in 3243 patient cells following treatment with selected drugs.....259

Chapter 1. Introduction

1.1 Mitochondrial biology

1.1.1 Origin of mitochondria

Mitochondria are ubiquitous double membraned organelles found in all nucleated human cells. Based on the endosymbiotic theory published by Lynn Margulis in 1967 (Sagan, 1967), mitochondria originated from a free-living organism that formed a union with a prokaryotic cell via endosymbiosis; this union evolved into the eukaryotic cell (Figure 1.1). The mitochondrion's double membrane structure, the lack of cholesterol in the inner membrane and its circular DNA are all remains of this bacterial origin. Phylogenetic analysis pinpoints the ancestor of mitochondria within alpha-proteobacteria, more specifically within the Rickettsiaceae (Anderson et al., 1981; Sicheritz-Ponten et al., 1998). The evolution of this symbiotic relationship resulted in cellular compartmentalization, which ultimately enabled eukaryotes to adopt new roles and provided a precursor to multicellularity. The symbiotic theory was recently challenged by the inside-out model for the evolution of eukaryotic cells (Baum and Baum, 2014), which describes an increasingly intimate mutualistic association between an archaeal host cell and α-proteobacteria (Figure 1.1). The inside-out model explains the formation of the nucleus, nuclear envelope and all other membrane bound organelles in a stepwise and orderly fashion as the host cell and mitochondrial ancestor grew closer and became one by the formation of the plasma membrane. Nevertheless, both of these models end up with the same final cellular structure that is intricate in nature.

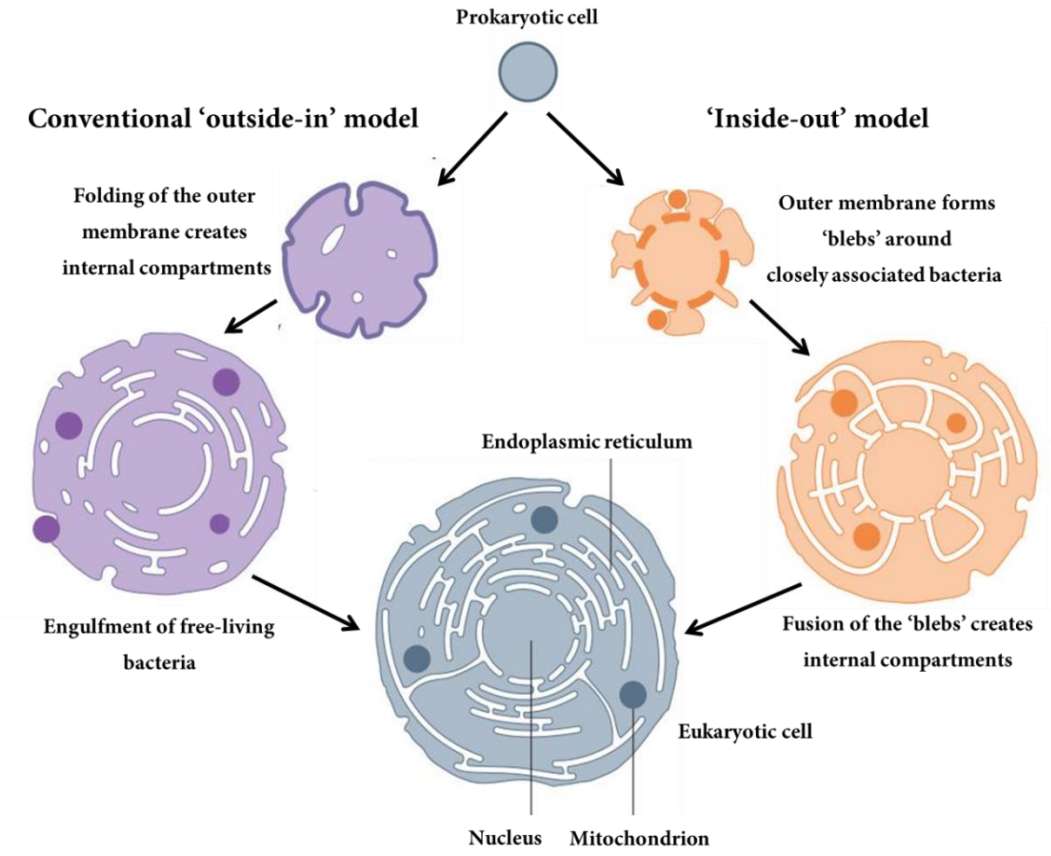

Figure 1.1 Current evolutionary models of the endosymbiotic theory
The conventional 'outside-in' model described the engulfment of free-living bacteria that will become mitochondria and the simultaneous invagination of the plasma membrane that will later form the internal compartments. The more recent 'inside-out' model is based on an increasingly intimate relationship developing between the ancestral prokaryotic cell and surface bacteria. Cellular compartments forming by extrusions of the cytoplasm, slowly engulfing the bacteria. The original plasma membrane will become the nuclear pore of the eukaryotic cell. Image was adopted from:
https://www.facebook.com/newscientist/photos/a.10150350736644589/10153087201264589/?type=1&theater

1.1.2 Structure of mitochondria

Mitochondria are commonly known as the energy producing, sausage-shaped organelles that serve as the power house of the cell. Mitochondria are dynamic organelles that move along microtubules and harbour an intimate relationship with the endoplasmic reticulum (ER) (Figure 1.2). Mitochondria are made up of an outer mitochondrial membrane (OMM) and a highly folded inner mitochondrial membrane

(IMM) that encloses the matrix (Figure 1.2). Folding of the IMM forms the cristae and houses the protein complexes of the oxidative phosphorylation (OXPHOS) system, whilst the space between the OMM and IMM is referred to as the intermembrane space. Owing to their bacterial origin, each organelle has their own rudimentary circular genome that is present in multiple copies within the matrix (Figure 1.2).

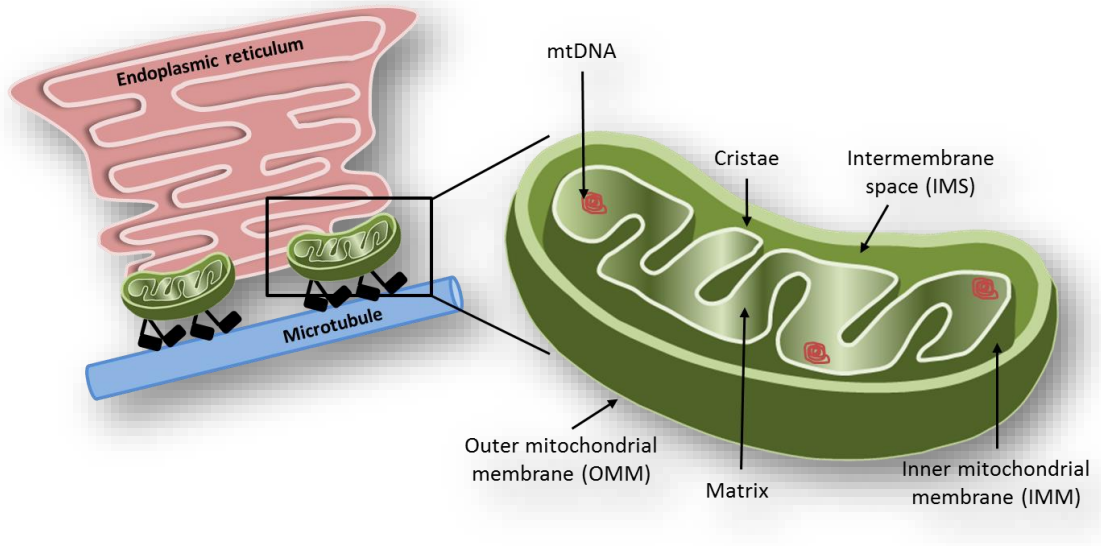

Figure 1.2 The structure of mitochondria
Mitochondria are dynamic organelles that move along microtubules within the cells and are closely associated with the ER. The structure of the organelle consists of an outer mitochondrial membrane (OMM), inner mitochondrial membrane (IMM) the folding of which forms the cristae, between the two is the intermembrane space (IMS) and finally the most inside compartment is the matrix. Mitochondrial DNA is located in the matrix and present in multiple copies.

1.1.3 Mitochondrial dynamics

Mitochondria are dynamic organelles that undergo constant fusion and fission (Bereiter-Hahn and Voth, 1994; Lackner, 2014). Mitochondrial fusion allows mixing of contents and therefore ensures the presence of a homogenous organelle population. Additionally, during nutrient starvation mitochondrial hyperfusion maximizes energy

production and protects the organelle from autophagic degradation (Gomes et al., 2011; Rambold et al., 2011). Fission ensures the partitioning of the existing mitochondrial pool during cell division (Mishra and Chan, 2014) while it also allows redistribution of mitochondria via active transport along microtubules according to the metabolic needs of the given cell (Frederick and Shaw, 2007). A fine balance between these two opposing forces is essential for the survival of the organelle as it constantly shapes the network according to the metabolic needs of the cell (Plecita-Hlavata et al., 2008). Selective mitochondrial fusion and fission aid the segregation of dysfunctional mitochondria from the rest of the network for degradation (Twig et al., 2008). Mitochondria with dysfunctional fission machinery were shown to accumulate oxidative damage that can lead to increased cell death (Kageyama et al., 2012). The current understanding of mitochondrial degradation will be discussed in section 1.3. The molecular drivers behind fusion and fission belong to the dynamin superfamily of GTPases (Figure 1.3). Separate but interacting machineries govern fusion of the inner and outer membranes. Fusion of the OMM is mediated by Mitofusin 1 (Mfn1) and to a certain extent by Mitofusin 2 (Mfn2) (Chen et al., 2003) both of which tether to the organelle by two N-terminal transmembrane domains while the rest of the protein is facing the cytosol with their C-terminal GTPase domain (Figure 1.3). According to the current model of OMM fusion, cis-dimerization of the Mfn proteins is followed by the association of adjacent mitochondrial membranes (Ishihara et al., 2004). The two Mfn proteins are not equally efficient in membrane tethering *in vitro,* which suggests their distinct functions (Ishihara et al., 2004). Indeed, Mfn2 is enriched at ER-mitochondria contact sites and was shown to regulate the tethering of the two membranes in mouse embryonic fibroblasts (de Brito and Scorrano, 2008). IMM fusion is regulated

by the dynamin-related protein optic atrophy 1 (OPA1) (Chen et al., 2005), that is anchored to the inner mitochondrial membrane with its active site facing the intermembrane space (Olichon et al., 2002) (Figure 1.3). The human OPA1 protein has eight variants resulting from alternative splicing of exons 4, 4b and 5b (Olichon et al., 2007). These variants have a tissue specific expression pattern and they undergo extensive post-translational processing during which long (L-OPA1) and short (S-OPA1) isoforms of the protein are created (Ishihara et al., 2006). These isoforms are associated with different functions. OPA1 knock-down induced mitochondrial fragmentation can only be rescued by the expression of L-OPA1 (Ishihara et al., 2006), while S-OPA1 regulates the formation and size of cristae junctions (Lee et al., 2017). The fusion activity of OPA1 is dependent on Mfn1 but not Mfn2 (Cipolat et al., 2004). Additionally, a small peptide generated by the cleavage of the exon 4b containing OPA1 isoform was implicated in mitochondrial genome maintenance, by contributing to the physical attachment of mitochondrial DNA to the matrix side of the IMM (Elachouri et al., 2011).

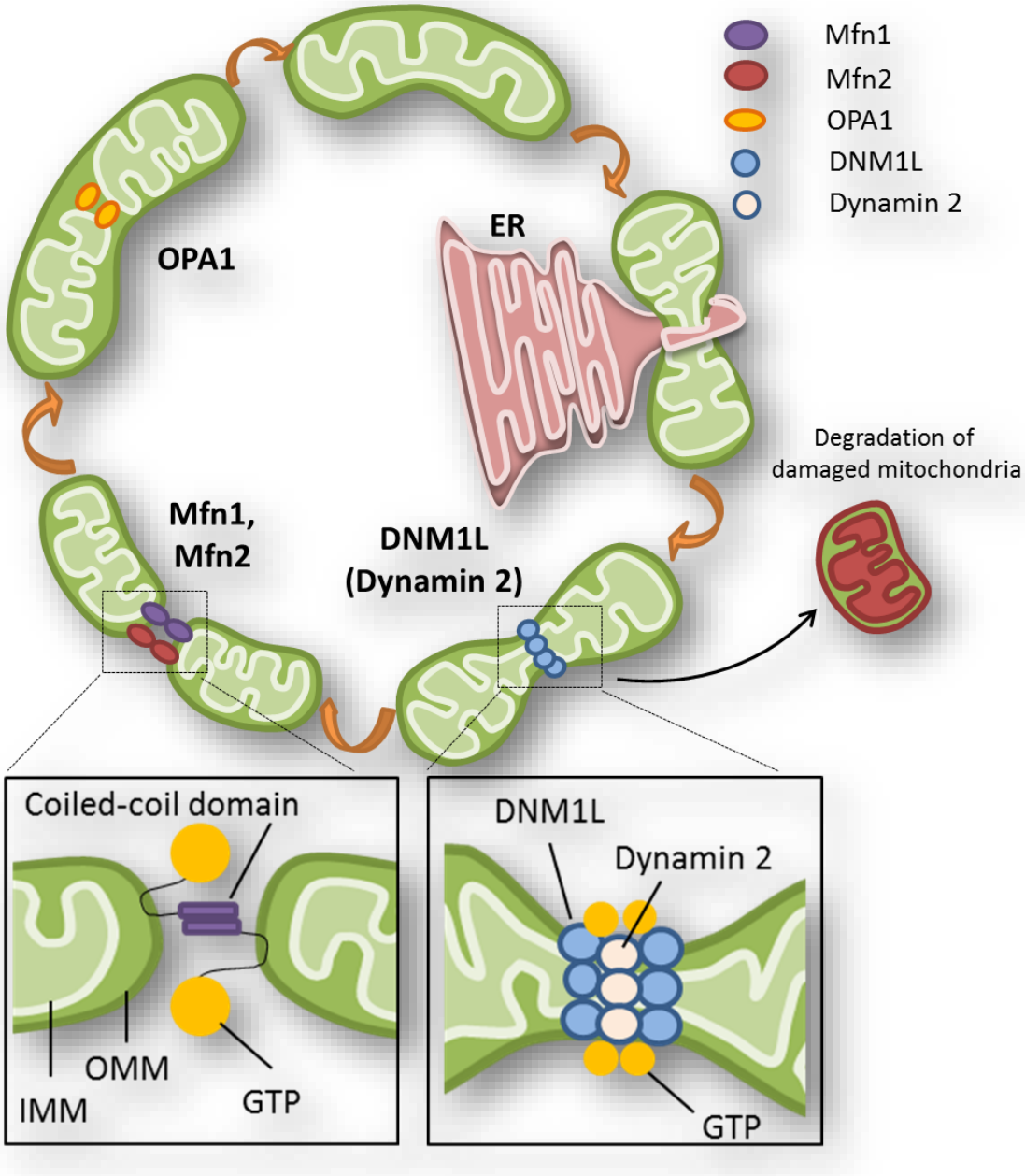

Figure 1.3 The mitochondrial fission and fusion machineries
Mitochondria are dynamic organelles that constantly fuse and divide. Fusion of the OMM is mediated by Mitofusin 1 and 2 (Mfn1/2), while IMM fusion is governed by optic atrophy 1 (OPA1). Fission is regulated by dynamin-like protein 1 (DNM1L) and Dynamin 2 that are recruited to ER marked division sites. The activity of all fusion-fission proteins is GTP-hydrolysis dependant.

The key regulator of mitochondrial fission is dynamin-like protein 1 (DNM1L) formerly known as dynamin-related protein 1 (DRP1), a highly conserved protein throughout the five kingdoms (Leger et al., 2015). DNM1L is recruited to the mitochondria at

division sites marked by the ER (Figure 1.3) (Friedman et al., 2011). The complete molecular mechanism behind DNM1L recruitment is still unknown, however, multiple OMM receptors, including fission protein 1 (Fis1) and mitochondrial fission factor (Mff), seem to be involved (Loson et al., 2013). DNM1L forms a ring around the division site by oligomerising at the mitochondrial surface (Figure 1.3). A conformational change resulting from GTP hydrolyses constricts the ring around the mitochondrion followed by the separation of the membranes (Mears et al., 2011). More recently, Dynamin 2 was shown to work in concert with DNM1L while coordinating the final step of mitochondrial membrane fission (Lee et al., 2016). Tight regulation of mitochondrial fission and fusion is essential, especially in non-replicating cells, as defects in mitochondrial dynamics have been related to an array of neurological disorders (Chen and Chan, 2009).

1.1.4 The mitochondrial genome

Mitochondria are the only organelles with extra-chromosomal DNA within mammalian cells. The human mitochondrial DNA (mtDNA) is 16,569-base pairs in length and encodes 37 genes in total with very little non-coding DNA present (Anderson et al., 1981). Out of those 37 genes only 13 are protein coding, providing instructions for complex subunits of the electron transport chain (ETC) (Figure 1.4). The rest of the mtDNA encodes for the 22 transfer RNAs (tRNAs) and 2 ribosomal RNAs (rRNAs) required for the translation of those 13 proteins (Figure 1.4).

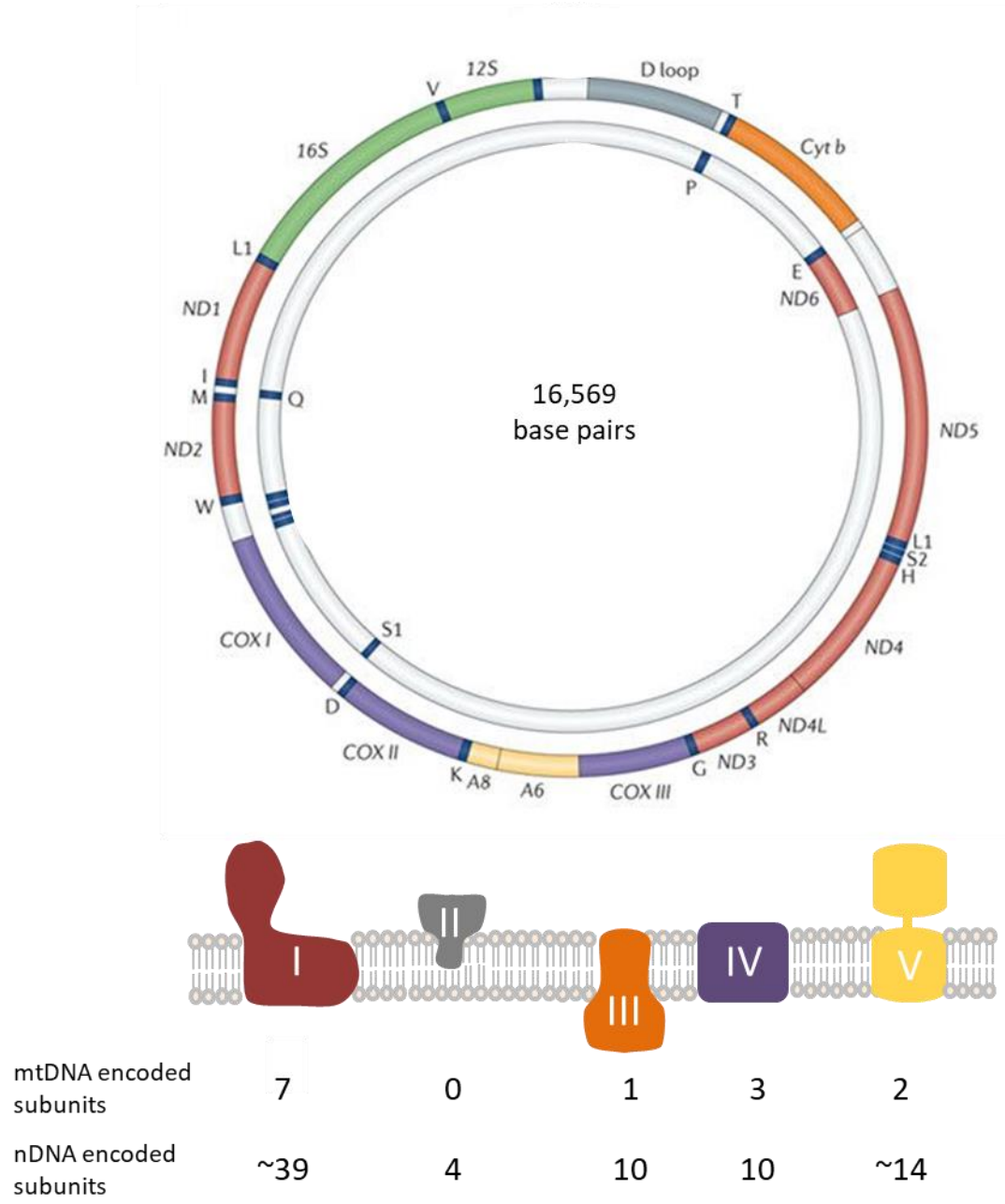

mtDNA encoded subunits	7	0	1	3	2
nDNA encoded subunits	~39	4	10	10	~14

Figure 1.4 The human mitochondrial genome
Mitochondrial DNA (mtDNA) is circular and double-stranded that encodes 37 genes. These are seven subunits of complex I (red), one subunit of complex III (orange), three subunits of complex IV (purple), two subunits of complex V (yellow), two rRNAs (12S and 16S, green) and 22 tRNAs (one-letter code). Adapted from (Schon et al., 2012).

Unlike nuclear DNA that is packaged into nucleosomes by histones, mtDNA is compacted into nucleoids associated with a wide range of proteins, but not histones (Bogenhagen, 2012). These nucleoids are located in the mitochondrial matrix and are tethered to the IMM (Elachouri et al., 2011; Gerhold et al., 2015). The predominant structural and functional organizer protein within mtDNA nucleoids is mitochondrial transcription factor A or TFAM (Bogenhagen, 2012; Kaufman et al., 2007). TFAM operates as both an enhancer of mitochondrial DNA transcription as well as a packaging protein via phased binding to non-promoter sites (Fisher et al., 1992; Parisi et al., 1993). Protein levels of TFAM tend to correlate with mitochondrial DNA content. TFAM is a functional protein essential for the maintenance and replication of mtDNA *in vivo,* as *Tfam* knock-out mice is embryonic lethal (Larsson et al., 1998). The number of mtDNA molecules included in a single nucleoid structure is still debated. Early studies reported multiple, 2-10 mtDNA molecules packaged together (Iborra et al., 2004; Legros et al., 2004). More recently, nucleoids were reported to contain a single mtDNA molecule (Kukat et al., 2015; Kukat et al., 2011). The list of additional proteins identified to closely interact with nucleoids is long (Bogenhagen, 2012; Bogenhagen et al., 2008). Some of the core nucleoid proteins include those involved in mitochondrial DNA replication, such as mitochondrial single-strand binding protein (mtSSB), mitochondrial polymerase gamma (poly γ) and the mitochondrial DNA helicase Twinkle. Mitochondrial DNA is maternally inherited; however, there are a few exceptional cases where bi-parental inheritance was reported (Luo et al., 2018).

1.1.5 Mitochondrial DNA replication

While an overwhelming proportion (~99%) of the human nuclear genome is made up of non-coding DNA, mtDNA contains almost no non-coding sequences. The exception is a 1.1kbp long stretch referred to as the displacement-loop (D-loop) that houses transcriptional promoters. Mitochondrial DNA is circular and double stranded. The two strands are named heavy (H) and light (L) according to their nucleotide composition and therefore their different masses that enables their separation using caesium-chloride preparation (Kasamatsu et al., 1974). Currently, there are competing models of mitochondrial DNA replication, all of which are briefly discussed below. The strand-displacement model of mtDNA replication (Figure 1.5 A) was proposed in the 1970s based on electron microscope images (Kasamatsu et al., 1971). It postulates that mitochondrial DNA replication is initiated at two origins, O_H of the heavy chain and O_L for the light chain in an asynchronous manner (Figure 1.5 A). First, replication is initiated at O_H and proceeds in a unidirectional and uninterrupted manner until reaching about two-thirds of the way. At this point, displacement of the parental H-strand exposes O_L, allowing assembly of the replication machinery and commencement of L-strand replication in the opposite direction (Clayton, 1982). In addition to the strand displacement model, in 2000 Holt and colleagues described a novel mtDNA replication mechanism referred to as the strand-coupled model (Figure 1.5 B) (Holt et al., 2000). According to this, replication of the H and L strands is synchronous and originates at or near to the previously defined O_H. Later, on the bases of these findings the RITOLS (**R**ibonucleotides are **I**ncorporated **T**hrough**O**ut the **L**agging **S**trand) model was developed (Figure 1.5 C) (Bowmaker et al., 2003). The RITOLS model proposes that replication originates at two sites, O_H and Ori-b, both of

which are located within the D-loop. During leading strand replication RNA is incorporated throughout the lagging strand. Later on, lagging strand DNA synthesis is initiated at O_L, and RNA is replaced (or converted to) DNA. The origin of the incorporated RNA stands undetermined. According to the latest "bootlace" model these are pre-formed RNA transcripts, as replication and transcription occurs simultaneously (Reyes et al., 2013).

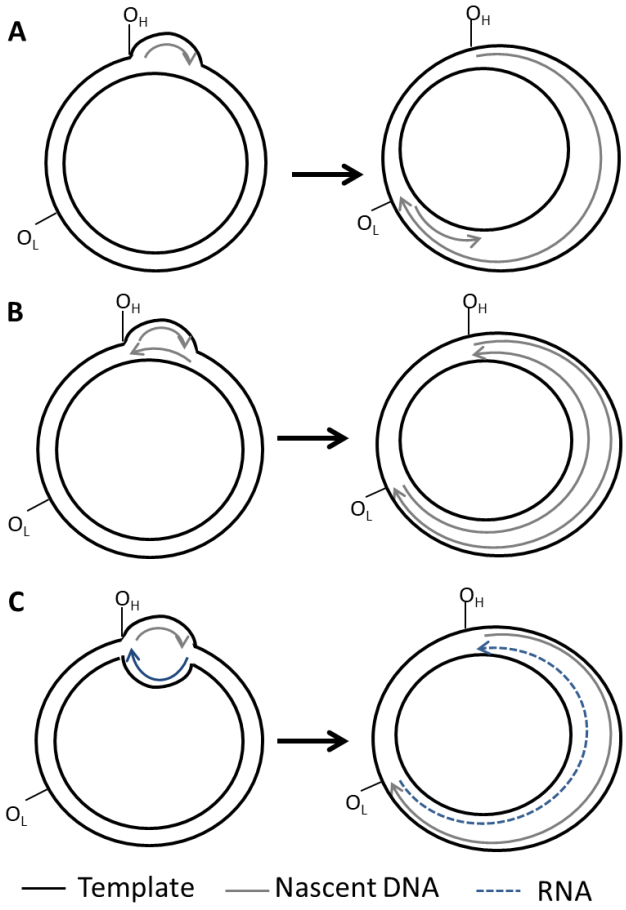

Figure 1.5 Current models of mitochondrial DNA replication
(A) Strand-displacement model of mtDNA replication during which heavy strand replication commences at O_H and once that reaches two-third DNA sequences light strand replication is initiated at O_L. (B) In the strand-coupled model replication of the heavy and light strands proceeds simultaneously from a single point of origin close to O_H. (C) The RITOLS model proposes asynchronous replication during which leading strand synthesis originates from the D-loop near O_H, while RNA is hybridised to the lagging strand. This later on is converted to DNA, originating from O_L. Adapted from (McKinney and Oliveira, 2013).

1.2 Mitochondrial functions – more than just a 'power house'

A long established function of mitochondria is to provide the cells with energy via oxidative phosphorylation. In the 1990s it became an emerging concept to consider mitochondria as important signalling hubs within the cell rather than just 'renewable batteries' (Figure 1.6) (Chandel, 2014). Additionally, mitochondria are also involved in the biosynthesis of several molecules.

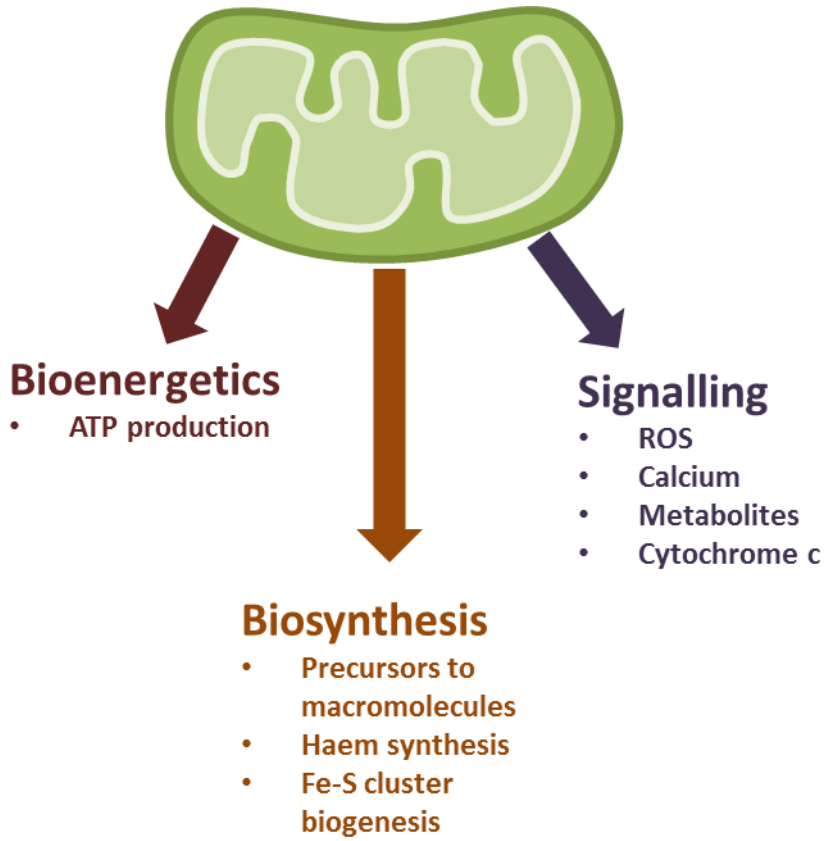

Figure 1.6 Mitochondria are involved in multiple cellular processes
Mitochondria are involved in three key cellular processes: bioenergetics, biosynthesis and signalling.

1.2.1 Mitochondria and ATP synthesis

The major source of cellular energy is glucose, which is initially metabolised via glycolysis into pyruvate in the cytoplasm. The subsequent steps of aerobic glucose metabolism all take place within mitochondria. Pyruvate is metabolised in the tricarboxylic acid (TCA) cycle to generate large amounts of ATP through the process of oxidative phosphorylation (OXPHOS). Certain cell types (e.g. cancer cells) preferentially use fermentation in order to meet their energy requirements (Lunt and Vander Heiden, 2011). Although this process does not require oxygen, it is considerably less efficient than aerobic glucose metabolism as it yields 2mol ATP per 1 mol glucose as opposed to the 36 mol ATP per 1 mol glucose through OXPHOS.

1.2.1.1 The TCA cycle

Pyruvate derived from glycolysis enters the mitochondria where it is converted into acetyl coenzyme A (acetyl-CoA) by pyruvate dehydrogenase (Figure 1.7). Acetyl-CoA enters the TCA cycle where it is completely oxidised into carbon dioxide and water through a series of reactions (Figure 1.7). The reactions of the TCA cycle also reduce three nicotinamide adenine dinucleotides (NAD^+) into NADH, and one equivalent of flavin adenine dinucleotide (FAD) into $FADH_2$. These will serve as substrates for OXPHOS.

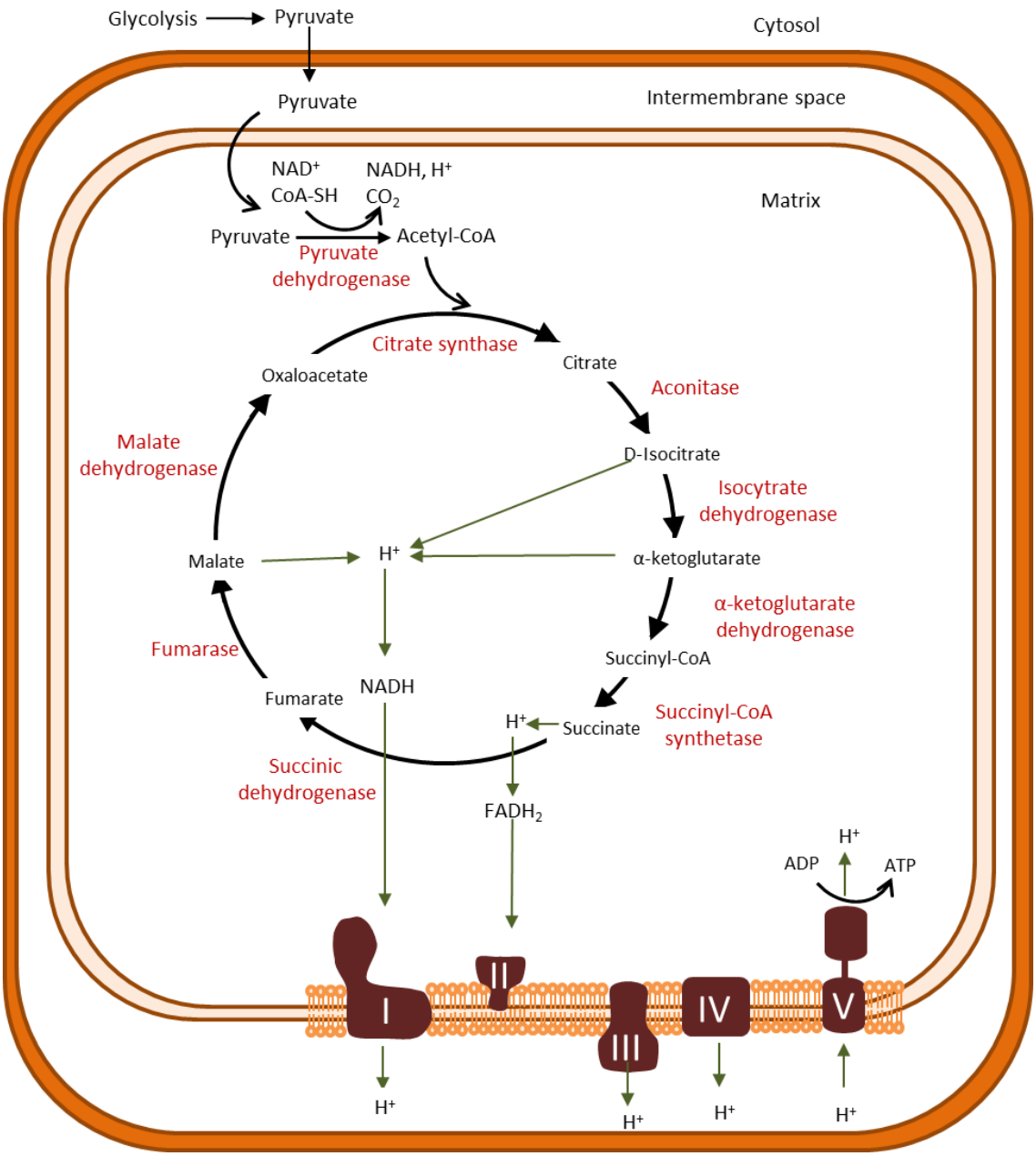

Figure 1.7 The TCA cycle
Acetyl-CoA enters the TCA cycle where it is completely oxidised into carbon dioxide and water through a series of reaction. Pyruvate dehydrogenase that converts pyruvate into Acetyl-CoA and the eight key enzymes of the TCA cycle are indicated in red. Adopted from (DiMauro and Schon, 2003).

1.2.1.2 Oxidative phosphorylation

NADH and $FADH_2$ generated through the TCA cycle enter the electron transport chain (ETC) through complex I (NADH dehydrogenase) and complex II (succinate dehydrogenase) respectively (Figure 1.8). NADH and $FADH_2$ are reduced to NAD^+ and FAD^+, and the electrons are transferred across the ETC from Complex I/II all the way to complex IV (cytochrome c oxidase) (Figure 1.8). Electron transfer between complex II and complex III (ubiquinol-cytochrome c oxidoreductase) is mediated by the lipid soluble ubiquinone (Q), while electron flow between complex III and IV is mediated by the water soluble cytochrome c (cyt c) (Figure 1.8). The final electron acceptor at complex IV is oxygen, which is then reduced to water. As the electrons travel from one complex to the next they lose energy, which is used by complexes I, III and IV to pump protons into the IMS. The accumulation of positively charged protons in the IMS creates an electrochemical gradient across the IMM. The IMM is impermeable to ions, therefore protons flow back to the matrix via the only available channel provided by complex V (ATP synthase). The enzyme uses the potential energy released for the synthesis of ATP from ADP and inorganic phosphate (Pi). Complexes of the electron transport chain assemble into supercomplexes, also called respirasomes, in order to increase the efficiency of electron transport and ATP production (Schagger, 2001). These functional units consist of CI, CIII, and CIV in various stoichiometries. The disruption of supercomplexes results in impaired oxygen consumption and increased mitochondrial reactive oxygen species production (Lopez-Fabuel et al., 2016).

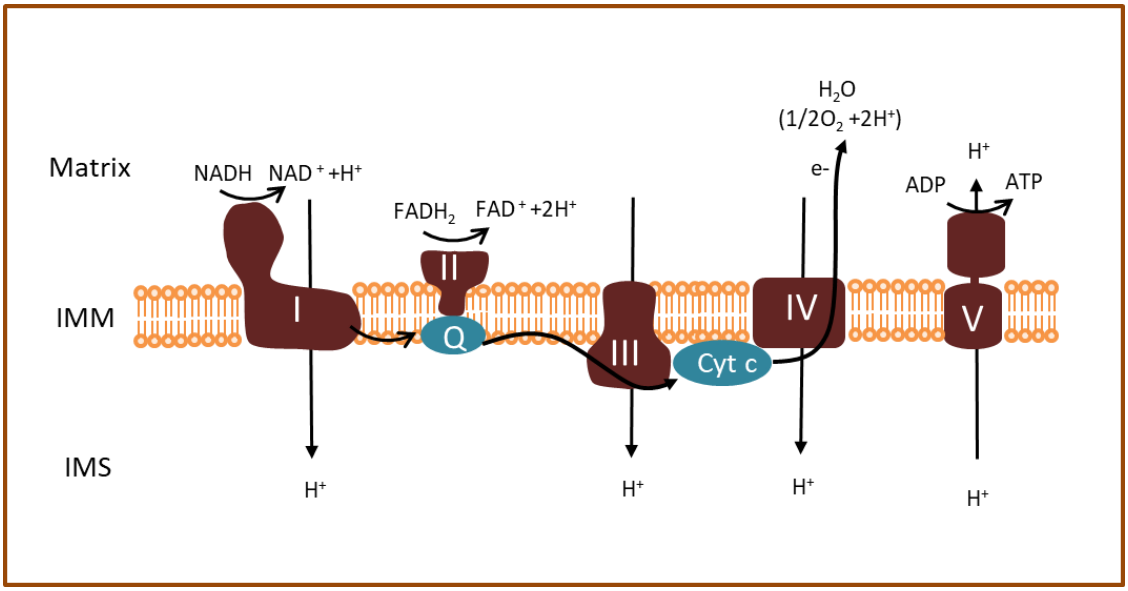

Figure 1.8 Oxidative phosphorylation and the generation of ATP through complexes of the electron transport chain
Electrons derived from the reduction of NADH and FADH2 travel through the electron transport chain complexes (I-IV) while protons are translocated to the IMS through complexes I, II and IV generating a proton motive force. This is harvested by complex V for ATP synthesis.

1.2.2 Mitochondria and iron metabolism

The greater part of cellular iron is utilized in mitochondria for the synthesis of haem (Ajioka et al., 2006) and iron-sulphur (Fe-S) clusters (Lill, 2009). The first and last steps of haem synthesis are carried out in the mitochondria, while the middle part is orchestrated in the cytoplasm. In mitochondria, haem synthesis is catalysed by the mitochondrial enzyme ferrochelatase that facilitates the incorporation of iron into protoporphyrin (Nishida and Labbe, 1959). Iron-sulphur clusters serve as inorganic co-factors for a wide range of proteins involved in catalysis, electron transport and sensing of ambient conditions (Lill, 2009). Fe-S cluster binding of ETC complexes I, II and III confer them the ability to undergo redox reactions (Napier et al., 2005). Biosynthesis of these Fe-S clusters requires an iron donor (frataxin), a sulphur donor

(cysteine desulfurase) and an assembly scaffold. Electrons are provided by ferredoxins and ferredoxin reductase (Rouault, 2012).

1.2.3 Mitochondria and calcium signalling

Calcium (Ca^{2+}) is involved in a vast repertoire of signalling processes that influence cellular functions such as neurotransmitter release and muscle contraction. It has long been observed that Ca^{2+} rapidly accumulates in functional mitochondria (Deluca and Engstrom, 1961), which implicates its involvement in calcium signalling and therefore several biological processes. Importantly, calcium also appears to regulate mitochondrial function (Duchen, 2000). The accumulation of positively charged Ca^{2+} ions in the mitochondrial matrix requires the passing of two double membranes. While the OMM is permeable to solutes with sizes below 5kDa, including Ca^{2+}, the availability of voltage gated ion channels (VDAC) was shown to influence the rate of Ca^{2+} uptake by mitochondria (Rapizzi et al., 2002). Passing through the IMM requires a transport system due to its selective permeability (Rizzuto et al., 2012). This is provided by the mitochondrial Ca^{2+} uniporter (MCU) (Figure 1.9) (Kirichok et al., 2004). Calcium uptake via MCU is tightly regulated by the mitochondrial calcium uptake proteins 1 and 2 (MICU1 and MICU2) and the essential MCU regulator (EMRE) based on cytosolic Ca^{2+} levels (Kamer and Mootha, 2015). Calcium is removed from the mitochondrial matrix by the sodium–calcium exchange protein (NCLX) and the Ca^{2+}/H^{+} exchanger (HCLX) via active transport (Figure 1.9) (Kamer and Mootha, 2015).

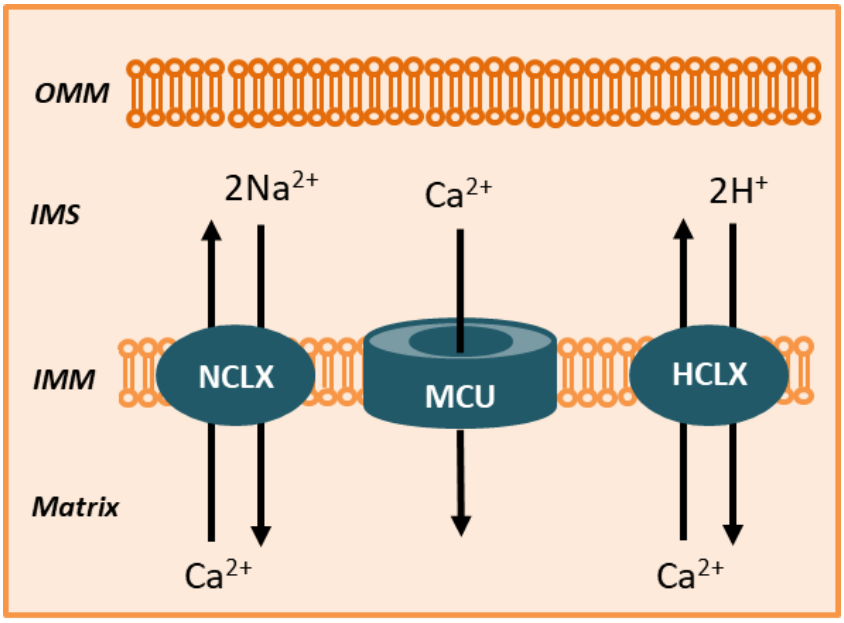

Figure 1.9 Calcium import and export through the inner mitochondrial membrane Positively charged Ca^{2+} ions are imported into the mitochondrial matrix through active transport via the mitochondrial Ca^{2+} uniporter (MCU) and removed by sodium–calcium exchange protein (NCLX) and the Ca^{2+}/H^{+} exchanger (HCLX). Adopted from (Kamer and Mootha, 2015).

Mitochondrial Ca^{2+} uptake is localised to micro-domains of high cytosolic Ca^{2+} in the vicinity of other calcium handling organelles and mediated by the formation of dynamic contact sites (Walsh et al., 2009). The best studied of these are mitochondria and endoplasmic reticulum (ER) contact sites (MERCs) (Csordás et al., 2006; Rizzuto et al., 1998). The portion of membranes involved in these interactions is dynamic and consists of specialised lipids. These are referred to as mitochondrial associated membranes (MAMs), which account for 5–20% of the mitochondrial network (Csordás et al., 2006). Other than calcium signalling, ER-mitochondria contact sites have been implicated in the regulation of several cellular processes, such as phospholipid exchange, mitochondrial biogenesis and mitophagy and even inflammasome formation (Paillusson et al., 2016).

1.2.4 Mitochondrial ROS signalling

The mitochondrial electron transport chain is a major site of reactive oxygen species production (ROS) (Brand, 2010). Mitochondrial ROS production has long been viewed as a contributor to many pathological conditions, especially neurodegenerative diseases as it can damage lipids, proteins as well as DNA and RNA (Manoharan et al., 2016). This perspective has changed as ROS slowly emerged as signalling molecules involved in normal physiological processes (Chandel, 2014). The primary reactive oxygen species generated on both sides of the IMM is superoxide (O_2^-) which can be converted to hydrogen peroxide (H_2O_2) by superoxide dismutase enzymes 1 and 2 (Shadel and Horvath, 2015). Mitochondrial ROS is involved in retrograde signalling from mitochondria to the cytosol and it was also shown to contribute to hypoxia signalling by stabilizing the hypoxia-inducible factor-1 alpha (HIF-1α) (Chandel et al., 2000), and to trigger potentially protective mitophagy (Frank et al., 2012; Xiao et al., 2017). While increased release of H_2O_2 was implicated in the regulation of cellular metabolism (Nemoto et al., 2000).

1.2.5 Mitochondria and apoptosis

Programmed cell death or apoptosis may be triggered either by the extrinsic, receptor-mediated pathway or via the intrinsic, mitochondria mediated pathway. Members of the B cell lymphoma-2 (Bcl-2) protein family are the gatekeepers of mitochondrial apoptotic signalling (Roufayel, 2016). Apoptosis is initiated by the cleavage of the anti-apoptotic Bcl-2 proteins, which allows pro-apoptotic members of the Bcl-2 family (Bax, or Bak) to stabilize on the surface of mitochondria resulting in membrane rupture and the release of cytochrome c (Figure 1.10). Subsequently,

cytosolic cyt c activates the caspase signalling cascade, resulting in programmed cell death (Wang and Youle, 2009).

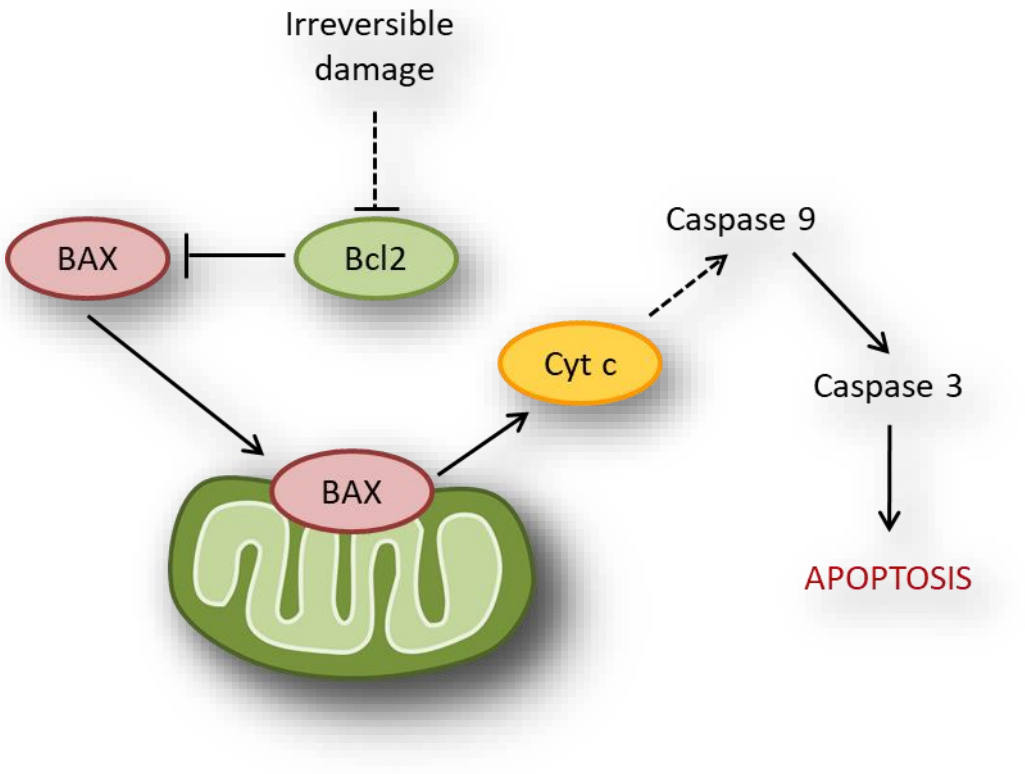

Figure 1.10 Overview of mitochondrial apoptotic signalling
Irreversible damage results in mitochondrial membrane rupture and the release of cyt c, which activates the caspase signalling cascade resulting in programmed cell death.

1.3 Mitochondrial quality control

Mitochondria are key to cellular homeostasis; therefore, their quality is ensured and tightly regulated. Mitochondrial quality control occurs in a stepwise manner according to the extent of the damage (Figure 1.11). While mitophagy may represent a last resort for individual organelles, additional mechanisms are in place to both limit the damage and facilitate the recovery of salvageable organelles. The failure of all these quality control mechanisms, which are discussed in the following sections, likely leads to apoptotic cell death.

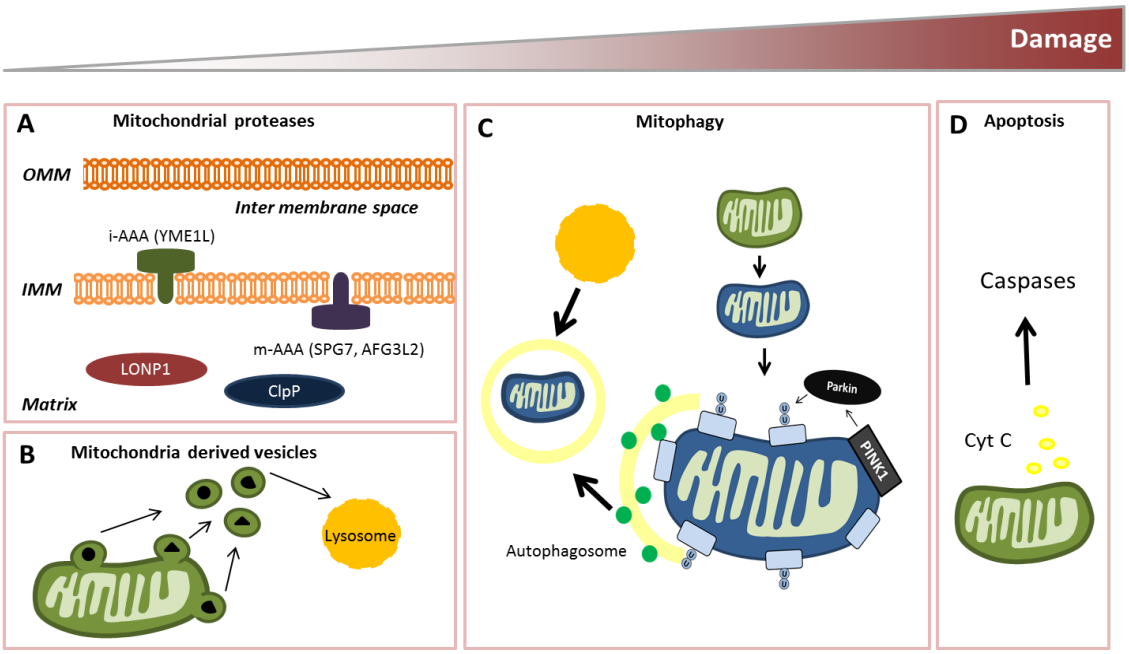

Figure 1.11 Mitochondrial quality control proceeds in a step wise manner
(A, B) Damaged parts of the organelle, such as oxidized or unfolded proteins are removed by resident proteases and mitochondria derived vesicles. (C) When the damage to the organelle is too extensive to be fixed by changing the parts, the whole organelle is recycled by mitophagy. (D) If mitophagy fails to restore cellular homeostasis the cells might undergo apoptosis.

1.3.1 Protecting the mitochondrial proteome - Mitochondrial proteases

A by-product of mitochondrial oxidative phosphorylation is the generation of ROS that are damaging to proteins. In order to avoid the accumulation of potentially toxic, oxidized and misfolded proteins mitochondria have their own protein quality control achieved by resident proteases (Figure 11.1 A) (Hamon et al., 2015). There are four ATP-dependent proteases within mitochondria, all of which are conserved from bacteria to higher eukaryotes (Gerdes et al., 2012). The i-AAA and m-AAA (ATPases associated with various cellular activities) proteases are embedded in the IMM with their catalytic sites facing the IMS and the matrix respectively (Figure1.11 A) (Leonhard et al., 1996). The i-AAA protease exists as a homo-hexamer made up of YME1L subunits (Coppola et al., 2000), while the m-AAA protease is found as two isozymes either as a homo-hexamer of AFG3 –like protein 2 (AFG3L2) subunits, or as a hetero-oligomer of alternating AFG3L2 and spastic paraplegia 7 (SPG7 or paraplegin) subunits (Koppen et al., 2007). Target proteins of these membrane bound proteases are either completely degraded, partially processed, or simply dislocated from the IMM (Glynn, 2017). Stable knock-down of YME1L leads to the accumulation of non-assembled respiratory chain subunits of complex I and complex IV (Stiburek et al., 2012). Additionally, YME1L is indirectly involved in the regulation of OPA1 processing (Rainbolt et al., 2016). The m-AAA protease was shown to degrade complex IV (Hornig-Do et al., 2012) and complex V (Richter et al., 2015) subunits encoded by the mitochondrial genome, as well as the unassembled EMRE subunit of the mitochondrial calcium uniporter (Tsai et al., 2017). Mutations in both m-AAA protease subunits have been associated with a wide range of neurological disorders

from hereditary spastic paraplegia (Wilkinson et al., 2004) to Parkinsonism (Magri et al., 2018).

Oxidized proteins in the matrix are degraded by two additional proteases, LONP1 and ClpP (Figure 1.11 A). The best studied of the two is LONP1, which was shown to regulate mitochondrial DNA copy number via the selective degradation of the mitochondrial transcription factor, TFAM (Matsushima et al., 2010). A decline in LONP1 function also contributes to the accumulation of oxidized proteins in the mitochondrial matrix during ageing (Ugarte et al., 2010).

There have been no mitochondrial proteases identified in the OMM. However, ubiquitinated proteins were shown to be degraded by the cytosolic ubiquitin-proteasome system (Taylor and Rutter, 2011). Mitochondrial proteases and the cytosolic ubiquitin-proteasome system are not only involved in proteomic quality control but also provide a regulatory mechanism by managing the expression levels of their target proteins.

1.3.2 Mitochondrial derived vesicles

Mitochondria are able to generate vesicles that are collectively called mitochondrial derived vesicles (MDVs, Figure 1.11 B) (Neuspiel et al., 2008; Soubannier et al., 2012a; Soubannier et al., 2012b). These form by budding off the OMM independently of the mitochondrial fission protein DRP1/DNM1L. MDVs positive for the OMM protein TOM20 selectively transport mitochondrial proteins and lipids to lysosomes for degradation (Soubannier et al., 2012b). MDVs were shown to accumulate in the presence of lysosomal inhibitors, suggesting that their formation is a constitutively active process (Soubannier et al., 2012a). Oxidative damage increases MDV generation carrying oxidized cargo, including components of electron transport chain

complexes (CII, CII and CIV) as well as outer membrane proteins (eg VDAC) (Soubannier et al., 2012b). Interestingly, proteins of complex I and V were not found in MDVs and neither was mtDNA.

1.3.3 Mitochondria specific autophagy – mitophagy

Superfluous or damaged mitochondria are turned over by an organelle specific autophagy pathway, termed mitophagy (Figure 1.11 C). During mitophagy, damaged mitochondria are sequestered by a double-membrane structure called the autophagosome and subsequently delivered to the lysosome for degradation. This process involves the combination of two distinct pathways:

I. Formation of the autophagosome, for which the molecular machinery is shared by all macro-autophagy pathways including mitophagy.
II. Mitochondrial 'eat-me' signalling for mitophagic degradation

1.3.3.1 Autophagosome formation

The core proteins involved in the formation of autophagosomes were first identified in yeast (Tsukada and Ohsumi, 1993) and were cumulatively named AuTophaGy (ATG) proteins (Klionsky et al., 2003). For his discoveries in the field of autophagy, in 2016 Yoshinori Ohsumi was awarded the Nobel Prize in Physiology or Medicine. Most of the ATG proteins discovered in yeast have mammalian homologues, emphasizing the high degree of conservation of this pathway throughout evolution. Although there are additional factors involved in autophagy that are specific to higher eukaryotes.

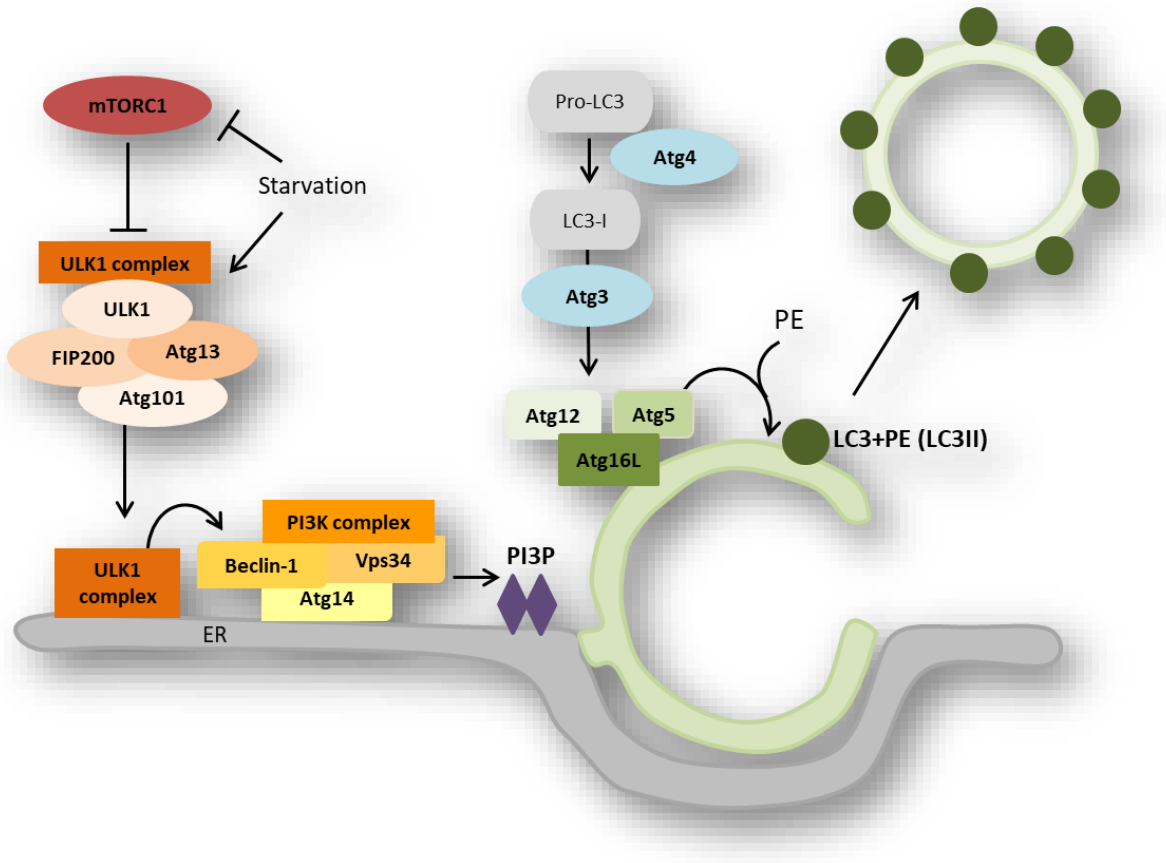

Figure 1.12 The molecular mechanism of autophagosome formation
The ULK1-Atg13-FIP200-Atg101 complex initiates autophagosome formation following mTORC1 inhibition. The ULK1 complex activates the PI3K protein complex (Beclin-1-Atg14-Vps34) that generates phosphatidylinositol-3-phosphate rich membranes for the recruitment of the Atg proteins that mediate membrane elongation. Adopted from:http://square.umin.ac.jp/molbiol/english/RESEARCH/index.html

Autophagosome formation is initiated by Unc-51-like kinase (ULK1) along with its binding partners Atg13, FIP200 and Atg101 (Figure 1.12) (Ganley et al., 2009; Hosokawa et al., 2009; Mercer et al., 2009). ULK1 is a serine-threonine kinase and the binding of Atg13 to ULK1 stabilizes the protein while stimulating its kinase activity (Jung et al., 2009). Active ULK1 phosphorylates its other binding partner FIP200 (Hara et al., 2008), and the ULK1-Atg13-FIP200-Atg101 complex initiates autophagosome formation. The role of ULK1 in autophagy initiation has primarily been studied in the

context of nutrient deprivation. In nutrient rich conditions, ULK1 is inhibited by the mechanistic/mammalian target of rapamycin complex 1 (mTORC1) through phosphorylation of ULK1 itself and some of its binding partners (Chan, 2009). The mammalian TORC1 complex is a key regulator of autophagy, dependent on the cell's metabolic status. Under nutrient rich conditions mTORC1 inhibits autophagy and promotes cell growth and proliferation, while during nutrient starvation mTORC1 inhibition triggers autophagy for which ULK1 is essential (Petherick et al., 2015). The signalling molecule(s) that initiate the recruitment and translocation of the ULK1 complex to the site of autophagosome formation remain unknown. ATG9 positive punctae were shown to be present at the sites of forming autophagosomes prior to ULK1 recruitment (Orsi et al., 2012). Additionally, RNAi mediated knock-down of ATG9 inhibits the appearance of GFP-LC3-positive dots during amino acid starvation (Orsi et al., 2012). Certain forms of autophagy, for example autophagy induced by glucose starvation, may proceed without the involvement of ULK1 (Cheong et al., 2011; Gammoh et al., 2013), or mTORC1 (Melser et al., 2013).

Initiation of autophagosome formation proceeds via the activity of a second protein complex that consist of Beclin-1, ATG14L and vacuolar protein sorting 34 (VPS34) (Figure1.12). The complex is initiated by ULK1 mediated phosphorylation of Beclin-1 and subsequent activation of its binding partners ATG14L and VPS34 (Russell et al., 2013). VPS34 is a class III phosphatidylinositol kinase (PI3K), therefore the complex is referred to as the PI3K complex, that generates phosphatidylinositol-3-phosphate (PI(3)P) rich membranes (Itakura et al., 2012). These provide the platforms for further ATG protein recruitment. Beclin-1 and the PI3K complex are dispensable for certain types of mitophagy (Chu et al., 2007; Lemasters, 2014).

Following initiation, elongation of the autophagosomal membrane is mediated by two ubiquitin-like conjugation systems (Figure 1.12) (Suzuki et al., 2007). Microtubule-associated protein-1 light chain-3 (LC3), a mammalian homologue of the yeast Atg8 protein is synthesized as a precursor with an additional C-terminal sequence, that is removed by Atg4, creating LC3-I (Kabeya et al., 2004). The LC3-I form of the protein is typically diffused in the cytoplasm. During autophagosome formation LC3-I is conjugated to phosphatidylethanolamine (PE) via Atg3, forming LC3-II. Additionally, the Atg12-Atg5-Atg16L conjugation system that resides on the surface of the forming autophagosome also facilitates the formation of LC3-II in cooperation with Atg3 (Hanada et al., 2007). While the Atg12-Atg5-Atg16L complex dissociates from the membrane once autophagosome formation is complete, LC3-II remains membrane bound. Therefore, labelling of LC3-II provides a unique tool for tracking autophagy progression within cells.

1.3.3.2 Mitochondrial 'eat-me' signals

The signalling pathways leading to the selective degradation of mitochondria are still not completely understood. The nature of the specific molecules involved seems to be dependent on the trigger and therefore there are multiple mechanisms by which mitochondria can be targeted for degradation. These can be broadly categorised into mitophagy receptors and mitophagy adaptors (Figure 1.13).

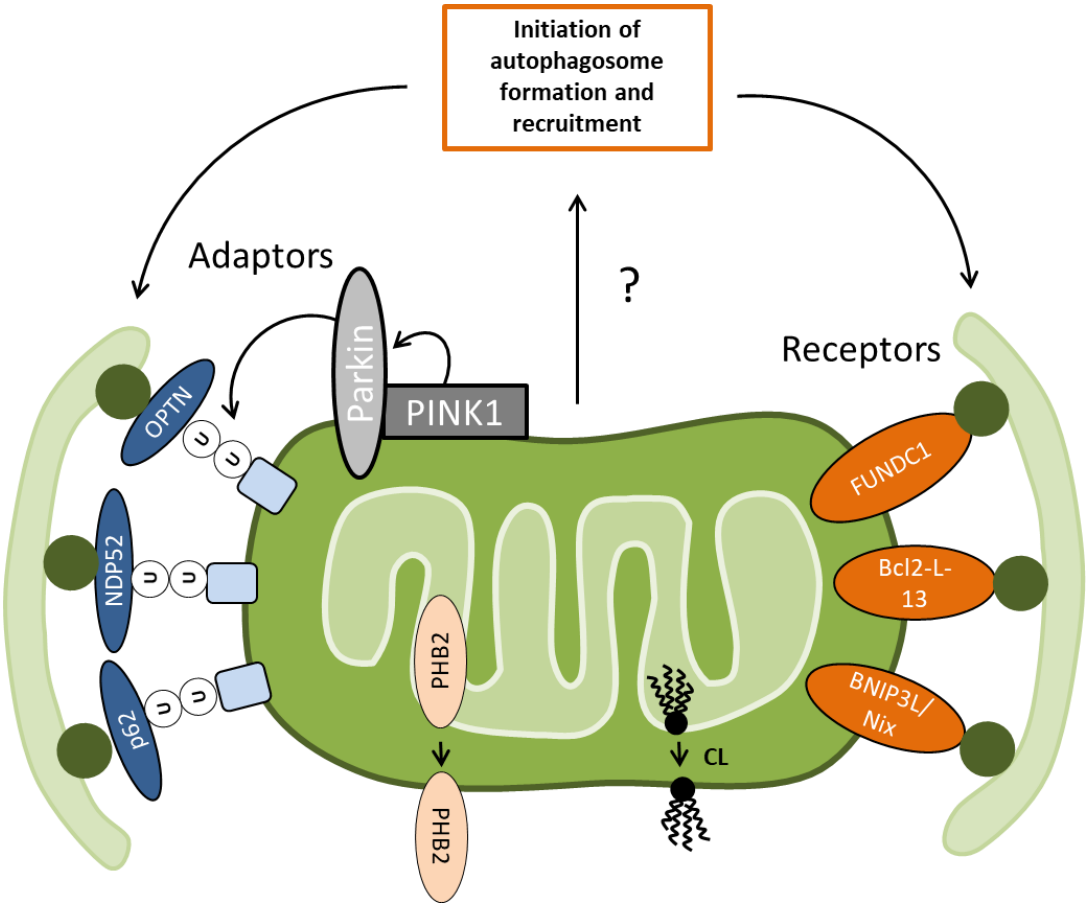

Figure 1.13 Mitophagy receptor and adaptors
Various molecules mediate mitochondrial signalling for mitophagy. Adaptors are molecules that bind to ubiquitinated OMM proteins while binding to LC3 on the forming autophagosome. Receptors are integral OMM proteins that upon stimulus readily bind to LC3. Two inner membrane components cardiolipin and PHB2 have also been implicated in mitophagy signalling. How the initiation complex of autophagosome formation is recruited to mitochondria is yet to be dissected.

The best-studied molecular pathway involves the recruitment of Parkin, an E3 ubiquitin ligase, to depolarized mitochondria (Narendra et al., 2008) by PTEN-induced putative kinase 1 (PINK1) (Matsuda et al., 2010), followed by the ubiquitination of OMM proteins in a Parkin dependent manner. The ubiquitin ligase activity of Parkin is promoted by its PINK1 mediated phosphorylation (Kondapalli et al., 2012). Additionally, PINK1 also phosphorylates ubiquitin at Ser65 which in turn initiates the recruitment of adaptor proteins, such as the nuclear dot protein 52kDa (NDP52) and optineurin (OPTN) (Lazarou et al., 2015). These adaptors also contribute to the

recruitment of the autophagy machinery and bind to LC3 via their LC3 interacting region (LIR). One of the earliest identified LC3 binding proteins was p62 (Geisler et al., 2010), however, it was later shown to coordinate the recruitment of ubiquitinated mitochondria into perinuclear clusters but was not essential for mitophagy (Narendra et al., 2010; Okatsu et al., 2010).

Signalling for mitophagy can also be mediated by specific receptors of the OMM (Figure 1.13) in both a Parkin dependent and independent manners. Bcl-2-like protein 13 (Bcl2-L-13) (Murakawa et al., 2015), Nix (or BNIP3L) (Melser et al., 2013), and FUN14 domain containing protein 1 (FUNDC1) (Liu et al., 2012) were all reported to mediate mitophagy. Bcl2-L-13 was identified based on its homology to the yeast mitophagy protein Atg32 (Murakawa et al., 2015). While Nix was first reported to mediate the removal of mitochondria during reticulocyte maturation (Sandoval et al., 2008; Schweers et al., 2007); it was also implicated in the turnover of mitochondria during a shift in mitochondrial energetic status (Melser et al., 2013). The role of FUNDC1 in mitophagy signalling is best characterized in hypoxic conditions (Chen et al., 2017; Liu et al., 2012; Wu et al., 2016; Wu et al., 2014). Externalized cardiolipin and prohibition 2 (PHB2), both integral parts of the IMM, were also shown to mediate mitophagy signalling by their externalization following mitochondrial damage (Chu et al., 2013; Wei et al., 2017). All the above mentioned receptors (Figure 1.13) possess at least one LIR domain and therefore are able to interact with LC3-coated autophagosomal membranes. How autophagosomes are recruited to the mitochondria remain to be elucidated. *De novo* autophagosome formation at the surface of the damaged mitochondria has also been suggested as opposed to the recruitment of a forming autophagosome (Itakura et al., 2012).

Although the identification of several molecules involved in mitophagy signalling represent significant advances in our understanding of mitochondrial turnover, the mitophagic pathways described in mammalian cells appear to be restricted to specific conditions. Many of these studies use pharmacologic agents in order to induce extensive mitochondrial damage; therefore, their physiological relevance remains controversial.

1.4 Current methods for investigating mitophagy

In cellular models, the most commonly used methods for investigating mitophagy are either electron microscopy (EM) or fluorescence microscopy. While EM allows excellent visualisation of mitochondria engulfed by autophagosomes, it is a laborious and not very quantitative method due to the small number of sections and cells. Fluorescence microscopy is widely used for monitoring the co-localisation between mitochondria and autophagosomes or lysosomes, utilising a wide range of labelling techniques. These allow imaging a much larger number of cells and can even be adapted for high-content imaging. Labelling of the organelles is either achieved by targeted fluorescent protein constructs or by using antibodies raised against a mitochondrial protein and typically LC3 for autophagosomes or lysosome-associated membrane protein 2 (LAMP2) for lysosomes. Co-localisation of mitochondria with autophagosomes indicates successful sequestration of the organelle, while co-localisation of mitochondria with lysosomes indicates successful delivery to the acidic compartment. In any case, none of these two outcomes are indicative of the turnover rate of mitochondria (flux). The use of lysosomal inhibitors is needed in order to be able to conclude mitophagic flux. Monitoring mitochondrial protein degradation by

western blot analysis could offer an alternative by measuring the degree of mitochondrial protein degradation (Williams et al., 2017). However, target proteins should be chosen with care as several members of the mitochondrial proteome are degraded by proteases as well as mitophagy. To overcome these hurdles, one can make use of the recently developed Mito-QC (Allen et al., 2013), mt-Keima (Katayama et al., 2011), and Rosella (Rosado et al., 2008) constructs that provide an end point measurement of mitochondrial degradation. Mito-QC consists of a tandem mCherry-GFP tag fused to the mitochondrial targeting sequence of the outer mitochondrial membrane protein FIS1 while mito-Rosella is the fusion of a pH-sensitive GFP (pHluorin) and a pH-stable RFP (DsRed.T3). Using either construct cytosolic mitochondria will appear yellow. Upon delivery to the lysosome the pH-sensitive GFP is quenched, yielding red only organelles. Mito-Keima is a pH-stable coral-derived fluorescent protein that was targeted to the mitochondrial matrix via fusion with COX8. The Keima protein responds to changes in pH by shifting its colour from green (neutral) to red (acidic).

1.5 Mitochondria and human disease

The umbrella term ‘mitochondrial diseases’ is used to describe an extremely heterogeneous group of genetic disorders with the common link of mitochondrial dysfunction. Mitochondrial diseases are among the commonest type of inherited neurological disorders in adults (Gorman et al., 2015), however, symptoms can occur at any age and the pathology may be isolated to a single organ or may involve multiple organ-systems (Lightowlers et al., 2015). Mitochondrial diseases include over 100 distinct diseases (Liang et al., 2014). The main function of mitochondria is to

provide ATP for cellular processes, therefore, mitochondria related diseases predominantly affect tissues with high energy demand. The symptoms most frequently involve the brain, muscle, heart, retina, cochlea and beta cells of the pancreas and liver. Common clinical presentations in children include failure to thrive, motor regression, metabolic encephalopathy, seizures, ptosis, external ophthalmoplegia and cardiomyopathy. The most frequent clinical manifestations associated with adult mitochondrial disease include diabetes, exercise intolerance, sensorineural hearing loss, ophthalmological abnormalities, muscle weakness, central nervous system involvement and cardiac manifestations (Liang et al., 2014)

1.6 Genetics of mitochondrial disease

Excluding 13 subunits of the electron transport chain encoded by the mitochondrial genome, all other proteins required for proper functioning of mitochondria are encoded by the nucleus. Therefore, mitochondrial disease may arise from mutations in the mitochondrial DNA or the nuclear DNA. Because both genomes are involved disease inheritance can be recessive, dominant, X-linked or maternally inherited. Additionally, mitochondrial disease may arise from *de novo* genetic variants (Burrage et al., 2014; Jeppesen et al., 2014; Morten et al., 1995).

1.6.1 MtDNA mutations and mitochondrial disease

Mitochondrial DNA nucleoids are located in the matrix, which makes them prone to oxidative damage. Partially attributed to such close proximity to free radicals (Lagouge and Larsson, 2013), the mutation rate of mtDNA is approximately 10 fold that of nuclear DNA in humans (Wallace and Chalkia, 2013). Mutations in the mitochondrial genome are maternally inherited. In each nucleated cell, mtDNA is

present in multiple copies. This gives rise to a unique feature of mtDNA mutations called heteroplasmy, when WT and mutant mtDNA coexist within the same cell (Figure 1.14). Heteroplasmic mtDNA diseases are often associated with a phenotypic threshold (Stewart and Chinnery, 2015), below which the mutation is tolerated without causing any symptoms (Figure 1.14). The actual value of this threshold varies between mutations, although it is hard to assess because the levels of mutant mtDNA may differ in different tissues. For example, individuals carrying the common m.8993T>G mtDNA point mutation affecting the MT-ATP6 subunit of complex V often remain asymptomatic if their heteroplasmy level remains below 70% (Sofou et al., 2014). On the other hand, individuals with 10-30% heteroplasmy harbouring the common m.3243A>G mutation may already develop diabetes, whereas those with 50-90% heteroplasmy manifest encephalomyopathies (Picard et al., 2014). Additionally, most individuals who carry the m.11778G>A pathogenic mutation remain asymptomatic throughout their life for reasons that are currently not understood (Giordano et al., 2014). Homoplasmy occurs when all the mtDNA molecules within a cell have the same genotype. In practice, this does not exist due to the presence of SNPs and neutral mutations. However, if a disease causing mtDNA mutation is present in 100% of the mitochondrial population that is referred to as homoplasmic. Although the occurrence of some specific mutations can be extremely rare (Gorman et al., 2015), the most common mtDNA mutation (m.3243A>G) is carried in 1 in 400 individuals (Manwaring et al., 2007) and pathogenic mtDNA mutations are estimated to be present in 1:200 of the population (Chinnery et al., 2012).

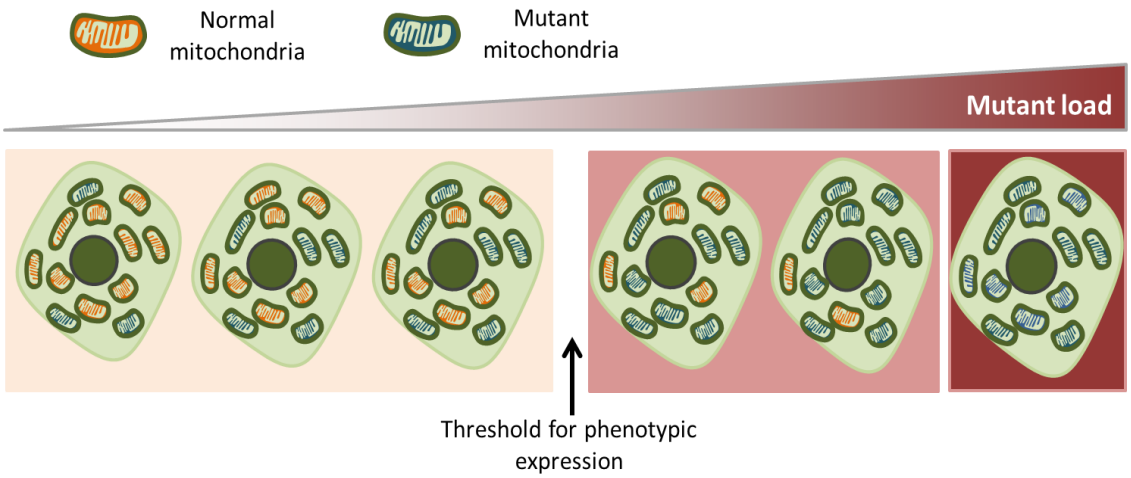

Figure 1.14 Heteroplasmy in mitochondrial DNA mutations
The co-existence of wild-type and mutant mtDNA within the same cell is referred to as heteroplasmy. Heteroplasmy levels often correlate with the severity of the disease, and the carrier remains asymptotic if the mutant load stays below a certain threshold.

The number of point mutations reported is over 600 affecting every single mtDNA encoded gene (Lott et al., 2013). Approximately 75% of the disease causing mtDNA mutations are inherited while the remaining 25% arise *de novo* (Sallevelt et al., 2017). Additionally to point mutations, single large-scale deletions ranging between 1-10kb account for mitochondrial disease in 1.2:100,000 of the population (Schaefer et al., 2008). These large-scale deletions often arise during embryonic development and tend to have a low recurrence risk (Chinnery, 2004). It is often difficult to predict the recurrence of mtDNA mutations as mtDNA segregation is not completely understood due to the genetic bottleneck that occurs during maternal transmission of mtDNA.

1.6.2 Nuclear DNA mutations and mitochondrial disease

Approximately 99% of mitochondrial proteins are encoded by the nuclear genome and pathogenic mutations have been reported in over 270 genes (Lott et al., 2013).

These most often follow Mendelian inheritance, however *de novo* (Ladds et al., 2018) and X-linked (Fernandez-Moreira et al., 2007) cases have also been reported.

1.6.3 Diagnosis of mitochondrial disease

Some of the manifestations carry a short differential diagnosis, but many are non-specific. Multi systemic involvement is a common feature of mitochondrial disease. Family history may provide important information when a diagnosis of mitochondrial disease is being considered. In most cases, the comprehensive diagnosis of mitochondrial disease requires the combination of a complex clinical investigation involving a wide variety of laboratory tests as well as histological and genetic investigations (Liang et al., 2014). The combination of clinical and functional studies is used to guide the genetic screening process, as the pathological relevance of novel mutations is not always established. Functional studies may involve the assessment of respiratory chain complex activities. A deficiency that is restricted to an individual respiratory chain complex greatly aids the selection of potential candidate genes for sequencing. Additional functional studies include histochemical and biochemical analysis of muscle biopsy samples. Mitochondrial DNA copy number is also often assessed to facilitate diagnosis of defects in mtDNA maintenance such as mitochondrial DNA depletion syndrome (MDS). Despite the tremendous advances in DNA sequencing, many patients still lack genetic diagnosis. While symptoms may be treated irrespective of the underlying genetic defect, a definitive genetic diagnosis is necessary for the testing of family members as well as for the evaluation of reproductive options.

1.7 Treatment options for mitochondrial disease

There is currently no cure for mitochondrial disease, treatment being largely supportive. Certain symptoms are managed by pharmacological intervention. For example, neuropathic pain is often treated by Duloxetine, while seizures are managed with a variety of anti-epileptic agents. Some aspects of mitochondrial disease may be managed surgically. For example, those with cardiomyopathy may benefit from a pacemaker. Additionally, surgical correction of droopy eyelids (ptosis) associated with some disorders, may considerably increase quality of life. Clinicians are frequently asked to prescribe co-factors and supplements that are unlikely to significantly benefit their patients, unless there is a specific biosynthetic defect. It is difficult to confirm improvement objectively as there are no good biomarkers and clinical scales can only confirm substantial changes.

1.8 Overall aims of this thesis

Mitochondria are traditionally considered the 'power house' of the cell. However, it is emerging that these organelles are involved in numerous cellular processes other than the production of ATP and therefore are essential for the maintenance of cellular homeostasis. Cell biological investigations into disease causing mutations tend to focus solely on isolated mitochondrial morphological and biochemical abnormalities when determining contributing factors to the pathology. Mitochondria specific autophagy, or mitophagy is the only currently known cellular mechanism that recycles redundant or damaged mitochondria and mitochondrial DNA. Mitophagy or rather the dysregulation of it is rarely considered as a contributing factor or as a potential therapeutic target in mitochondrial disease. An earlier study on patients with dominant optic atrophy, result of mutation(s) in the nuclear DNA encoded OPA1 gene, established that mitophagy was increased in these patients that appeared to be excessive and poorly selective (Liao et al., 2017). Similarly, increased mitochondrial turnover was reported in two unrelated individuals harbouring the common heteroplasmic m.3234A>G mutation (Diot et al., 2015) as well as in a cohort of POLG patients (unpublished) that might be a contributing factor to the severe mtDNA depletion associated with POLG disorders.

Therefore, the overall aims of this thesis are:

I. To investigate mitophagy in fibroblasts derived from patients with confirmed mitochondrial disease either due to nDNA or mtDNA mutations using high-content imaging and further characterise selected patient cells using a combination of cell biological and biochemical approaches.

II. To investigate whether mtDNA depletions are associated with increased and potentially excessive mitophagy, and whether that can be rescued by nucleotide supplementation in POLG mutant cell.

III. Finally, given that mtDNA mutant load may fall if mitophagy is activated, to identify drug modulators of mitophagy that can be implemented as potential novel therapies for mitochondrial disease.

Chapter 2. Materials and methods

2.1 Materials

2.1.1 Consumables

96-well plastic plates	Nunc/Thermo Fisher
96-well optical bottom plates	PerkinElmer
6-well plastic plates	Thermo Fisher
Disposable pipettes (2ml, 5ml, 10ml, 25ml)	Sigma-Aldrich/Merck
Disposable tissue culture flasks ($25cm^2$, $75cm^2$, $175cm^2$)	Sigma-Aldrich/Merck
Cryotubes	Nunc/Thermo Fisher
Falcon tubes (15ml, 50ml)	Sarsted

2.1.2 Chemicals and reagents

2.1.2.1 Tissue culture

DMEM high-glucose	Sigma-Aldrich/Merck
DMEM no glucose	Thermo Fisher Scientific
EZ-PCR Mycoplasma Test Kit	Geneflow
Fetal Bovine Serum	Sigma-Aldrich/Merck
Galactose	Sigma-Aldrich/Merck
Glucose	Sigma-Aldrich/Merck
L-glutamine	Sigma-Aldrich/Merck
Penicillin-Streptomycin	Sigma-Aldrich/Merck
Phosphate buffered saline (500ml)	Sigma-Aldrich/Merck
Sodium pyruvate	Sigma-Aldrich/Merck
Trypsin	Sigma-Aldrich/Merck

Uridine	Sigma-Aldrich/Merck

2.1.2.2 Antibodies and live cell stains

LC3 mouse monoclonal (rabbit)	MB Laboratories
TOM20 mouse monoclonal (mouse)	Santa Cruz Biotechnology
DRP1 (rabbit)	Cell Signalling Technologies
Phosphor-DRP1 S616 (rabbit)	Cell Signalling Technologies
Phospho-DRP1 S637 (rabbit)	Cell Signalling Technologies
Mitofusin 2 (rabbit)	Cell Signalling Technologies
Opa1 (rabbit)	Abcam
Total OXPHOS Human Antibody Cocktail (mouse)	Abcam
beta actin (rabbit)	Cell Signalling Technologies
Alexa-Fluor 488 goat anti-rabbit	Life technologies
Alexa-Fluor 546 goat anti-mouse	Life technologies
Goat anti-mouse horse radish peroxidase	Dako
Goat anti-rabbit horse radish peroxidase	Dako
Tetramethylrhodamine, Methyl Ester, Perchlorate (TMRM)	Sigma-Aldrich/Merck
Quant-iT™ PicoGreen™ dsDNA Reagent (PicoGreen)	Thermo Fisher Scientific
Lyso ID Red	Enzolifesciences
4’,6-diamidino-2-phenylindole (DAPI)	Sigma-Aldrich/Merck
Hoechst	Sigma-Aldrich/Merck

2.1.2.3 Staining reagents

eBioscience™ Permeabilisation buffer 10X	Thermo Fisher scientific
Pierce™ Methanol Free Formaldehyde 16%	Thermo Fisher Scientific
Opti-MEM reduced serum medium	Thermo Fisher Scientific

2.1.2.4 Drugs and small molecules

5-Aminoimidazole-4-carboxamide ribonucleotide (AICAR)	Sigma-Aldrich/Merck
Antimycin A	Sigma-Aldrich/Merck
Carbonyl cyanide-4-(trifluoromethoxy)phenylhydrazone (FCCP)	Sigma-Aldrich/Merck
2-deoxy glucose (2DG)	Sigma-Aldrich/Merck
Doxorubicin	Sigma-Aldrich/Merck
Duloxetine	Sigma-Aldrich/Merck
E64d	Sigma-Aldrich/Merck
Librium (Chlorodiazepoxide)	Sigma-Aldrich/Merck
Metformin	Sigma-Aldrich/Merck
Pepstatin A	Sigma-Aldrich/Merck
Rotenone	Sigma-Aldrich/Merck
Cycloheximide	Sigma-Aldrich/Merck

2.1.2.5 Western blot reagents

4X Bolt® LDS Sample Buffer	Thermo Fisher Scientific
10X Bolt® Sample Reducing Agent	Thermo Fisher Scientific
20X Bolt® MES SDS Running Buffer	Thermo Fisher Scientific
Bolt™ 4-12% Bis-Tris Plus Gels, 15-well	Thermo Fisher Scientific

Ethanol	Sigma-Aldrich/Merck
Methanol	Sigma-Aldrich/Merck
Phosphate buffered saline (tablet)	Sigma-Aldrich/Merck
Nitrocellulose membrane	Amersham™ , GE Healthcare Life Sciences
Blotting paper	Amersham™ , GE Healthcare Life Sciences
WESTAR® Supernova HRP Detection Substrate	Geneflow

2.1.2.6 DNA extraction, precipitation and purification reagents

Chloroform	Sgma-Aldrich/Merck
Ethanol	Sigma-Aldrich/Merck
illustra Nucleon BACC2 Genomic DNA Extraction Kit	GE Healthcare Life Sciences
RNase	Thermo Fisher Scientific
TE Buffer	Ambion

2.1.2.7 Polymerase chain reaction and sequencing reagents

Apa I	Sigma-Aldrich/Merck
KAPA2G Fast HotStart ReadyMix PCR Kit	Kapa Biosystems
OneTaq® 2X Master Mix with Standard Buffer	New England Biolabs
Taq DNA polymerase	Roche
Taq DNA Polymerase	Thermo Fisher Scientific

2.1.2.8 Gel electrophoresis reagents

Agarose	Sigma-Aldrich/Merck

DNA ladder	New England Biolabs
Ethidium bromide	Sigma-Aldrich/Merck
Gel loading dye	New England Biolabs
Tris base, acetic acid and EDTA buffer (TEA)	Thermo Fisher Scientific

2.1.2.9 Primer and probe sequences

All custom primers were ordered from Integrated DNA technologies unless otherwise stated

MELAS1b (L)	5' CAA ATT CCT CCC TGT ACG AA 3'
MELAS2APAL (H)	5' AGG GGC CTA CAA CGT TGG GCC CTT TGC GTA 3'
MELAS1bHEX	5' HEX-CAA ATT CCT CCC TGT ACG AA 3'

2.1.3 Solutions

Mili-Q® water was used to prepare the solutions listed below.

Protein lysis buffer
50mM Tris-HCl (pH7.4), 150mM NaCl, 1mM EDTA, 1% Triton, 0.1%SDS, Halt™ Protease and Phosphatase Inhibitor Cocktail (ThermoFisher Scientific 78444)

10X Western Blot transfer buffer
144g glycine, 90.2g Tris and 1L water

1X Western Blot transfer buffer
100ml 10X transfer buffer, 200ml ethanol, 700ml water

10X Permeabilisation buffer
Pre-ordered from eBiosciences

1X Permeabilisation buffer
5mL of 10X permeabilisation buffer and 45ml water

10X Phosphate buffered saline (PBS)
50xPBS tablets in 1L water

1X Phosphate buffered saline
100ml 10X PBS and 900ml water to obtain a 137 mM NaCl, 2.7 mM KCl and 10 mM phosphate buffer solution

4% paraformaldehyde (PFA)
10ml 16% formaldehyde and 30ml PBS

PBS-Tween
50ml 10X PBS, 1ml Tween, 449ml water

PBS-Tween with milk (Western Blot blocking buffer)
50ml PBS-Tween, 2.5g skimmed milk powder

2.2 Methods

2.2.1 General tissue culture

Skin biopsies were performed following informed consent. Human fibroblasts were established from skin explants following standard procedure. Cells were maintained in Dulbecco's modified Eagle's medium (DMEM high-glucose) supplemented with 10% FCS, 100U/ml Penicillin and 100µg/ml streptomycin, 2mM L-glutamine and 50µg/ml uridine at 37°C in a humidified incubator with 5% CO_2. Media was changed every 3-4 days. Cells were routinely cultured in T25/T75 tissue culture flasks and split when reached ~80-90% confluency. All procedures were performed using aseptic techniques, sterile equipment and reagents in a Class II biological cabinet. Periodically, cells were tested for possible mycoplasma contamination using the EZ-PCR™ Mycoplasma Test Kit (Geneflow) following manufacturer's instructions.

2.2.2 Cell harvesting and counting for experimental set up

Medium, PBS and trypsin were pre-warmed at 37°C prior to use. Spent media was aspirated using a vacuum line; cells were washed with PBS. Trypsin (1.5 ml/T75 flask, 0.5 ml/T25 flask) was added to cover the surface of the flask, which was then incubated in a 37°C incubator for 1-2 minutes to dislodge the cells. Trypsin was

deactivated using at least 2X volume complete growth media. Detached cells were transferred to 15ml falcon tubes and pelleted by centrifugation at 1500rpm for 3 minutes. The supernatant was removed and the cells were resuspended in growth medium for counting (various volumes depending on cell density). Cell numbers were established using a haemocytometer by loading 20µL cell aliquot distributed between the two counting areas. Cells were counted in 8 squares (1mm^2 each) and the number of cells in the original aliquot was established using the following equation: (Total number of cells counted) / 8 = the number of cells in the original aliquot (per ml) x 10

2.2.3 High-content fluorescent microscopy

2.2.3.1 Set up of fibroblasts for mitophagy and mtDNA/ mitochondrial membrane potential analysis

Fibroblasts were harvested and counted as described in section 2.2.2. Cells were plated in optical bottom 96-well plates at a density of 3000 cells per well in triplicates for each condition and left to attach overnight. Media was changed the next day to either high-glucose (25mM), high-glucose with lysosomal inhibitors E64d and Pepstatin A (EP, 10µg/ml each), low glucose (3mM) media, low glucose media with EP, galactose media (0mM glucose, 10mM galactose) or galactose media with EP. Low glucose and galactose media was prepared using DMEM no glucose supplemented with 10% FCS, 100U/ml Penicillin and 100µg/ml streptomycin, 1mM sodium pyruvate, 50µg/ml uridine and either 3mM glucose or 10mM galactose respectively. A sample layout for a plate is presented in Figure 2.1. Cells were treated for 24 hours followed by either the fixation or live imaging of the plate. E64d and

Pepstatin A were stored at -20°C as 1000X stock solutions diluted in ethanol and methanol respectively.

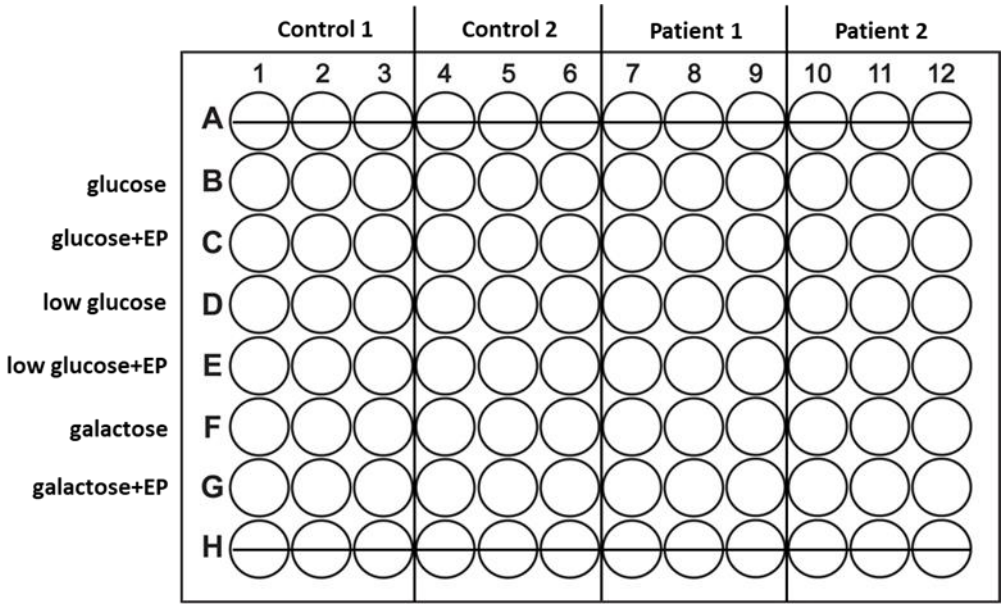

Figure 2.1 Representative plate layout used for mitophagy and mtDNA/TMRM analyses

2.2.3.2 Cell fixation

At the end of treatment, the plates were washed 1X with 100µl PBS. PBS was gently tipped out and 50µl 4% PFA was added per well. Cells were incubated at room temperature in the dark for 15 minutes, rocking. PFA was removed and the plate was washed 2X with 100µl PBS per well. On the last wash PBS was left in the wells and the plate was stored at 4°C in the dark until immunostaining.

2.2.3.3 Immunostaining of fixed cells for mitophagy analysis

PBS was removed from each well and cells were washed with 100µl permeabilisation buffer. Fibroblasts were incubated with primary antibodies monoclonal mouse anti-TOM20 antibody (1:200) and polyclonal rabbit anti-LC3 antibody (1:500) diluted in permeabilisation buffer (50µl per well) to label mitochondria and autophagosomes

respectively. Incubation was at room temperature in the dark for 2 hours. Following the removal of the primary antibody mix cells were briefly washed with 1X permeabilisation buffer and incubated with secondary antibodies Alexa Fluor 488 goat anti-rabbit and Alexa Fluor 546 goat anti-mouse diluted in permeabilisation buffer (50µl per well) for 40 minutes in the dark. Plates were washed with 100µl PBS and nuclei were labelled using DAPI. DAPI was diluted in PBS (1:1000) and 50µl per well was added to each plate for 5 minutes. Plates were incubated at room temperature in the dark. Cells were subsequently washed with 100µl PBS 2X and plates were finally imaged in a final volume of 150µl PBS.

2.2.3.4 Imaging of fixed fibroblasts for mitophagy analysis

Acquisition protocol: nuclei were imaged in the blue channel; cell body and autophagososomes were imaged in the green channel, and mitochondria in the red channel. 20X images were acquired in 12 fields for each well. The position of each field was chosen randomly, however they remained constant across the same plate. Representative images of control fibroblasts are shown in Figure 2.2.

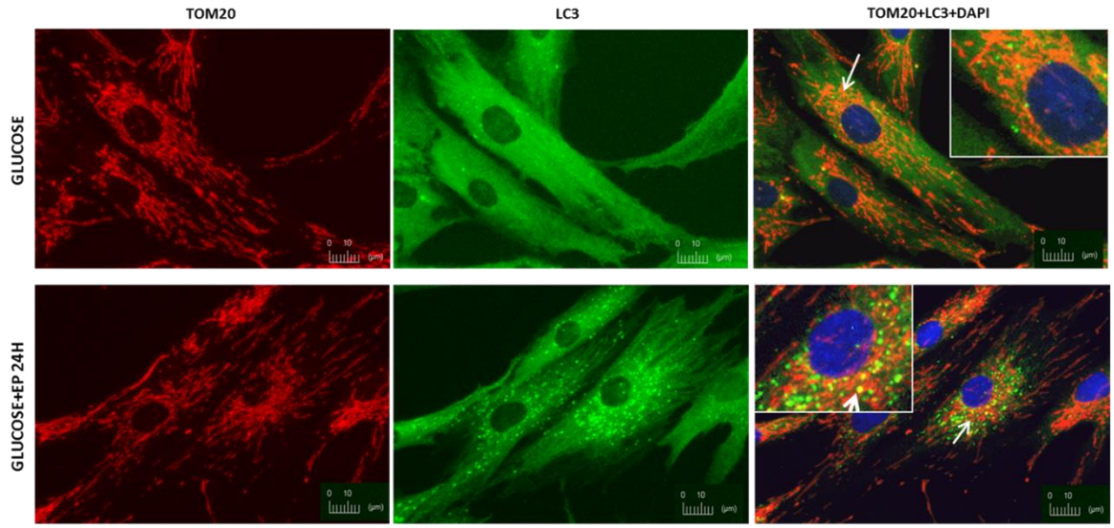

Figure 2.2 Representative images of DAPI,TOM20 and LC3 labelled control fibroblast
Nuclei of control fibroblasts are labelled with DAPI (blue), mitochondria with TOM20 (red) and autophagosomes/cytoplasm with LC3 (green). Cells were cultured in glucose (25mM) media with or without lysosomal inhibitors E64d and Pepstatin A (EP). Co-localising mitochondria and autophagosomes following EP treatment are highlighted by the white arrow. Scale bar 10µm.

2.2.3.5 Live cell staining of fibroblasts for mtDNA and mitochondrial membrane potential analysis

The Quant-iT™ PicoGreen™ dsDNA Reagent was received as a stock solution in DMSO and was stored at -20°C. The staining procedure was adopted from (Ashley et al., 2005), who validated it for the detection of mtDNA content within live cells. TMRM was received as a powder and was diluted to a 50µM stock dilution in DMSO, stored at -20 °C. For live cell staining, PicoGreen and TMRM stocks were diluted in cell culture media 1:333 (3µl/ml) and 1:2000 respectively. 100µl of staining solution was added to each well of a 96-well plate. Fibroblasts were incubated in the staining solution for 30 mins at 37°C in a humidified incubator with 5% CO_2. The staining solution was removed and replaced with 150µl pre-warmed reduced serum Opti-MEM media for imaging.

2.2.3.6 Imaging of fibroblasts for mtDNA and mitochondrial membrane potential analysis

Acquisition protocol: PicoGreen stained nuclei and mitochondrial DNA nucleoids were imaged in the green channel, TMRM labelled mitochondria were imaged in the red channel. 20X images were acquired in 9 fields for each well. As previously, the position of each field was chosen randomly, however they remained constant across the same plate. Representative images of control fibroblasts are shown in Figure 2.3.

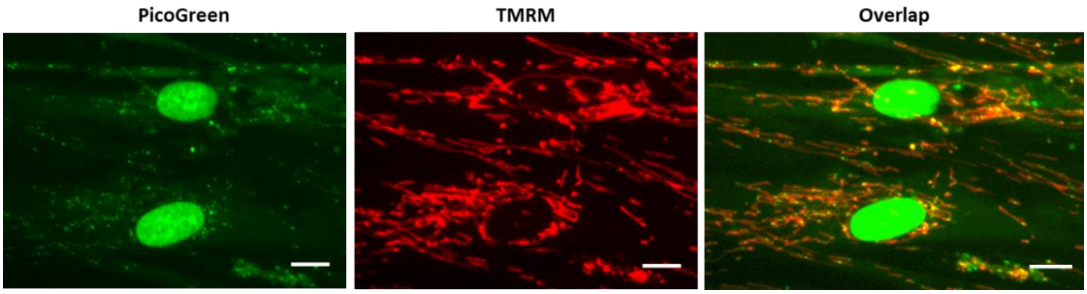

Figure 2.3 Representative images of PicoGreen and TMRM labelled control fibroblasts
Nuclei and mtDNA nucleoids of control fibroblasts are labelled with PicoGreen, mitochondria are labelled with the membrane potential sentivive dye TMRM (red). Scale bar 10µm.

2.2.3.7 Analysis of image stacks

Image stacks were analysed by an in-house written protocol using the IN Cell Developer software (GE Healthcare) (Diot et al., 2015). The mitophagy protocol was previously validated using a range of mitophagy inducers and lysosomal inhibitors (Diot et al., 2015). The workflow of the image analysis process outlined in Figure 2.4. A series of target sets were created by the segmentation of cellular components. These target sets were then linked together in order to create a set of cells with all the labelled organelles in which various measurements were carried out on a cell-by-cell bases.

The definition of target sets and the subsequent linking process (Figure 2.4):

Nuclei were segmented in the blue channel (DAPI) and the cell body was segmented in the green channel (cytosolic LC3 signal). The 'cell' was defined by a 'one to one' link between the nucleus and the corresponding cell body. Cells around the edges of the field were excluded from the analysis. → Cell

Autophagosomes were distinguished from the cell body in the green channel based on their size and intensity. A 'one to many' link was created between the previously defined cell and the autophagosomes within. The overlap criteria between the two target sets was set to 90%. → Cell+autophagosomes

TOM20 labelled mitochondria was segmented into two separate target sets: short → Cell+autophagosome+short mito; and long mitochondria → Cell+autophagosome+short mito+long mito. The 'Cell+autophagosome+short mito+long mito' target set defines a cell with a single nucleus, autophagosomes and long/short mitochondria within. Mitochondrial length and area measurements were derived from this target set.

Finally, overlapping mitochondria and autophagosomes were segmented (Overlap) and linked to the previous target set to define a cell with a single nucleus, autophagosomes, long/short mitochondria and autophagosomes overlapping with mitochondria. Autophagy and mitophagy measurements were derived from this target set. Therefore, in this thesis mitophagy is defined as co-localising mitochondria and autophagosmes. During the analysis process mitophagy was quantified in two ways:

(1) by counting the co-localisation events between mitochondria and autophagososmes (Mitophagy events per cell) or

(2) by measuring the area of mitophagy and expressing that as the percentage of total mitochondrial area (mitophagy as % of total mitochondrial area).

In this thesis I decided to present mitophagy measured as the percentage of mitochondrial area.

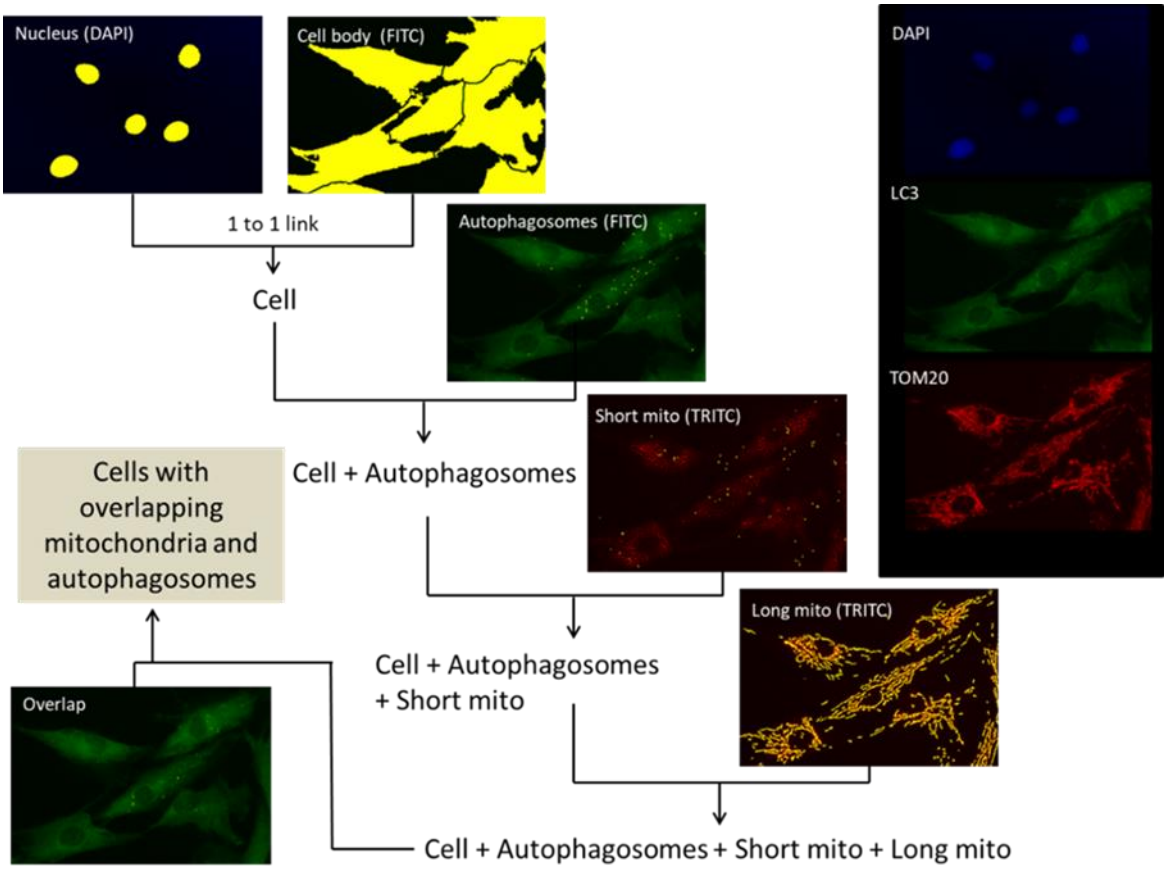

Figure 2.4 Workflow of the image analyses protocol – mitophagy assay
The definition of target sets and the subsequent linking process used for the analysis of the mitophagy assay.

The analyses protocol of PicoGreen/TMRM image stacks was built following the same principles. The cell body, the nucleus and mtDNA were segmented in the green channel (PicoGreen). Mitochondria were segmented in the red channel (TMRM). Mitochondrial DNA was distinguished from the nucleus by the application of a size criterion during the analysis procedure.

2.2.3.8 Statistical analysis of the IN Cell output (Chapters 3, 4 and 5)

The n number for each experiment is defined as the number of biological replicates, in other words, the number of plates ran. From the analyses of a single plate the outputs are provided on a cell by cell basis. For each experiment where outputs were available these cell by cell measurements were merged into a single dataset. Statistical analysis was carried out using Graphpad Prism (version 7). The merged data was subjected to a ROUT outliers test (Q=1%). All the outliers identified were excluded from the data set. The data set was then subjected to a Shapiro-Wilk normality test. The dataset that followed Gaussian distribution was analysed using One-way ANOVA with multiple comparison. The datasets that did not follow normal distribution (majority) were analysed using the Kruskall-Wallis non-parametric test with multiple comparison.

2.2.3.9 Limitations of the high-throughput imaging method

Both the mitophagy and the mtDNA/TMRM method produce results with large plate to plate variations. Although the differences between the same control and patient cells remain constant between runs the numbers vary. In order to identify the source of variation I have compared two plates that were set up, treated, fixed and stained at the same and imaged subsequently. The results obtained from these two plates are almost identical (Figure 2.5). While this experiment does not clarify whether the variation between runs results from differences in cell biology or staining quality it is generally reassuring.

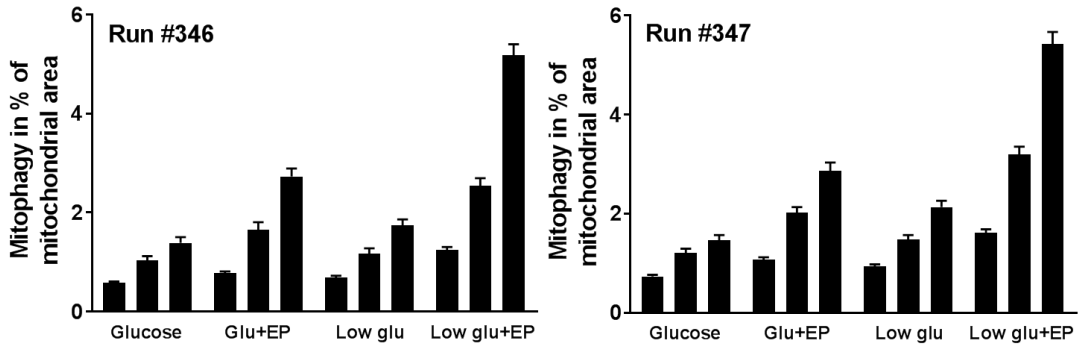

Figure 2.5 Comparison of two plates set up, fixed and stained at the same time
The results shown above are from two different plates with exactly the same cells that were set, treated, fixed and stained in parallel.

2.2.4 Western blot analysis

2.2.4.1 Preparation of samples

Frozen cell pellets were dissolved in protein lysis buffer (200-300µl) at room temperature, rocking for 30 minutes. For each sample 13µl of the lysate was mixed with 5µl of 4X LDS Sample Buffer and 2µl of 10X Sample Reducing Agent in a 1.5ml Eppendorf tube. The mixture was incubated in a heating block at 90°C for 5 minutes, except for samples used for the detection of ETC complexes using the OXPHOS antibody cocktail (Abcam). These samples were not heated above 70°C. The tubes were spun briefly.

2.2.4.2 Gel electrophoresis

For electrophoresis a Mini Gel Tank (Bolt - Thermo Fisher) was used that is able to house two 15-well Bolt Bis-Tris Plus gels at a time. 20µl of the prepared sample described above was loaded into one well of a Bolt Bis-Tris Plus gels. Samples were run at 100-120V in 1X Bolt MES Running Buffer (400ml/gel) until the samples reached the bottom of the gel (1h-1.5h).

2.2.4.3 Protein transfer

For protein transfer a Bio-Rad transfer system was used. Prior to protein transfer the nitrocellulose membrane was briefly soaked in methanol followed by 1X transfer buffer for 10 minutes. Two sponges and 6 pieces of blotting paper (cut to the appropriate size) per gel were also pre-soaked in 1X transfer buffer. Upon removal from the electrophoresis tank gels were transferred to 1X transfer buffer for at least 5 minutes. The transfer sandwich consisted of a sponge, 3 pieces of blotting paper, nitrocellulose membrane, gel, 3 pieces of blotting paper and finally another sponge. Proteins were transferred at 40V for 2 hours. Successful protein transfer was confirmed by Ponceau S.

2.2.4.4 Membrane immunoblotting

The membranes were blocked for at least 30 minutes in PBS-T with 5% milk. Membranes were incubated over night at 4°C with the specified primary antibodies diluted in blocking buffer. The membranes were washed 3X with 10ml PBS-T for 10 minutes per washes. Secondary HRP-conjugated antibodies were also diluted in blocking buffer. Membranes were incubated for 1 hour at room temperature followed by 3X 5 minutes washes with PBS-T.

2.2.4.5 Signal detection

Following the final washes the membranes were incubated with WESTAR ® Supernova HRP detection substrate (Geneflow) for 1 minute. Chemiluminescent signal was detected using the G:BOX system (Geneflow). A manually set up protocol was used to image all membranes (chemi series 3X with 15s, 30s and 1min 30s exposure times, 3x3 binning).

2.2.5 Oxygen consumption measurements using the Seahorse XF96 platform

Oxygen consumption rate (OCR) in adherent fibroblasts was measured using the Mito Stress Test protocol with an XF96 Extracellular Flux Analyzer (Seahorse Bioscience, Billerica, MA, USA). All materials and access to the instrument were provided by Dr Brent Ryan (DPAG, University of Oxford). Cell plating density and FCCP concentration were previously optimized using a trial run on Control 1 fibroblasts. Control and patient fibroblasts were seeded into XF96 Agilent Seahorse XF Cell Culture Microplates at a density of 20000 cells per well. Fibroblasts were left to attach overnight and media was changed the next day, 24 hours prior to the assay. The, the assays were initiated following the manufacturer's instructions by replacing the growth medium in each well with 1175µl of Seahorse XF assay media supplemented with 10mM glucose, 1Mm pyruvate, 2mM L-glutamine adjusted to pH 7.4 and pre-warmed to 37 °C. Cells were incubated at 37 °C for 60 min to allow temperature and pH equilibration. Oxygen consumption rate was measures every 18 minutes and 3 times were each condition. Following 3 baseline OCR measurements Oligomycin was injected (1µM final concentration). This was followed by FCCP injection (1µM final concentration) in order to uncouple oxygen consumption from ATP production. Finally, rotenone and antimycin A were injected at the same time (1µM final concentration) in order to inhibit complexes I and III, respectively. The addition of these drugs were used to calculate basal respiration (baseline OCR 3 – rotenone/Antimycin A OCR); maximal respiration (FCCP OCR - rotenone/Antimycin A OCR); spare respiratory capacity (maximal OCR – baseline OCR)and ATP-linked respiration (basal respiration – oligomycin OCR) (Figure 2.6).

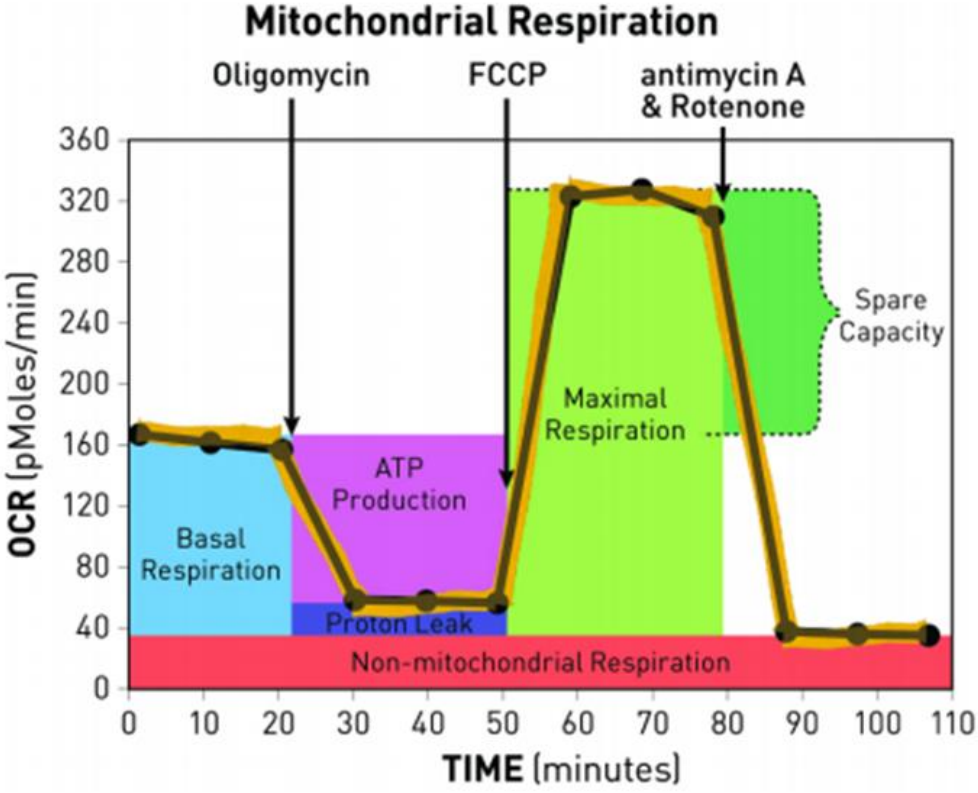

Figure 2.6 Key parameters of mitochondrial respiration measured during the Seahorse Cell Mito Stress
Image from:
https://www.agilent.com/cs/library/usermanuals/public/XF_Cell_Mito_Stress_Test_Kit_User_Guide.pdf

The OCR rates measured were normalized to the protein content in each well. At the end of the assay media was removed from each well and the cells were washed with PBS. The plate was stored at -20°C until protein content was measured. 200µl of protein lysis buffer was added to each well and the plate was incubated for at least 30 minutes at room temperature, rocking. Protein content in each wall was measured using a Pierce™ BCA Protein Assay Kit following manufacturer's instructions.

2.2.6 Cell growth experiments to determine dependency on glucose

Fibroblasts were seeded into 6 well plates at a density of 15,000 cells per well. Cells were left to attach overnight. The next day (day 0) the media was changed to either baseline (25mM glucose) or galactose (0mM glucose) and cells were cultured for 9 days. Media was changed on day 3 and day 6. On day 9 the cells were tripsinized and counted manually as described in section 2.2.2. The number of cells remaining in galactose media was expressed as the percentage of the same cells counted at baseline. The experiment was designed based on a protocol provided by Dr Heather Mortiboys (Sheffield).

2.2.7 Statistical analysis

Statistical analysis was performed using Graphpad Prism (version 7). The different result groups were compared using One-way ANOVA. The n numbers indicated below each graph represent biological replicates.

Chapter 3. Characterization of fibroblasts derived from patients with mitochondrial disease resulting from mitochondrial DNA mutations

3.1 Introduction

The first disease causing point mutation in mtDNA was identified in 1988 (Wallace et al., 1988). Since then, the recognition of specific mitochondrial as well as nuclear genetic causes of mitochondrial disease has rapidly escalated. The cumulative prevalence of mitochondrial diseases is estimated to be 1 in 5000, although many milder cases are likely to go undiagnosed. Furthermore, the number of asymptomatic carriers is predicted to be 1 in 250 per live births (Falk and Sondheimer, 2010). Mitochondrial DNA mutations are either transmitted from mother to offspring or may arise *de novo*. Either way, they affect essential protein subunits of the electron transport chain enzyme complexes that carry out mitochondrial oxidative phosphorylation. Although the human mitochondrial genome has only 16569 base pairs, more than 600 point mutations spread across the 37 genes encoded by the mtDNA have been reported (Lott et al., 2013), many of these are likely benign. Confirmed pathogenic mutations account for approximately one third of all paediatric and two thirds of adult mitochondrial disease cases diagnosed (Falk and Sondheimer, 2010). The most common defined syndromes associated with mtDNA mutations are listed in Table 3.1. The focus of this chapter will be fibroblasts derived from patients with single mtDNA point mutations in genes encoding either complex I or complex V subunits. For the purposes of the present thesis, I refer to these as deficiencies of complexes l and V. In practise, diagnosis of these clinical syndromes is based on mtDNA analysis, neither complex l nor complex V measurements being either required or easily carried out.

Table 3.1 Most common disorders associated with mtDNA mutations

Syndrome	Pathological description
Mitochondrial myopathy, encephalopathy, lactic acidosis& stroke-like episodes (MELAS)	Progressive multisystem disorder mainly affecting muscles and the nervous system. Age of onset varies, ranging from age 4 to age 40, but most patients show symptoms before the age of 20. The disease is progressive and fatal, although cause of death varies from hyperglycaemia/ketoacidosis to cardiac arrest, and in many cases remains unknown. The MELAS phenotype is associated with the m.3243G>A mutation which accounted for almost 30% of the patients diagnosed (Barends et al., 2016).
Leber's Hereditary Optic Neuropathy (LHON)	LHON is an inherited form of visual loss characterised by bilateral, painless, subacute visual failure due to the atrophy of the optic nerve. The onset of the disease in most cases begins in young adulthood, rarely in early childhood or late adulthood. Over 95% of the documented LHON cases are the result of three mtDNA point mutations, 11778G>A, 3460G>A, and 14484T>C.
Leigh syndrome (LS)	Early onset, severe mitochondrial disease commonly presents with progressive loss of mental and movement abilities. A rapidly progressing condition affects approximately 1 in 30,000 to 1 in 40,000. LS can develop due to mutations in either mitochondrial DNA or nuclear DNA, the latter being the more common cause.
Neuropathy, ataxia, and retinitis pigmentosa (NARP)	Childhood or early adulthood onset disease that mainly affects the nervous system. Characterized by sensory and/or motor neuropathy manifesting with weakness, problems with balance and loss of vision. It is a rare disorder estimated to have a prevalence of about 1 in 100,000 live births and it is caused by mutations in the *MT-ATP6* gene of the mitochondrial genome.
Myoclonic epilepsy with ragged red fibres (MERRF)	A multisystem disorder that particularly affects muscles and the nervous system. Features vary widely among affected individuals. The features of MERRF vary widely from individual to individual. Mutations in the mitochondrial *MT-TK* gene account for over 80% of the cases diagnosed.
Chronic progressive external ophthalmoplegia (CPEO)	CPEO is a condition characterized by the weakness of the eye muscles. The initial presentation is often droopy eyelids. CPEO worsens over time with weakness and fatigue involving other muscles. It as an adult onset disease commonly presenting in early adulthood. CPEO can be caused by mutations in many different genes (eg. POLG) as well as by large-scale mtDNA deletions.
Maternally inherited diabetes and deafness (MIDD)	MIDD typically develops in mid-adulthood, although age of onset may vary. Diabetes that is often accompanied by hearing loss.

3.1.1 An overview of complex I structure and deficiency

Complex I (NADH:ubiquinone oxidoreductase) is the first enzyme complex of the ETC and the largest OXPHOS complex with a total mass of almost 1000 kDa. It consists of 37 nDNA encoded subunits and the additional 7 integral membrane subunits are encoded by the mtDNA (Carroll et al., 2006; Zickermann et al., 2015). The enzyme is L-shaped (Figure 3.1) with a hydrophilic 'upper' arm concerned with the oxidation of NADH, FeS clusters for electron transfer and a ubiquinone binding site. The 'lower' hydrophobic arm consists of antiporter like domains that 'pump' protons into the inter-membrane space (Figure 3.1) (Vinothkumar et al., 2014). The 'core' enzyme that is sufficient for catalysis, highly conserved from bacteria to humans, is made up of only 14 subunits (Supplementary Table 1), that provide all the structurally critical elements (Yip et al., 2011). The rest of the so-called 'supernumerary' subunits wrap around the core as if forming a protective layer, are required for assembly and stability. Additional functions for some of these auxiliary subunits are currently being described that may go beyond electron transfer and proton translocation. For example, PINK1 dependent phosphorylation of NDUFA10, a supernumerary subunit that sits on top of ND2 (Figure 3.1), was shown to influence complex I activity (Morais et al., 2014), placing the link between PINK1 and Parkinson's disease into a new perspective.

Complex I is the main site of mitochondrial ROS production (Murphy, 2009) that can cause mtDNA damage as well as the oxidation of proteins that has been implicated in Parkinson's disease (Dias et al., 2013) as well as ageing (Stefanatos and Sanz, 2018). While complex I dysfunction has been associated with many human disorders, including Leber's Hereditary Optic Neuropathy (LHON) and Leigh syndrome (Table

3.1) (Fassone and Rahman, 2012). LHON is a result of mtDNA point mutations with an estimated prevalence of 1 in 25,000 in the British population (Yu-Wai-Man et al., 2002), making it the most common inherited neurological disorder. It is a form of maternally inherited blindness that typically presents with bilateral, painless, subacute visual failure due to the atrophy of the optic nerve (Chinnery and Hudson, 2013). Over 95% of the documented LHON cases are the result of three mtDNA point mutations, 11778G>A (ND4), 3460G>A (ND1), and 14484T>C (ND6) (Mackey et al., 1996). These primary mutations are generally found as homoplasmic.

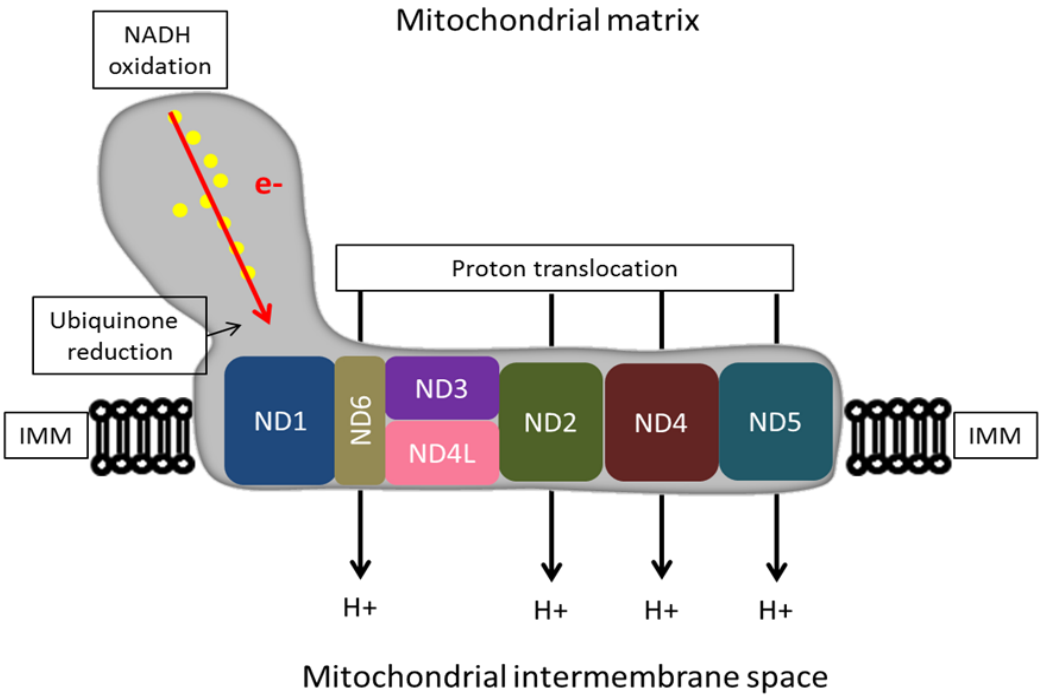

Figure 3.1 Schematic representation of the structure and function of Complex I
The mitochondrial ETC Complex I consists of 37 nDNA encoded subunits and 7 integral membrane subunits encoded by the mtDNA that are indicated here. These are all considered ‘core’ subunits. The hydrophilic 'upper' arm that stretches into the matrix is responsible for the oxidation of NADH and the transfer of electrons via the FeS clusters (yellow dots) to the final ubiquinone acceptor. The ‘lower’ hydrophobic arm consists of antiporter like domains that ‘pump’ protons into the inter-membrane space.

3.1.2 An overview of complex V structure and deficiency

Electron transport chain complexes I-IV transport electrons from donors (NADH and FADH) via redox, coupled with the transfer of protons (H^+) across the inner membrane to the intermembrane space. Complex V, otherwise referred to as ATP synthase, uses the electrochemical gradient created by H^+ translocation for the synthesis of ATP from ADP and inorganic phosphate. The mammalian ATP synthase consists of 17 subunits (Figure 3.2). Two of these subunits, A6L (or 8) and *a* are encoded by the *MT-ATP8* and *MT-ATP6* genes respectively in the mitochondrial genome. The enzyme complex is made up of the F_1 catalytic domain that protrudes into the matrix, and the membrane embedded F_0 domain. The two domains are connected by a central and a peripheral stalk or stator (Zhou et al., 2015). The mitochondrial encoded subunit *a* and a ring of 10-15 *c* subunits constitute the membrane embedded proton channel, while the A6L subunit provides the physical connection between the proton channel and the stator (Jonckheere et al., 2012).
A plethora of diseases and defined syndromes are associated with mutations in both *MT-ATP8* and *MT-ATP6* including maternally inherited Leigh syndrome and NARP (Table 3.1) (Dautant et al., 2018). The most common and hence the best studied mtDNA point mutations affect the same highly conserved amino acid residue (8993T>G and 8993T>C) in the *a* subunit. Patients with heteroplasmy levels ranging from 70% to 90% typically develop NARP (Table 3.1), while a mutant load above 90% often manifests in MILS (Table 3.1) (Makela-Bengs et al., 1995). The 8993T>G mutation severely compromises mitochondrial ATP production without affecting complex V assembly and therefore often associated with early clinical presentation of more serious illness (Cortes-Hernandez et al., 2007). The 8993T>C mutation usually

presents with a milder phenotype (Vilarinho et al., 2001). An intriguing feature of the 8993 mtDNA point mutations is their skewed segregation in oocytes. While mtDNA analysis of oocytes from women with most mtDNA point mutations shows a distribution of heteroplasmic load scattered around the woman's own level of mutant, the 8993 point mutations frequently segregate either close to 0% or over 90%, indicating a bottleneck, or small number of segregating units in mtDNA inheritance (Blok et al., 1997; Sallevelt et al., 2013). Recent investigators have suggested a positive selection for m.8993T>G, but this does not explain both a high and a low level of mutant mtDNA (Otten et al., 2018).

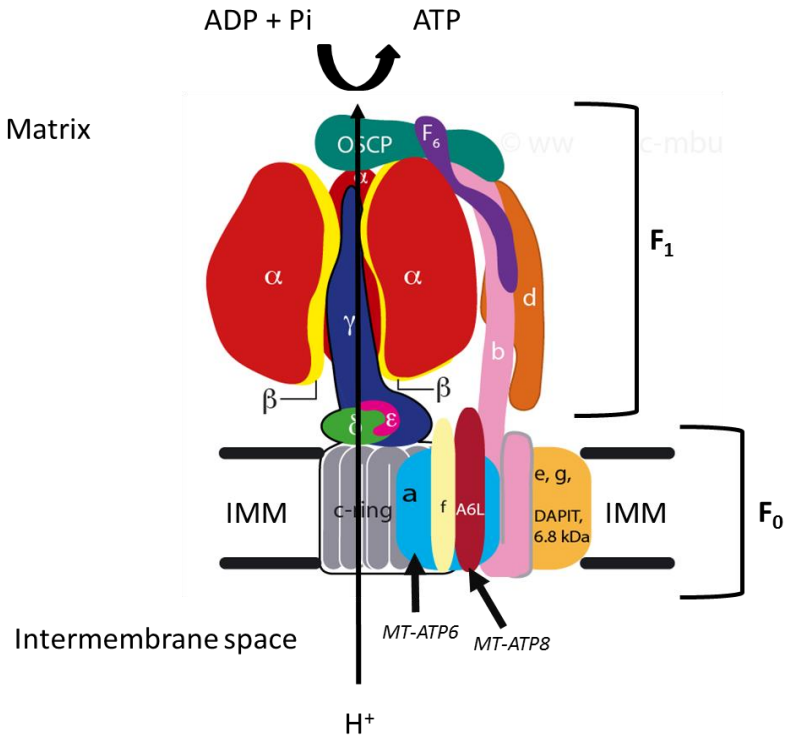

Figure 3.2 Schematic representation of the structure and function of complex V
The mammalian ATP synthase consists of 17 subunits. Two of these subunits, A6L and *a* are encoded by the *MT-ATP8* and *MT-ATP6* genes respectively in the mitochondrial genome (indicated by arrows). The complex is made of the F_1 catalytic domain that protrudes into the matrix, and the membrane embedded F_0 domain. The two domains are connected by a central and a peripheral stalk. Image was modified from: http://www.mrc-mbu.cam.ac.uk/projects/2679/subunit-composition

3.2 Aims of chapter 3

I. To investigate mitophagy in fibroblasts derived from patients with confirmed mitochondrial disease due to mtDNA mutations using high-content imaging.

II. To further characterise selected patient cells using a combination of cell biological and biochemical approaches

3.3 Materials and methods

3.3.1 Patient and control fibroblasts

Twenty-two anonymised control fibroblast cultures were established from skin explants in-house and maintained as described in section 2.2.1. These were obtained with parental consent from children undergoing diagnostic skin biopsy for karyotyping and where cytogenetics was normal (n = 10), and from healthy consented adults aged 18–81 years (n = 12). For the experiments presented here I used a culture with the mean mitophagic activity which was also the median age of the series (Control 1) of 22 cultures. I also used a paediatric control culture (Control 2, male, 5 years old) as most patient cultures were derived from paediatric patients. Patient fibroblast cultures were donated by patients in Professor Jo Poulton's outpatient clinic and established in house with the approval of the UK National Research Ethics Service (South Central-Berkshire, n=10) except for 13051D cells, these were sent for investigation from the Newcastle Mitochondrial Disease Clinic for Adults and Children.

For all other materials and methods please refer to Chapter 2.

3.4 Results

Fibroblast cultures were available from ten patients, each harbouring a single pathogenic point mutation in the mitochondrial genome. Four unrelated patients were diagnosed with the m.11778G>A mutation affecting the ND4 subunit of complex I, and hence putative complex I deficiency. An additional four patients, three of whom were related were diagnosed with complex I deficiency due to the rare m.13051G>A mutation in the ND5 subunit of complex I. Two fibroblasts cultures were derived from unrelated patients with complex V deficiency, harbouring pathogenic mutations at the same nucleotide position. Both the 8993T>G and 8993T>C nucleotide change affect the *a* subunit of the mitochondrial ATP synthase/complex V. Mitophagy was measured in these cells by measuring the area of co-localising LC3 punctae and mitochondria, and expressing that as the percentage of total mitochondrial area. The results of the preliminary screen for dysregulated mitophagy are summarized in Table 3.2. Mitophagy was increased in eight patient cultures with complex I deficiency when compared to control cells, indicated by ↑ (p<0.05). While mitophagy was below control levels in two complex I deficient cultures (↓; p<0.05), one harbouring the 11778G>A mutation and the other the 13051G>A mutation. Furthermore, mitophagy was also significantly decreased (↓, p<0.05) in both fibroblast cultures derived from patients harbouring complex V mutations.

Table 3.2 Summary of mitophagy results on fibroblasts derived from patients with various mtDNA mutations

Patient identifier	Gene	Mutation	Adult	Child	Mitophagy
13051A	*MT-ND5*	m.13051G>A		1	↑
13051B	*MT-ND5*	m.13051G>A		1	↓
13051C	*MT-ND5*	m.13051G>A	1		↑
13051D	*MT-ND5*	m.13051G>A	1		↑
11778A	*MT-ND4*	m.11778G>A		1	↑
11778B	*MT-ND4*	m.11778G>A		1	↑
11778C	*MT-ND4*	m.11778G>A	1		↑
11778D	*MT-ND4*	m.11778G>A	1		↓
8993TC	*MT-ATP6*	m.8993T>C		1	↓
8993TG	*MT-ATP6*	m.8993T>G		1	↓

The fibroblast cultures highlighted (grey) in Table 3.2 were selected for further characterization. Representative images of those patient cultures that are not discussed further in detail in this chapter are shown in Figure 3.3.

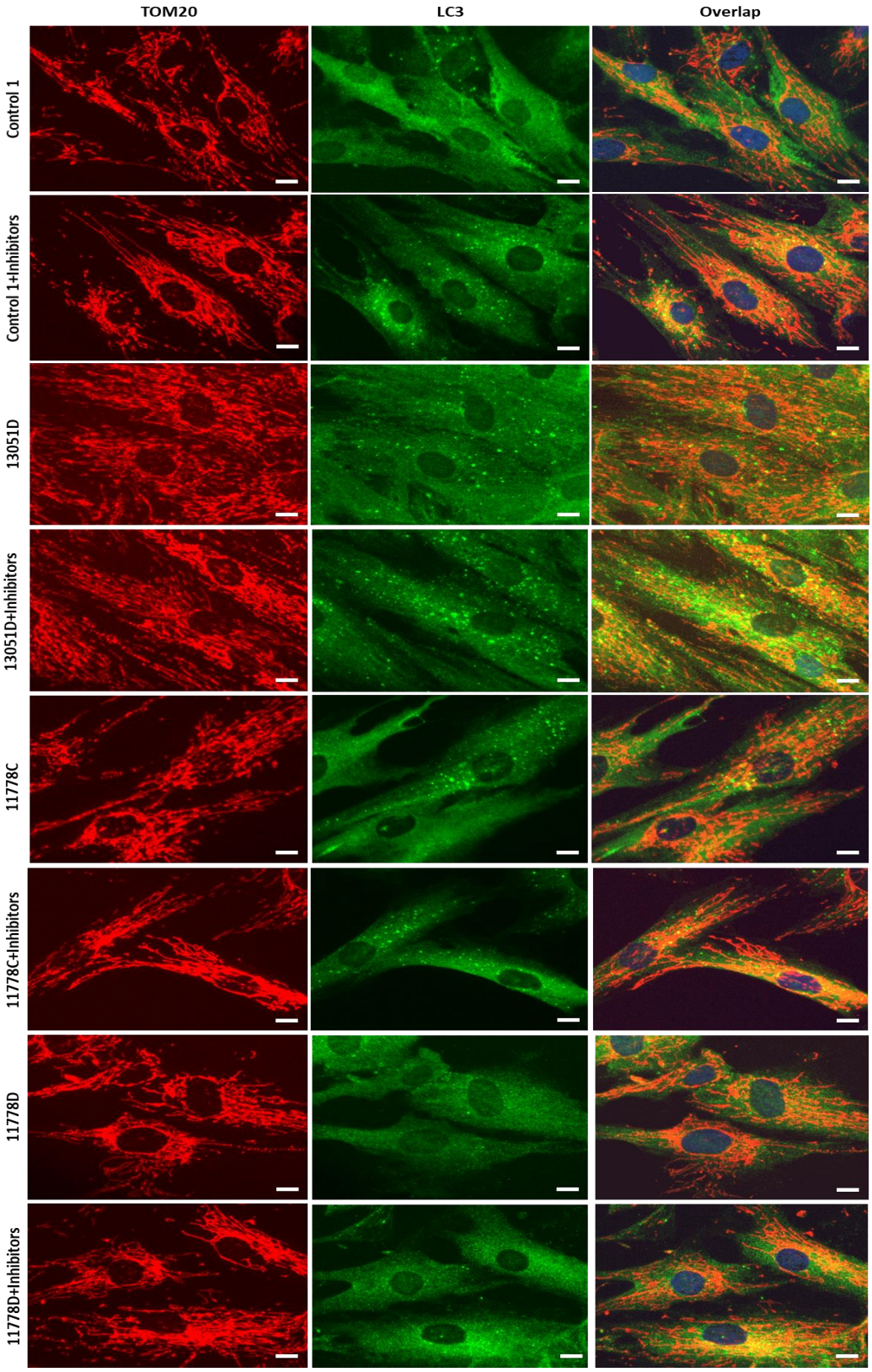

Figure 3.3 Representative images of Control 1 and complex I patient fibroblasts Showing TOM20-labelled mitochondria and LC3-labelled autophagosomes cultured either at baseline or with the addition of lysosomal inhibitors E64d and Pepstatin A. Scale bar 10µm.

The 13051G>A mtDNA mutation was first described in the literature in a single family where affected individuals were presenting with LHON (Howell et al., 2003). Since then this mutation has only been reported by our group in the individuals presented here (Dombi et al., 2016). Patients 13051A and 13051B are siblings presented with a much more severe Leigh disease/LHON phenotype compared to their mother (13051C) who was presented with classical LHON (Table 3.3 and Figure 3.4). Leigh syndrome (LS) (Table 3.1) is a neurological mitochondrial disorder that is the most common paediatric presentation resulting from both mtDNA and nDNA mutations. LS is mainly characterized by progressive encephalopathy, patients developing bilateral lesions in the brain stem and basal ganglia (Lake et al., 2016). Increased mitophagy was previously reported in patients 13051A and 13051C (Dombi et al., 2016). Fibroblasts were not yet available from patient 13051B at the time of publication. The low levels of mitophagy documented in 13051B fibroblasts is intriguing considering the intermediate phenotypic presentation of the patient; while her mother (13051C) and sister (13051A) had increased mitophagy documented. Therefore, 13051A and 13051B fibroblasts were selected for further characterisation. 13051C fibroblasts derived from the mother were included in some of the experiments for comparison. 11778A and 11778B fibroblasts were derived from two unrelated patients both of whom were presented with a Leigh disease/LHON phenotype that is uncommon for the 11778G>A mtDNA mutation. Additionally, patient 11778A started developing symptoms at the age of 4. This is the youngest presentation of the 11778G>A mutation ever seen in the Oxford NHS Clinical Service for Rare Mitochondrial Disorders. These cells were selected for further experiments in the anticipation that they could shed some light on the unusual pathology of the

patients. Fibroblasts derived from two unrelated patients with complex V defects were selected for further characterisation as a result of the low mitophagy documented in these patients and its potential connection to the skewed segregation of the 8993 mtDNA mutations documented in oocytes.

3.4.1 Characterisation of fibroblasts with complex I mutations

In this section, I will characterise fibroblasts derived from five patients. Three patients from the same family harboured the 13051G>A mtDNA mutation in the ND5 subunit of complex I (Figure 3.4 A and B). Additionally, cells from two unrelated individuals harbouring the common 11778G>A mtDNA mutation in the ND4 subunit of complex I (Figure 3.4 C). All patients presented here were homoplasmic for the respective mutations. A short clinical description of all patients presented in this section is available in Table 3.3.

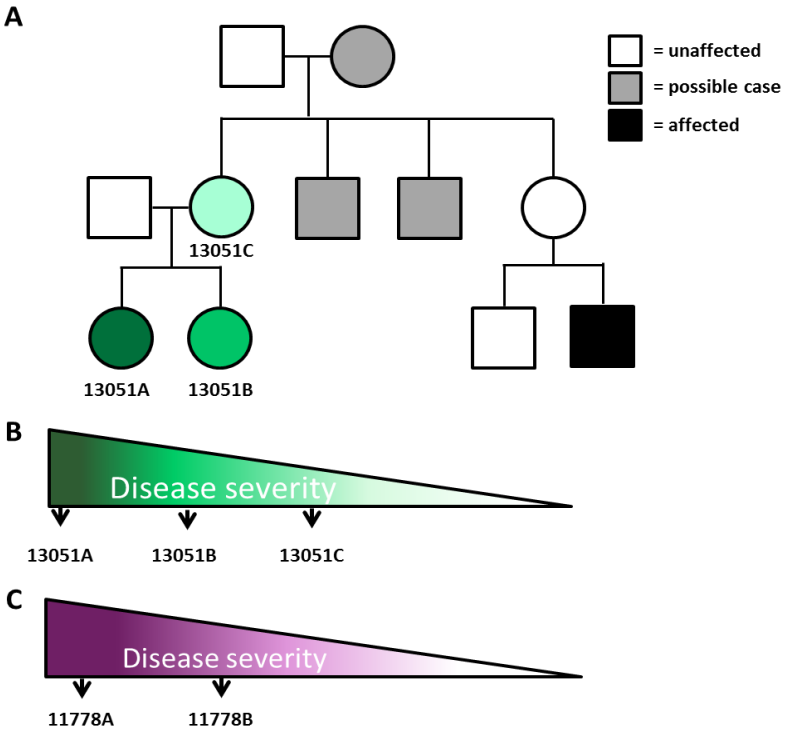

Figure 3.4 Family tree of patients with the 13051G>A mtDNA mutation and relative disease severity of all complex I patients
(A) The three patients presented here are indicated by the green symbols. Individuals represented by white are unaffected family members. Grey symbols are potential cases with unconfirmed diagnosis. Black symbols are documented affected family members. Squares are males and circles are females. (B) Within the family harbouring the 13051 mutation patient 13051A has the most severe phenotype followed by 13051B. The least severe patient is 13051C. (C) Amongst the two unrelated patients carrying the 11778 mutation the presentation of patient 11778A is more severe than that of 11778B.

Table 3.3 Clinical description of complex I patients

Patient/Diagnosis	Clinical presentation
13051A LHON/Leigh disease	She had auditory verbal agnosia and selective language regression due to bilateral sensorineural hearing loss at the age of 4 years old. MRI showed high signal in the basal ganglia and brainstem-suggesting necrosis. At 5 years of age visual acuities were 1.5 for the right eye and 0.2 for the left eye. No deterioration was noted in visual acuity at her last examination at age 8 years. She is non-ambulant, ventilator dependent, tube fed and has no recognisable speech.
13051B Leigh disease	She had motor delay from 18 months onwards with subsequent learning difficulties. She developed dystonic movements but remains ambulant. At the age of 11 there was no evidence of optic nerve disease with normal retinal and optic nerve examinations.
13051C LHON	Acute onset of bilateral visual loss with a typical LHON phenotype at the age of 45. At presentation the visual acuities were 0.62 for the right eye and 0.62 for the left eye. Visual fields showed significant loss of central fields extending to 20 degrees, with no recordable colour vision on Ishihara testing. Examination revealed optic nerve atrophy.
11778A Leigh disease	She has intellectual delay and profound movement disorder (non-ambulant), vision apparently normal, borderline low mtDNA copy number in muscle (40%).
11778B LHON/Leigh disease	He was diagnosed with LHON, movement disorder (non-ambulant), depression, cardiomyopathy and urinary incontinence.

3.4.1.1 Mitophagy and autophagy in complex I mutant fibroblasts

Mitophagy was measured in both 13051 and 11778 mutant cells by measuring the area of co-localization events between TOM20-labelled mitochondria and LC3 positive autophagosomes (Figure 3.5). The values were expressed as the percentage of total mitochondrial area. Mitophagy was reduced in both 13051 fibroblasts at baseline (25mM glucose media) when compared to control cells. However, following the addition of lysosomal inhibitors E64d and Pepstain A (EP) for 24 hours in order to assess mitophagic flux, 13051A cells showed increased accumulation of co-localizing mitochondria and autophagosomes, while mitophagy in 13051B fibroblasts remained significantly below that measured in control cells (Figure 3.5 A). Mitophagy was significantly increased in 11778 fibroblast cultures when measured at baseline as well as following treatment with inhibitors EP when compared to control cells (Figure 3.5 B). In 11778 cells mitophagy was the highest in fibroblast derived from the less severe patient moving to a lower value in cells from the more severe patient and lowest in control cells. There was no correlation between mitophagy levels and disease severity in 13051 cells. Representative images of TOM20-labelled mitochondria and LC3-labelled autophagosomes from controls and complex I patients are shown in Figure 3.6 for 13051 fibroblasts and Figure 3.7 for 11778 fibroblasts.

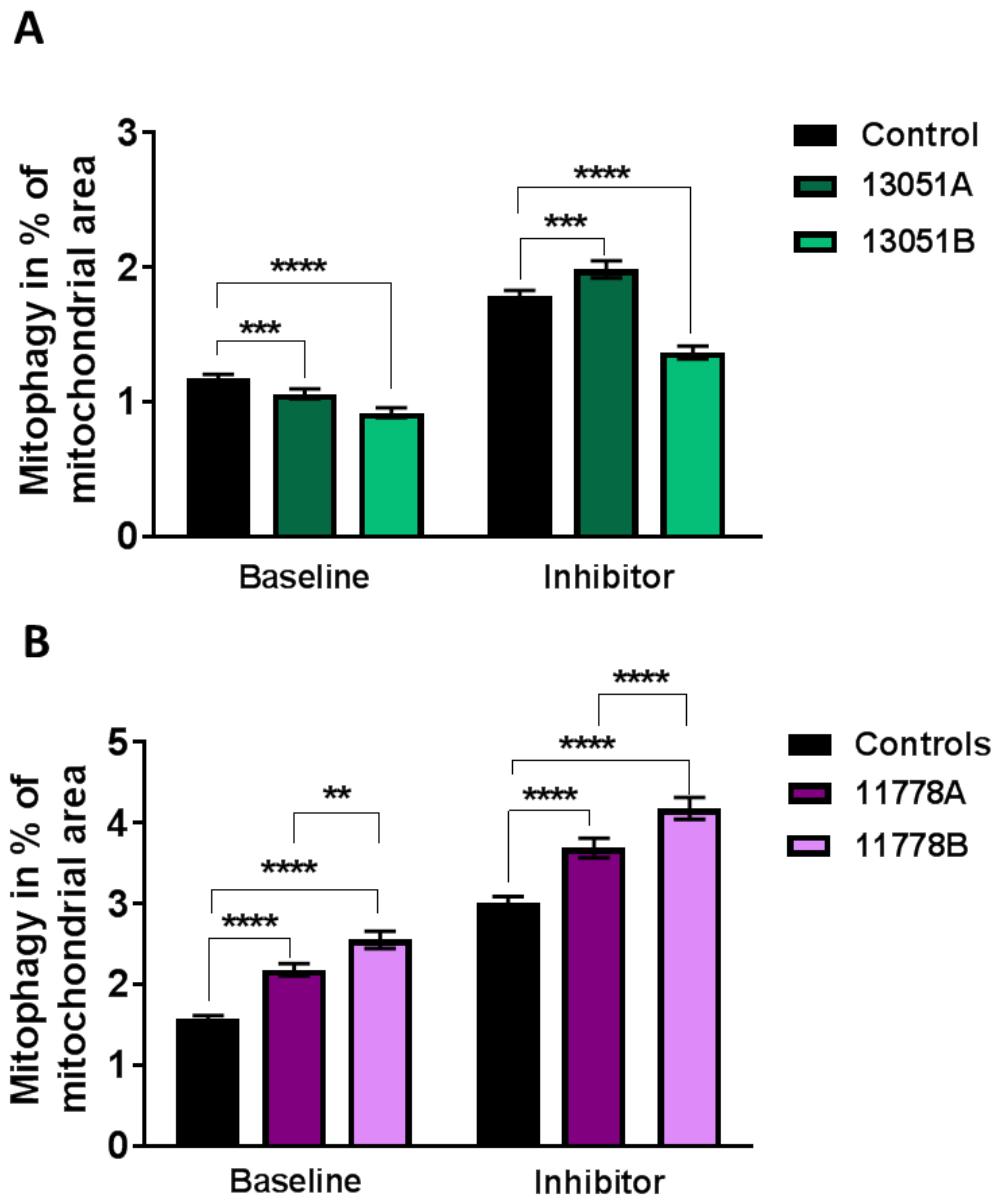

Figure 3.5 Mitophagy in complex I mutant fibroblasts in 25mM glucose
Mitophagy measured as the area of TOM20 labelled mitochondrial fragments co-localising with LC3 labelled autophagosomes, expressed as the percentage of total mitochondrial area. Mitophagy was measured in parallel at baseline (25mM glucose media only) or after the addition of lysosomal inhibitors E64d and pepsatin A for 24 hours. (A) Mitophagy in 13051G>A mutant fibroblasts, n=3, minimum of 1279 cells analysed per condition. (B) Mitophagy in 11778>A mutant fibroblasts, n=3, minimum of 1156 cells analysed per condition. Mean +/- 95% CI, **=p<0.01, ***=p<0.001, ****=p<0.0001

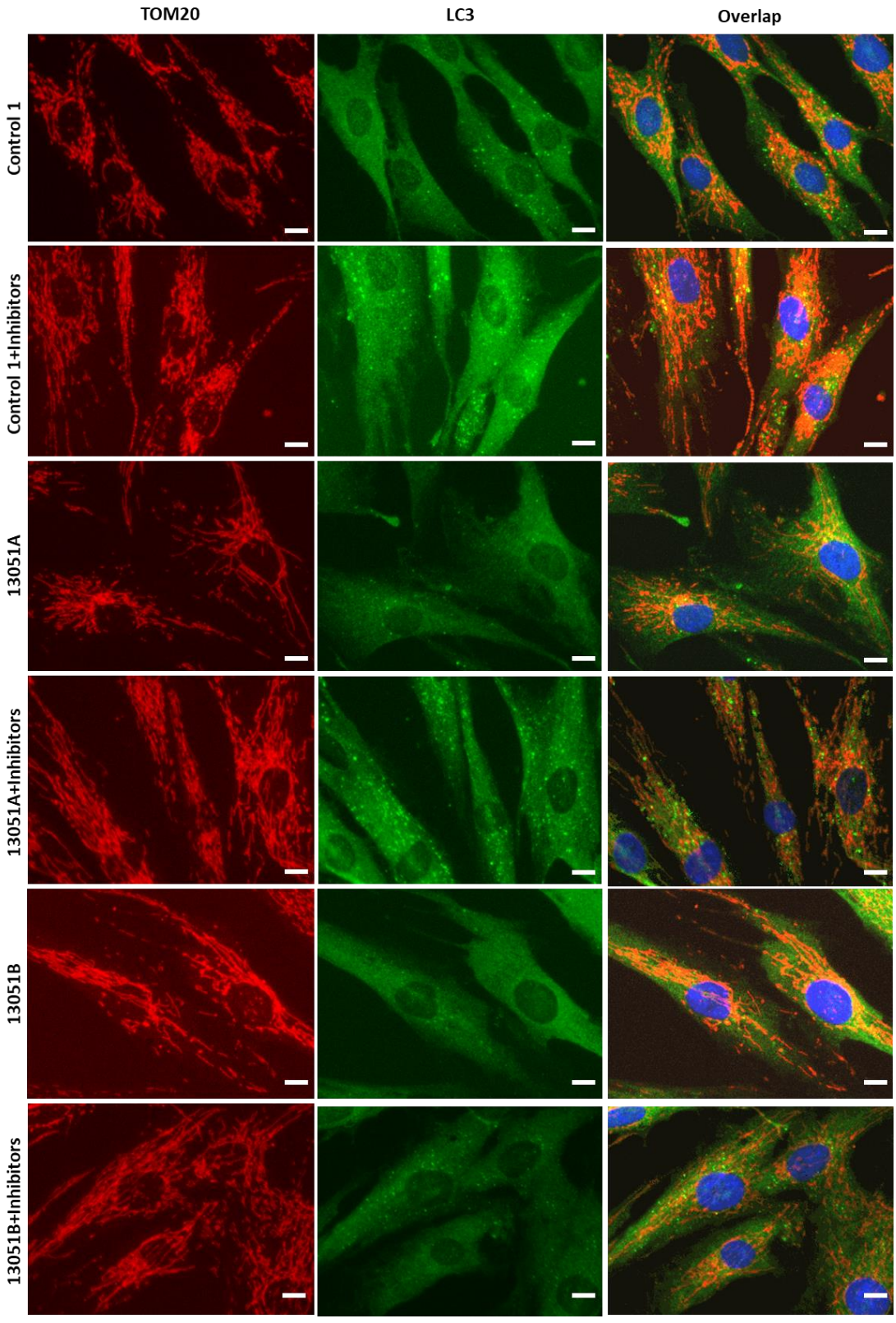

Figure 3.6 Representative images of Control 1 and 13051 fibroblasts
Showing TOM20-labelled mitochondria and LC3-labelled autophagosomes cultured either at baseline or with the addition of lysosomal inhibitors E64d and Pepstatin A. Scale bar 10µm.

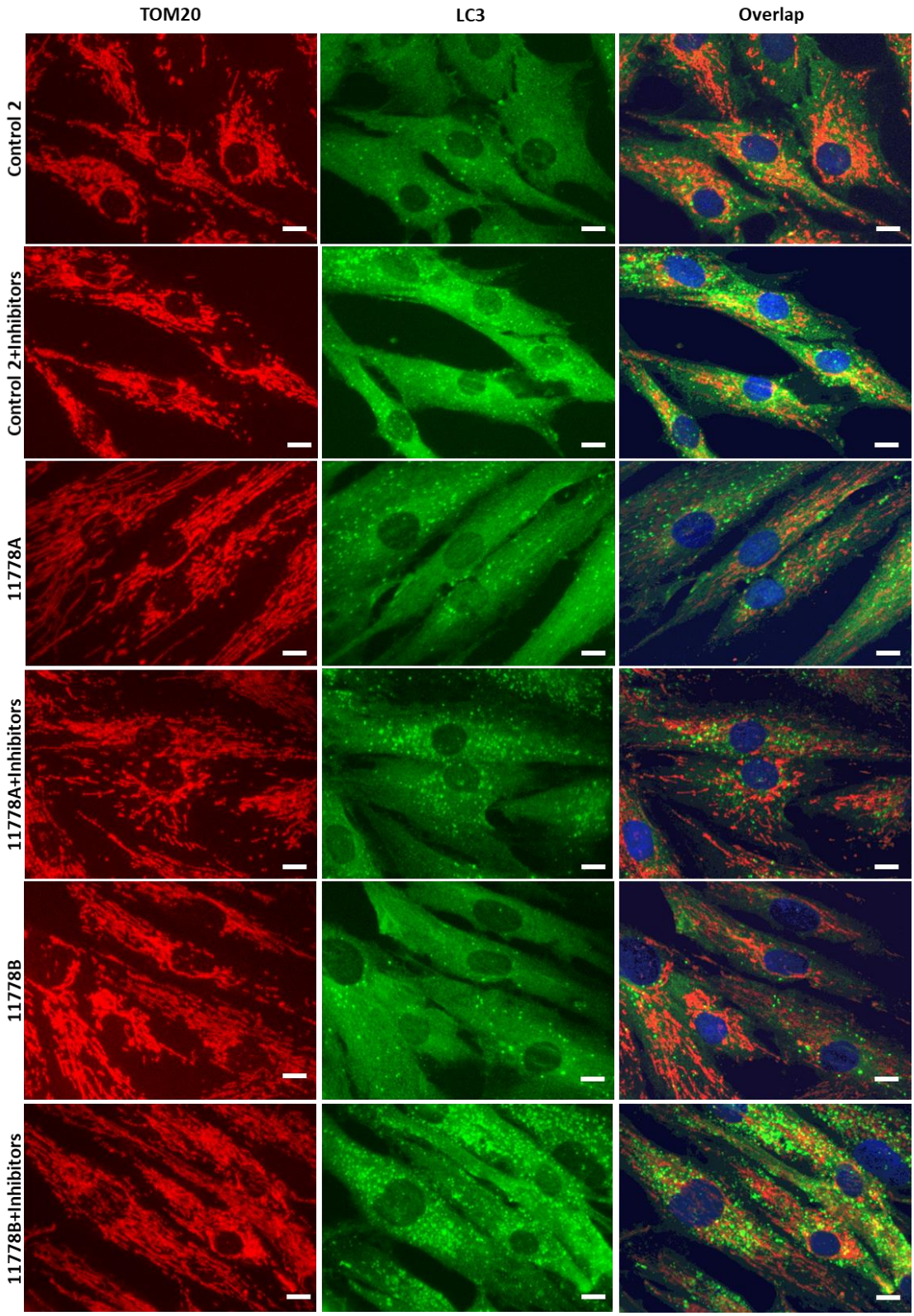

Figure 3.7 Representative images of Control 2 and 11778 fibroblasts
Showing TOM20-labelled mitochondria and LC3-labelled autophagosomes cultured either at baseline or with the addition of lysosomal inhibitors E64d and Pepstatin A. Scale bar 10µm.

The most efficient way for eukaryotic cells to meet their energy requirements when the availability of glucose is limited is to produce ATP via oxidative phosphorylation. However, the conventional culture medium for fibroblasts contains 25mM glucose that is above physiological levels and allows cells to rely more on glycolysis for ATP production. Glucose deprivation or starvation of cultured cells is a known inducer of both mitophagy and autophagy. Additionally, prolonged culture in galactose media was shown to remodel oxidative energy metabolism and increase mitochondrial content in myotubes in the long term (Kase et al., 2013). Therefore, complex I deficient fibroblasts were cultured in either low glucose (3mM) or galactose (0mM glucose) media for 24 hours with or without lysosomal inhibitors. The aim was to determine how a change in glucose availability influences mitophagy both in patient and control fibroblasts. Mitophagy was reduced at baseline in 13051A and 13051B cells cultured both in low glucose and galactose media when compared to controls (Figure 3.8 A). Following incubations with lysosomal inhibitors for 24 hours mitophagy was maintained at controls levels in 13051A cells while it remained significantly low in 13051B fibroblasts in both 3mM glucose and galactose media when compared to control cells (Figure 3.8). Meanwhile mitophagy in both 11778 cultures remained consistently increased, treated either with 3mM glucose or with galactose media (Figure 3.8 B). Mitophagy was also increased in these patient cells when compared to controls at both baseline as well as following EP treatment.

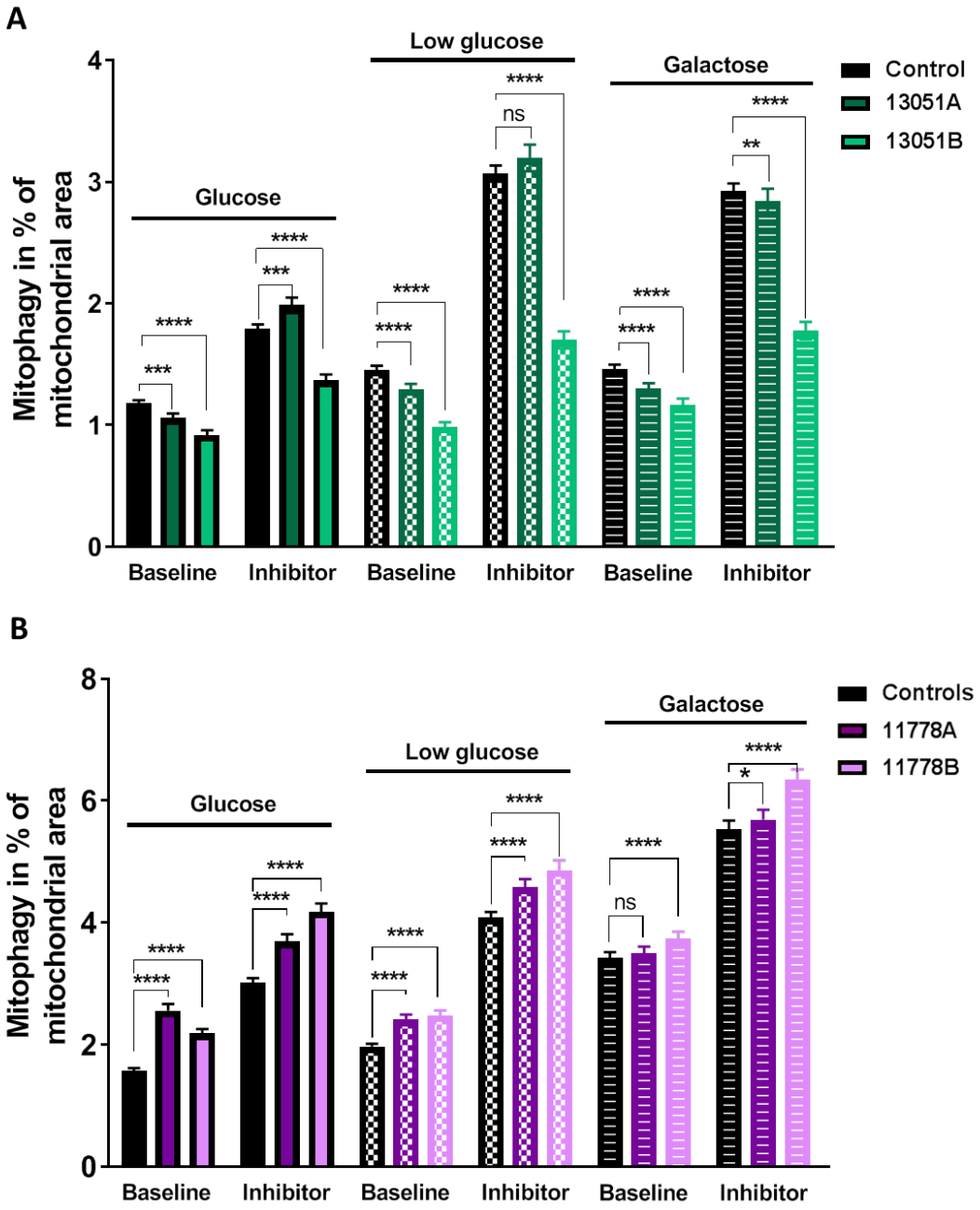

Figure 3.8 Mitophagy in complex I mutant fibroblasts under energetic stress
(A) Mitophagy in 13051G>A mutant fibroblasts, n=3, minimum of 877 cells analysed per condition. (B) Mitophagy in 11778>A mutant fibroblasts, n=3, minimum of 1145 cells analysed per condition. Lysosomal inhibitors are E64d, Pepstatin A. Low glucose media is 3mM glucose, and galactose media is 0mM glucose supplemented with 10mM galactose.
Mean +/- 95% CI, *=p<0.05, **=p<0.01, ***=p<0.001, ****=p<0.0001

Mitophagy is an organelle specific form of autophagy, the housekeeping recycling mechanism within cells that is also activated during various stress conditions such as hypoxia, ER-stress and inflammation (Ravanan et al., 2017). Considering the central role of mitochondria within cellular homeostasis it is plausible that mitochondrial dysfunction could trigger a systemic stress response leading not only to an increase in mitophagy but general autophagy as well. Autophagy was measured by counting the number of LC3 positive punctae within cells corresponding to autophagosomes (Figure 3.9). The number of autophagosomes was increased in both 13051 mutant fibroblasts (Figure 3.9 A and B) as well as 11778 cells when compared to controls (Figure 3.9 C and D) at baseline. Treatment with lysosomal inhibitors further increased the number of LC3 positive punctae in both control and patient cells. Autophagosome count remained elevated in patient derived cells following EP treatment when compared to controls. The increase in autophagy was confirmed by Western blot analysis of the autophagosome marker protein LC3 (Figure 3.9 E).

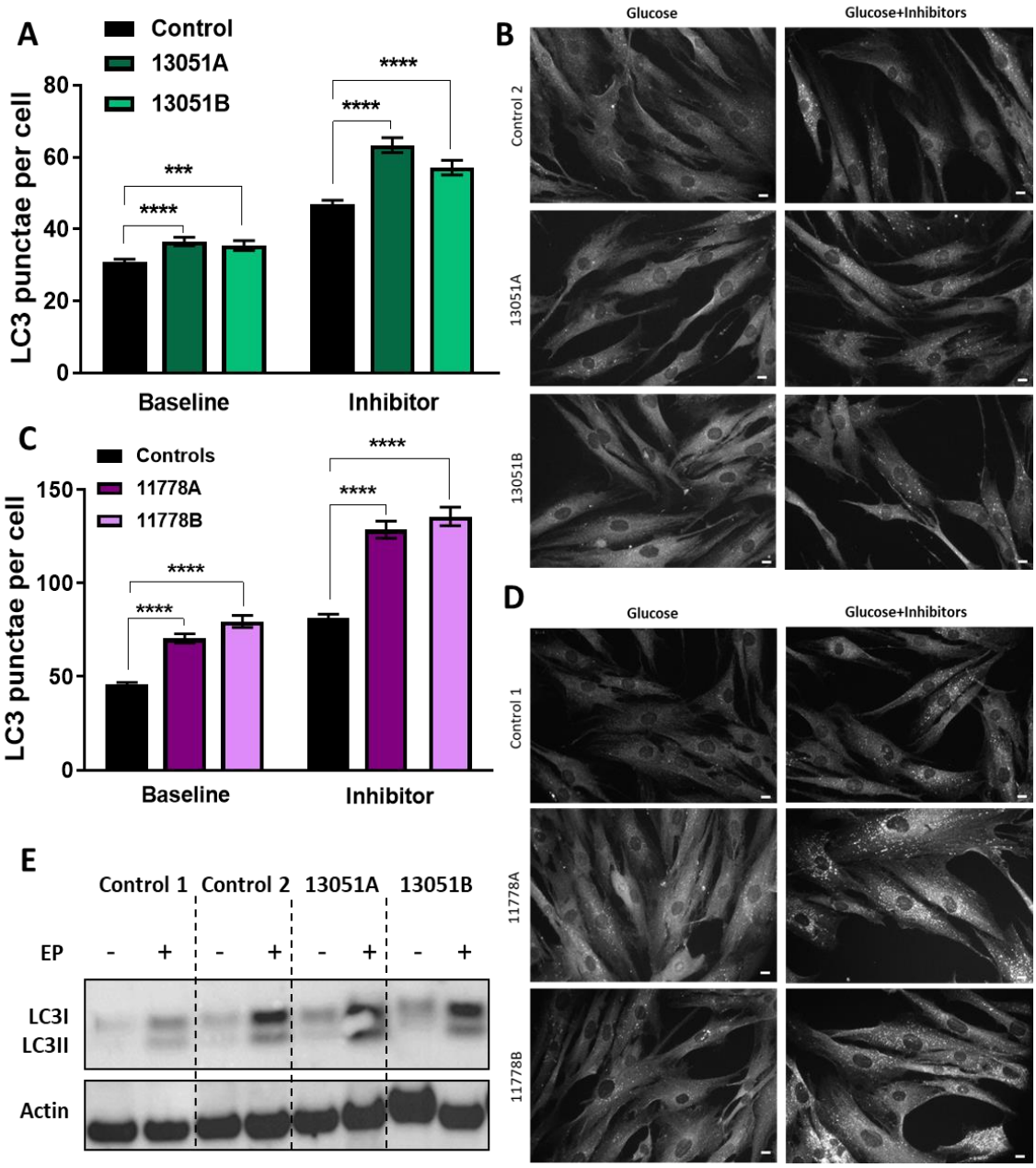

Figure 3.9 Autophagy in complex I mutant fibroblasts in 25mM glucose
Autophagy was measured by counting the number of LC3 positive punctae within cells. Autophagy was measured in parallel at baseline (25mM glucose media only) or after the addition of lysosomal inhibitors E64d and Pepsatin A (EP) for 24 hours. (A) Autophagy in 13051G>A mutant fibroblasts, n=3, minimum of 1279 cell analysed per condition. (B) Representative images of LC3 labelled cells, scale bar=10µm (C) Autophagy in 11778>A mutant fibroblasts, n=3, minimum of 1156 cells analysed per condition. (D) Representative images of LC3 labelled cells, scale bar=10µm (D) Western blot analysis of the autophagosome marker protein LC3, n=1, EP= lysosomal inhibitors E64d and Pepstatin A. Mean +/- 95% CI, ***=p<0.001, ****=p<0.0001

Autophagy was increased in all complex I mutant cells cultured in high-glucose media both at baseline and following treatment with lysosomal inhibitors when compared to control cells (Figure 3.9). As described previously, control and patient fibroblasts were cultured in either low glucose or galactose media for 24 hours in order to determine the effect of glucose availability on general autophagy. Culture in either low glucose or galactose further increased autophagy in both control and patient cells (Figure 3.10). With the exception of 13051B fibroblasts, autophagy was increased in complex I deficient cells when compared to controls under energetic stress (Figure 3.10). While 13051B cells were unable to raise their autophagosome counts like the other patient fibroblasts investigated, autophagy was not reduced in these cells when compared to controls. The low levels of mitophagy detected in 13051B cells (Figure 3.5 and 3.8) is therefore unlikely to be the result of defects in the autophagy process, but rather seems to specific to mitophagy.

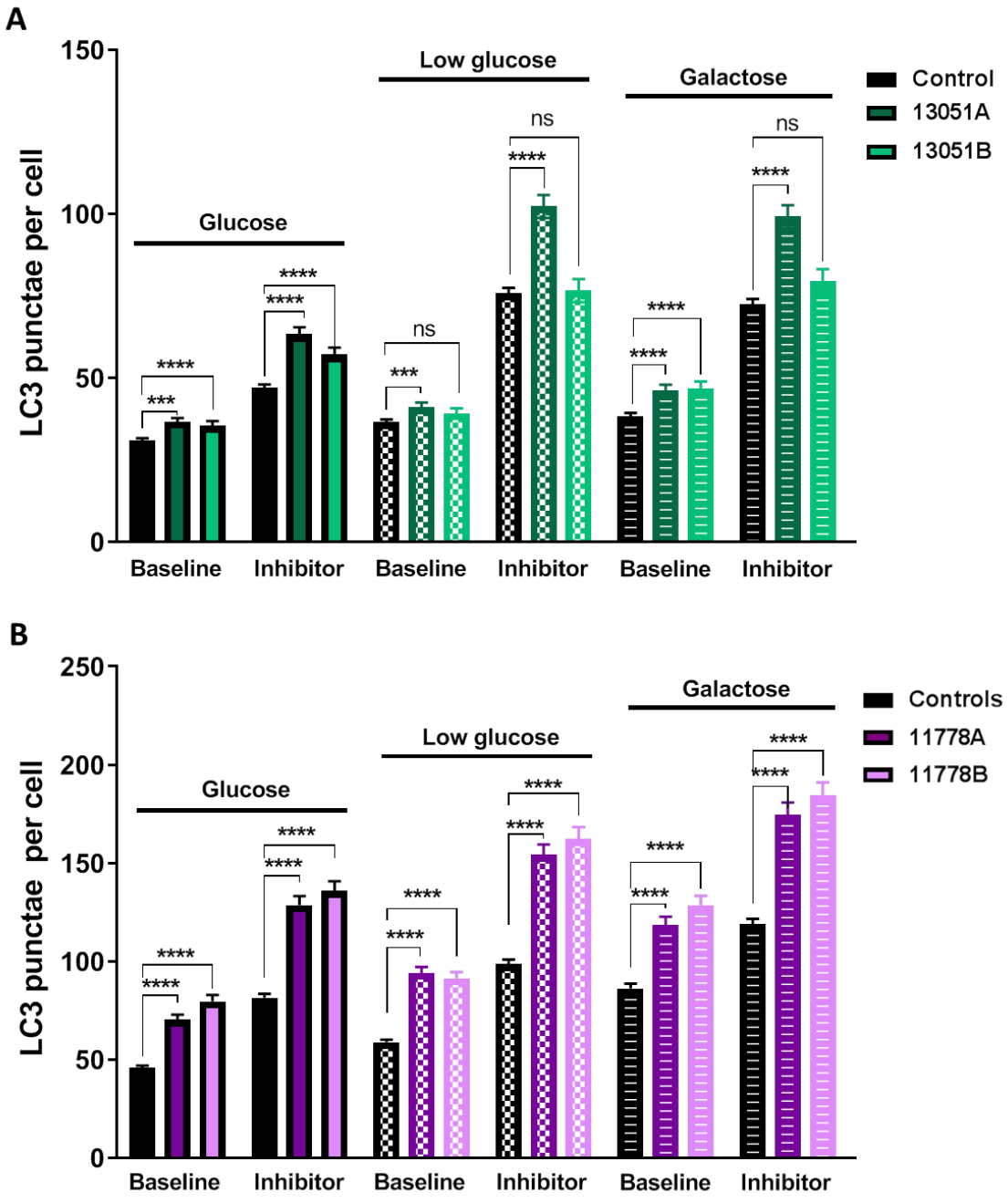

Figure 3.10 Autophagy in complex I mutant fibroblasts under energetic stress
(A) Autophagy in 13051G>A mutant fibroblasts, n=3, minimum of 877 cell analysed per condition. (B) Autophagy in 11778>A mutant fibroblasts, n=3, minimum of 1145 cells analysed per condition. Lysosomal inhibitors are E64d, Pepstatin A. Low glucose media is 3mM glucose, and galactose media is 0mM glucose supplemented with 10mM galactose.
Mean +/- 95% CI, *=p<0.05, **=p<0.01, ***=p<0.001, ****=p<0.0001

A limiting factor for autophagy, as well as mitophagy, to proceed is the availability of lysosomes. Chronic mitochondrial dysfunction was shown to negatively affect lysosomal biogenesis (Fernandez-Mosquera et al., 2017). The number of lysosomes in fibroblasts was assessed using Lyso-ID red staining. Lysosome count in 13051B cells was comparable with controls both at baseline and following 4 hours treatment with chloroquine (Figure 3.11). The number of lysosomes was also comparable to control levels in 11778 fibroblasts at baseline, however, significantly increased following chloroquine treatment (Figure 3.11). In the previously cited study carried-out by Fernandez-Mosquera *et al.* chronic lysosomal dysfunction was achieved by prolonged treatment with mitochondrial poisons oligomycin and antimycin A. The detrimental effect of these drugs on mitochondria is unlikely to mimic the dysfunction caused by the point mutations presented here.

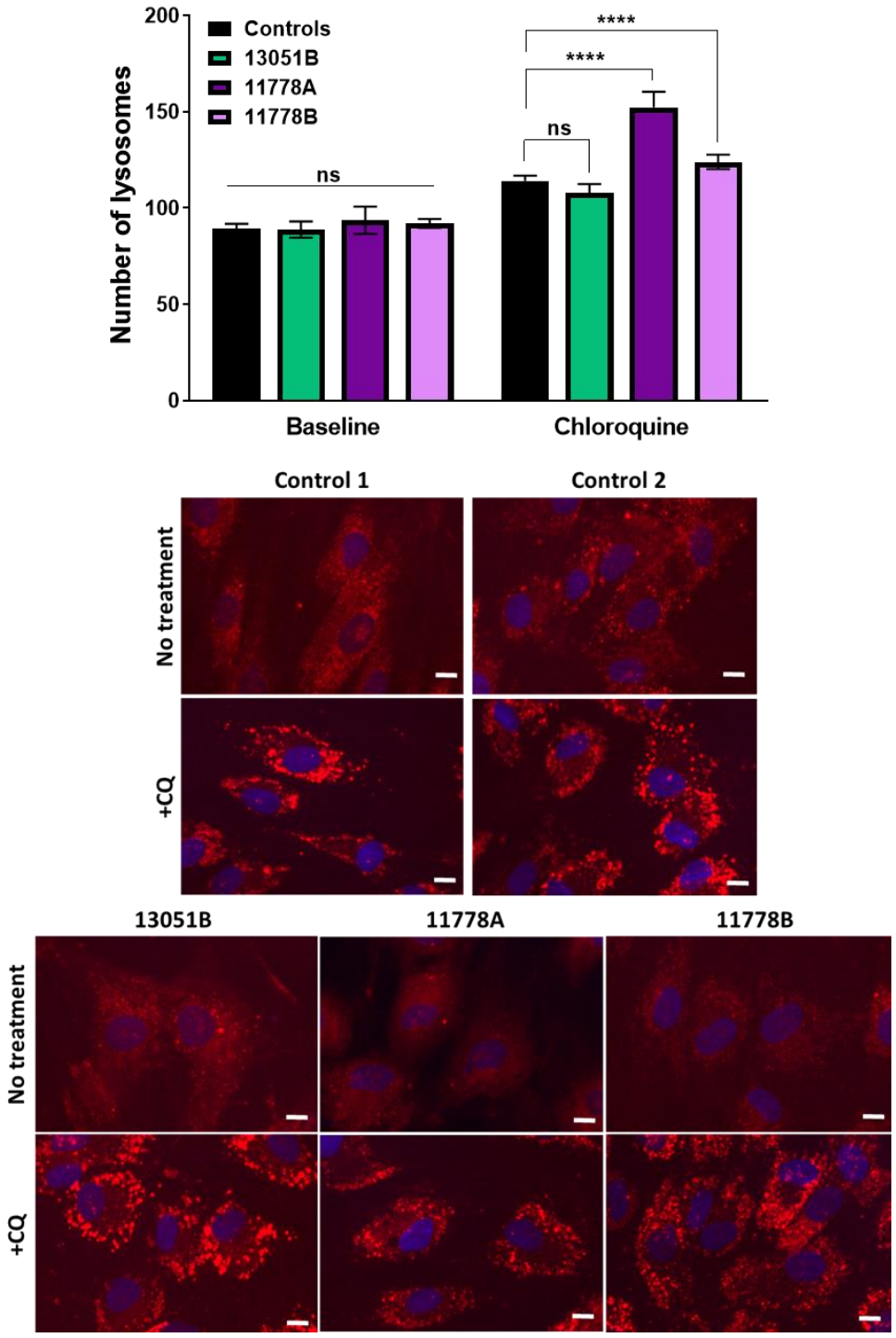

Figure 3.11 Lysosomal content of complex I mutant fibroblasts
Number of lysosome counted by Lyso-ID staining of fibroblasts cultured either in 25mM glucose media (baseline) only or supplemented with 60µM chloroquine (CQ) for 4 hours prior to imaging. Mean +/- 95% CI, ****=p<0.0001, n=2, minimum of 542 cell analysed. Representative images of Lyso-ID (red) and Hoechst (blue) labelled fibroblasts with or without chloroquine (CQ) treatment. Scale bar 10µm.

3.4.1.2 Mitochondrial network properties of complex I mutant fibroblasts

Mitochondrial fragmentation (Liao et al., 2017; Twig and Shirihai, 2011) and a reduced membrane potential (Narendra et al., 2008) have both been shown to trigger mitochondrial turnover by mitophagy. Mitochondrial length was measured in fixed labelled with anitbodies against the OMM protein TOM20. Despite the increased mitophagy observed in 13051A cells mitochondrial length was increased in these cells when compared to controls (Figure 3.12 A). Contrarily, mitochondrial length was reduced in 13051B cells with low mitophagy when compared to control fibroblast (Figure 3.12 A). Mitochondrial membrane potential measured by TMRM intensity was decreased in both 13051 patient cultures compared to control ones (Figure 3.12 B). Both mitochondrial length (Figure 3.12 C) and membrane potential (Figure 3.12 D) was reduced in 11778A and 11778B cells compared to controls. The 13051 and 11778 point mutations affect membrane embedded subunits of the respiratory complex that are responsible for the pumping of protons across the IMM (Figure 3.1). Disturbances in proton translocation across the IMM may account for the reduction in membrane potential in patient derived cells.

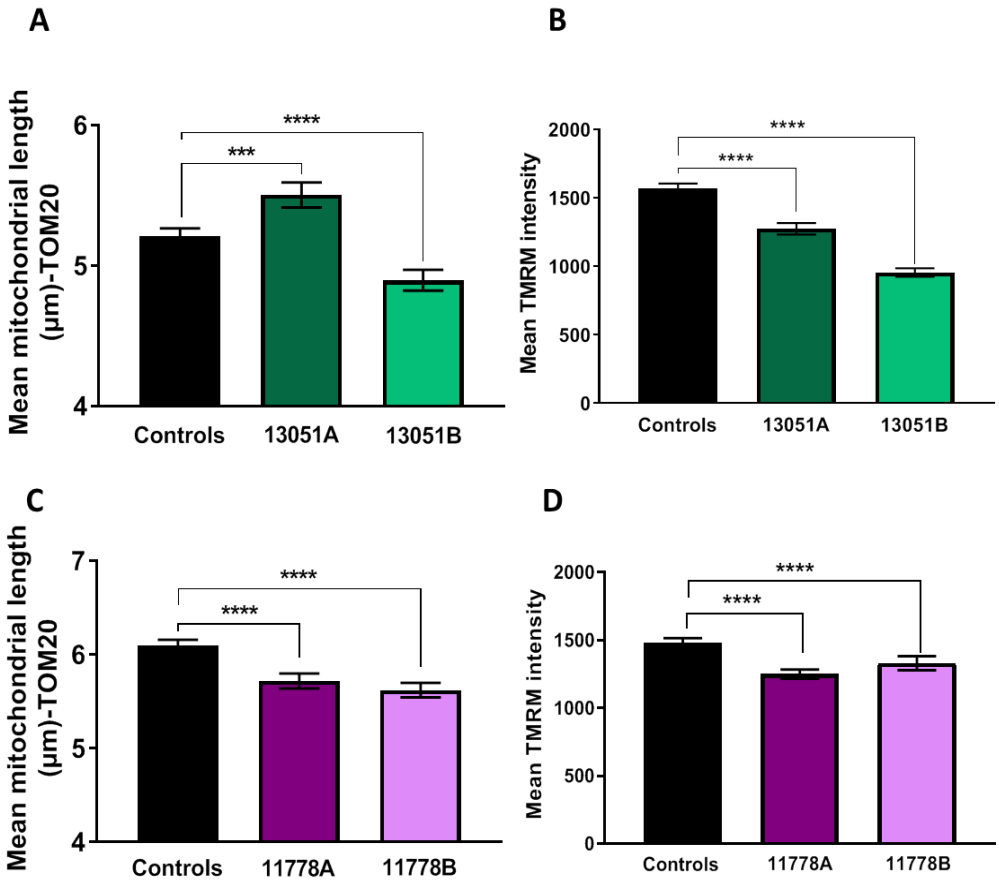

Figure 3.12 Mitochondrial network properties of complex I mutant fibroblasts
(A) Mitochondrial length (TOM20) and (B) membrane potential (TMRM) in 13051 mutant fibroblasts, n=3, minimum of 1298 cell analysed per condition.
(C) Mitochondrial length (TOM20) and (D) membrane potential (TMRM) in 11778 mutant fibroblasts, n=3, minimum of 853 cells analysed per condition
Mean +/- 95% CI, ***=p<0.001, ****=p<0.0001

3.4.1.3 Bioenergetics of complex I mutant fibroblasts

The 13051G>A mutation is located in the ND5 subunit while the 11778 G>A mutation is located in the ND4 subunit of complex I. Both of these subunits are part of the evolutionary conserved 'core' subunits that are imperative for complex I function (Figure 3.1). The 11778G>A mutation expressed in cybrids was shown to significantly reduce complex I activity and to cause subsequent biochemical defects (Brown et al., 2000; Floreani et al., 2005). Additionally, disturbed mitochondrial membrane potential (Figure 3.12) may also affect oxidative phosphorylation. Therefore, oxygen consumption was measured in 13051 fibroblasts using the Seahorse XF96 (Agilent) platform (Figure 3.13). 13051C fibroblasts were also included here to see how the milder phenotype of the patient might affect cellular respiration. Basal respiration is calculated by the subtraction of non-mitochondrial respiration; measured following the last injection by Rot/Ant A, from baseline cellular oxygen consumption. Maximal respiratory capacity is derived by subtracting non-mitochondrial respiration from the OCR measured following FCCP injection. ATP-linked respiration is calculated by subtracting the OCR measured after oligomycin treatment from basal respiration. The values were corrected for protein concentration within each well. Basal respiration, maximal and ATP-linked respiration was significantly decreased in 13051A and 13051B fibroblasts when compared to control cells (Figure 3.13). These are the cells derived from the siblings presented with a severe Leigh disease phenotype. There was no difference between control and 13051C fibroblasts derived from the mother who has the mildest LHON phenotype (Figure 3.13). There was no difference between 13051A and 13051B fibroblasts.

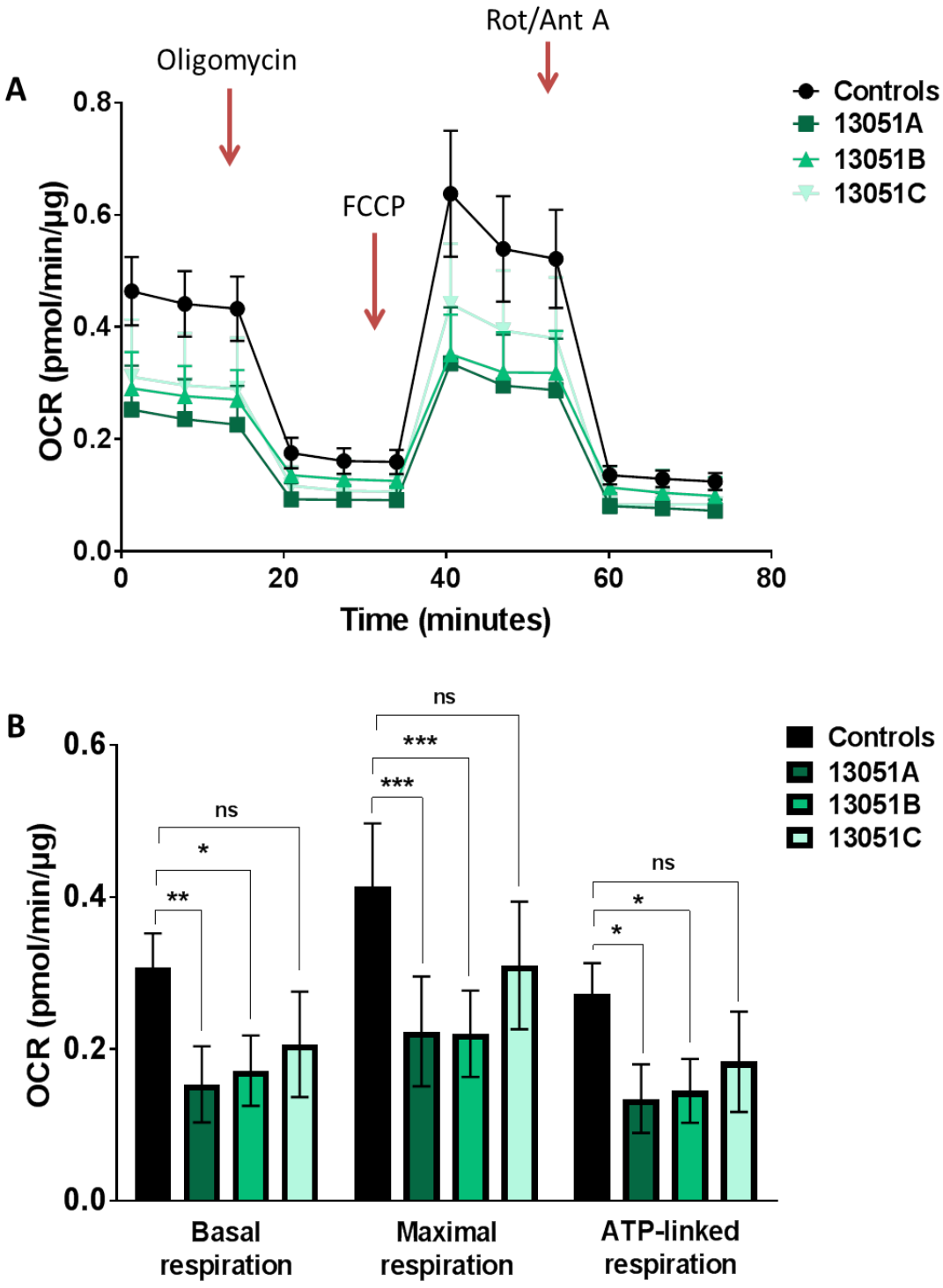

Figure 3.13 Oxygen consumption of 13051 mutant fibroblasts
(A) Oxygen consumption measured at baseline and following the addition of rotenone (complex V inhibitor), FCCP (protonophore, to collapse membrane potential) and rotenone (complex I inhibitor)/ antimycin A (complex III inhibitor). (B) Calculated basal, maximal and ATP-linked respiration of control and 13051 cells. Mean +/- 95% CI, n=1, *=p<0.05, **=p<0.01, ***=p<0.001

Following the oxygen consumption results, protein expression of a single subunit from each OXPHOS complex was measured using western blot analysis and the Abcam OXPHOS antibody cocktail. According to the manufacturer, antibodies in the cocktail were chosen because they are against subunits that are easily altered when their respective complex is not assembled. Protein expression of the NDUF8B subunit of complex I was visibly reduced in 13051B and 13051C fibroblasts compared to control cells (Figure 3.14). On the contrary, complex I subunit along with complex II and complex IV subunit proteins were increased in fibroblast derived from patient 13051A with the most severe phenotypic presentation (Figure 3.14).

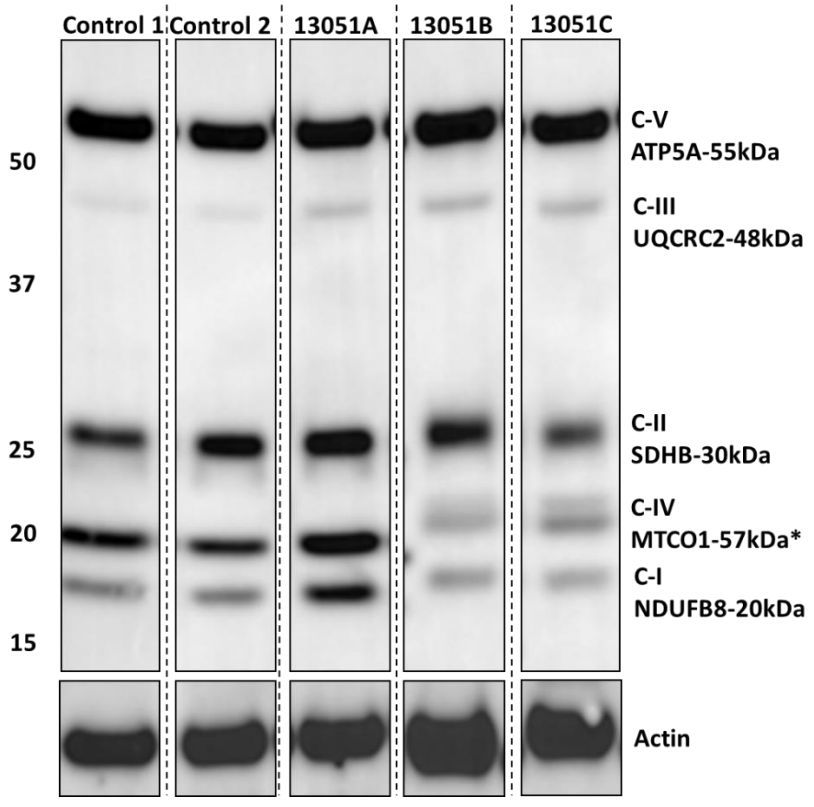

Figure 3.14 Protein expressions of OXPHOS complex subunits in 13051 mutant fibroblasts
*Highly hydrophobic mtDNA encoded protein. Real MW is 57kDa but migrates differently in different systems according to the manufacturer.

Sufficient oxidative phosphorylation is essential for the replication and subsequently the survival of cells cultured in glucose free galactose media as galactose is a non-glycolytic substrate. In order to determine the dependence of complex I mutant fibroblasts on glucose availability control and complex I mutant cells were cultured in either baseline (25mM glucose) or galactose (0mM glucose) media for 9 consecutive days. 15000 cells per well were seeded into 6 well plates. At day 9, cells were counted in each well. The number of cells remaining in the galactose culture after 9 days was expressed as the percentage of the cells counted in 25mM glucose (Figure 3.15). The percentage of 13051A and 13051B cells remaining in galactose media after 9 days was significantly reduced compared to control cells (Figure 3.15 A). The percentage of 13051C fibroblast remaining in culture after 9 days was not different from control cells. Although the growth of 13051 cells in galactose media seemed to show a graded response according to phenotype severity, there was no significant difference between the 13051A and 13051B cells (Figure 3.15 A). The survival of both 11778 cultures was significantly reduced in galactose media compared to control cells (Figure 3.15 B) suggesting the presence of a similar OXPHOS defect seen in 13051A and 13051B cells (Figure 3.13).

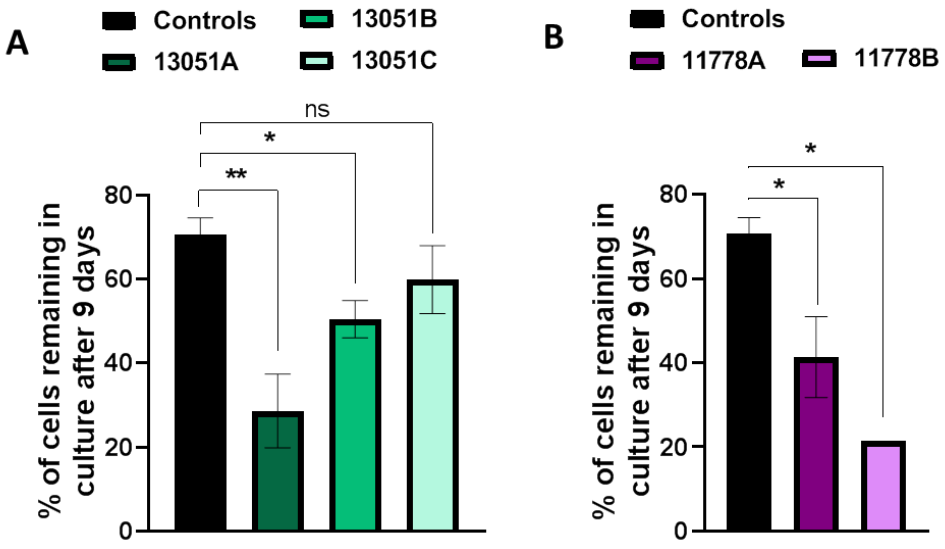

Figure 3.15 Survival of complex I mutant cells cultured galactose media for 9 days
The number of cells remaining in galactose culture after 9 days in (A) 13051 mutant cells and (C) 11778 cells, expressed as the percentage of the same cells counted in the parallel baseline (25mM glucose) culture.
Mean +/- SEM derived from 3 technical replicates, n=1, *=p<0.05, **=p<0.01

3.4.1.4 Mitochondrial DNA content in fibroblasts with complex I mutations

LHON is characterised by incomplete penetrance. It means that an mtDNA mutations is necessary but not always sufficient to cause symptoms. Approximately 50% of males and 10% of females who carry pathogenic mutations develop optic neuropathy (Yu-Wai-Man et al., 2002). The reason for this is poorly understood. Giordiano and colleagues attributed this variable disease penetrance to an increase in mtDNA copy number owing to the compensatory activation of mitochondrial biogenesis (Giordano et al., 2014). When investigated in three large pedigrees of Italian and American-Irish origin, mitochondrial DNA copy number measured in peripheral white blood cells was the highest in asymptomatic carriers, moving progressively towards lower values in affected carriers and the lowest in healthy controls (Giordano et al., 2014).

Mitochondrial DNA copy number in 13051 and 11778 mutant fibroblasts was

measured using PicoGreen staining and subsequent live cell imaging (Ashley et al., 2005). The number of mtDNA nucleoids was increased in fibroblasts derived from all complex I patient cells when compared to controls (Figure 3.16 A, B and C). Additionally, mitochondrial content, measured by antibody labelling of the mitochondrial reticulum against the OMM protein TOM20, was also increased in patient derived cells compared to control ones (Figure 3.16 D and E). Fibroblasts derived from patient 13051C were included in this assay as her phenotype is the mildest within the 13051 family. Although mitochondrial DNA content did not show any pattern that would associate with the severity of the pathological presentation of the patients, mitochondrial content (TOM20 area) did show a graded response (Figure 3.16 D and E). Mitochondrial content was the highest in fibroblasts derived from the least severe patient in the 13051 family (13051C) and declined continuously reaching the lowest value in healthy control cells (Figure 3.16 D). Similarly, fibroblasts derived from the milder patient carrying the m.11778G>A mutation had the highest mitochondrial content (Figure 3.16 E). Unfortunately, fibroblasts were not available from asymptomatic maternal relatives for comparison.

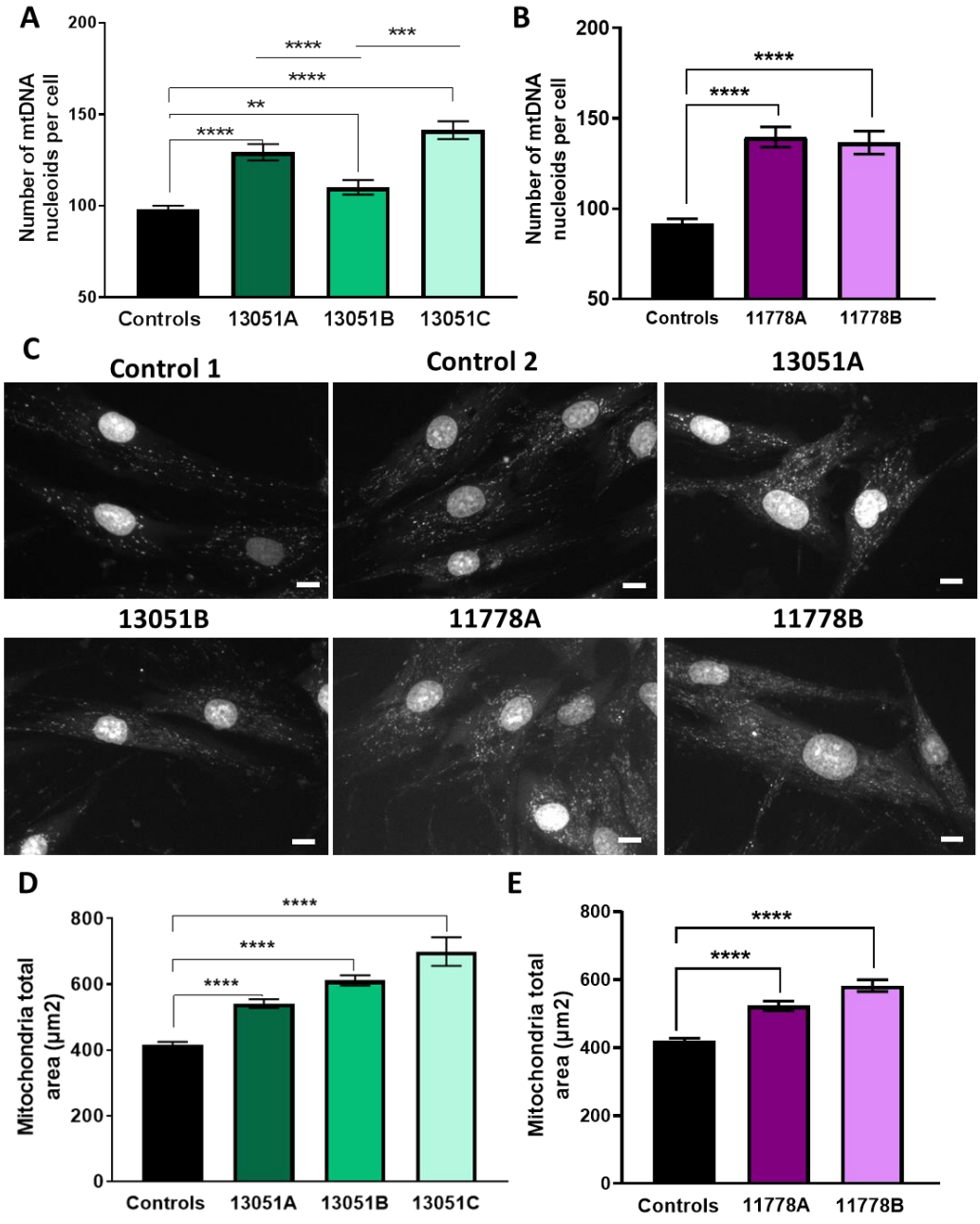

Figure 3.16 Analysis of mDNA nucleoid and mitochondrial content in complex I mutant fibroblasts

(A) mtDNA nucleoid number in 13051G>A mutant fibroblasts. (B) mtDNA nucleoid number in 11778>A mutant fibroblasts. (C) Representative images of PicoGreen labelled nucleoids of control and patient cells, scale bar 10µm. (E) Mitochondrial content (total area of TOM20 labelled mitochondria) in 13051G>A mutant fibroblasts. (D) Mitochondrial content in 11778>A mutant fibroblasts.

Mean +/- 95% CI, **=p<0.01, ***=p<0.001, ****=p<0.0001

3.4.2 Discussion of complex I mutations specific findings (Section 3.4.1)

A visual summary of all data presented in section 3.4.2 is available in Table 3.5. I investigated three related patients with the m.13051G>A mutation and two unrelated individuals with the m.11778G>A mutation. Cells from two 13051 patients with a severe LHON/Leigh's disease phenotype (13501A and 13051B) grew more slowly in galactose and had lower respiratory chain activity than the cells derived from the patient with the milder classical LHON phenotype (13051C) or controls. All complex I mutant fibroblasts had increased mtDNA and mitochondrial content compared to control ones. This suggests that the cells are generally stressed, compensating by increasing mitochondrial mass and mitochondrial DNA copy number at the expense of cell growth. Autophagy was also increased in these cells compared to controls. Mitophagy was also increased in both 11778 cultures as well as 13051A fibroblasts. Contrarily, 13051B fibroblasts had low mitophagy compared to 13051A and control fibroblasts even following glucose starvation. There was no decrease in the number of lysosomes.

Complex I deficiency is often associated with elevated ROS production (Taddei et al., 2012; Tretter et al., 2004). Therefore, the treatments currently available (Gueven et al., 2017) or under development (Beyrath et al., 2018; de Haas et al., 2017) are focused on redox modulation. In a previous study we reported increased ROS in 13051A fibroblasts using DHR fluorescence (Dombi et al., 2016). ROS production was measured in 13051C and 11778A cells using the mitochondrial superoxide indicator MitoSOX (Supplementary figure 1). There was no difference between control and patient cells in MitoSOX fluorescence, however measuring superoxide produced only by mitochondria might not be sufficient to detect overall differences in ROS levels.

Others also failed to detect differences in ROS levels using MitoSOX using complex I mutant fibroblast while succeeding with alternative probes (Beyrath et al., 2018). Elevated levels of ROS have previously been linked to the activation of mitophagy (Ding et al., 2010). More recently, the mitochondrial 18-kDa translocator protein (TSPO) was shown to be involved in the coordination of mitophagy in a ROS dependent manner (Gatliff et al., 2014). Although TSPO was first identified as a peripheral benzodiazepine receptor (Braestrup and Squires, 1977), its actual function is to facilitate the transport of cytosolic cholesterol into mitochondria for steroid synthesis (Li et al., 2016) and was also shown to have a high-binding affinity for porphyrins (Li et al., 2015). TSPO overexpression negatively regulates mitophagy (Gatliff et al., 2014). There is a common nucleotide polymorphism (rs6971) associated with TSPO that involves a c.439A>G nucleotide change and a p.Ala147Thr amino acid change (Costa et al., 2009). The 'G' allele; most common within the general population; is associated with altered TSPO protein structure and a four- to five fold lower binding affinity for cholesterol and porphyrin, compared to that in the presence of the 'A' allele (Li et al., 2015). A range of our control fibroblasts were sent for genotyping and found that the control cells with the 'AA' genotype had consistently low mitophagy. Fibroblast derived from complex I mutant patients also underwent genotyping. 13051B and 11778D cells were the only complex I mutant cells in which low mitophagy was detected (Table 3.2). Both of these were heterozygous for the c.439A>G nucleotide change ('AG' genotype), which might contribute to reduced mitophagy levels seen in these patients when compared to TSPO 'GG' controls. The rest of the complex I patients who were genotyped were homozygous for the A>G TSPO polymorphism ('GG') (Supplementary table 2).

Complex I deficient cells all had increased mitochondrial content as well as increased mtDNA nucleoid numbers compared to control cells. These are common features of several pathological conditions (Vafai and Mootha, 2012). Additionally, compensatory increase in mtDNA copy was implicated as the reason behind the incomplete penetrance of LHON mutations (Giordano et al., 2014). Transcriptional regulation of *de novo* mitochondrial biogenesis is coordinated by the PGC-1 family of transcriptional coactivators (Scarpulla, 2011). On the other hand, the fine-tuning of the two opposing processes; de novo biogenesis and turnover by mitophagy co-ordinately regulates mitochondrial content. The antagonistic activities of these two pathways constantly accommodate the mitochondrial content of a cell to meet energy requirements in response to cellular metabolic state (Palikaras et al., 2015a). The uncoupling of these two processes was shown to contribute to the proliferation of damaged mitochondria in a *C. elegans* model of ageing (Palikaras et al., 2015b). Mitochondrial DNA content was significantly increased in all complex I deficient fibroblasts when compared to controls, even in 13051B cells with decreased mitophagy. However, these cells had the least increase compared to 13051A or 13051C ones. Low mitophagy is a potential contributor to the less efficient compensatory biogenesis. 13051 mutant fibroblasts presented in this section are derived from members of the same family, nonetheless the clinical presentation of the three patients is spread across the clinical spectrum ranging from severe Leigh syndrome (13051A) through a mixture of LS/LHON (13051B) to a classical LHON (13051C) phenotype (Figure 3.4). This family is a good representation of the extreme heterogeneity associated with mitochondrial diseases. Reduced mitophagy could contribute to the phenotypic differences between patient 13051B and 13051C by

promoting the accumulation of damaged mitochondria. Mitophagy was increased in 13051A cells derived from the most severely affected member of the family. In this case additional unknown genetic components are the most likely reasons behind the differences in disease pathology.

3.4.3 Results continued - Characterisation of fibroblasts with complex V mutations

In this section I will characterise fibroblasts derived from two unrelated patients harbouring the 8993T>G and 8993T>C mtDNA mutations in the *a* subunit of the mitochondrial ATP synthase or otherwise referred to as complex V (Figure 3.2). The patients presented here were heteroplasmic, however, the mutant load in both patients was approximately 90%. A short clinical description of the complex V patients is available in Table 3.4.

Table 3.4 Clinical description of complex V patients

Patient	Diagnosis	Clinical presentation
8993TG	Leigh syndrome	He presented with Leigh syndrome shortly after birth with intellectual delay, epilepsy and raised CSF lactate. Patient passed away before his first birthday.
8993TC	Leigh syndrome	Leigh syndrome presented with encephalopathy and respiratory failure. Patient is still alive now in his 20s with intellectual delay, mild movement disorder and urinary incontinence.

3.4.3.1 Mitophagy and autophagy in complex V mutant fibroblasts

Mitophagy was measured as described previously (section 3.4.1.1) by measuring the area of co-localising TOM20-labelled mitochondria and LC3 positive autophagosomes. The values were expressed as a percentage of total mitochondrial area. Mitophagy was decreased in both 8993 patient cultures at baseline and following 24 hours treatment with lysosomal inhibitors (EP) when compared to control cells (Figure 3.17 A). The two patient cultures were not different from each other at baseline. However, following the addition of EP, 8993TG fibroblasts derived from the more severe patient showed the lowest levels of mitophagy (Figure 3.17 A) followed by 8993TC fibroblasts. Autophagy levels measured by counting the number of LC3 positive punctae showed a similar pattern (Figure 3.17 B). The number of autophagosomes was significantly reduced in both patient derived cultures when compared to control cells at baseline. Autophagosome count remained below control levels in 899TG fibroblasts following EP treatment but was not different form controls in 8993TC cells. Representative images of TOM20 and LC3 labelled control 1 and patient fibroblasts are shown in Figure 3.18. A limiting factor for mitophagy and autophagy to occur is the availability of lysosomes. Lysosomal content was assessed by Lyso-ID labelling of live fibroblasts at baseline condition (25mM glucose) and following chloroquine treatment for 4 hours (60µM) (Figure 3.17 C). Lysosomal content of 8993TG fibroblasts was comparable with control levels both at baseline and after chloroquine treatment. The number of lysosomes detected in 8993TC cells was not different to control at baseline but significantly increased following chloroquine treatment. Representative images are shown in Figure 3.19.

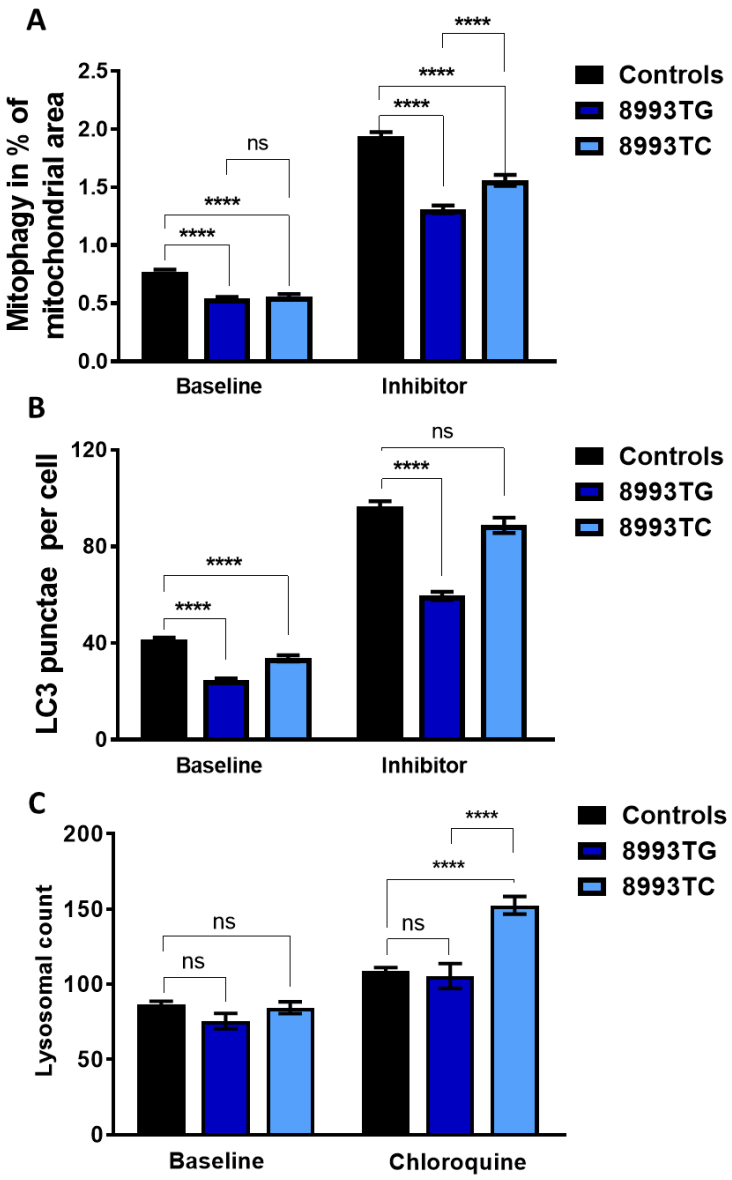

Figure 3.17 Mitophagy and autophagy in complex V mutant fibroblasts in 25mM glucose

(A) Mitophagy in 8993TG and 899TC mutant fibroblasts measured by the co-localisation of TOM20-labelled mitochondria and LC3 labelled autophagosomes expressed as the percentage of total mitochondrial area. (B) Autophagy in 8993TG and 899TC mutant fibroblasts was measured by counting the number of LC3 positive punctae. n=4, minimum of 1336 cell analysed per condition. Lysosomal inhibitors are E64d and Pepstatin A. (C) Number of lysosome counted by Lyso-ID staining of fibroblasts cultured either in 25mM glucose media (baseline) only or supplemented with 60µM chloroquine for 4 hours prior to imaging, n=2, minimum of 198 cell analysed per condition

Mean +/- 95% CI, **=p<0.01, ***=p<0.001, ****=p<0.0001

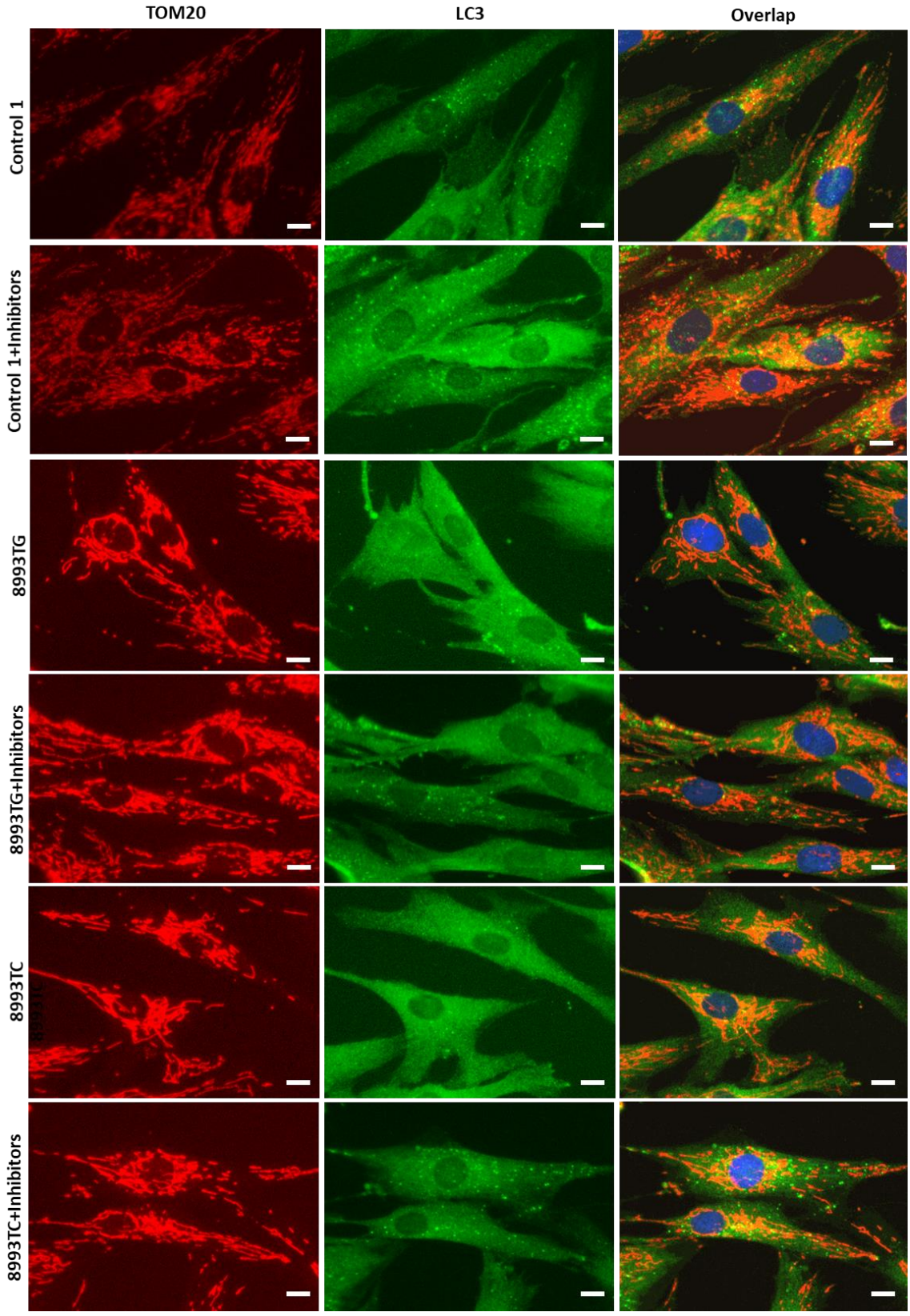

Figure 3.18 Representative images of Control 1 and 8993 fibroblasts
Showing TOM20-labelled mitochondria and LC3-labelled autophagosomes cultured either at baseline or with the addition of lysosomal inhibitors E64d and Pepstatin A. Scale bar 10µm.

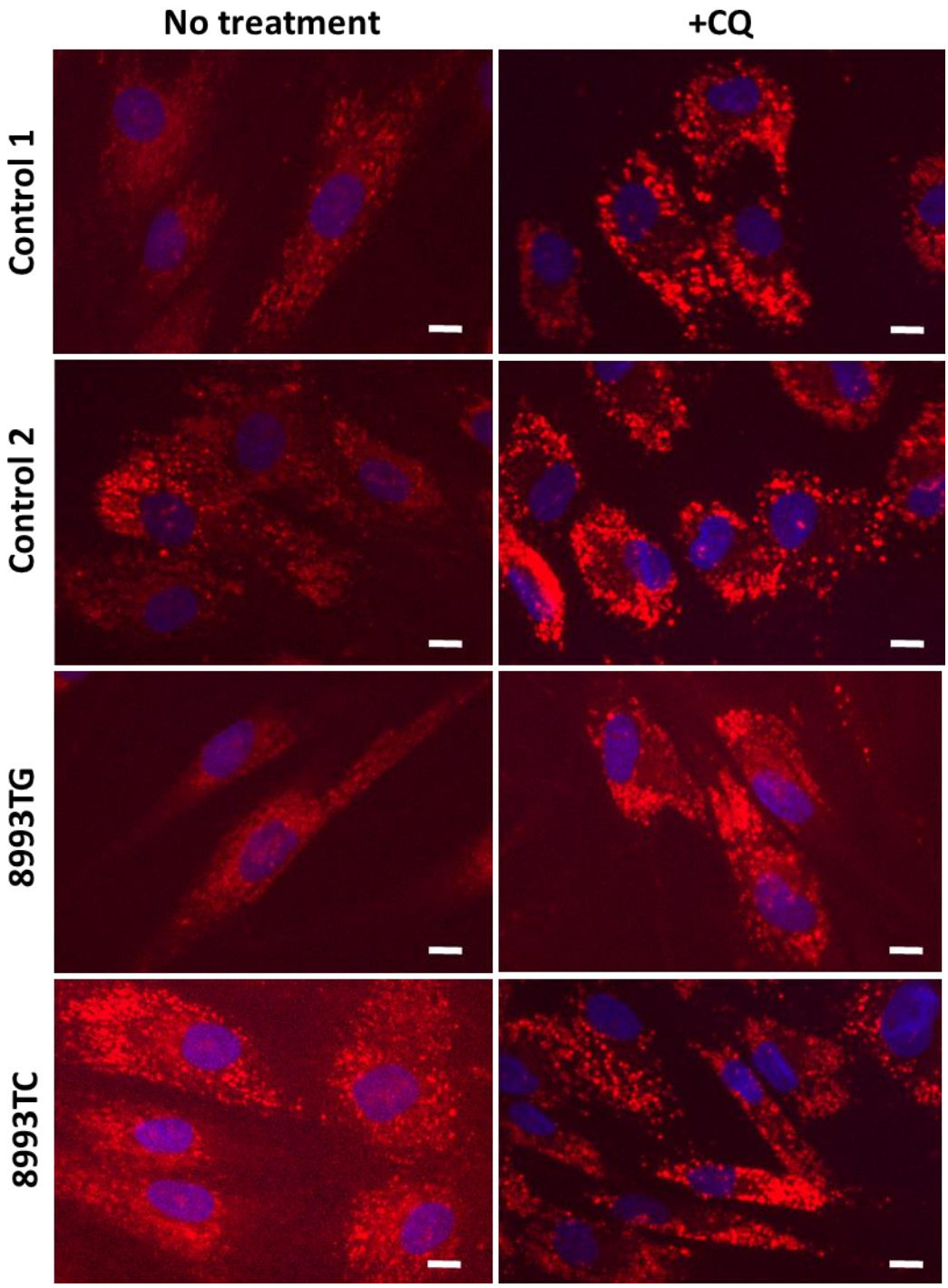

Figure 3.19 Representative images of control and 8993 fibroblasts labelled with Lyso-ID

Showing Lyso-ID (red) and Hoechst (blue) labelled fibroblasts with or without chloroquine (CQ) treatment. Scale bar 10µm.

In order to stimulate mitophagy and autophagy, 8993 mutant cells were subjected to the same energetic stress conditions as complex I mutant cells previously (section 3.4.1.1). Control and patient cells were cultured in either low glucose (3mM glucose) or galactose (0mM glucose, 10mM galactose) media for 24 hours prior to imaging. In 8993TG fibroblast mitophagy remained significantly below control levels in low glucose as well as galactose media without lysosomal inhibitors (EP) while 8993TC cells maintained their mitophagy at control levels under energetic stress (Figure 3.20 A). Following treatment with EP, mitophagy remained significantly below control levels in both patient cultures in low glucose as well as galactose (Figure 3.20 A). The low mitophagy observed was more pronounced in 8993TG fibroblasts derived from the patient with the more severe disease presentation. Autophagosome count in complex V mutant cells following 24 hours glucose starvation followed a similar pattern to that seen in high-glucose media (Figure 3.20 B). The number of LC3 punctae was significantly lower in 8993TG cells cultured in either low glucose or galactose media without additional treatment with lysosomal inhibitors when compared to control cells and remained significantly below control levels even after EP treatment. Nevertheless, the autophagsome count was not different from controls when 899TC fibroblasts in either in low glucose or galactose (Figure 3.20 B).

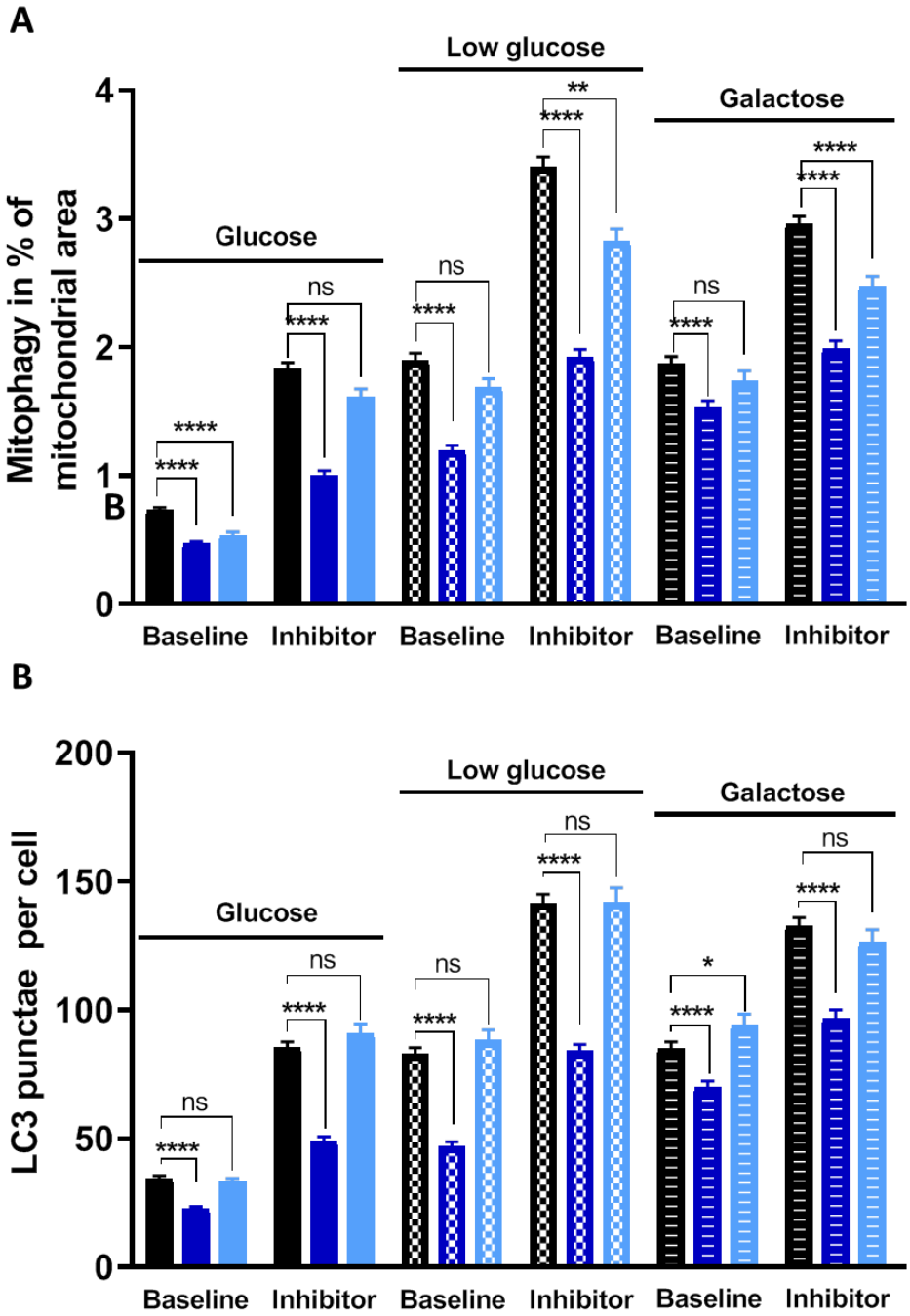

Figure 3.20 Mitophagy and autophagy in complex V mutant fibroblasts under energetic stress

(A) Mitophagy in 8993TG and 8993TC mutant fibroblasts. (B) Autophagy in 8993TG and 8993TC mutant fibroblasts. Lysosomal inhibitors are E64d and Pepstatin A. n=2, minimum of 863 cells analysed per condition, mean +/- 95% CI, *=p<0.05, **=p<0.01, ***=p<0.001, ****=p<0.0001

3.4.3.2 Mitochondrial network properties of complex V mutant fibroblasts

Mitochondrial fusion and fission plays a critical role in mitochondrial quality control. Dysfunctional mitochondria are separated from the rest of the network by fission and often refused re-entry to the healthy reticulum by the prevention of fusion and subsequent degradation via mitophagy (Twig et al., 2008). Nevertheless, stress-induced mitochondrial hyperfusion was shown to be protective during starvation by raising ATP levels and protecting functional mitochondria from degradation (Gomes et al., 2011). Mean mitochondrial length was significantly increased in both 8993 cultures when compared to control cells (Figure 3.21 A). There was no significant difference in length between the two patients. Mitochondrial membrane potential measured by TMRM staining was decreased in 8993TC fibroblasts derived from the milder patient but was not different from controls in 8993TG cells derived from the more severe patient (Figure 3.21 B).

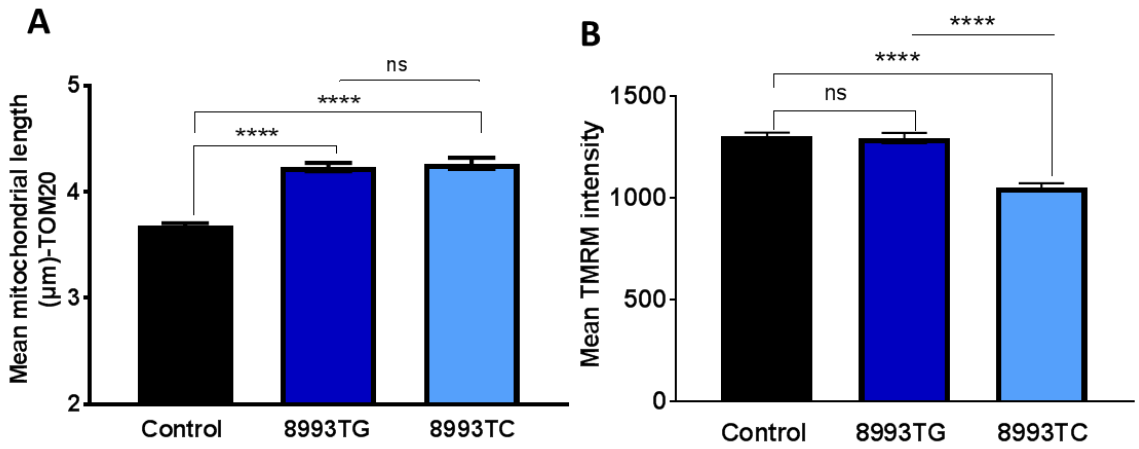

Figure 3.21 Mitochondrial network properties of complex V mutant fibroblasts
(A) Mitochondrial length measured by TOM20 staining, n=4, minimum of 1336 cell analysed per condition**.** (B) Mitochondrial membrane potential measured by TMRM staining, n=2, minimum of 1094 cells analysed per condition
Mean +/- 95% CI, ***=p<0.001; ****=p<0.0001

3.4.3.3 Bioenergetics of complex V deficient fibroblasts

Multiple investigations of the 8993 mtDNA mutations revealed that pathologic nucleotide changes at this position have a negative impact on ATP synthesis, the T>G nucleotide change more so than the T>C. However, neither of these mutations affect the assembly of complex V, but rather proton translocation and/or coupling efficiency (Cortes-Hernandez et al., 2007). Western blot analysis of OXPHOS complex subunits reinforces this notion as there was no visible difference in the protein levels of complex V subunit ATP5A between control and patient derived cells (Figure 3.22). Although neither the 8993TG nor the 8993TC mutations had an effect on ATP5A expression; complex I, II and IV subunit levels were all visibly reduced in patient cells compared to control ones. This was more pronounced in 8993TG fibroblast derived from the severe patient.

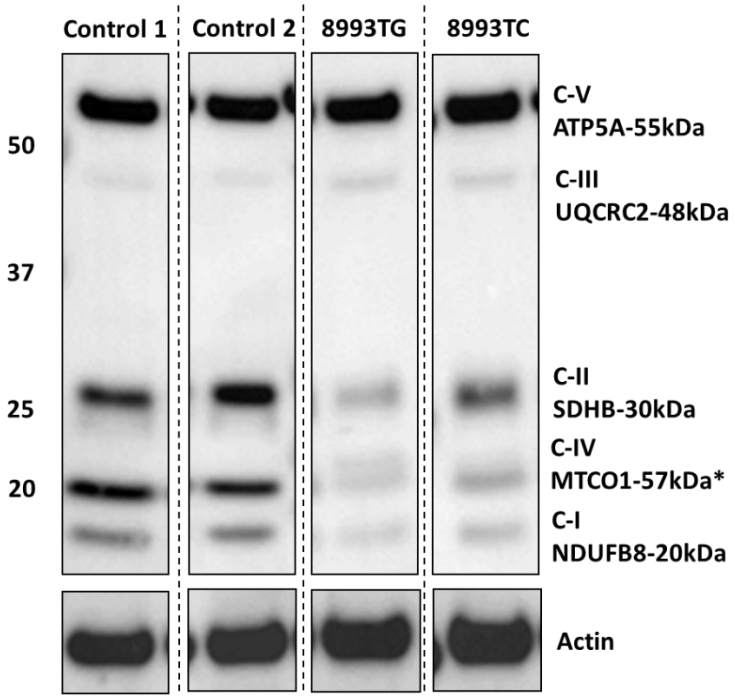

Figure 3.22 Protein expressions of OXPHOS complex subunits in complex V mutant fibroblasts
*Highly hydrophobic mtDNA encoded protein. Real MW is 57kDa but migrates differently in different systems according to manufacturer. n=2, representative image

Even though complex V assembly and structure seem to remain intact in 8993 mutant cells, the dysfunction caused by these mutations has a considerable impact on the rest of the electron transport chain. The reduced protein levels of the other complex subunits could negatively impact the bioenergetic status of these cells. Therefore, oxygen consumption rates were measured as described previously (section 3.4.1.3). There was no difference between the oxygen consumption rates of 899TG and control cells (Figure 3.23). The basal and ATP-linked respiration of 8993TC cells was comparable to control levels. However, maximal respiration was significantly lower in these cells compared to control ones (Figure 3.23).

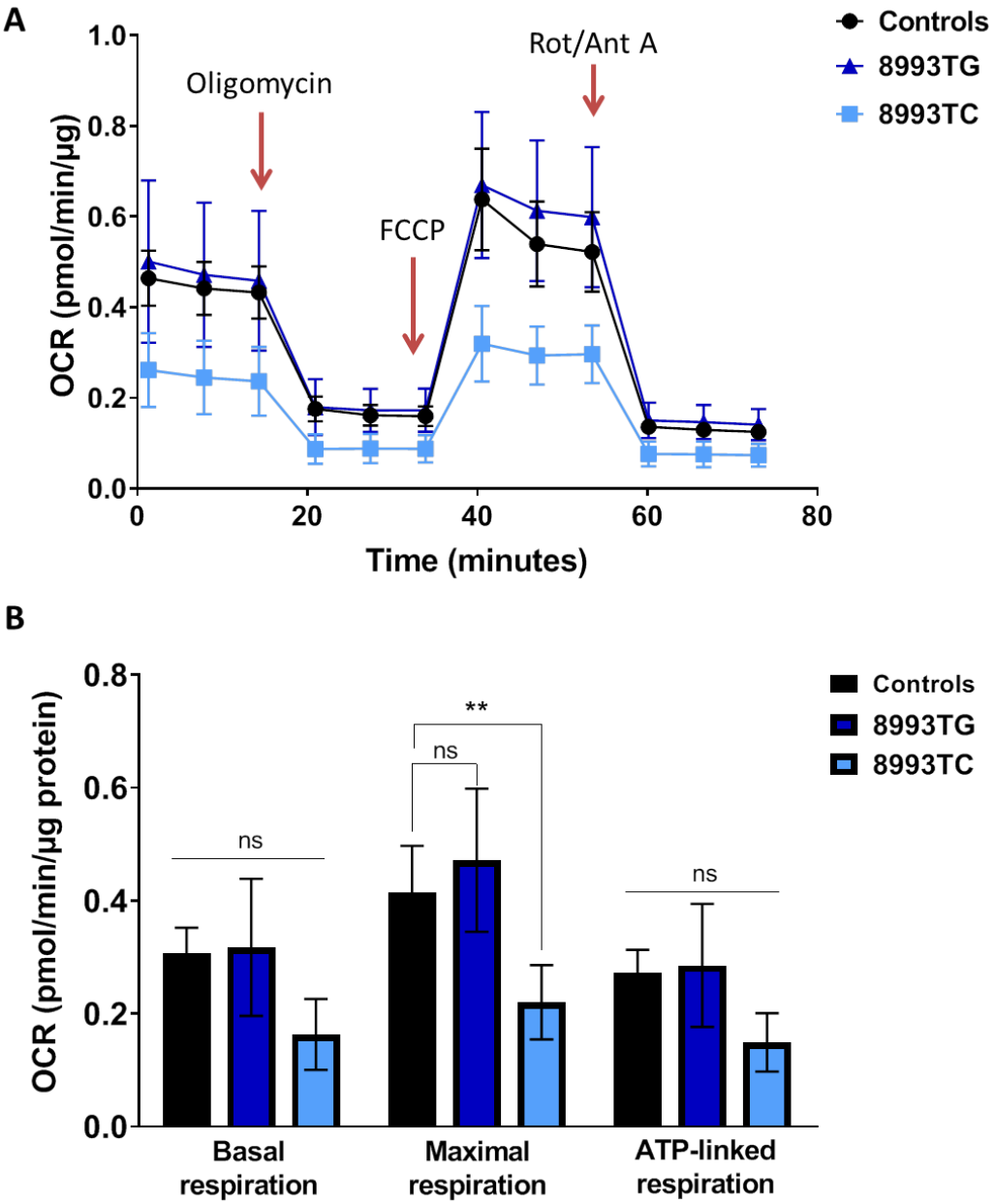

Figure 3.23 Oxygen consumption of 8993 mutant fibroblasts
(A) Kinetic graph of oxygen consumption measured at baseline and following to addition of rotenone (complex V inhibitor), FCCP (protonophore, to collapse membrane potential) and rotenone (complex I inhibitor)/ antimycin A (complex III inhibitor). (B) Calculated basal, maximal and ATP-linked respiration
Mean +/- 95% CI, **=p<0.01, n=1

3.4.3.4 Mitochondrial DNA content in fibroblasts with complex V mutations

A sufficient increase in mitochondrial DNA content in non-affected mutation carriers may contribute to incomplete penetrance in LHON (Giordano et al., 2014). It is also a common compensatory mechanism observed in relation to many mitochondrial diseases. The number of mitochondrial DNA nucleoids was assessed using the DNA specific dye PicoGreen. While mitochondrial DNA content of 8993TG fibroblasts was comparable to control levels, there was a significant increase detected in 8993TC cells derived from the milder patient (Figure 3.24 A). On the other hand, the total area of TOM20 labelled mitochondria did not increase simultaneously in 8993TC cells while in 8993TG fibroblasts it was significantly reduced (Figure 3.24 B).

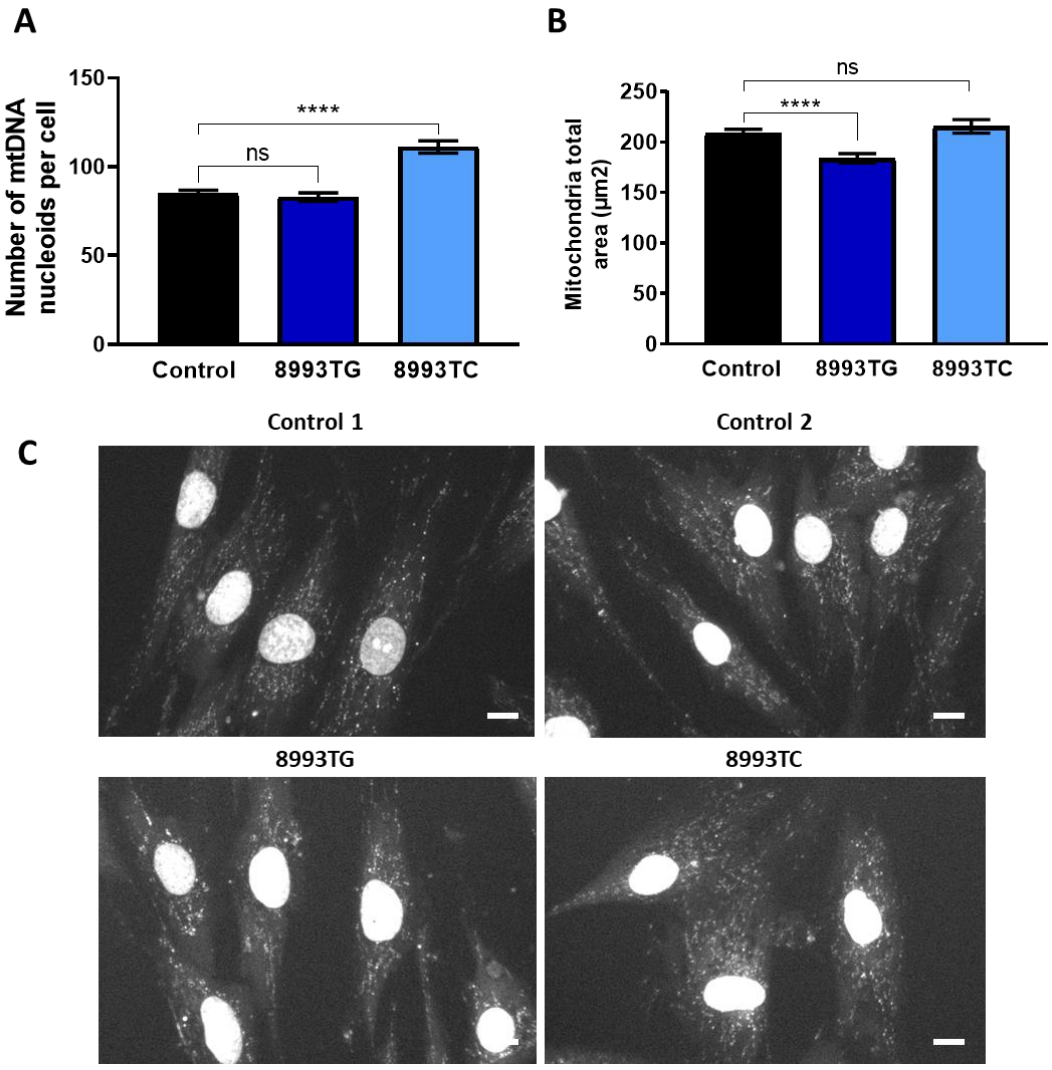

Figure 3.24 Mitochondrial DNA nucleoid and mitochondrial content in complex V mutant fibroblasts

(A) Number of mtDNA nucleoids measured by PicoGreen staining. (B) Mitochondrial content measured as the area of TOM20 labelled mitochondria. n=2, minimum of 1094 cells analysed per condition (C) Representative images of PicoGreen labelled control and patient fibroblasts, scale bar 10µm.

Mean +/- 95% CI, ****=p<0.0001

3.4.4 Discussion of complex V mutant specific findings (section 3.4.3)

A visual summary of all findings is presented in Table 3.5. I have shown that fibroblasts from patients with mutations at base pair 8993 have elongated mitochondria, with decreased mitophagy. This reduced mitophagy does not appear to be driven by mitochondrial membrane potential because only the 8993TC cells derived from the patient with the milder phenotype had reduced oxygen consumption and membrane potential. As in the complex I patients, his mitochondrial DNA content was increased in 8993TC cultures. This may reflect a compensatory mechanism for the depolarization in both groups of patients. However, the patient with the more severe defect (8993TG) had no change in membrane potential or mtDNA content. Previous investigators have shown that the more severe m.8993T>G mutation (Leu156Arg) prevents synthetic activity of the enzyme by impairing intra enzyme coupling between functional proton transport and c-ring rotation, thus preventing ATP synthesis (Baracca et al., 2007) while others suggested a blockage of the proton channel (Sgarbi et al., 2006). In case of m.8993T>C (Leu156Pro) the coupling is preserved but the proton translocation is inhibited by approximately 30% thus down regulating the ATP synthesis to a similar extent. Preservation of the proton translocation presumably explains why the m.8993TC cells are depolarized relative to m.8993TG cells. Additionally, 899TG cells demonstrated a general autophagy defect, which was not apparent in 8993TC cells. The reduced mitophagy in 8993 mutants may be very relevant to a pressing problem for genetic management of affected families, namely the mitochondrial bottleneck, which occurs due to the dilution of mtDNA during oocyte maturation. Most mtDNA mutations are transmitted at various and unpredictable heteroplasmy levels but

often show a heteroplasmy scattered around the woman's own level (Sallevelt et al., 2017). The only exception is the 8993 point mutation that shows a skewed segregation that is either close to 0% or over 90% (Blok et al., 1997; Sallevelt et al., 2013). This unique pattern of segregation could have several different causes; however, mitophagy is the only currently known mechanism to turn over mtDNA as part of the whole organelle. The reduced mitophagy detected in 8993 fibroblast may contribute to the unusual segregation pattern of these mutations by allowing the unrestricted clonal proliferation of mutant mtDNA.

Neither the decreased mitophagy nor the low levels of autophagy in 8993TG fibroblasts was secondary to a decrease in lysosomal content in the cells, although there were no functional assays performed. The mitochondrial network was significantly elongated in fibroblasts derived from both patients. Tondera and colleagues described that stress-induced mitochondrial hyperfusion protects mitochondria from turnover by mitophagy during nutrient starvation while increasing the efficiency of ATP production (Tondera et al., 2009). Mean mitochondrial length was significantly increased in both patient cultures compared to control cells, which may contribute to decreased mitochondrial turnover, however, it does not account for the general autophagy defect detected in 8993TG fibroblasts.

3.5 Overall chapter discussion

The aim of this chapter was to investigate mitophagy in fibroblasts derived from patients with mitochondrial disease due to various mtDNA mutations. For a visual representation of all the results from sections 3.4.2 and 3.4.4 please refer to Table 3.5.

Although efficient mitophagy should ensure the presence of a healthy and well-functioning mitochondrial pool within cells, it is often overlooked when investigating mitochondrial disease. I showed that mitophagy was increased in six out of eight fibroblast cultures with complex I mutations and substantially decreased in the two complex V mutant cultures investigated. The heterozygous presence of the common c.439A>G TSPO polymorphism in two complex I mutant cultures could be a major contributor to the low mitophagy detected in these cells. TSPO is a mitochondrial OMM protein that coordinates cholesterol and porphyrin transport from the cytosol into the organelle (Li et al., 2016), and was shown to regulate ROS dependent mitophagy (Gatliff et al., 2014). This is a novel finding as the relationship between the c.439A>G polymorphism, which is present in the majority of the population; and mitophagy has never been investigated to our knowledge.

Table 3.5 Summary of the main findings

Patient	Gene	Mutation	Mitophagy (+EP)	Autophagy (+EP)	OXPHOS defect	Membrane potential	mtDNA content	Mito fragmentation (TOM20)	Perinuclear clustering of mitochondria	Lysosomal content (+CQ)
13051A	*MT-ND5*	m.13051G>A	↑	↑	yes	↓	↑	elongated	No	N/A
13051B	*MT-ND5*	m.13051G>A	↓	↑	yes	↓	↑	yes	No	↔
11778A	*MT-ND4*	m.11778G>A	↑	↑	N/A	↓	↑	yes	No	↑
11778B	*MT-ND4*	m.11778G>A	↑	↑	N/A	↓	↑	yes	No	↑
8993TG	*MT-ATP6*	m.8993T>G	↓	↓	no	↔	↔	elongated	No	↔
8993TC	*MT-ATP6*	m.8993T>C	↓	↔	yes	↓	↑	elongated	No	↑

There may be multiple causes for the increased mitophagy detected in six fibroblast cultures with complex I mutations. NADH:ubiquinone oxidoreductase is the largest enzyme complex of the ETC. It is also the main site of ROS production (Murphy, 2009). While reactive oxygen species are important intracellular signalling molecules (Chandel, 2014), their excessive generation can lead to lipid peroxidation as well as DNA damage. These ultimately would have a detrimental effect on the entire organelle. Each fibroblast culture investigated harboured a single point mutation in either the ND4 or the ND5 subunit of complex I. Both of these complexes are part of the evolutionarily conserved 'core' enzyme (Yip et al., 2011) and therefore are essential for complex assembly and function. Complex I, III and IV were shown organize into so called respiratory supercomplexes in various stoichiometric ratios (Schagger, 2001). This assembly confers structural advantages by stabilization, as well as functional ones by increasing efficiency of both electron and proton transport while reducing leakage (Schagger, 2001; Dudkina et al., 2010). Defects in complex I assembly would disrupt supercomplex assembly and compromise the entire electron transport chain. Western blot analysis also revealed reduced protein expression of complex I, II and IV protein subunits in 8993 mutant cells. This suggests that the reasons behind the pathological effect of these mutations are beyond just isolated complex V dysfunction. Additionally, to ATP deficiency, heightened oxidative damage as a result of increased ROS is also suspected to contribute to the pathology of complex V deficiency (Baracca et al., 2007).

3.6 Limitations of this study

Oxygen consumption data is derived from a single run (n=1), although a minimum of five wells were used for each fibroblasts culture. Additional biological replicates are needed to confirm the differences presented here prior to publication.

There were no cells available from non-symptomatic family members of the complex I patients presented here. Measuring mitophagy in fibroblast of non-symptomatic mutation carriers would greatly add to the findings presented here.

3.7 Future directions

Considering the novel discovery of a potential relationship between mitophagy and the common c.439A>G TSPO polymorphism, our group has received funding to genotype a range of our control and patient fibroblasts for the presence of this nucleotide change.

Mitophagy was shown to be dysregulated in numerous patient derived fibroblasts although the molecular drivers of this phenomenon remain unknown. Dissecting the molecular pathways participating in the various forms of mitophagy would increase the attractiveness of targeting this process for therapy not just for mitochondrial disease but also age related neurological disorders and potentially cancer.

Further investigating mitophagy in 8993 mutant cells could shed some light on the connection between mtDNA segregation and mitophagy.

Chapter 4. Characterisation of fibroblasts derived from patients with mitochondrial disease resulting from nuclear DNA mutations

4.1 Introduction

Mitochondrial DNA has 37 genes of which 13 are protein coding and the remaining 24 encoding tRNAs and rRNAs necessary for their translation. The remaining mitochondrial proteins required for the correct functioning of mitochondria are encoded by the nuclear genome, translated in the cytoplasm and are imported into the mitochondria based on a mitochondrial targeting signal (MTS). Additionally, there are proteins such as the mitochondrial fission proteins DNM1L that do not form an integral part of the organelle, but is part of the mitochondrial proteome. DNM1L is located in the cytoplasm and recruited to mitochondria by OMM receptors (Loson et al., 2013). Genes that are predicted to and/or experimentally verified to encode mitochondrial proteins have been collated into publicly available databases such as MitoCarta. Currently there are 1158 genes listed in MitoCarta 2.0 with strong support of mitochondrial localization (Calvo et al., 2016). This represents an estimated 85% of the actual mitochondrial proteome, which would total around 1,400 proteins.

The application of next generation sequencing has greatly advanced the diagnosis of mitochondrial disease, and many genes that cause Mendelian mitochondrial disorders have now been identified. As a result, further members of the mitochondrial proteome have been recognised and characterized. In 2012 over 240 nuclear encoded proteins that are targeted to mitochondria were linked to human diseases (Koopman et al., 2012). These proteins can be broadly categorised by their functions into structural OXPHOS elements, OXPHOS assembly factors, mtDNA maintenance, mitochondrial homeostasis, internal quality control proteins and proteins that regulate mitochondrial dynamics (Lightowlers et al., 2015).

4.2 Aims of chapter 4

I. To investigate mitophagy in fibroblasts derived from patients with confirmed mitochondrial disease due to nDNA mutations using high-content imaging.

II. To further characterise selected patient cells using a combination of cell biological and biochemical approaches.

4.3 Materials and methods

4.3.1 Patient and control fibroblasts

The control fibroblast cultures used in this chapter are the same as the ones described in chapter 3 (section 3.3.1).

FBXL4 fibroblasts were received from Professor Ellen Crushell, Temple Street Children's University Hospital, Dublin 1, Ireland.

CHCHD10 S59L fibroblasts were received from Professor Veronique Paquis-Flucklinger IRCAN, UMR CNRS 7284/INSERM U1081/UNS, School of Medicine, Nice Sophia-Antipolis University, and Department of Medical Genetics, National Centre for Mitochondrial Diseases, Nice Teaching Hospital, France.

DNM1LB fibroblasts were received from Dr Andrea Whitney, Department of Paediatrics, University Hospital Southampton NHS Foundation Trust.

The remaining fibroblast cultures were donated by patients in JP's outpatient clinic with the approval of the UK National Research Ethics Service (South Central-Berkshire).

For all other materials and methods please refer to chapter 2.

4.4 Results

Fibroblast cultures were available from seventeen patients with mitochondrial disease due to nuclear genetic mutations and an additional two cultures were derived from new-borns who passed away unexpectedly and therefore were diagnosed with sudden unexplained death in infancy (SUDI). A preliminary screen for dysregulated mitophagy was concluded on all nineteen fibroblast cultures. Mitophagy was measured as described previously by quantifying the area of co-localising LC3 punctae and mitochondria, and expressing that as the percentage of total mitochondrial area both at baseline (25mM glucose) and following treatment with lysosomal inhibitors E64d and Pepstatin A (EP). The results of the screen are summarized in Table 4.1. Of the nineteen patient derived fibroblast cultures, sixteen showed robustly increased mitophagy following treatment with lysosomal inhibitors E64d and Pepstatin A (EP), indicated by ↑ (p<0.05). Mitophagy was not significantly different from control cells (↔) in the remaining four fibroblast cultures. Fibroblasts derived from eight patients were selected for further investigation; these are highlighted in Table 4.1 (grey). Representative images of those patient cultures that are not discussed further in detail in this chapter are shown in Figure 4.1 for mutations in OXPHOS assembly factors, in Figure 4.2 for OXPHOS structural genes and in Figure 4.3- and 4.4 for mutations in proteins involved in mitochondrial homeostasis.

Table 4.1 Summary of mitophagy results on fibroblasts derived from patients with nuclear genetic mutations

Patient identifier	*Gene*	Mutation	Mitophagy
ACAD9A	*ACAD9*	c.1168G>A (p.Ala390Thr); c.1150G>A (p.Val384Met)	↔
ACAD9B	*ACAD9*		↑
NDUFS7	*NDUFS7*	c.1390897C>G (p.Leu86Val) 1390975G>A (p.Ala112Thr)	↑
NDFUA6	*NDUFA6*	c.191G>C (p.Arg64Pro), c.265G>T (p.Glu89*)	↔
POLG	*POLG*	c.752C>T (p.Thr251Ile); c.1760C>T (p.Pro587Leu)	↑
OPA1	*OPA1*	c.2708_2711delTTAG (p.Val903fs); c.1146A>G (Ile382Met)	↑
MFN2	*MFN2*	*De novo* missense c.310C>T mutation (F) (p.Arg104Trp)	↑
DNM1LA	*DNM1L*	c.1207C>T (p.Arg403Cys)	↑
DNM1LB	*DNM1L*	c.1207C>T (p.Arg403Cys)	↑
FBXL4A	*FBXL4*	c.1641_1642delTG: (p.Cys547*); c.1790A>C: (p.Gln597Pro)	↑
FBXL4B	*FBXL4*	c.1641_1642delTG: (p.Cys547*); c.1790A>C: (p.Gln597Pro)	↑
G58R	*CHCHD10*	c.172G>C (p.Gly58Arg)	↑
S59L	*CHCHD10*	c.176C>T (p.Ser59Leu)	↑
SPG7	*SPG7*	c.1454_1462del (p.Arg485_487del) c.1672A>T (p.Lys558*)	↑
PIGN1	*PIGN1*	c.283C>T (p.Arg95Trp)	↑
TRIAP1	*TRIAP1*	c.194delT (p.M65fs)	↑
CNTNAP1	*CNTNAP1*	c.635T>C (p.Leu212Pro); c.1677G>A (p.Trp559Ter)	↑
SUDI	*N/A*	N/A	↔
SUDI	*N/A*	N/A	↑

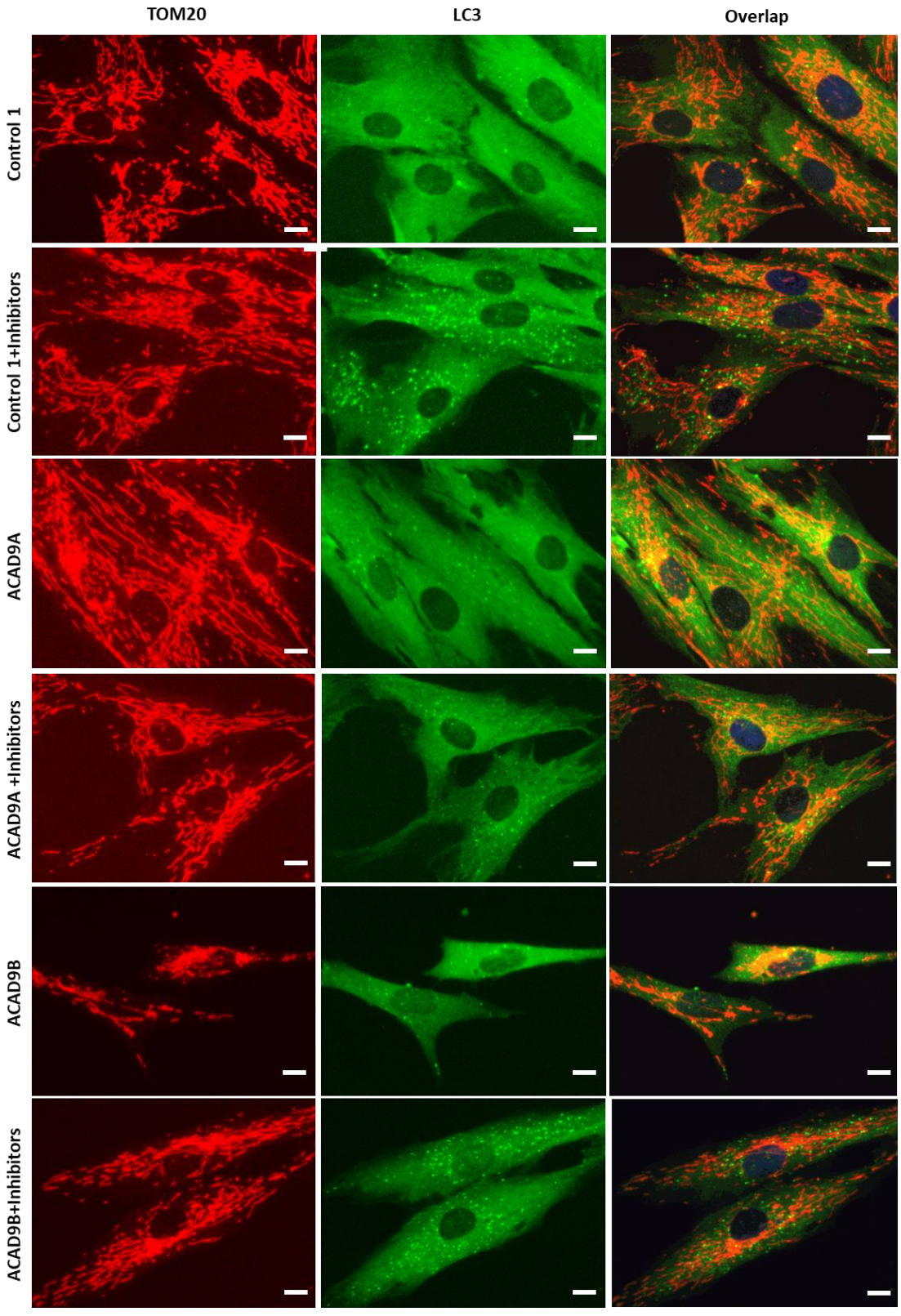

Figure 4.1 Representative images of Control 1 and patient fibroblasts with mutations in OXPHOS assembly factors

Showing TOM20-labelled mitochondria and LC3-labelled autophagosomes cultured either at baseline or with the addition of lysosomal inhibitors E64d and Pepstatin A. Scale bar 10µm.

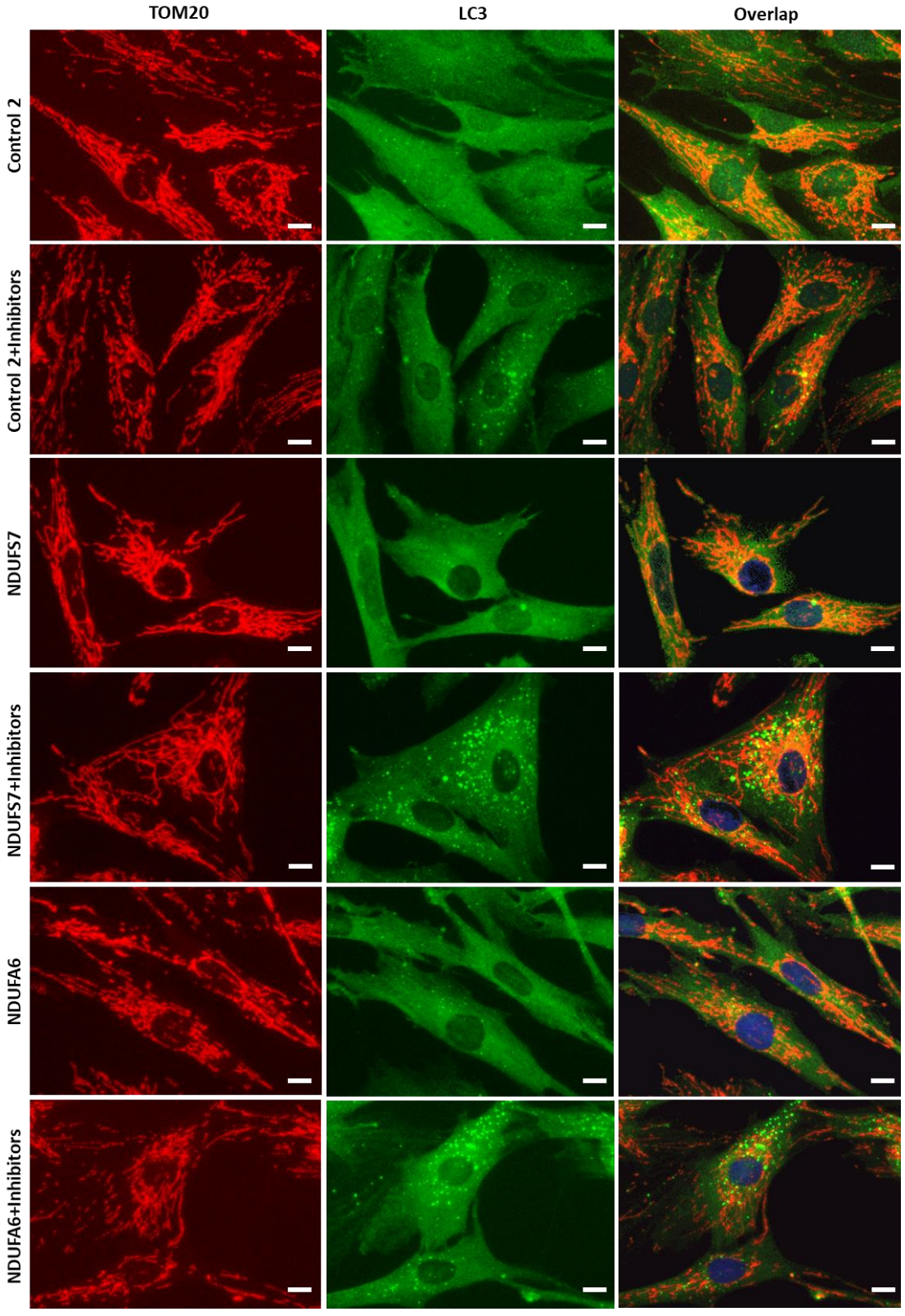

Figure 4.2 Representative images of Control 2 and patient fibroblasts with mutations in OXPHOS structural genes

Showing TOM20-labelled mitochondria and LC3-labelled autophagosomes cultured either at baseline or with the addition of lysosomal inhibitors E64d and Pepstatin A. Scale bar 10µm.

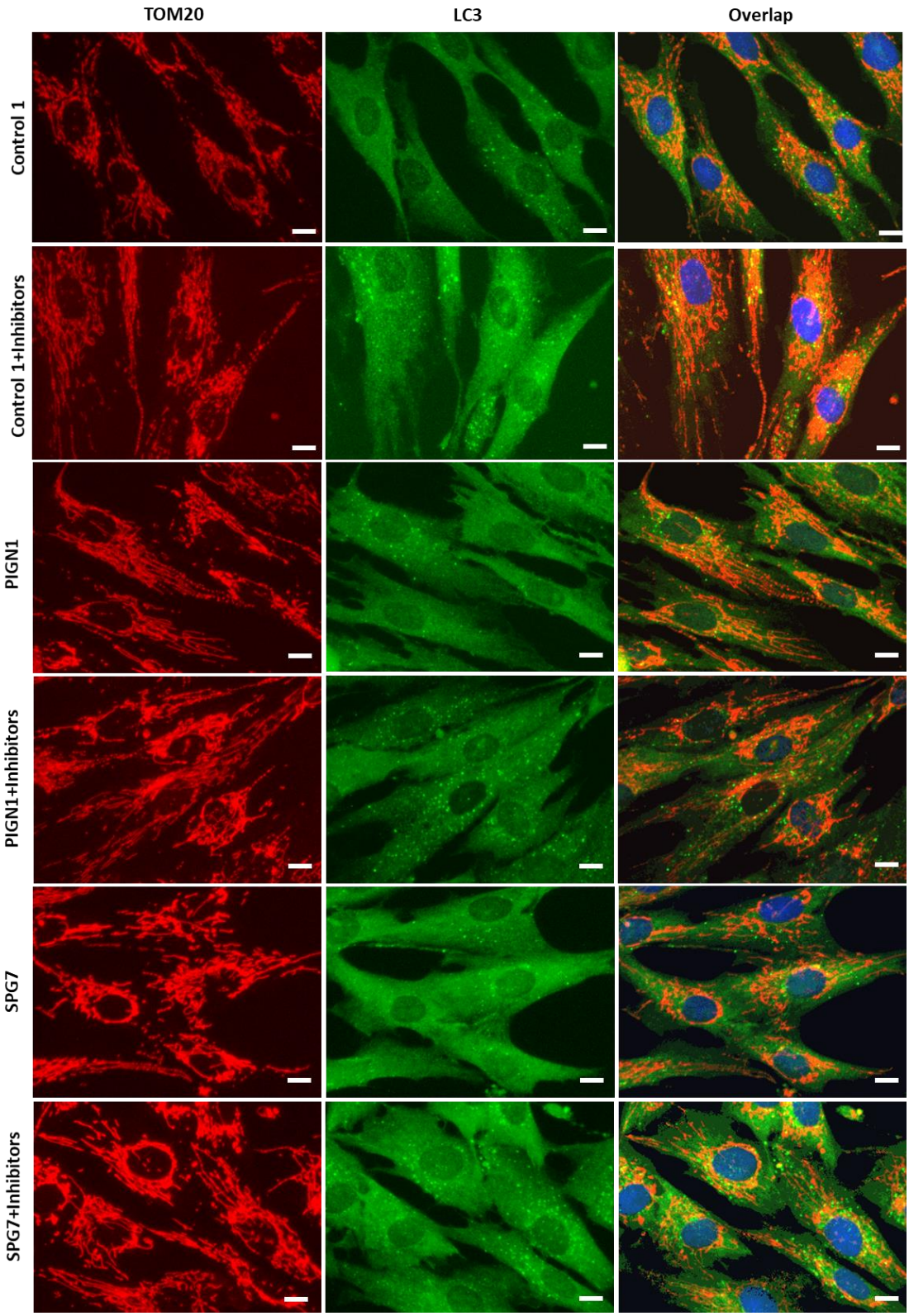

Figure 4.3 Representative images of Control 1 and patient fibroblasts with mutations in genes involved in mitochondrial homestasis-1
Showing TOM20-labelled mitochondria and LC3-labelled autophagosomes cultured either at baseline or with the addition of lysosomal inhibitors E64d and Pepstatin A. Scale bar 10µm.

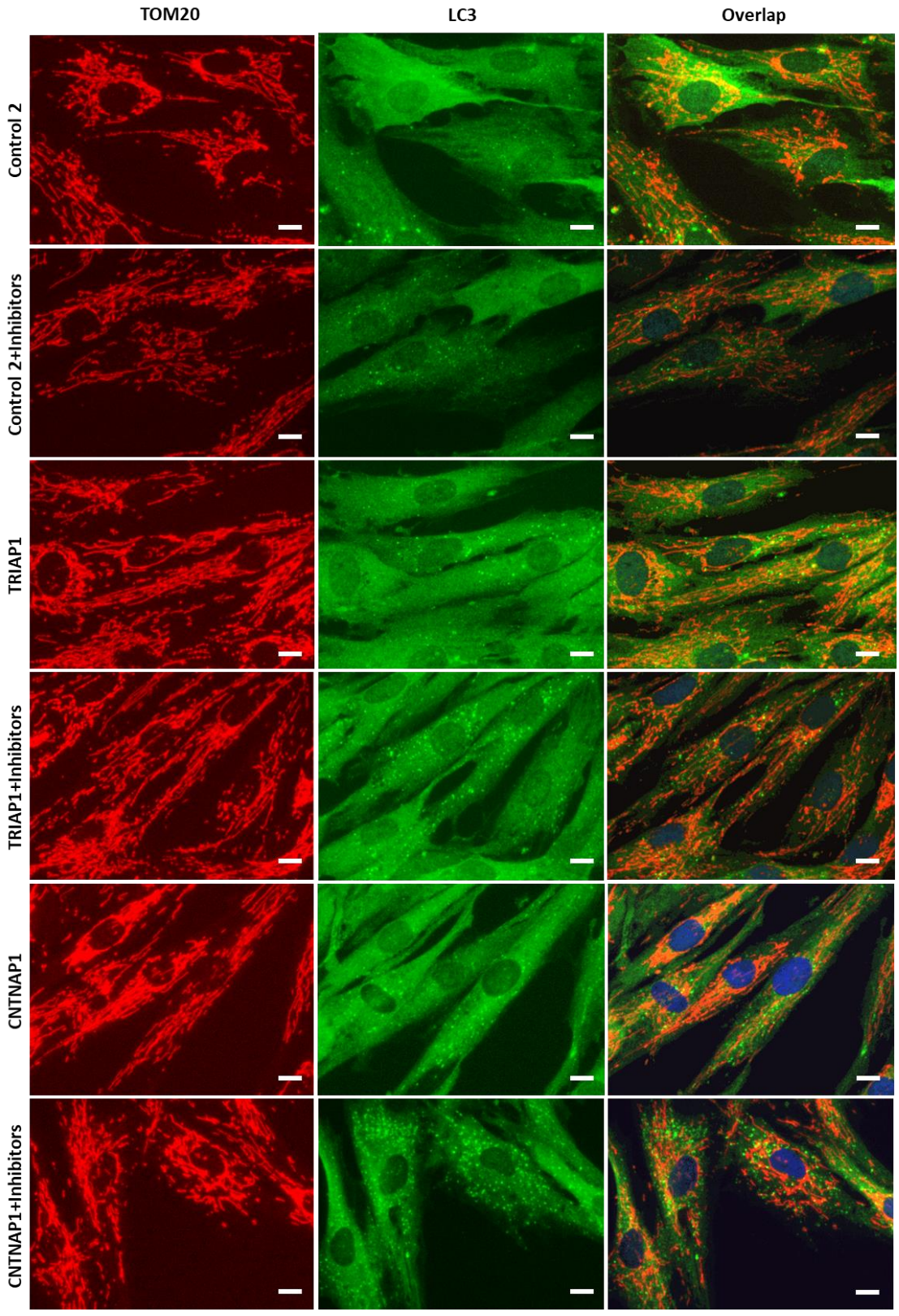

Figure 4.4 Representative images of Control 2 and patient fibroblasts with mutations in genes involved in mitochondrial homestasis-2
Showing TOM20-labelled mitochondria and LC3-labelled autophagosomes cultured either at baseline or with the addition of lysosomal inhibitors E64d and Pepstatin A. Scale bar 10µm.

Half of the selected patients had defects in proteins affecting mitochondrial dynamics (DNM1L, OPA1 and MFN2). Two patients had mutations in genes encoding pro-fusion proteins. One of them is a *de novo* missense mutation affecting the OMM protein MFN2 and the other is a compound heterozygous mutation in OPA1, encoding the IMM fusion protein. Additionally, two non-related patients were selected who carried the same homozygous mutation in DNM1L, altering the mitochondrial fission protein. The other half of the selected patients harboured mutations in genes that regulate mitochondrial homeostasis. The exact function of the proteins encoded by these genes is still unknown. Two siblings with heterogeneous pathologies were compound heterozygous for the same mutations in FBXL4. While two unrelated patients carried mutations affecting neighbouring amino acids in CHCHD10. Furthermore, fibroblasts derived from a patient with compound heterozygous POLG mutations resulting in severe mtDNA depletion will be discussed in Chapter 5. Mutations in OPA1 (Liao et al., 2017), DNM1L (Ladds et al., 2018) and FBXL4 (Almannai et al., 1993) have also been associated with mitochondrial DNA depletion syndromes. Additional results on the selected eight patient cultures are presented in the following sections. A short introduction on patient pathology and the currently known functions of the affected protein is included at the beginning of each section.

4.4.1 Patients with *DNM1L* mutation and mitochondrial fission defects

Mitochondria are dynamic organelles and their ability to perform fusion and fission is important for efficient function in the several physiological processes they are involved in (Section 1.1.3). Mitochondria undergoes symmetric fission in order to replicate and expand the mitochondrial pool. On the other hand, asymmetric fission maintains mitochondrial fitness by isolating damaged organelle components for recycling by mitophagy (de Castro et al., 2010; Shirihai et al., 2015). Additionally, fission is necessary for the efficient transport of mitochondrial fragments required for the local energy requirements of the cell.

The main mediator of mitochondrial fission is DNM1L, a member of the dynamin superfamily of GTPases (Smirnova et al., 2001). DNM1L is a cytosolic protein that is recruited to the mitochondria by OMM receptors (Loson et al., 2013) and forms a homo-oligomeric ring around the division site. DNML1 constricts the mitochondrial tubule in a GTP-dependent manner. The final step of the division process is executed by another GTPase called Dynamin 2 (Lee et al., 2016). The ER plays an important role in DNM1L-dependent division, as a projection of ER membrane wraps around the mitochondria to mark the division site (Friedman et al., 2011). A large proportion of ER-marked DNM1L-dependent division events occur in the close vicinity of newly synthesized mtDNA nucleoids, suggesting that DNM1L also plays a vital role in the distribution of mtDNA throughout the network, by contributing to nucleoid division.

Mutations in DNM1L were reported to cause cardiomyopathy in the mouse (Ashrafian et al., 2010), while in humans the commonest phenotypes are epileptic encephalopathy (Fahrner et al., 2016) and lethal infantile encephalopathy (Chao et al., 2016). In this section I will present data on fibroblasts derived from two unrelated

individuals harbouring the same *de novo* recurrent mutation (c.1207C>T p.Arg403Cys) (Ladds et al., 2018). The R403C mutation impacts a critical amino acid residue within the middle domain of DRP1 and was shown to act by a dominant-negative by reducing the oligomerization of the protein, and therefore, mitochondrial fission activity (Fahrner et al., 2016).

Patient DNM1LA presented with moderate language delay, and prolonged partial seizures at the age of three following a viral illness. Muscle biopsy showed atrophy of type II muscle fibres. Muscle mtDNA content was 33% of normal levels, which is classed as borderline depletion. He also had a borderline low CIV activity. Patient DNM1LB had mild general developmental delay and seizures triggered by febrile illness at the age of 5. Muscle biopsy showed a few cytochrome oxidase negative fibres but mtDNA content and respiratory chain activities were normal. Lipid content was increased in muscle from both patients.

4.4.1.1 Mitophagy and autophagy in DNM1L fibroblasts

The R403C mutation was shown to reduce fission activity of the DNM1L protein by impairing oligomerization of the protein as well as its recruitment to mitochondria (Fahrner et al., 2016). Despite the presumed fission defect, mitophagy was increased in both DNM1L cultures compared to controls (Figure 4.5 A). The increase was significant at baseline and following EP treatment. Mitophagy was highest in inhibitor treated DNM1LB cells derived from the milder patient. The number of LC3 positive punctae corresponding to autophagy followed a similar pattern (Figure 4.5 B). Representative images of TOM20 and LC3 labelled fibroblasts are shown in Figure 4.6. Autophagy was increased in both patient derived cultures compared to control ones. The increase was significant at baseline and after inhibitor treatment. Much the same as mitophagy, autophagy was the highest in DNM1LB fibroblasts. Lysosomal count was available from DNM1LA cells only (Figure 4.5 C). The number of lysosomes detected in DNM1LA cells was significantly lower both at baseline and following 4 hours chloroquine treatment when compared to control cells (Figure 4.5 C). Representative images are shown in Figure 4.7.

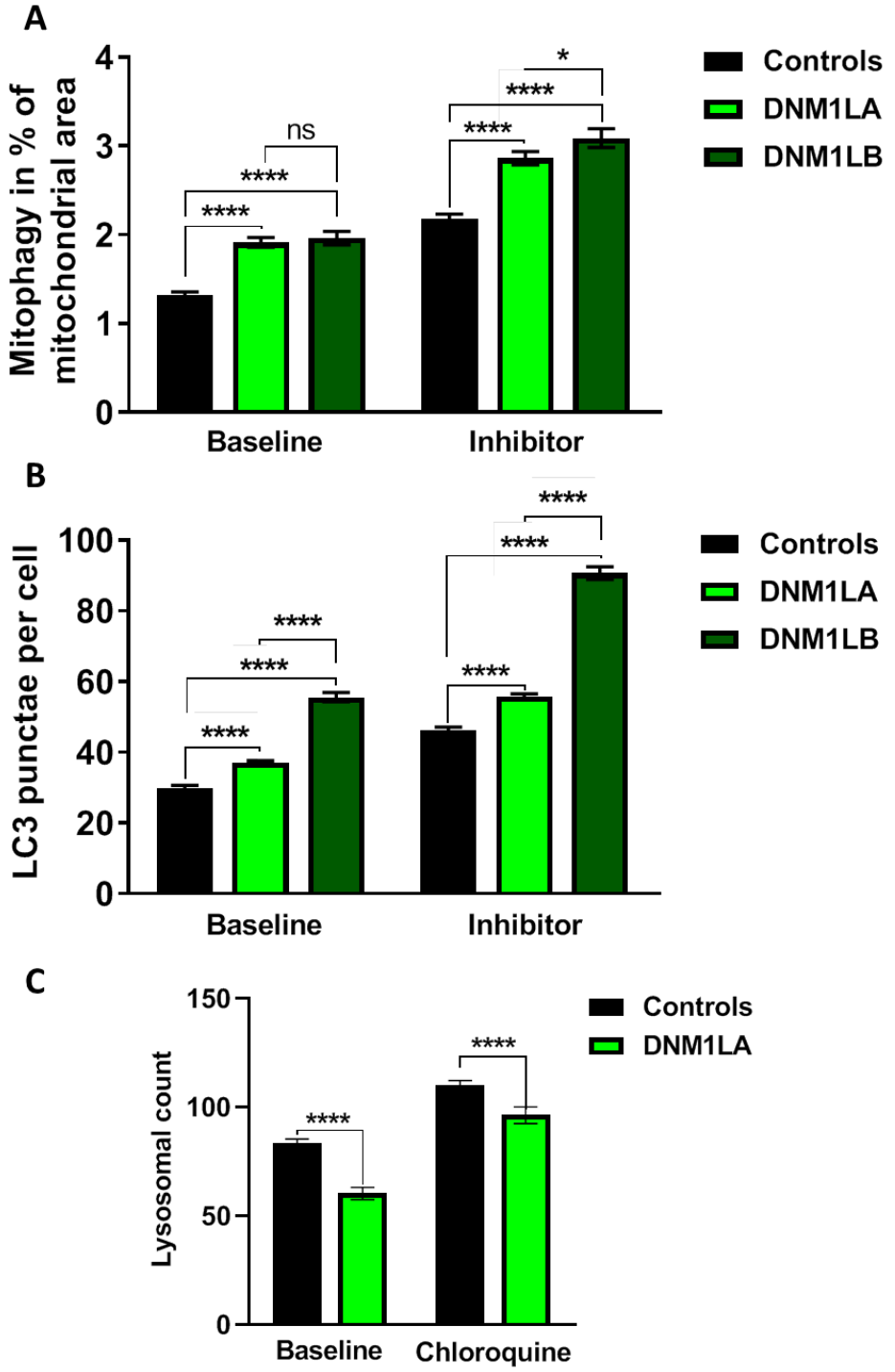

Figure 4.5 Mitophagy and autophagy in DNM1L fibroblasts
(A) Mitophagy and (B) autophagy measured at baseline and following 24 hours treatment with lysosomal inhibitors E64d and Pepstatin A (EP, 10µg/ml), n=3, minimum of 1128 cells analysed per condition, (C) Lysosome count at baseline and following 4 hours chloroquine (60µM) treatment, n=2, minimum of 621 cells analysed. Mean +/- 95% CI, *=p<0.05, ****=p<0.0001

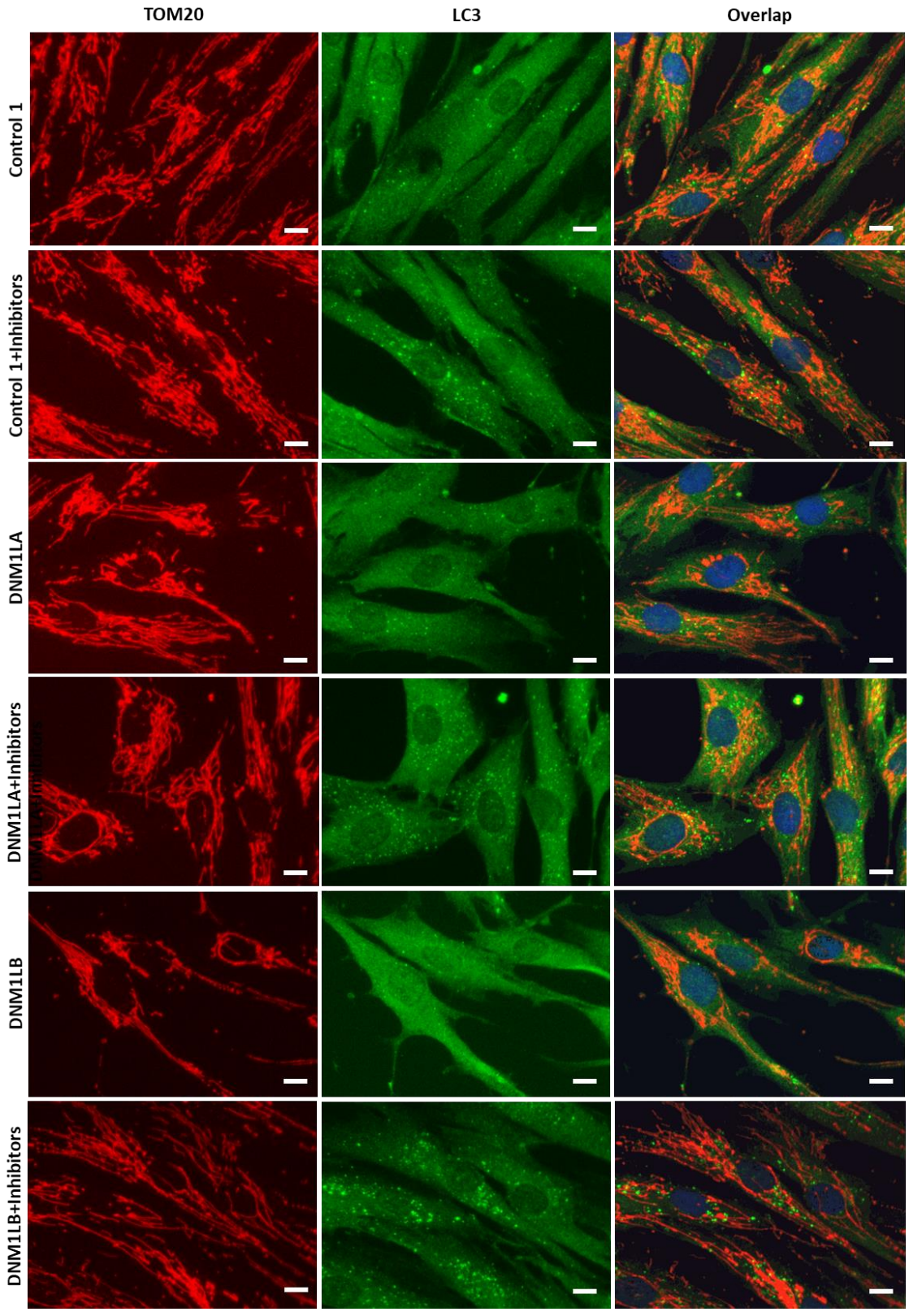

Figure 4.6 Representative images of Control 1 and DNM1L fibroblasts
Showing TOM20-labelled mitochondria and LC3-labelled autophagosomes cultured either at baseline or with the addition of lysosomal inhibitors E64d and Pepstatin A. Scale bar 10µm.

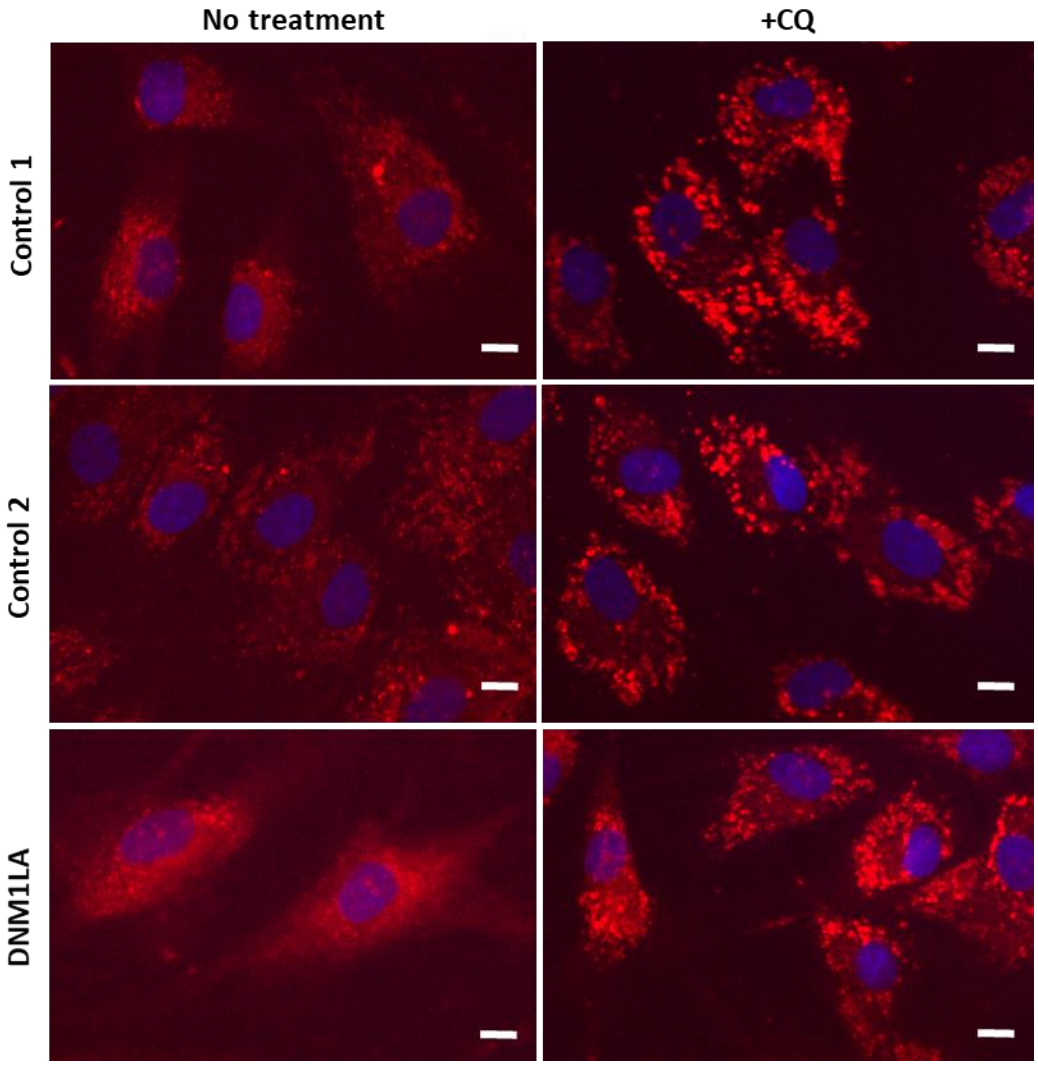

Figure 4.7 Representative images of control and DNM1L fibroblasts labelled with Lyso-ID
Showing Lyso-ID (red) and Hoechst (blue) labelled fibroblasts with or without chloroquine (CQ) treatment. Scale bar 10µm.

4.4.1.2 Mitochondrial network properties of DNM1L fibroblasts

Mean mitochondrial length was measured in fixed cells of TOM20 labelled mitochondria (Figure 4.8). In line with a fission defect, mean mitochondrial length was increased in both patient derived cultures when compared to control ones (Figure 4.8 A). The increase was more pronounced in DNM1LA fibroblast derived from the patient with the more severe phenotype. DNM1L activity is regulated by post-translational modification. Phosphorylation of the protein at residue Ser-616 (S616) was shown to activate fission activity of the protein, while phosphorylation at Ser-637 (S637) was shown to have an inhibitory effect (Hu et al., 2017). Phosphorylation at S616 was visibly increased in DNM1LB fibroblasts compared to control and DNM1LA cells (Figure 4.8 B). Expression of S637 pDNM1L was the highest in control cells. There was no visible difference between control and DNM1L mutant cells in the expression of the pro-fusion protein OPA1 (Figure 4.8 B) suggesting that lengthening of mitochondria is the result of unopposed fusion rather than upregulation of fusion activity. TMRM intensity corresponding to mitochondrial membrane potential was significantly increased in both DNM1L cultures when compared to control cells (Figure4.8 C). There was no difference between the two patient cultures.

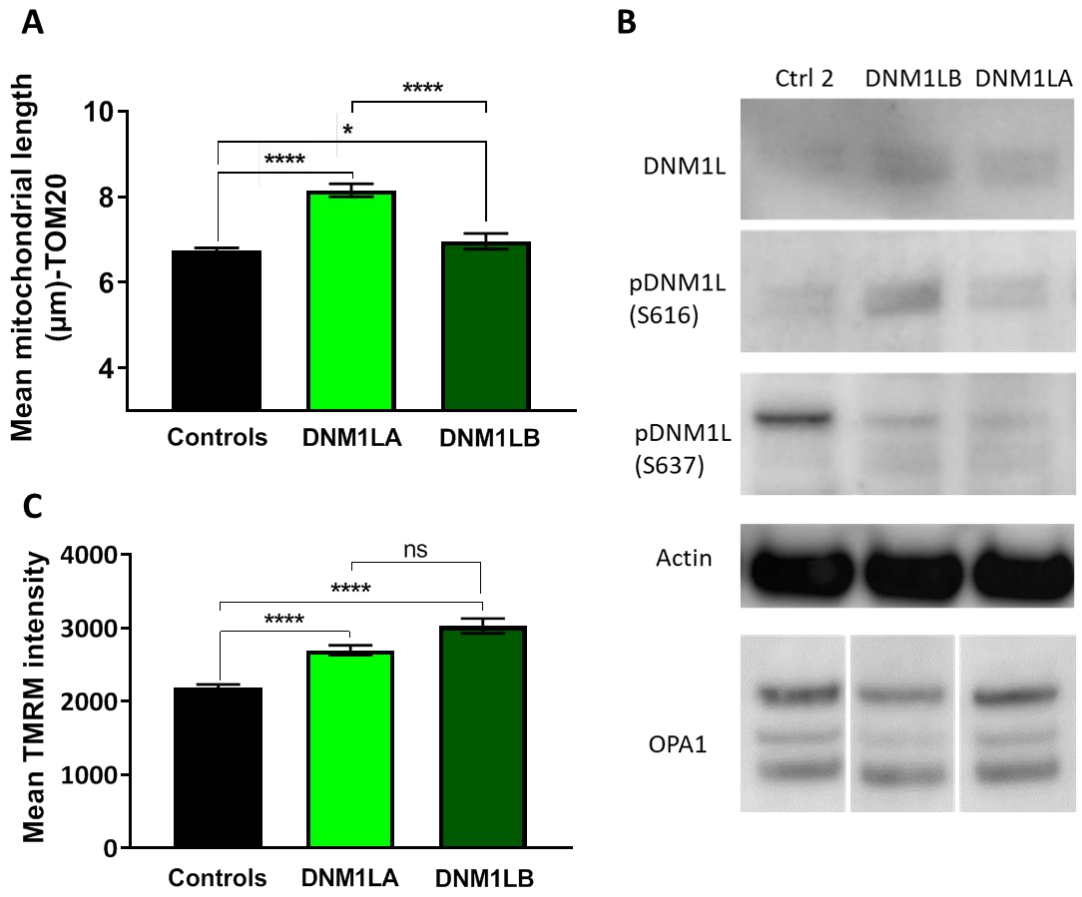

Figure 4.8 Mitochondrial network properties of DNM1L fibroblasts
(A) Mitochondrial length measured by TOM20 labelling, n=3, minimum of 1144 cells analysed per condition. (B) Total DNM1L, phosphorylated DNM1L and OPA1 protein expression, n=1. (C) Mitochondrial membrane potential measured by TMRM staining, n=3, minimum of 1829 cells analysed per condition.
Mean +/- 95% CI, *=p<0.05, ****=p<0.0001

4.4.1.3 Oxygen consumption and mitochondrial respiration in DNM1L fibroblasts

Investigation of mitochondrial activity in muscle biopsies showed a mild reduction in complex IV activity from patient DNM1LA but was normal in DNM1LB (Ladds et al., 2018). Oxygen consumption and mitochondrial respiration was measured in fibroblasts from both patients using the Seahorse platform. There was no difference in oxygen consumption or respiration between DNM1LB and control fibroblasts (Figure 4.9). Oxygen consumption was reduced in DNM1LA cells compared to control and DNM1LB fibroblasts. Basal respirations, maximal respiration and ATP-linked respiration were all significantly lower in DNM1LA fibroblasts compared to control cell (Figure 4.9 B).

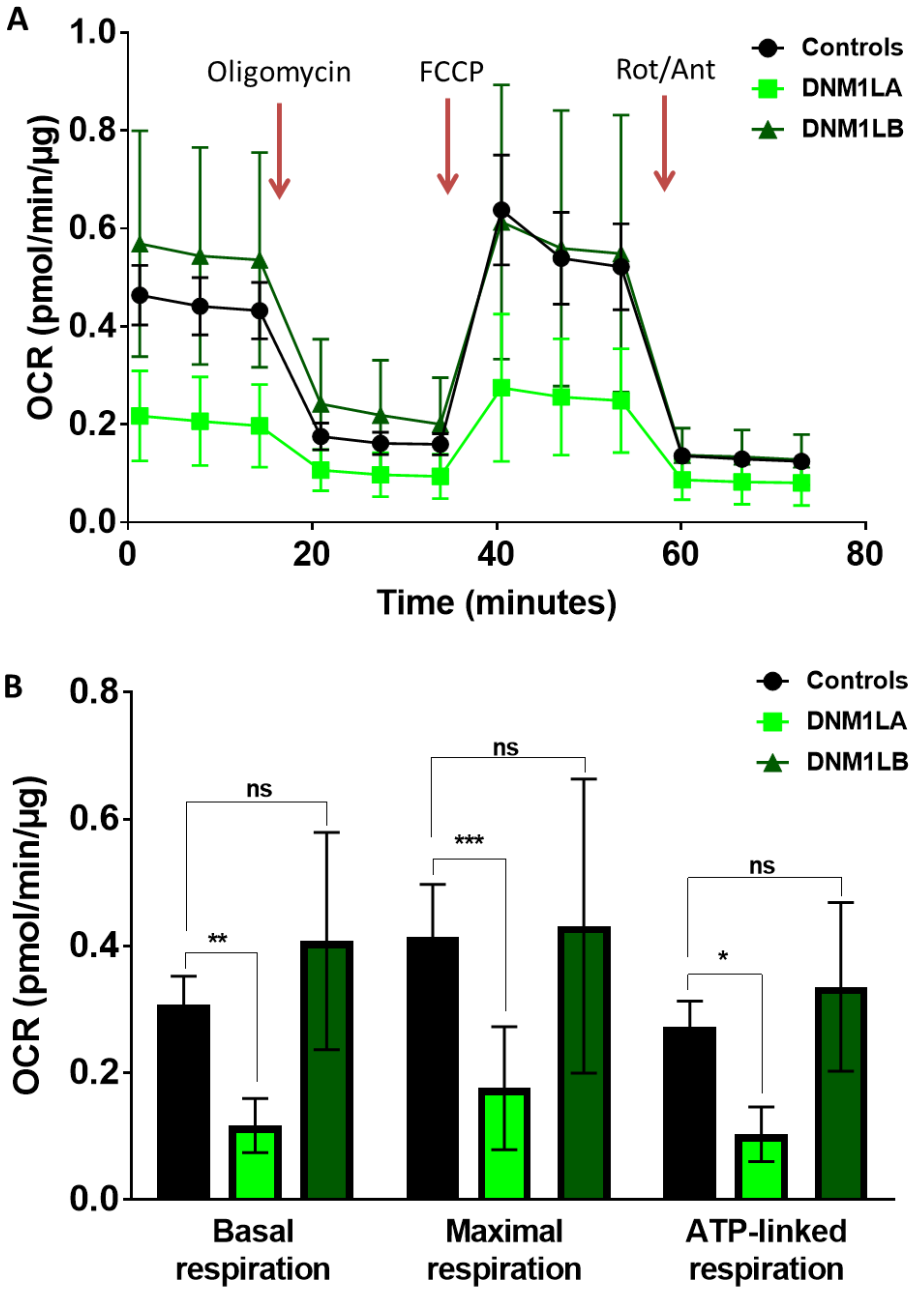

Figure 4.9 Oxygen consumption and mitochondrial respiration in DNM1L fibroblasts
(A) Oxygen consumption measured at baseline and following the addition of rotenone (complex V inhibitor), FCCP (protonophore, to collapse membrane potential) and rotenone (complex I inhibitor)/ antimycin A (complex III inhibitor). (B) Calculated basal, maximal and ATP-linked respiration.
Mean +/- 95%CI from a single experiment based on at least 4 technical replicates, *=p<0.05, **=p<0.01, ***=p<0.001

4.4.1.4 Mitochondrial DNA content and organisation in DNM1L fibroblats

Borderline mitochondrial DNA depletion (33%) and a reduced mtDNA content (71%) were reported in muscle biopsies obtained from DNM1LA and DNM1LB respectively (Ladds et al., 2018) . Mitochondrial DNA content was reduced in fibroblasts derived from patient DNM1LA by approximately 17% (Figure 4.10). This reduction was highly significant compared to controls. Mitochondrial DNA content was also reduced in DNM1LB fibroblasts, but to a much lesser extent, by approximately 5% (Figure 4.10 A). Fluorescent imaging of PicoGreen stained fiboblasts showed the presence of enlarged nucleoids in DNM1LA cells (Figure 4.10 C) that was not observed in control cells. Quantification of the images showed a significant increase in nucleoid diameter in DNM1LA fibroblasts in comparison to controls (Figure 4.10 B). Nucleoid diameter was also increased in DNM1LB cells, although to a much lesser extent (Figure 4.10 B). TMRM labelled portions of the mitochondrial network corresponding to the enlarged nucleoids had an unusual blobby appearance (Figure 4.10 C). These were previously observed in DNM1L KO cells and were referred to as ‘mito-bulbs’ (Ban-Ishihara et al., 2013).

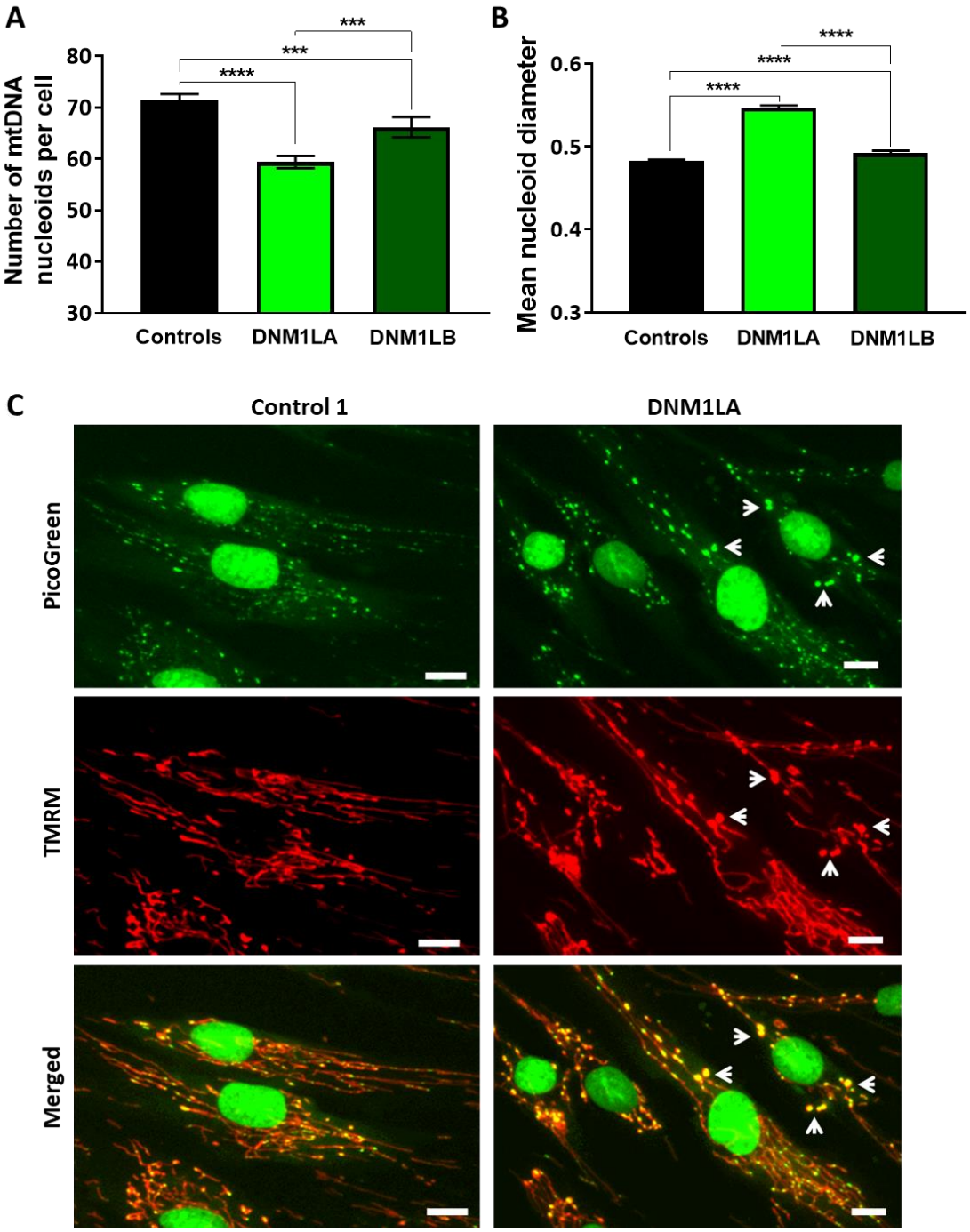

Figure 4.10 Mitochondrial DNA nucleoids in DNM1L fibroblasts
(A) Quantification of PicoGreen labelled mitochondrial DNA nucleoids (B) Quantification of PicoGreen labelled mtDNA nucleoid diameter (C) Representative images of PicoGreen labelled mtDNA nucleoids of control and DNM1LA fibroblasts and TMRM labelled mitochondria. Some enlarged nucleoids and the corresponding mitohcondria are indicated by white arrows.
n=3, minimum of 1829 cells analysed per condition, mean +/- 95% CI, ****p*=<0.001, ****=*p*<0.0001, scale bar 10µm

4.4.1.5 Discussion of DNM1L specific findings

In this section I investigated fibroblasts from two unrelated individuals harbouring the same R403C mutation in the mitochondrial fission protein DNM1L. Although both patients harboured the same recurrent mutation, patient DNM1LA presented with a more severe disease and an earlier onset compared to DNM1LB. The R403C mutation prevents oligomerisation and mitochondrial recruitment of the protein via a dominant negative effect (Fahrner et al., 2016). This results in abnormally long mitochondrial due to the unopposed activity of the mitochondrial fusion proteins. I showed that the mitochondria in fibroblasts from both patients are lengthened and hyperpolarised. Lengthening was more pronounced in DNM1LA fibroblasts suggesting that the effect of the mutation is more detrimental to DNM1L protein function in these cells compared to DNM1LB fibroblasts. The reason behind this is currently unknown.

I also documented reduced mtDNA content in fibroblasts consistent with the borderline low mtDNA content in skeletal muscle from patient DNM1LA. Both DNM1L patients had abnormally large nucleoids, although the clustering was more prominent in DNM1LA fibroblasts derived from the more severe patient. Previously, HeLa cells produced similarly enlarged mtDNA nucleoids following siRNA mediated knock-down of DNM1L (Ban-Ishihara et al., 2013). High-resolution microscopy showed that these large structures in DNLM1L KD HeLa cells were formed by the clustering of multiple mtDNA nucleoids and that the portion of the mitochondrial tubule housing the cluster of nucleoids also appeared bulgy-looking (‘mito-blubs’) due to the formation of stacked cristae. Mitochondria maintain an intimate connection with the ER at highly specialized segments of the membrane referred to

as MAMs. These contact sites are required for mtDNA synthesis to occur (Lewis et al., 2016). A large proportion of DNM1L-dependent mitochondrial fission was shown to proceed in the vicinity of mtDNA nucleoids, at division sites marked by the ER (Friedman et al., 2011). Therefore, it is possible that the role of DNM1L in mitochondrial division is coupled with a role in mitochondrial DNA maintenance. Mitochondrial fission was deemed to be a pre-requisite for mitophagy to occur (MacVicar, 2013; Rambold et al., 2011). Despite a hyperfused mitochondrial network patient derived cells had increased mitophagy. This suggests that fission is not always a pre-requisite for mitophagy to occur. Indeed, Lemasters showed that Beclin-1 dependent mitophagy triggered by nutrient deprivation does not require fission or depolarization of the mitochondrial fragment prior to engulfment by the autophagosome (Lemasters, 2014). It is also plausible that there are alternative, DNM1L independent fission mechanisms that remain to be elucidated. Indeed, recently Bcl2-L-13, a novel mitophagy receptor was implicated in DNM1L-independt mitochondrial fission (Murakawa et al., 2015).

Between the two mutant cultures investigated in this section, the extent of mitochondrial hyperfusion and mtDNA clustering seemed to correlate with the severity of phenotypic presentation. DNM1LA fibroblast derived from the more severe patient (DNM1LA) had longer mitochondria and more prominent, larger nucleoid clusters. On the contrary, there was an inverse correlation between phenotypic presentation and the levels of mitophagy and autophagy; both being the highest in DNM1LB cells derived from the milder patient. Additionally, increased co-localisation of mitochondria with autophagosomes may be the result of slower

turnover in DNM1LA cells, as lysosomal content was substantially reduced compared to control fibroblasts.

4.4.2 Patients with *MFN2* and *OPA1* mutations

Mitochondrial fusion allows the exchange of contents, DNA, and metabolites between neighbouring mitochondria and therefore promote their proper functioning and survival (Section 1.1.3) . Mitochondria are double membrane organelles and the fusion of the outer and inner mitochondrial membranes are assisted by two distinct machineries. OMM fusion depends on two GTPase family members: MFN1 and MFN2 (Hoppins and Nunnari, 2009). Deletion of either of these proteins is embryonic lethal in mice (Chen et al., 2003). MFN2 also functions as a mitochondria-ER tether, and thereby a regulator of mitochondrial Ca^{2+} uptake in mouse (de Brito and Scorrano, 2008). Whether MFN2 positively (Naon et al., 2016) or negatively (Filadi et al., 2017) regulates the number of mitochondria-ER contact sites is still debated. The IMM fusion protein OPA1 is equally versatile in its functions (Del Dotto et al., 2017). Long isoforms of of the protein, L-OPA1 mediate inner membrane fusion while S-OPA1 isoforms are invloved in cristae modelling and mtDNA mainatance.

Defects in either of the fusion machineries may result in several kinds of pathologies. Mutations in *MFN2* are most commonly associated with Charcot–Marie–Tooth neuropathy type 2A (CMT2A), characterised by axonal degeneration of both sensory and motor neurons (Zuchner et al., 2004). Pathogenic mutations in *OPA1* are the major underlying cause for autosomal dominant optic atrophy (DOA), the commonest autosomal form of mitochondrial optic neuropathy. DOA is dominantly inherited in the majority of cases and is characterised by progressive visual failure secondary to optic nerve neurodegeneration. A subgroup of patients with *OPA1* mutations develop a multisystemic neurologic phenotype, known as DOA plus. Other obligate *OPA1* mutation carriers are visually asymptomatic (Liao et al., 2017). Disease phenotypes as

a result of OPA1 mutations are either caused by haploinsufficiency or a dominant-negative effect, with DOA plus patients most commonly harbouring a single missense mutations in the GTPase domain. Occasionally bi-allelic DOA plus patients harbour two mutations, a nonsense mutation in *trans* with a missense mutation (Liao et al., 2017).

In this section, fibroblasts were available from two patients with mitochondrial disease due to defects in the fusion proteins MFN2 and OPA1. Patient MFN2 harboured the c.310C>T (Arg104Trp) *de novo* missense mutation in exon 4 of the *MFN2* gene. Patient OPA1 harboured the c.2708_2711delTTAG(Val903fs); c.1146A>G (Ile382Met) bi-allelic mutations in the *OPA1* gene. Ile382Met is located in exon 12 and affects the GTPase domain. It is denoted a hypomorphic allele, in that homozygotes are phenotypically normal. The Val903fs mutation is located in exon 27 that forms part of the assembly domain. Bioinformatic analysis of OPA1 structure revelaled two coiled coil domains, one spanning residues 226-268 and the other 940-969 potentially involved in protein-protein interactions (Thiselton et al., 2002). The second coiled-coil is completely removed by the Val903fs mutation. Interestingly, the penetrance of this mutation is not 100%, but closer to 60% (Thiselton et al., 2002).

4.4.2.1 Mitophagy and autophagy in OPA1 and MFN2 fibroblasts

Mitophagy was increased OPA1 and MFN2 mutant cells at baseline and following treatment with lysosomal inhibitors for 24 hours when compared to control cells (Figure 4.11 A). The increase was more striking in MNF2 mutant cells. Autophagy, measured by counting the number of LC3 positive punctae was increased in both patient cultures when compared to control cells at baseline (Figure 4.11 B). Autophagy remained significantly above control levels in MFN2 fibroblast following EP treatment but was not different from controls in OPA1 cells (Figure 4.11 B). Representative images of TOM20 and LC3 labelled control and patient fibroblasts are shown in Figure 4.12.

The number of lysosomes was assessed on OPA1 fibroblast using Lyso-ID labelling. Lysosomal count was reduced in OPA1 fibroblasts when compared to controls bot at baseline and following 4 hours treatment with chloroquine (Figure 4.11 C). Lysosomal data was not available for MFN2 cells. Representative images of Lyso-ID labelled control and OPA1 fibroblasts are shown in Figure 4.13.

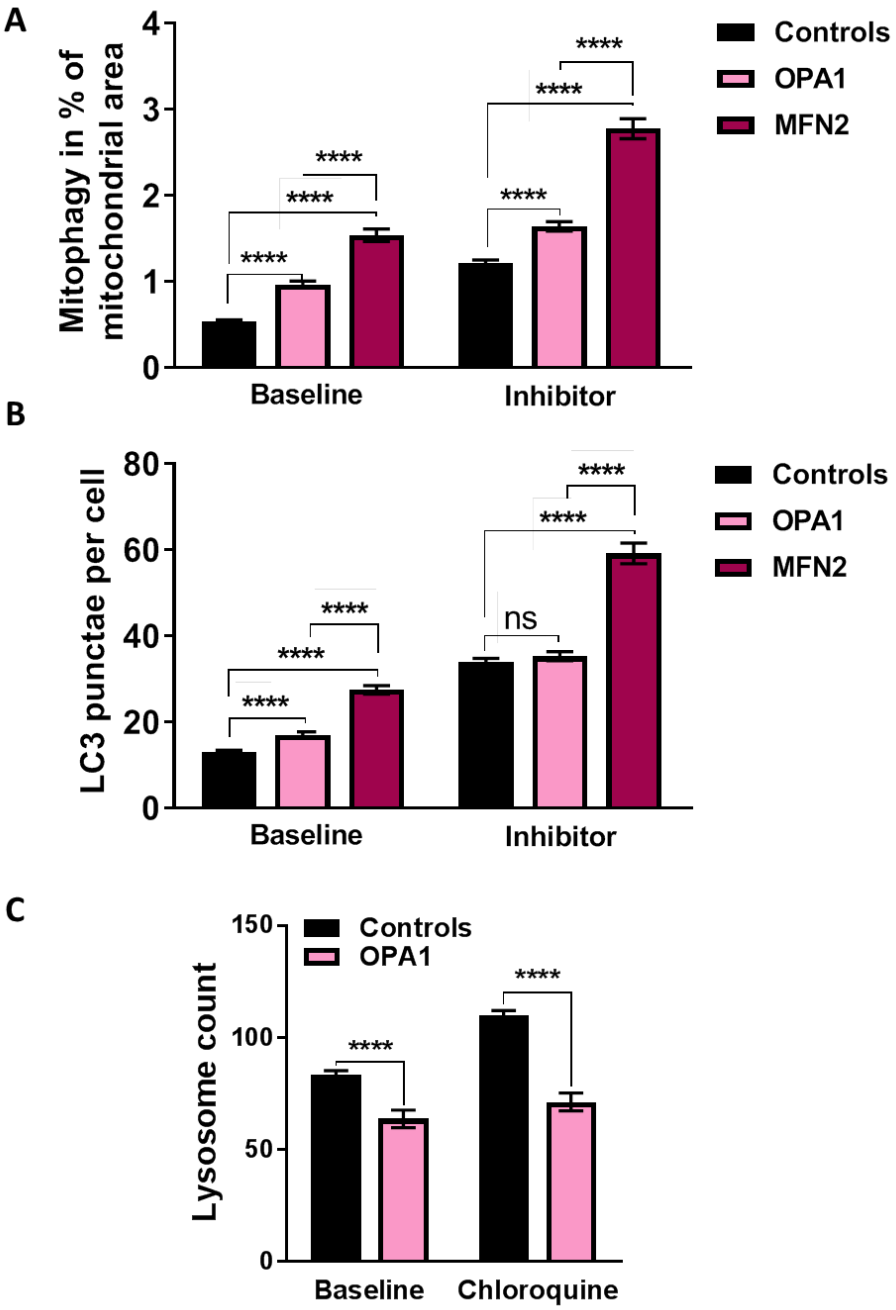

Figure 4.11 Mitophagy and autophagy in OPA1 and MFN2 fibroblasts
(A) Mitophagy and (B) autophagy measured at baseline and following 24 hours treatment with lysosomal inhibitors E64d and Pepstatin A (10µg/ml), n=3, minimum of 1196 cells analysed per condition. (C) Lysosomal content measured by Lyso-ID labelling at baseline and following 4 hours chloroquine treatment (60µM), n=2, minimum of 139 cells analysed per condition.
Mean +/- 95% CI, ****=p<0.0001

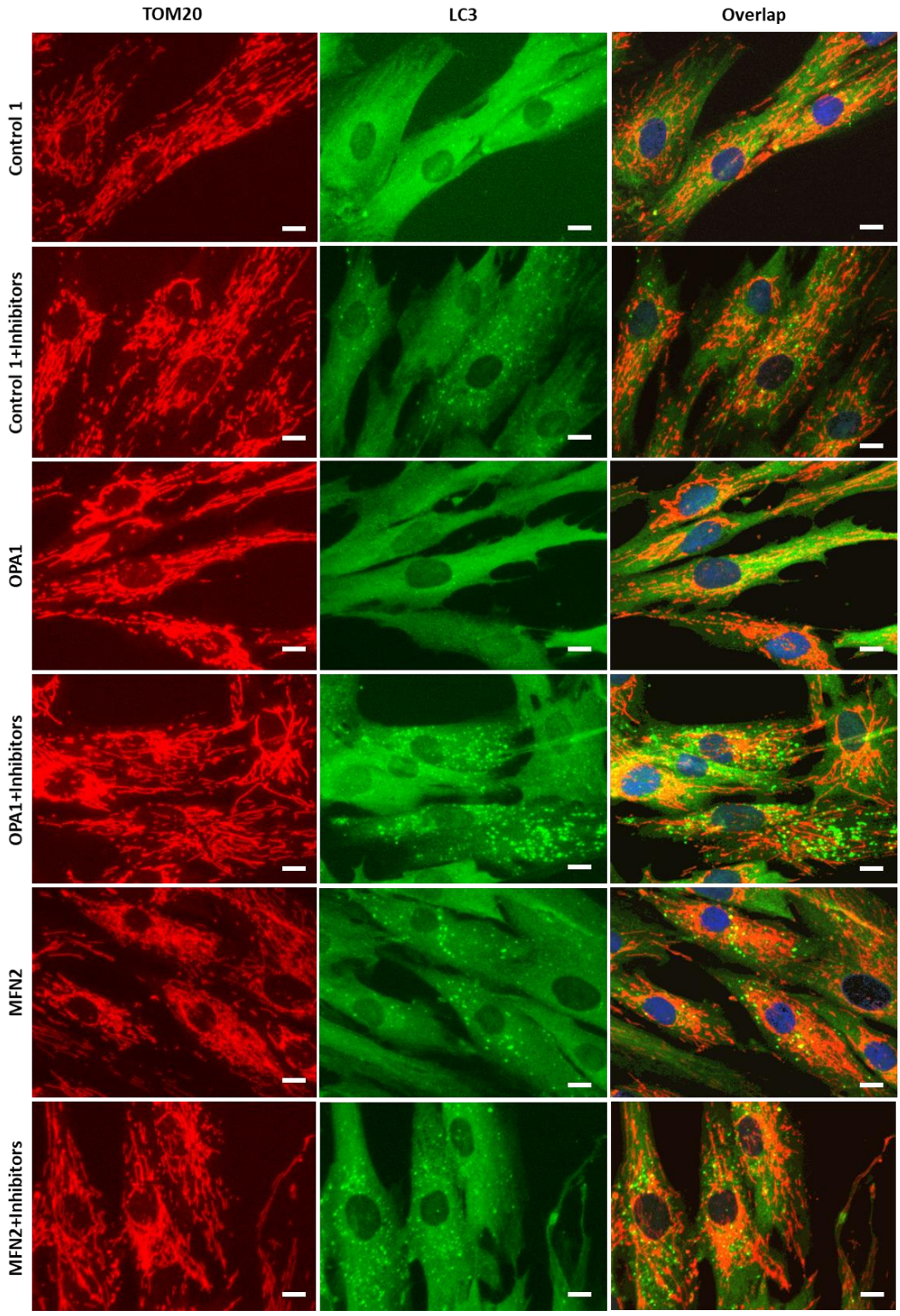

Figure 4.12 Representative images of Control 1, OPA1 and MFN2 fibroblasts Showing TOM20-labelled mitochondria and LC3-labelled autophagosomes cultured either at baseline or with the addition of lysosomal inhibitors E64d and Pepstatin A. Scale bar 10µm.

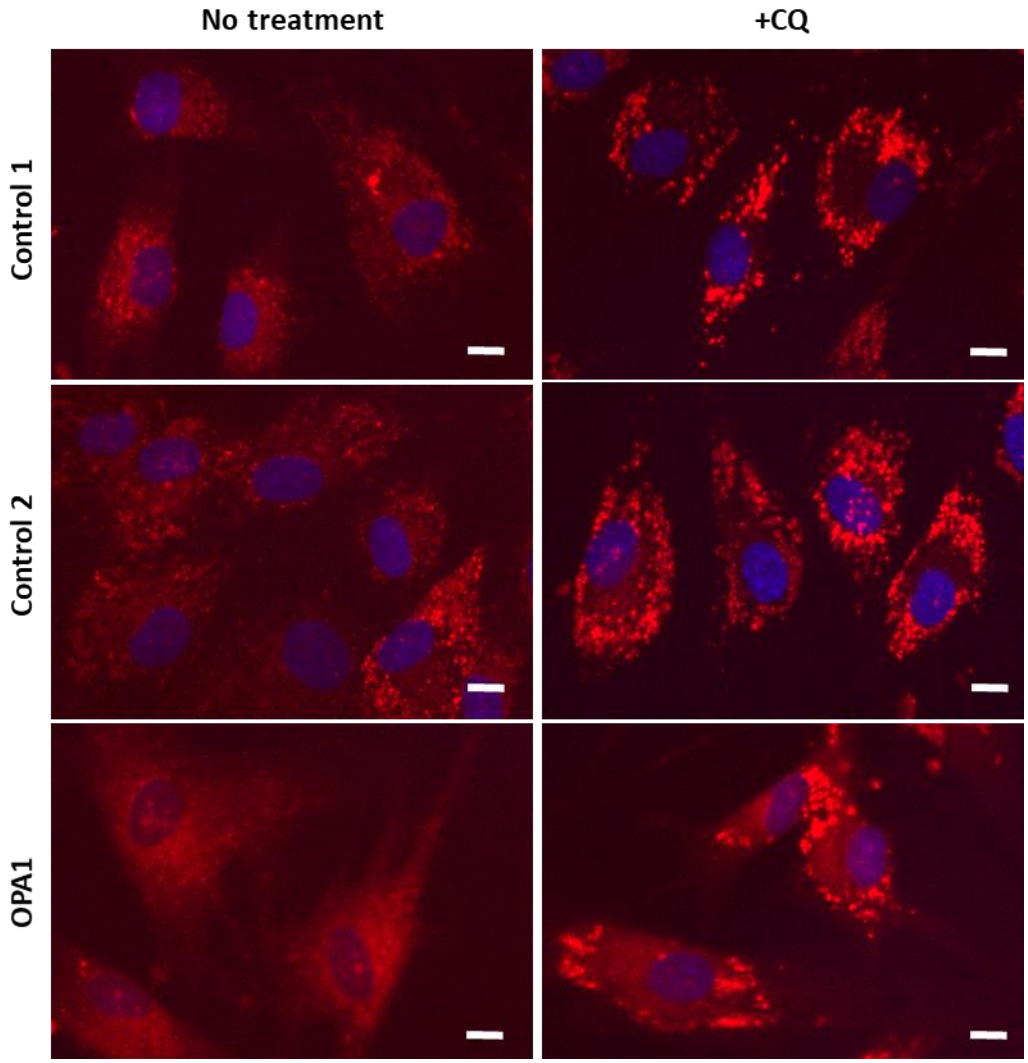

Figure 4.13 Representative images of Control and OPA1 fibroblasts labelled with Lyso-ID
Showing Lyso-ID (red) and Hoechst (blue) labelled fibroblasts with or without chloroquine (CQ) treatment. Scale bar 10µm.

4.4.2.2 Mitochondrial network properties of fibroblasts with fusion defects

OPA1 and MFN2 are both key regulators of mitochondrial fusion, therefore measuring mitochondrial length seems evident (Figure 4.14). When the mean length of TOM20 labelled mitochondria was measured, there was no difference between control and OPA1 fibroblasts (Figure 4.14 A). Mean mitochondrial length was significantly reduced in MFN2 cells compared to controls as well as to OPA1 cells (Figure 4.14 A). TOM20 is an OMM protein therefore mitochondrial length might appear undisturbed if there is no defect present in the fusion machinery of the outer membranes. On the other hand, fusion defects of both IMM and OMM have a detrimental impact on mitochondrial membrane potential. TMRM accumulates in the matrix compartment of the organelle; therefore, it would indicate any defect in inner membrane fusion. Mitochondrial membrane potential measured by TMRM intensity was significantly reduced in both OPA1 and MFN2 mutant cells when compared to controls (Figure 4.14 B). It is possible, that the excessive fragmentation seen in MFN2 cells makes it difficult for the cells to maintain their membrane potential.

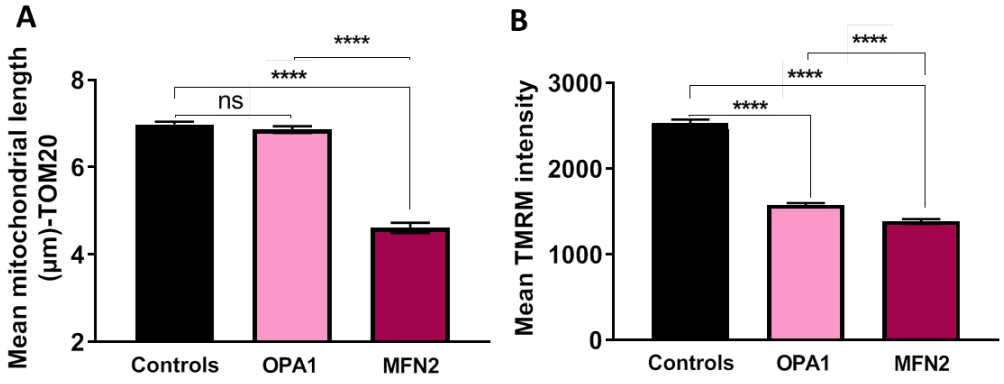

Figure 4.14 Mitochondrial network properties of OPA1 and MFN2 fibroblasts
(A) Mitochondrial length measured by TOM20 labelling, n=3, minimum of 1191 cells analysed per condition. (B) Mitochondrial membrane potential measured by TMRM intensity, n=2, minimum of 984 cells analysed per condition, mean +/- 95% CI, ****=p<0.0001

4.4.2.3 Mitochondrial DNA content of OPA1 and MFN2 fibroblasts

The short isoforms of OPA1 have a pivotal role in cristae structure and mitochondrial DNA maintenance. Mitochondrial DNA is depleted when control fibroblasts are treated with siRNA against OPA1 (Liao et al., 2017). Quantification of mtDNA nucleoids in fibroblast showed a reduction in nucleoid numbers in OPA1 fibroblasts compared to control cells (Figure 4.15 A). There was no significant difference in mtDNA nucleoid numbers between MFN2 and control cells (Figure 4.15 A). Representative images of PicoGreen and TMRM labelled Control 2, OPA1 and MFN2 fibroblasts are shown in Figure 4.16. On these images, mtDNA nucleoids appear larger in OPA1 cells and seem to cluster closer to the nucleus. When quantified, the size of mtDNA nucleoids was significantly larger in OPA1 fibroblasts compared to controls (Figure 4.15 B). Similar findings were observed in DNM1L fibroblasts (Figure 4.10), with the exception of the perinuclear localisation, that was only apparent in OPA1 cells (Figure 4.15 C). These observations may vary, depending on how we define the perinuclear region. In our automated analyses protocol, the perinuclear region is defined by the dilation of the nuclear mask. The number of mtDNA nucleoids in this region is expressed as the percentage of the total number of nucleoids within the cell. MFN2 fibroblasts showed the complete opposite to OPA1 cells. Nucleoid diameter was significantly reduced in MFN2 cells when compared to controls and OPA1 cells, resulting in tiny nucleoids (Figure 4.15 B and 4.16). This may have led to an underestimation of mtDNA content in these cells, as some of the nucleoids might have been under the detection threshold of our analysis protocol. This is supported by the images presented in Figure 4.16, in which judging by eye MFN2 cells have more PicoGreen labelled nucleoids than control fibroblasts.

Furthermore, mitochondrial content measured by the total area of TOM20 labelled mitochondria was significantly increased in MFN2 cells when compared to controls, while showing the opposite in OPA1 fibroblasts correlating with their mtDNA content (Figure 4.15 D).

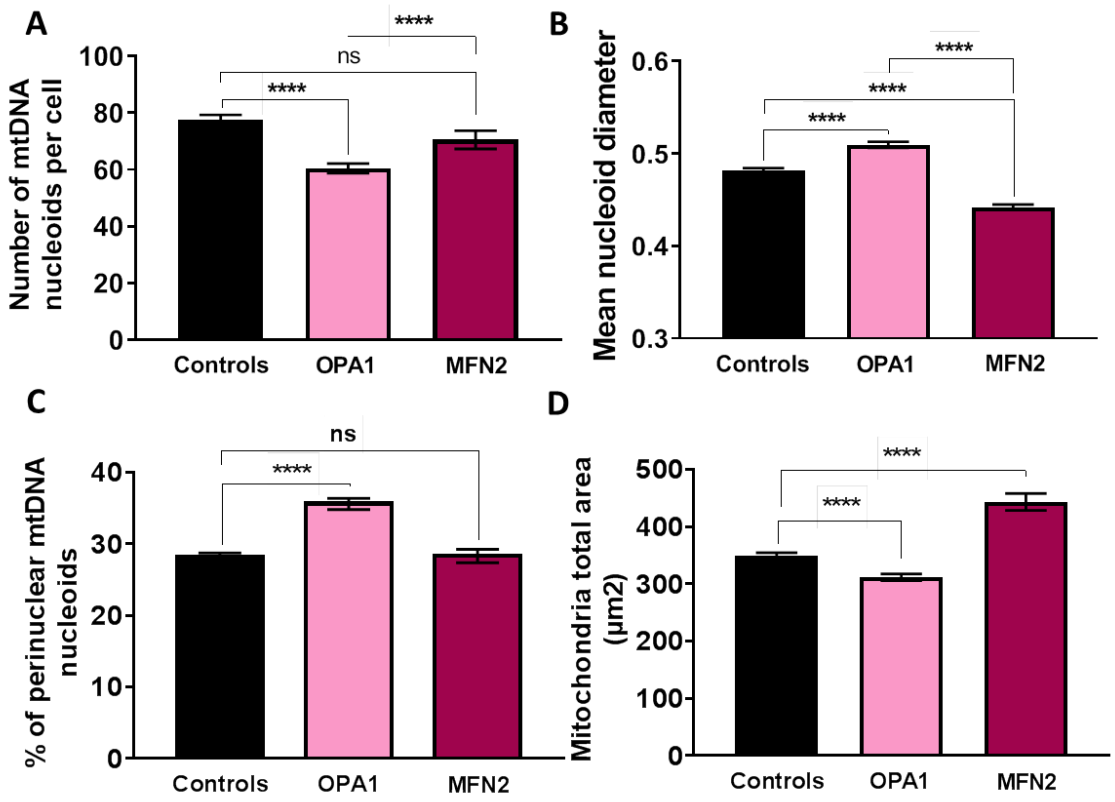

Figure 4.15 Mitochondrial DNA content in OPA1 and MFN2 fibroblasts
A) Quantification of PicoGreen labelled mitochondrial DNA nucleoids. (B) Quantification of PicoGreen labelled nucleoid diameter. (C) Percentage of perinuclear mtDNA nucleoids in area, n=3, minimum of 1297 cells analysed per condition. (D) Total mitochondrial area, n=3, minimum of 1191 cells analysed per condition. Mean +/- 95% CI, ****=p<0.0001

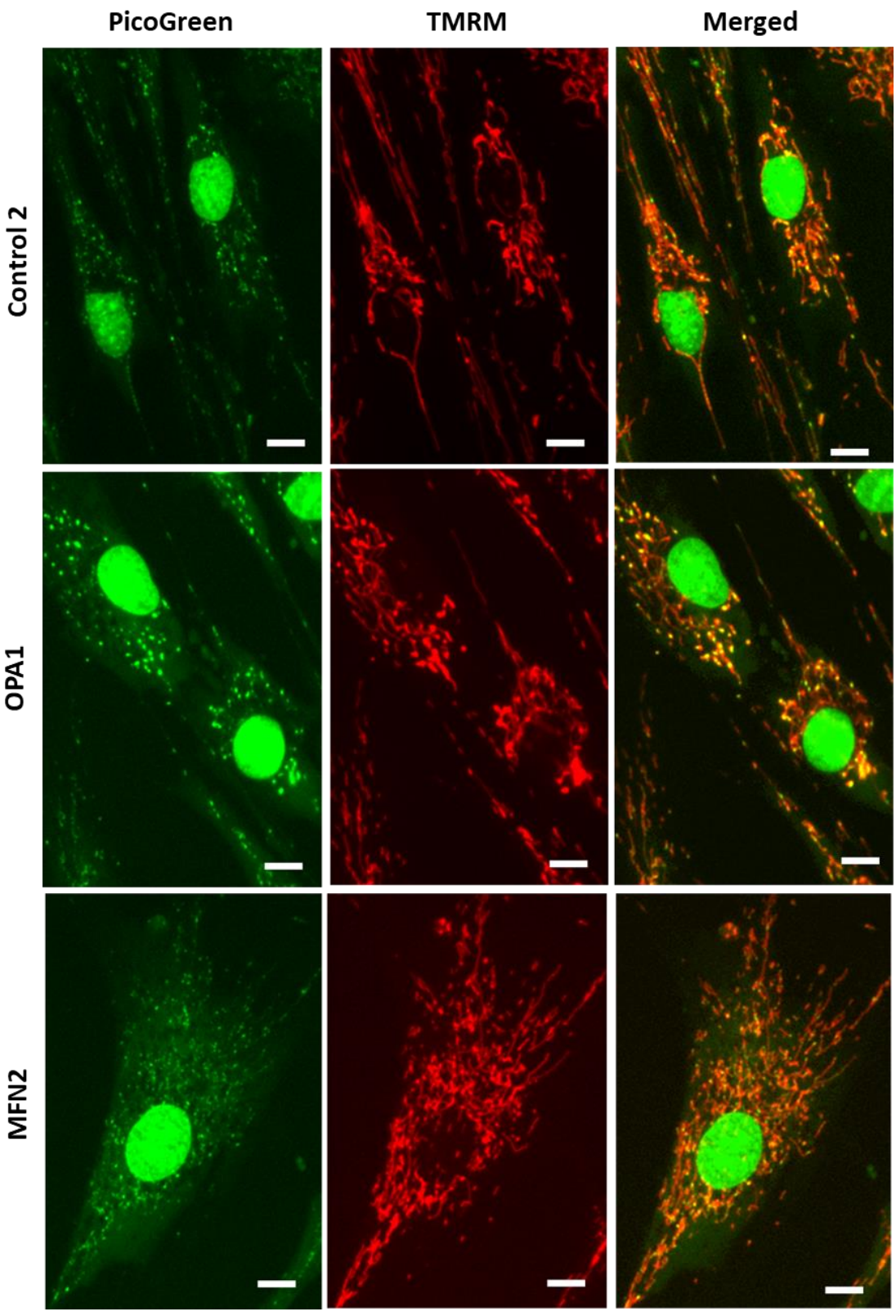

Figure 4.16 Representative images of PicoGreen and TMRM labelled OPA1 and MFN2 cells
Scale bar 10µm

4.4.2.4 Discussion of OPA1 and MFN2 specific findings

I showed that mitochondria in MFN2 mutant fibroblasts are fragmented, consistent with defective OMM fusion. There was no difference in mean mitochondrial length between OPA1 and control cells despite the excessive fragmentation documented in a previous patient cohort harbouring dominant-negative OPA1 mutations (Liao et al., 2017). Transcripts of OPA1 produce several isoforms of the protein with distinct functions (Del Dotto et al., 2017). Western blot analysis of whole cell lysates of OPA1 mutant fibroblasts revealed that there was normal expression of L-OPA1 that functions in inner membrane fusion (Supplementary figure 2). On the contrary, there was reduced expression of S-OPA1 isoforms involved in cristae organisation and mtDNA maintenance. In line with this, OPA1 cells had reduced mtDNA content with large nucleoids that clustered in the perinuclear region of the cells. OPA1 fibroblasts investigated in this chapter harbour bi-allelic mutations in the *OPA1* gene, one of which (Val903fs) affects the C-terminal region of the protein. This region is also implicated in the regulation of ER-mitochondria contact sites during mTORC1 inactivation (Sood et al., 2014) therefore contributing to the structural remodelling of the organelle during metabolic stress.

MFN2 mutant cells harboured significantly smaller mtDNA nucleoids compared to control cells. MFN2 is a known mediator of mtichondria-ER contact sites, however, more recently ablation of MFN2 was shown to increase rather than diminsh the number of of these site between the two organelles (Filadi et al., 2017). This is supported by my findings that MFN2 fibroblasts have drastically increased mitochondrial content and tiny mtDNA nucleoids when compared to healthy control cells. We did not detect an increase in mtDNA copy number, however, the size of

mtDNA nucleoids might be below detection level in these cells when using PIcoGreen staining.

4.4.3 Patients with mitochondrial encephalopathy due to mutations in FBXL4

FBXL4 belongs to the family of FBX (F-box) proteins that are characterised by the presence of an F-box motif of approximately 50 amino acids at the amino terminal, which functions as a site of protein-protein interactions (Bai et al., 1996). FBX proteins often contain additional motifs implicated in protein-protein interactions, the most common in humans being WD (tryptophan-aspartic acid) or leucine-rich repeats (LRR) located towards the carboxy-terminal. FBXL refers to all FBX proteins containing an F-box motif combined with LRRs, and the proteins are numbered in the order of their discovery (Cenciarelli et al., 1999). In 2013 two independent groups described patients harbouring multiple mutations in FBXL4 presenting as mitochondrial encephalomyopathy with mtDNA depletion (Bonnen et al., 2013; Gai et al., 2013). Both groups reported the presence of a mitochondrial targeting signal at the N-terminal region of the protein (amino-acids 1-26), an F-box domain (amino acids 277-332) and at least nine leucine-rich repeats (LRRs) (amino acids 340–609) (Figure 4.17). Additionally, they found exclusive mitochondrial localisation of the FBXL4 protein using overexpressed recombinant HA-tagged FBXL4 either in fibroblasts or HEK293T cells. Furthermore, Gai et al. (2013) pinpointed the localisation of the protein to the intermembrane-space and immunoblot analysis indicated that FBXL4 is present in a quaternary protein complex. This contrasts with earlier data from the time when FBX proteins were first identified when FBXL4 was shown to localise both to the cytoplasm and the nucleus (Cenciarelli et al., 1999). Additionally, FBX proteins are well known components of SCF (Skp, Cullin, F-box protein) ubiquitin ligase complexes (Skowyra et al., 1997). There are multiple SCF

complexes in humans that only differ in their F-box protein component as these confer substrate specificity of the ubiquitin ligase (Petroski and Deshaies, 2005). FBXL4 was reported to regulate chromatin structure via the ubiquitination of the histone demethylase JMJD2 (Jumonji Domain Containing 2A) as part of the SKP1-Cul1-F-box and leucine-rich repeat protein 4 (SCF-FBXL4) ubiquitin ligase (Van Rechem et al., 2011) which would support its nuclear localisation. Conversely, a large scale proteomic study aimed to identify candidate targets for FBXL proteins found Endoplasmic Reticulum Lectin 1 (ERLEC1) to interact with FBXL4, an ER stress response element (Tan et al., 2013). Considering all the publications reviewed above, it is safe to say that both the subcellular localisation and precise function of FBXL4 is still controversial.

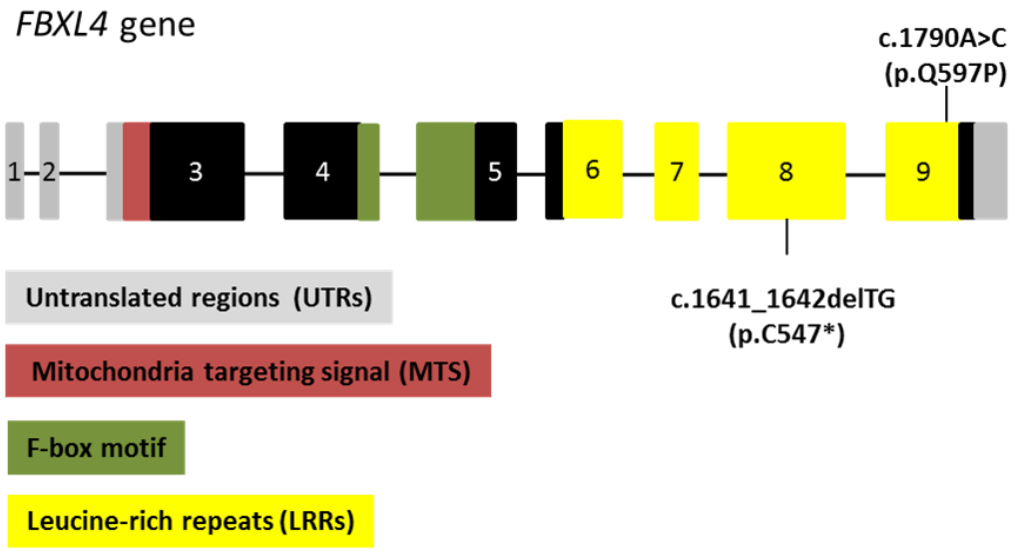

Figure 4.17 Structure of the FBXL4 gene and location of the reported mutations
Coding exons are coloured and non-coding exons are represented by grey boxes. The N-terminal region of exon 3 harbours the mitochondrial targeting signal. The F-box motif (aa 277-332) characteristic of the whole protein family spans across exons 4 and 5. Exons 6, 7 8 and 9 encode the N-terminal leucine-rich repeat region of the protein. The paternally-inherited truncating deletion (c.1641_1642delTG: p.(Cys547*) exon 8) and a maternally-inherited missense variant (c.1790A>C: p.(Gln597Pro) exon 9) was identified in both patients. Adopted from: (Gai et al., 2013).

The fibroblast cultures presented in this section were derived from two siblings who harboured a paternally-inherited truncating deletion (c.1641_1642delTG: p.(Cys547*)) and a maternally-inherited missense variant (c.1790A>C: p.(Gln597Pro)) in the FBXL4 gene. The patients presented with early onset encephalopathy, lactic acidosis, dysmorphic features and global developmental delay. Patient FBXL4A had a mild reduction in complex IV in muscle but her mtDNA copy number was normal. Patient FBLX4B also developed seizures at age 2 and he had a mild reduction in complex II/III and IV in muscle. Mitochondrial DNA copy number was within normal range (50-70%). He died at 8 years of age.

4.4.3.1 Mitophagy and autophagy in FBXL4 fibroblasts

Mitophagy was increased in both cultures derived from FBXL4 patients compared to control cells at baseline as well as after EP treatment (Figure 4.18 A). When compared to each other, mitophagy was the highest in FBXL4B cells derived from the patient with a slightly more severe presentation, significantly higher than in FBXL4A cells. LC3 count, used to measure autophagy, followed the same pattern (Figure 4.18 B). Autophagy was the highest in FBXL4B fibroblasts followed by FBXL4A cells. LC3 count in both cases was significantly higher than in control cells. Although it was not measured directly, mitophagic and autophagic flux are likely increased in patient cells. This is apparent from the results following treatment with lysosomal inhibitors. Representative images of TOM20 and LC3 labelled fibroblasts are shown in Figure 19. When lysosomes were labelled using Lyso-ID and the number of lysosomes was counted it was increased in both patient cultures compared to controls at baseline and following chloroquine treatment (Figure 4.18 C). There was no significant difference between the two patient cultures. Representative images of Lyso-ID labelled control and patient fibroblasts are shown in Figure 4.20.

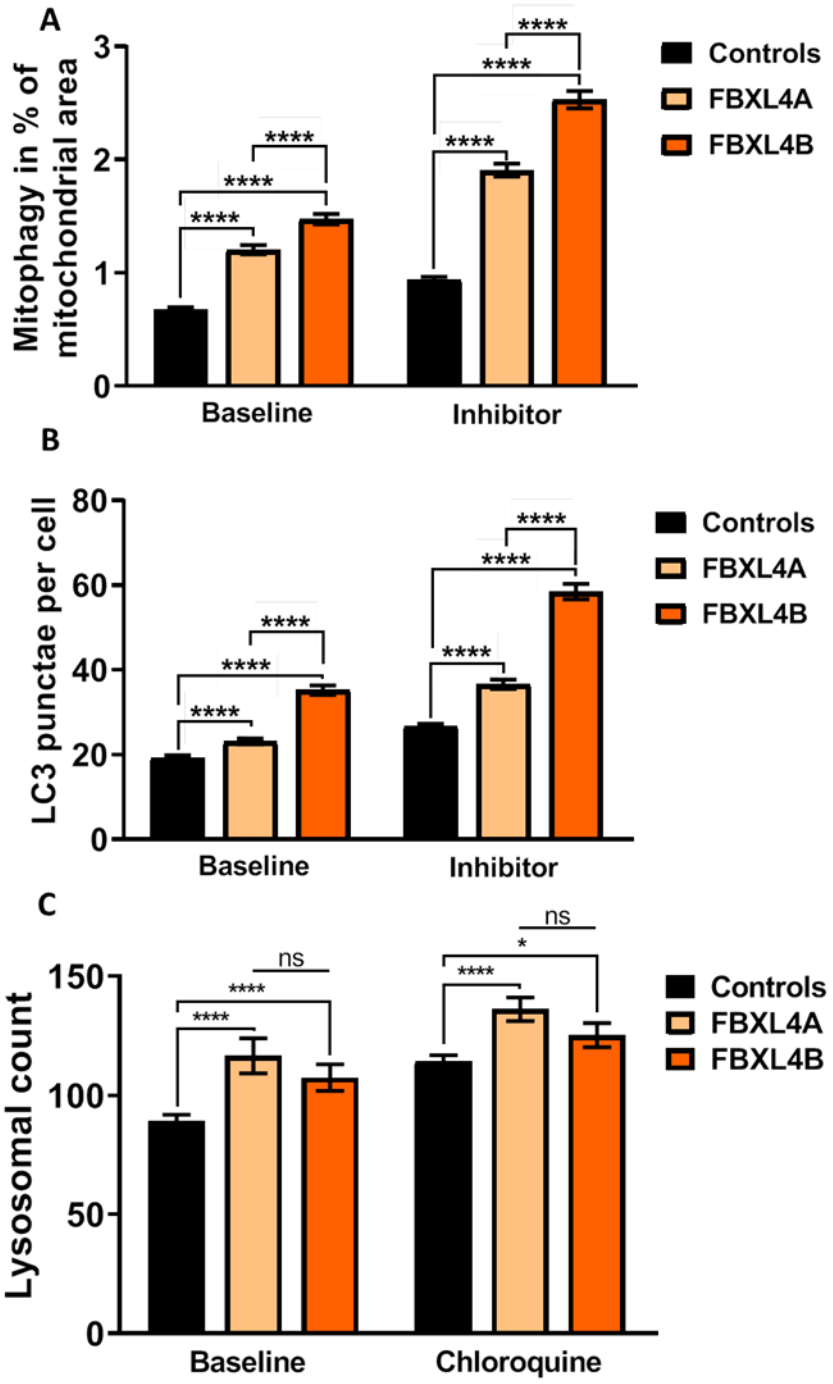

Figure 4.18 Mitophagy and autophagy in FBXL4 fibroblasts
(A) Mitophagy and (B) autophagy were measured in standard growth media (25mM)=baseline as well as after 24 hours treatment with lysosomal inhibitors E64d and Pepstatin A=Inhibitors, n=3, minimum 1702 cells analysed per condition. (C) The number of lysosomes at baseline and following 4 hours treatment with chloroquine (60µM). n=2, minimum of 716 cells analysed per condition.
Mean +/- 95%CI, *=p<0.05, ****=p<0.0001

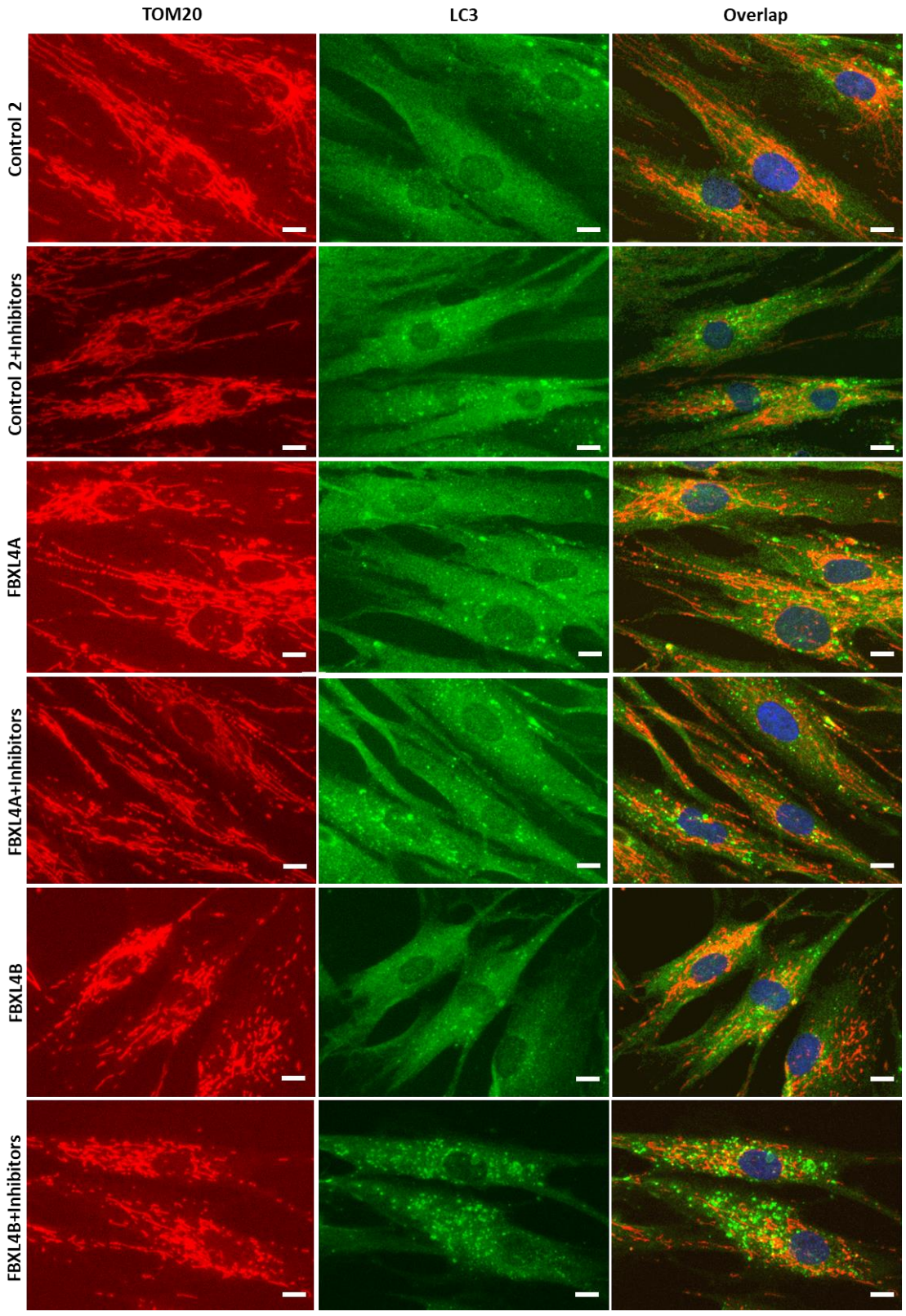

Figure 4.19 Representative images of Control 2 and FBXL4 fibroblasts
Showing TOM20-labelled mitochondria and LC3-labelled autophagosomes cultured either at baseline or with the addition of lysosomal inhibitors E64d and Pepstatin A. Scale bar 10µm.

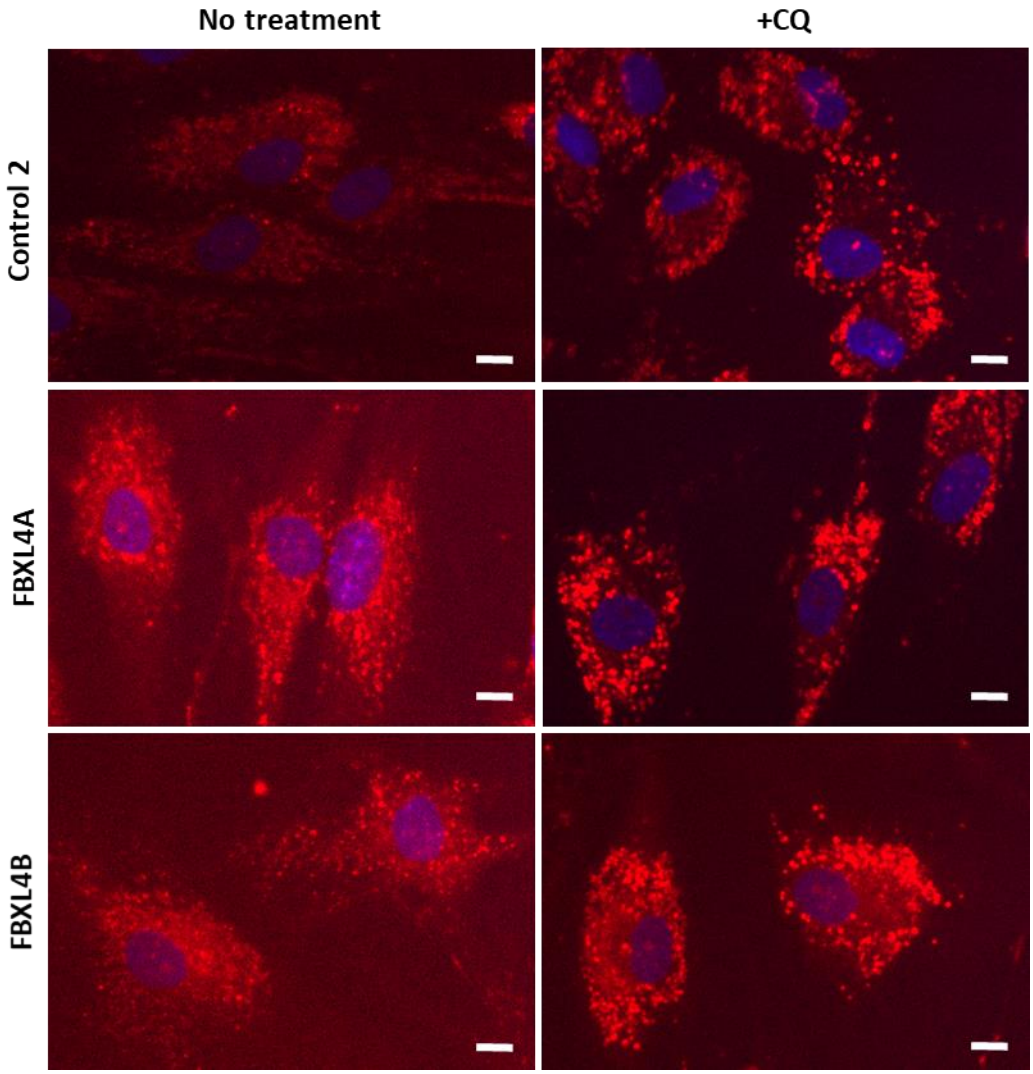

Figure 4.20 Representative images of Control 2 and FBXL4 fibroblasts labelled with Lyso-ID
Showing Lyso-ID (red) and Hoechst (blue) labelled fibroblasts with or without chloroquine (CQ) treatment. Scale bar 10µm.

4.4.3.2 Mitochondrial network properties of FBXL4 fibroblasts

Mitochondrial dynamics plays an important role in mitophagy. The mitochondrial network in FBXL4 fibroblasts was assessed using TOM20 labelling of mitochondria in fixed cells as well as using the membrane potential sensitive live cell dye TMRM. Mean mitochondrial length (TOM20) was increased in FBXL4A fibroblasts compared to controls while FBXLB fibroblasts showed fragmentation (Figure 4.21 A). Mitochondrial membrane potential was significantly lower in both patient cultures compared to control cells (Figure 4.21 B). The decrease was the most prominent in FBXL4B cells.

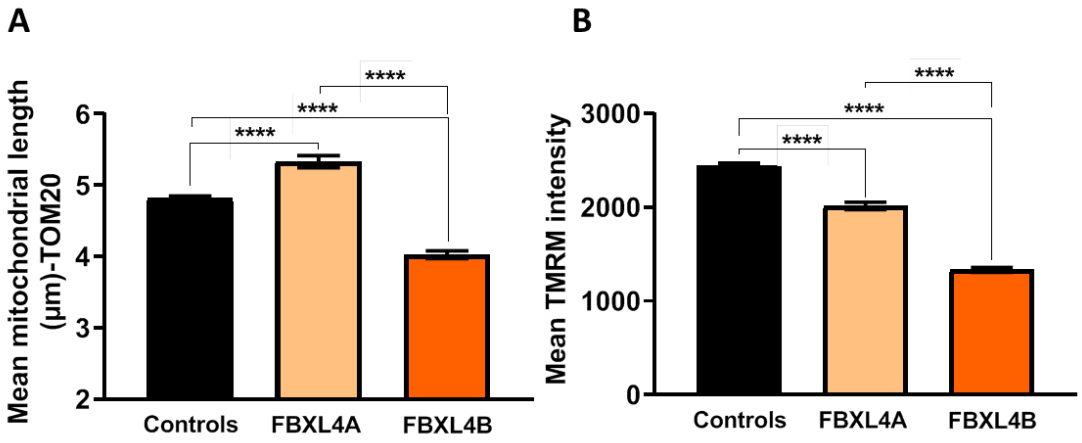

Figure 4.21 Mitochondrial network properties of FBXL4 fibroblasts
(A) Mean mitochondrial length measured by TOM20 labelling, n=3, minimum of 1840 cells analysed per condition, (B) Membrane potential measured by TMRM intensity, n=2, minimum of 1142 cells analysed per condition.
Mean +/- 95% CI, ****= p<0.0001

4.4.3.3 Oxygen consumption rate and mitochondrial respiration in FBXL4 fibroblasts

Fragmentation of the mitochondrial reticulum and reduced membrane potential can result in deficient oxidative phosphorylation. Measuring mitochondrial respiration is a common practice in order to determine the 'fitness' of the mitochondria within cells. Oxygen consumption rate was measured in patient and control fibroblasts using the Seahorse platform (Agilent). The rate of oxygen consumption is expressed as pmol/min which was normalized to µg protein content in each well. Measures of mitochondrial respiration, including basal respiration, ATP-linked respiration, and reserve capacity were derived by the sequential addition of pharmacological agents to the cells. Initially baseline cellular oxygen consumption is measured followed by oligomycin injection, an inhibitor of complex V. In the next step FCCP is added, an uncoupling agent that abolishes the linkage between the respiratory chain and the phosphorylation system. Finally, a combination of Rotenone and Antimycin A (Rot/Ant A) is injected in order to inhibit complex I and complex III respectively and thereby the whole respiratory chain. For each parameter, three repeated rates of oxygen consumption are made over an 18 minute period. Figure 4.22 A shows the rate of oxygen consumption measured at each point. Basal respiration was reduced in FBXL4 cells when compared to controls (Figure 4.22 B). Maximal respiration was significantly reduced in both FBXL4A and FBXL4B fibroblasts compared to control cells, while there was no significant difference in ATP-linked respiration between control and either of the patient cultures (Figure 4.22 B). Previous biochemical investigations revealed that patient FBXL4B had a mild reduction of complex II/III and IV in muscle, which was not reported in FBXL4A cells. Agreeing with these results the

protein expression of OXPHOS complex II/III and IV subunits as well as complex I was visibly lower in FBXL4B fibroblasts when compared to control or FBXL4A ones (Figure 4.23).

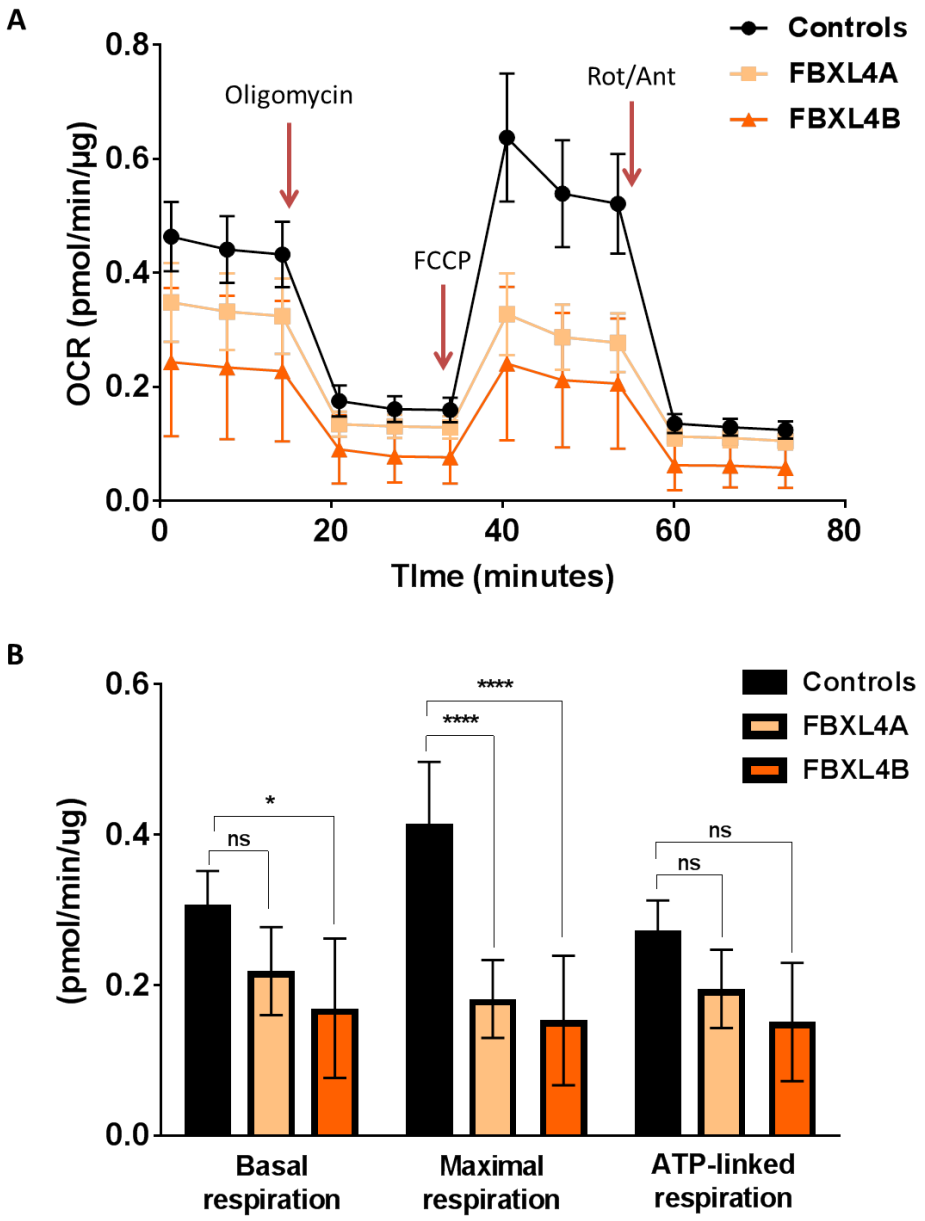

Figure 4.22 Oxygen consumption rate and mitochondrial respiration in FBXL4 fibroblasts

(A) Oxygen consumption rate measured every 18 minutes normalized to protein content, all injections indicated. Rot/Ant A = Rotenone and Antimycin A. (B) Baseline, maximal and ATP linked respiration calculated from the results shown in graph A. Mean +/- 95%CI from a single experiment based on at least 4 technical replicates, *=p<0.05, ****=p<0.0001

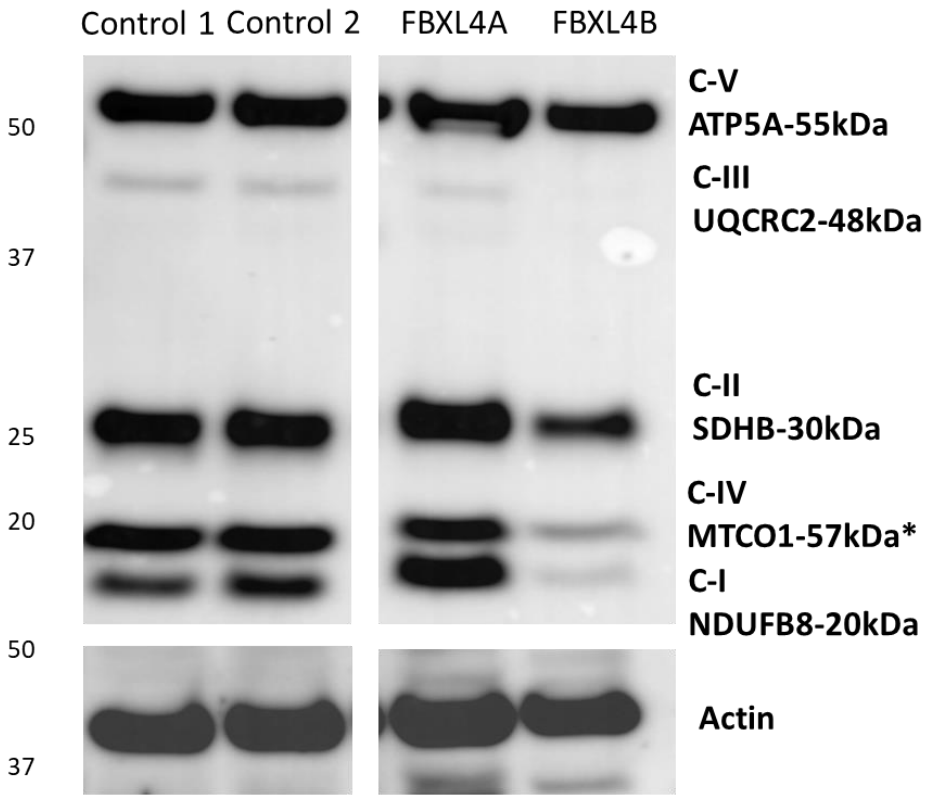

Figure 4.23 Protein expression of OXPHOS complex subunits
*Highly hydrophobic mtDNA encoded protein. Real MW is 57kDa but migrates differently in different systems according to the manufacturer.

4.4.3.4 Mitochondrial DNA content in FBXL4 fibroblasts

Mitochondrial DNA depletion in skeletal muscle has previously been reported in some but not all patients with confirmed FBXL4 mutations (Bonnen et al., 2013; Gai et al., 2013) which could contribute to low oxygen consumption and reduced OXPHOS complex protein expression. Mitochondrial DNA depletion was not reported in muscle derived from these patients. However, mtDNA copy number below 30% of expected in skeletal muscle is classified as mtDNA depletion, while 30-50% is considered borderline low, and over 50% is classed as normal. Regardless, lesser alterations in mtDNA content may also contribute to the pathology resulting from these mutations. Therefore, mitochondrial DNA content was investigated by PicoGreen staining. The number of mtDNA nucleoids was reduced by an approximate 35% in FBXL4A fibroblasts and an approximate 20% in FBXL4B fibroblasts compared to control cells (Figure 4.24 A). Mitochondrial total area corresponding to mitochondrial content followed a similar pattern to mtNDA as it was significantly reduced in both patient derived cultures compared to control cells (Figure 4.24 B). The drop in mitochondrial content was most prominent in FBXL4A fibroblasts. Mitochondrial DNA nucleoids in patient derived cells appeared abnormal in size (Figure 4.24 C and E) similarly to DNM1L and OPA1 mutant cells (Figure 4.10, 4.15 and 4.16). Subsequent quantification of nucleoid diameter showed a significant increase in nucleoid size in both patients compared to control cells (Figure 4.24 C). Nucleoid distribution also appeared abnormal in patient fibroblasts with apparent clustering in the perinuclear region of the cells as opposed to an even distribution throughout the cytoplasm as seen in controls (Figure 4.24 D and E). Similar pattern of perinuclear clustering of mtDNA nucleoids was reported by a different group in

fibroblasts from patients harboring single homozygous mutations in the *FBXL4* gene (S1 and S2 in Bonnen et al., 2013).

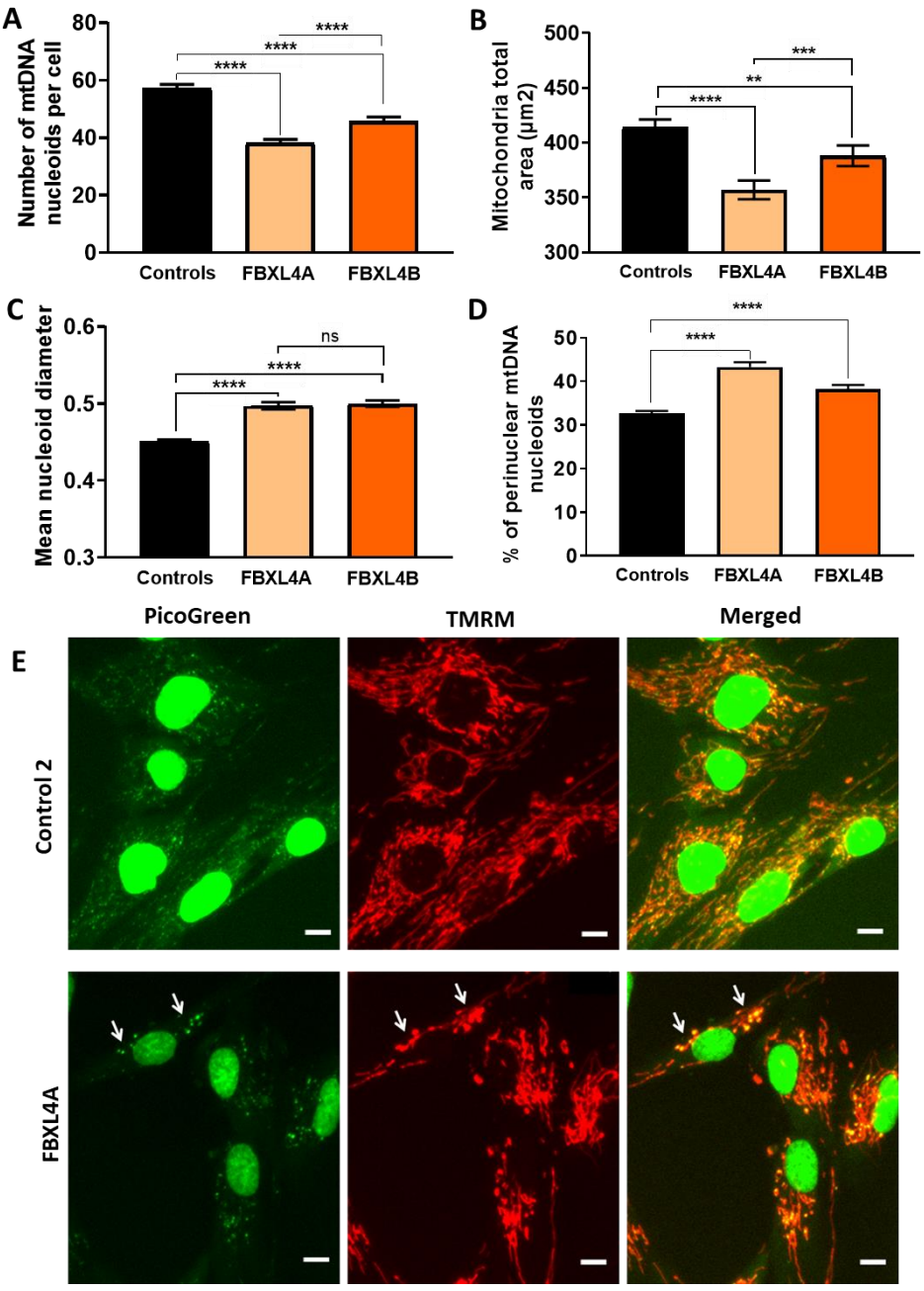

Figure 4.24 Mitochondrial DNA content in FBXL4 cells
(A) Quantification of PicoGreen labelled mtDNA nucleoids. (B) Mitochondrial area measured by TOM20 labelling. (C) Quantification of mtDNA nucleoid diameter. (D) Representative images of control and FBXL4A fibroblasts cells stained with PicoGreen and TMRM, enlarged nucleoids in FBXL4A are indicated by white arrows.
n=2, Minimum of 1138 cell analysed per condition, mean +/- 95% CI, ****=p<0.0001, scale bar 10µm

4.4.3.5 Discussion of FBXL4 specific findings

The results presented here are in agreement with previously described cases. FBXL4A and FBXL4B fibroblasts had reduced mitochondrial DNA content and deficient mitochondrial bioenergetics. Mitochondrial organisation was affected, mitochondrial area being decreased and nucleoids were enlarged and clustered in the perinuclear region, consistent with previous studies (Bonnen et al., 2013). Enlarged mtDNA nucleoids are often seen in patients with defects in mitochondrial DNA maintenance (unpublished data). Mitochondrial nucleoids consist of all the proteins necessary for the transcription and replication of mtDNA; however, the molecular mechanism of nucleoid formation remains poorly understood. Even though mutations in FBXL4 have been identified in patients with either severe mitochondrial DNA depletion or reduced mitochondrial DNA content above the threshold to be classified as depletion the protein's function is currently unknown. Hence, it is not clear which if any of these abnormalities is the primary problem. While reduced mtDNA content and bioenergetics have been associated with mtDNA perinuclear clustering in OPA1 knockdown, this is probably due to increased mitophagy resulting from profound mitochondrial fragmentation. As FBXL4 mutations appear to elongate rather than fragment mitochondria it does not phenocopy OPA1. FBXL4 has recently been associated with ERLEC1, an ER stress response element (Misiewicz et al., 2013). FBXL4 was implicated in the regulation of ERLEC1 expression based on the well-established function of F-box proteins in ubiquitin mediated protein degradation (Kipreos and Pagano, 2000; Skowyra et al., 1997). This places FBXL4 into a role in both mtDNA maintenance and in a potentially ER-associated function.

4.4.4 Patients with mutations in *CHCHD10*

Coiled-Coil-Helix-Coiled-Coil-Helix Domain-Containing Protein 10 (CHCHD10) is a mitochondrial protein localised in the intermembrane space and especially enriched at cristae junctions (Bannwarth et al., 2014). Mutations in *CHCHD10* were reported in patients with frontotemporal dementia and amyotrophic lateral sclerosis like phenotypes (Bannwarth et al., 2014; Johnson et al., 2014), mitochondrial myopathy (Ajroud-Driss et al., 2015) , axonal Charcot-Marie-Tooth disease (Auranen et al., 2015) as well as Parkinson's disease (Rubino et al., 2017). CHCHD10 is ubiquitously expressed in humans, however expression levels vary from tissue to tissue. In line with the phenotypes observed in patients harbouring *CHCHD10* mutations the encoded protein have the highest expression levels in tissues with high energy demand such as the liver, muscle and heart (Bannwarth et al., 2014). Additionally, in the central nervous system CHCHD10 is strongly expressed in dopaminergic neurons of the substantia nigra as well as in spinal cord neurons which are the most affected in Parkinson's disease (Burstein et al., 2018). Fibroblasts derived from a patient with FTD-ALS-like disease due to the Ser59Leu pathogenic variant of CHCHD10 showed disorganised cristae and mitochondrial DNA nucleoids which lead to the conclusion that CHCHD10 is part of the mitochondrial contact site and cristae organizing system (MICOS) (Genin et al., 2016). The MICOS complex is located in the IMM and involved in the maintenance of cristae junctions, inner membrane architecture and formation of contact sites with the OMM. More recent studies reported that CHCHD10 forms a complex with its paralogue CHCHD2 and together they regulate oxidative phosphorylation (Purandare et al., 2018; Straub et al., 2018). CHCHD2 is found in both the mitochondria and the nucleus. In the mitochondria, it binds to cytochrome

oxidase c (complex IV) and in the nucleus it functions in the transcriptional regulation of genes that contain a highly conserved promoter motif termed the oxygen-responsive element (Aras et al., 2015). Both CHCHD10 and CHCHD2 are rapidly turned over, in a matter of hours, which is more supportive of a regulatory function for these proteins rather than a structural role (Burstein et al., 2018).

CHCHD10 is a 142 amino acids long protein encoded by four exons with a MTS at the N-terminus end (amino acids 1-16) and a C-terminal CHCH domain (amino acids 102-133) (Figure 4.25 A) (Ajroud-Driss et al., 2015). CHCHD10 mutant fibroblasts were available from two unrelated individuals harbouring a single mutation at highly conserved neighbouring residues (Figure 4.25 B). Patient G58R carried the c.172G>C (p.Gly58Arg) missense mutation in exon 4 (Figure 4.25). He presented at aged 6 years with lipid storage myopathy and scanty cytochrome oxidase negative fibres due to a mixed respiratory chain deficiency in skeletal muscle (complex ll+lll 0.027 (0.04-0.204), complex lV 0.005 (0.014-0.034) with normal mtDNA copy number. Later in childhood he developed dilated cardiomyopathy and underwent a heart transplant. He died of lymphoma as a side effect of the immunosuppression required for his transplant at the age of 19. Patient S59L was presented as V-10 in Bannwarth et al. (2014), harboured the c.176C>T (p.Ser59Leu) missense mutation affecting the neighbouring amino acid. She had a milder phenotype with an age of onset 49 years with cerebellar syndrome including ataxia, cognitive impairment and areflexia. Patient S59L's fibroblasts showed borderline low activities of all respiratory chain complexes and she was still alive at the time of the publication (Bannwarth et al., 2014).

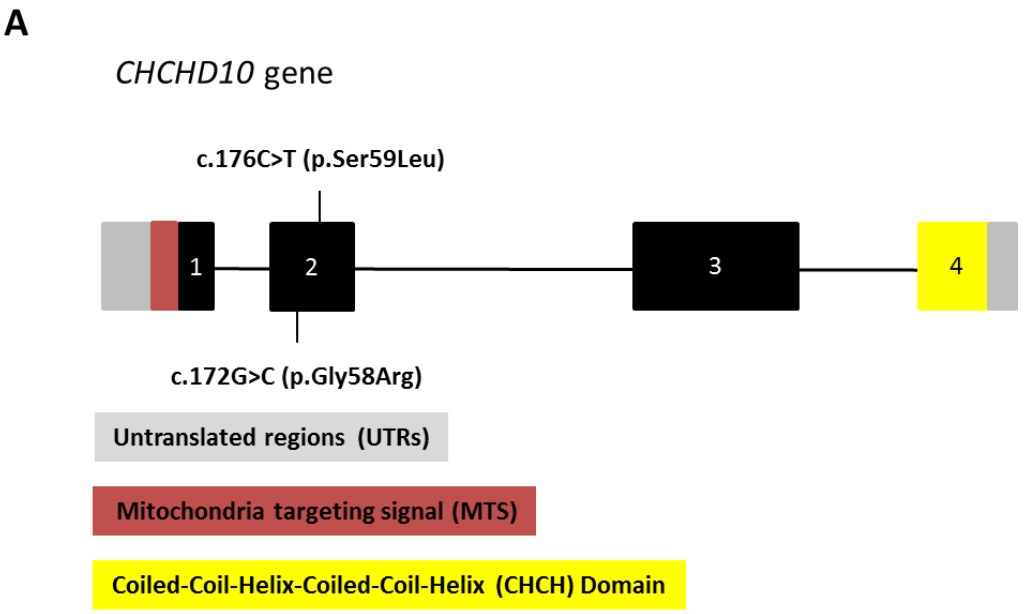

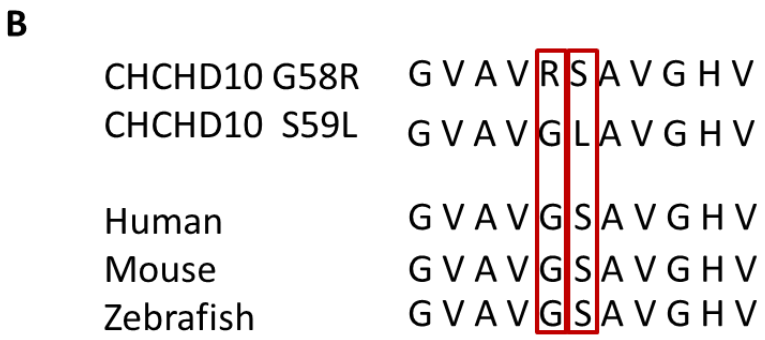

Figure 4.25 CHCHD10 gene structure and currently investigated mutations
(A) CHCHD10 is a 142 amino acids long protein encoded by 4 exons with a MTS at the N-terminus end (amino acids 1-16) and a C-terminal CHCH domain (amino acids 102-133) (B) Both Gly58Arg and Ser59Leu mutations are found in a region of highly conserved residues. Image adopted from Bannwarth et al., 2014, not to scale

4.4.4.1 Mitophagy and autophagy in *CHCHD10* mutant fibroblasts

The CHCHD10 mutations investigated in this section affect neighbouring amino acid residues. Regardless, the phenotypic presentation of the two patients is very different. Mitophagy in G58R fibroblast derived from the more severe patient had increased mitophagy both at baseline and after treatment with lysosomal inhibitors when compared to controls (Figure 4.26 A). In S59L cells mitophagy was only increased following EP treatment when compared to control cells. There was a significant difference between the two patients. Mitophagy was exceedingly higher in G58R cells when compared to S59L ones. Autophagy, measured as the number of LC3 positive punctae, was increased in both patient cultures at baseline as well as after EP treatment when compared to control cells (Figure 4.26 B). Similarly to mitophagy, autophagy was significantly higher in G58R fibroblasts derived from the more severe patient when compared to S59L cells. Representative images of TOM20 and LC3 labelled control and patient fibroblasts are shown in Figure 4.27.

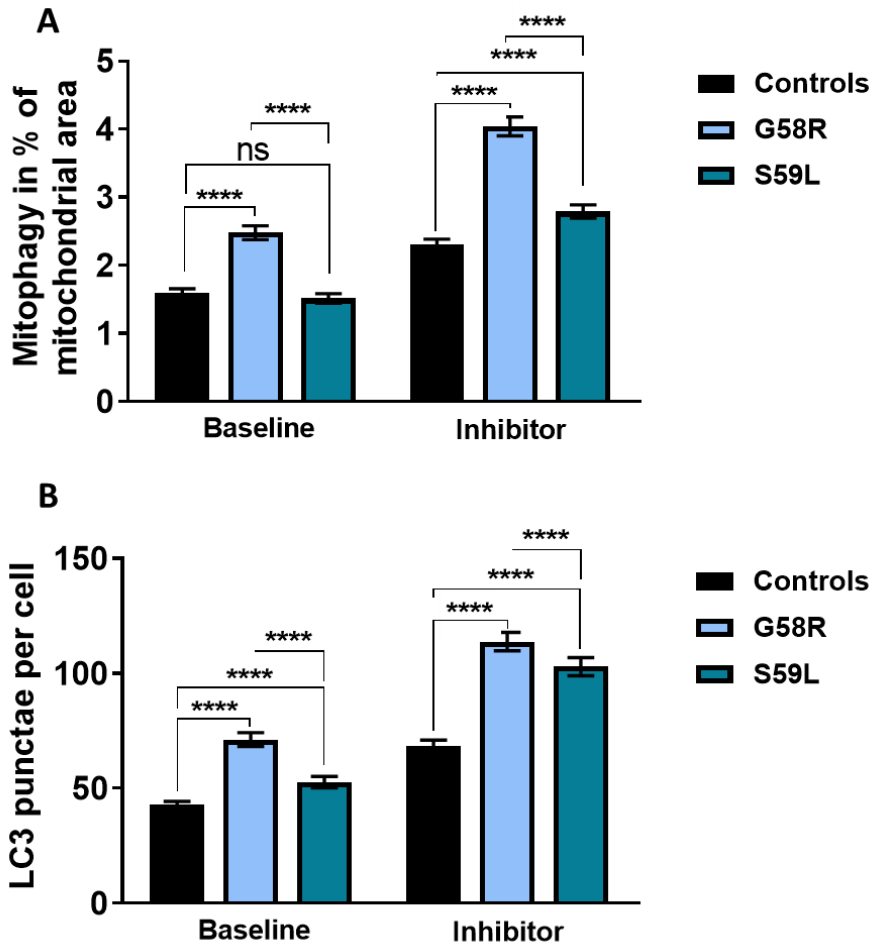

Figure 4.26 Mitophagy and autophagy in CHCHD10 fibroblast
(A) Mitophagy and (B) autophagy measured at baseline and following 24 hours treatment with lysosomal inhibitors E64d and Pepstatin A (10µg/ml).
n=3, minimum of 943 cells analysed per condition, mean +/- 95% CI, ***=*p*<0.0001

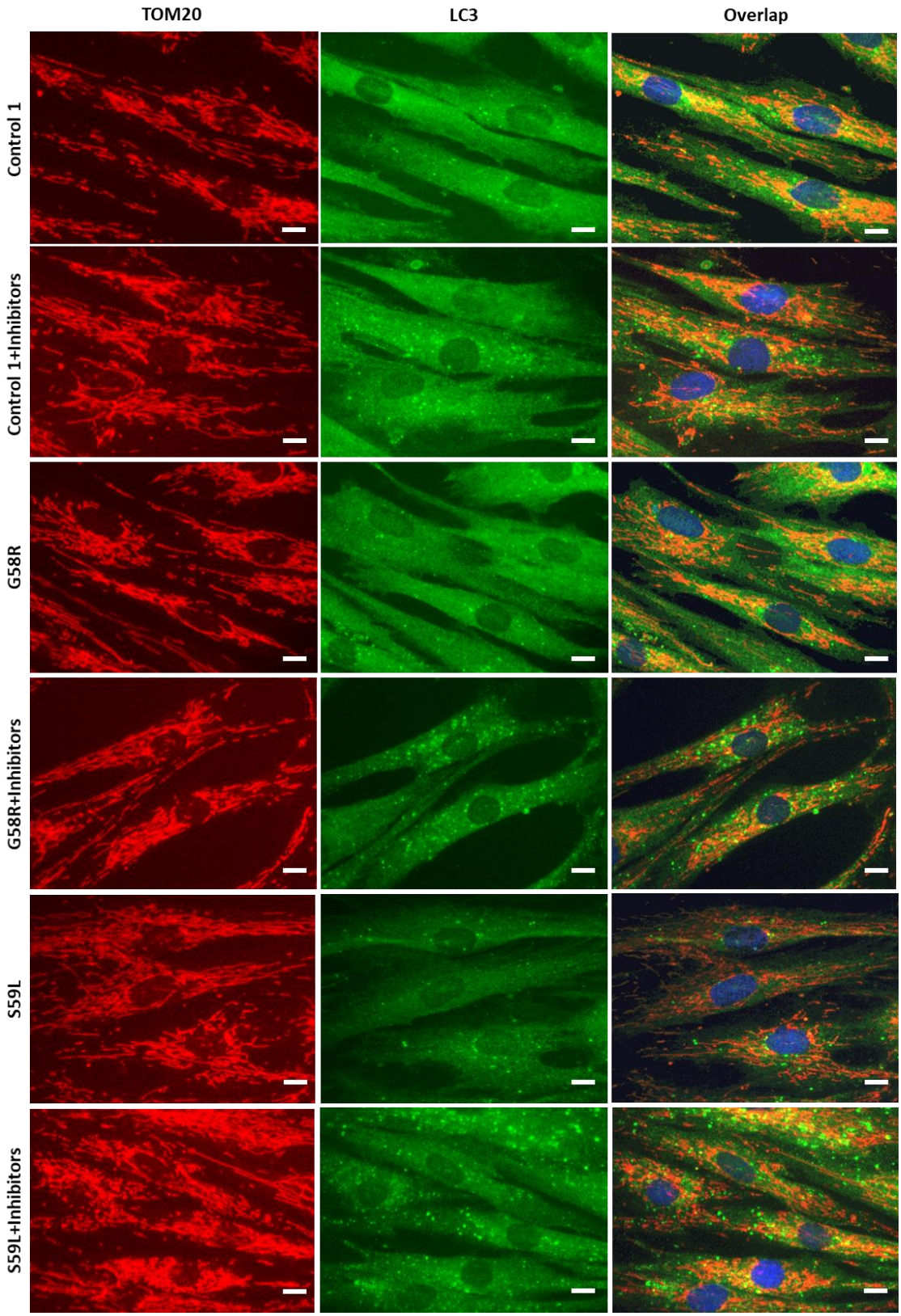

Figure 4.27 Representative images of Control 1 and CHCHD10 fibroblasts
Showing TOM20-labelled mitochondria and LC3-labelled autophagosomes cultured either at baseline or with the addition of lysosomal inhibitors E64d and Pepstatin A. Scale bar 10µm.

4.4.4.2 Mitochondrial network properties of CHCHD10 fibroblasts

Fragmentation of the mitochondrial network was reported in S59L fibroblasts (Bannwarth et al., 2014) as well as in HEK293 cells expressing G58R mutant CHCHD10 protein (Ajroud-Driss et al., 2015). However, in our assay G58R cells had elongated mitochondria, while S59L fibroblasts showed a fragmented mitochondrial network when compared to control cells (Figure 4.28 A). This is consistent with the previously published results on the S59L cells (Bannwarth et al., 2014) but not with HeLa cells expressing the G58R mutation (Ajroud-Driss et al., 2015). Mitochondrial membrane potential measured by TMRM showed an opposite trend. TMRM intensity was reduced in G58R fibroblasts as opposed to increased membrane potential in S59L cells when compared to controls (Figure 4.28 B).

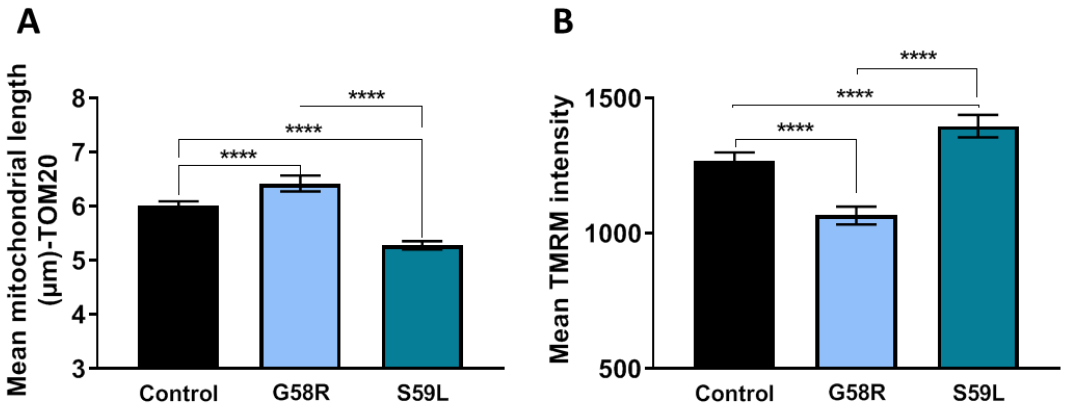

Figure 4.28 Mitochondrial network properties of CHCHD10 fibroblasts
(A) Mean mitochondrial length measured by TOM20 labelling, n=3, minimum of 983 cell analysed per condition. (B) Mitochondrial membrane potential measure by TMRM intensity, n=2, minimum of 581 cells analysed per condition. Mean +/- 95% CI, *=p<0.05, ****=p<0.0001

4.4.4.3 Bioenergetics of CHCHD10 fibroblasts

Oxygen consumption data is only available on S59L fibroblasts. There was no difference in basal, maximal or ATP-related respiration between control and S59L patient cells (Figure 4.29) which agrees with the normal respiratory chain function reported in the patient's muscle.

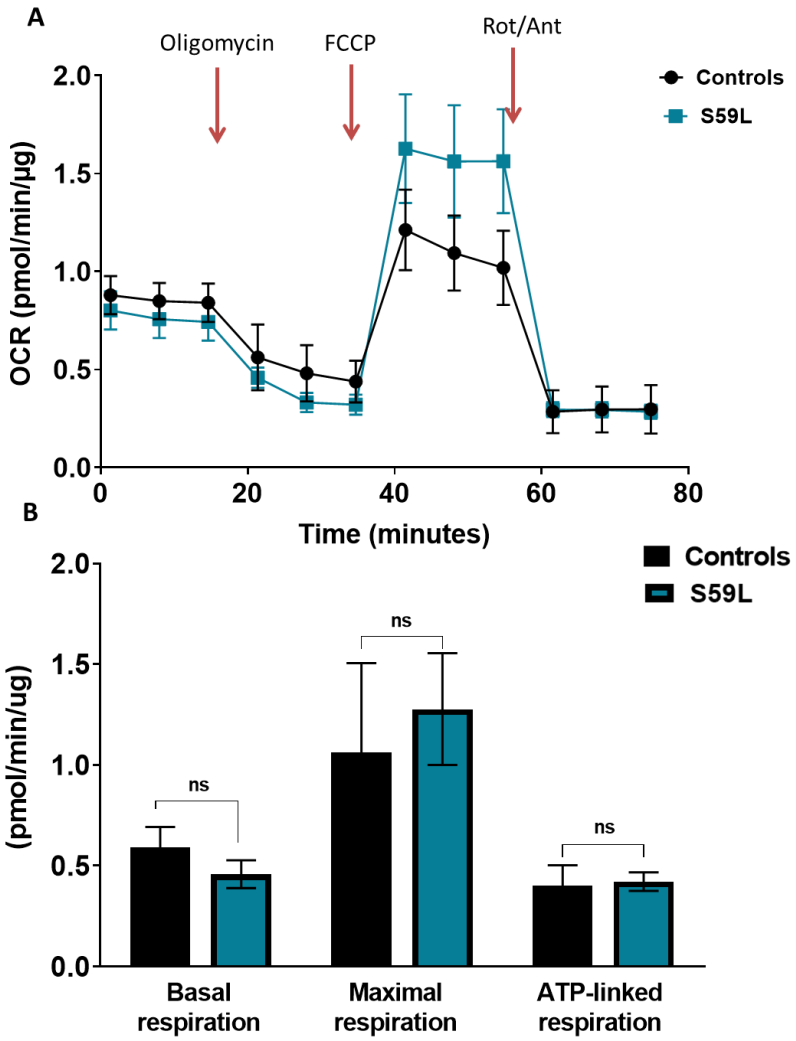

Figure 4.29 Oxygen consumption rate and mitochondrial respiration in CHCHD10 fibroblasts
(A) Oxygen consumption rate measured every 18 minutes normalized to protein content, all injections indicated. Rot/Ant A = Rotenone and Antimycin A. (B) Baseline, maximal and ATP linked respiration calculated from the results shown in graph A. Mean +/- 95%CI from a single experiment based on at least 4 technical replicates.

4.4.4.4 Mitochondrial content in CHCHD10 fibroblasts

CHCHD10 is predicted to have a role in mitochondrial DNA maintenance. Multiple mitochondrial DNA deletions in muscle and disorganised mtDNA nucleoids are a common feature in patient derived cells with *CHCHD10* mutations. Despite previous reports of reduced mitochondrial DNA content in CHCHD10 mutant cells (Bannwarth et al., 2014) the number of mtDNA nucleoids measured by PicoGreen staining was increased by approximately 30% in both G58R and S59L fibroblasts compared to control cells (Figure 4.30 A). Representative images of PicoGreen and TMRM labelled control and patient fibroblasts are shown in Figure 4.30 C. Along with this, mitochondrial content was also increased in fibroblasts from both patients (Figure 4.30 B). The increase was more prominent in S59L cells derived from the milder patient.

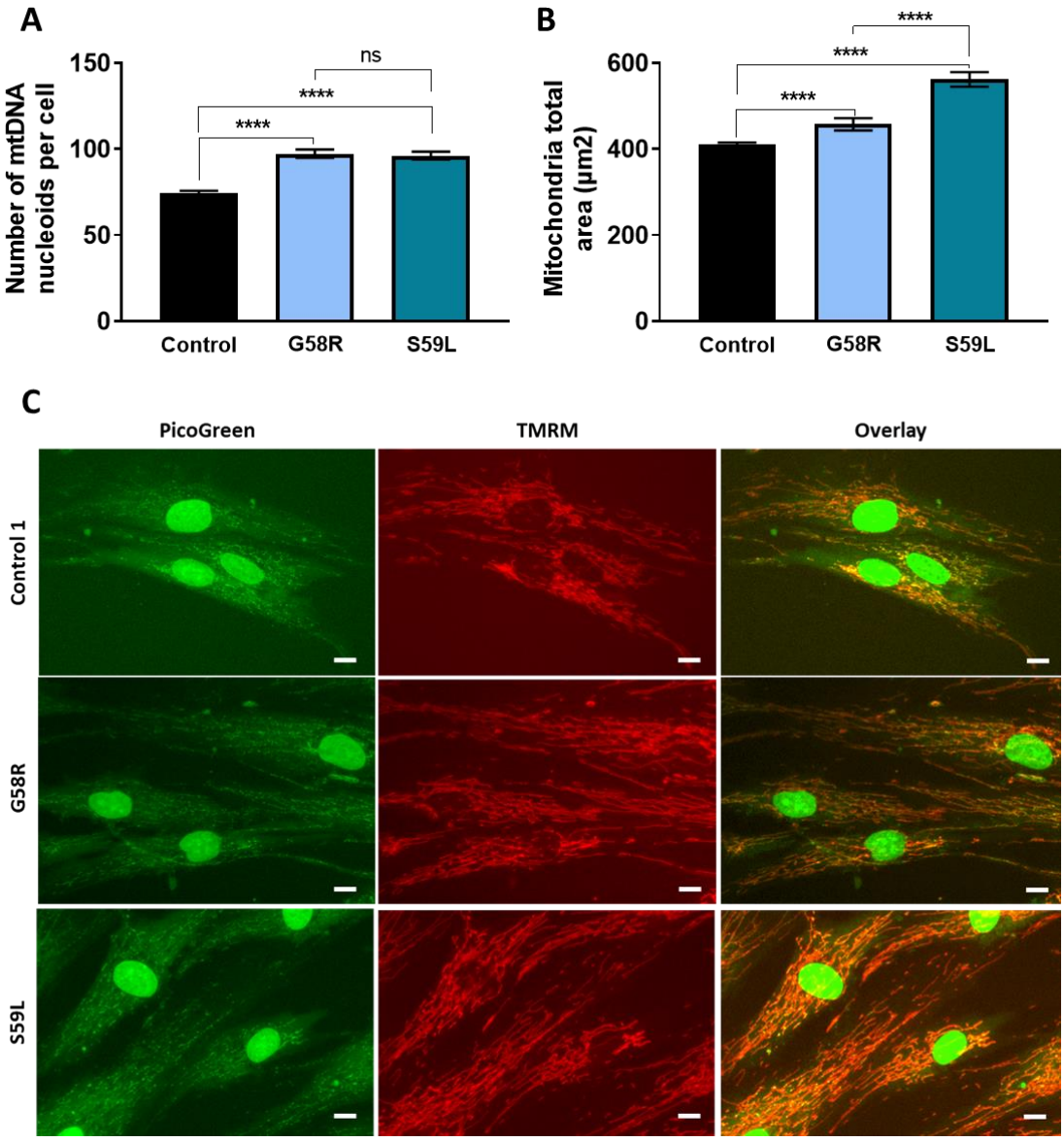

Figure 4.30 Mitochondrial content in CHCHD10 fibroblasts
(A) Quantification of PicoGreen labelled mitochondrial DNA nucleoids; n=3, minimum of 943 cells analysed per condition. (B) Mitochondrial content measured as the total area of TOM20 labelled mitochondria n=3, minimum of 983 cell analysed per condition (C) PicoGreen and TMRM labelled fibroblasts, scale bar 10µm
Mean +/- 95% CI, *=p<0.05, ****=p<0.0001

4.4.4.5 Discussion of CHCHD10 specific findings

In this section I presented two unrelated patients with different point mutations in the *CHCHD10* gene. The clinical presentation of the two patients was very different despite their CHCHD10 mutations affecting neighbouring amino acid residues that are highly conserved. The results show increased mtDNA copy number in both patients, but mitochondrial organisation and membrane potential differed markedly between the patients.

CHCHD10 mutations reported in the literature are mostly associated with neurodegenerative phenotypes, such as ALS, FTD or Parkinson's disease of which patient S59L is typical. Our patient and his family harbouring the G58R mutation comprises the only CHCHD10 family described with cardiomyopathy, a feature that is seen in a new CHCHD10 mouse model (Paquis-Flucklinger, personal communication). The reason for this is currently unknown. It was proposed that the mutations associated with the neurodegerative phenotypes are making the protein more hydrophobic but not the G58R mutation (Huang et al., 2018). Nonetheless, how this feature confers such tissue specificity is unknown. In order to untagle the not so obvious relationship between genotype and phenotype determination of CHCHD10 protein function is essential. Currently CHCHD10 is implicated as an integral protein of the MICOS complex that organises the cristae junctions within cells (Genin et al., 2018). On the contrary, CHCHD10 has also been reported to regulate oxydative phosporylation in mitochondria as well as to media hypoxia response in tandem with CHCHD2 (Straub et al., 2018).

I showed increased mitophagy and autophagy in fibroblasts from both patients. The magnitude of the increase compared to control cells seemed to correlate with the

severity of the phenotype with both mitophagy and autophagy being the highest in G58R cells. This graded response may reflect the overall stress level these cells are under as a result of their corresponding mutations.

4.5 Overall chapter discussion

A visual summary of all findings in this chapter is presented in Table 4.2. Dysregulated autophagy and mitophagy were found to be common features of fibroblasts derived from patients with mitochondrial disease secondary to mutations in nuclear encoded mitochondrial proteins. These included proteins involved in mitochondrial dynamics (pro-fission protein DNM1L and pro-fusion proteins OPA1 and MFN2) and two proteins of unknown function (FBXL4 and CHCHD10). Loss of mitochondrial membrane potential is a known inducer of PINK1/Parkin mediated mitophagy (Narendra et al., 2009). We have observed a substantial loss of membrane potential in FBXL4, CHCHD10 G58R, OPA1 and MFN2 fibroblast which could contribute to the increased co-localisation of mitochondria with autophagosomes in these cells. Despite the increased co-localisation events there was a significant reduction in the number of lysosomes in OPA1 and DNM1L cells. Hence, in these cells increased mitophagy measured as co-localising mitochondria and autophagosomes may reflect slower degradation limited by the number of lysosomes, rather than increased turnover. Previously, increased mitophagy was documented in fibroblasts derived from a cohort of patients with dominant-negative OPA1 mutations (Liao et al., 2017). These fibroblast also demonstrated excessive fragmentation of the mitochondrial network. It was concluded that the fragmentation could contribute or even drive the increased mitophagy seen in these cells. On the other hand, fibroblasts harbouring OPA1 mutations such as the Ile382Met mutation found in the OPA1 patient presented here result in haploinsuffiency due to the loss of the short-OPA1 isoforms only, and therefore a mildly fragmented mitochondrial network (Kane et al., 2017).

Fibroblast harbouring mutations resulting in haploinsuffciency were also found to have reduced autophagy as well as mitophagy (Kane et al., 2017). The OPA1 mutations harboured by our patient likely result in haploinsufficiency. We did not see excessive fragmentation like in the dominant negative patients (Chunyan Liao, 2016). Unravelling whether increased mitophagy and autophagy are a result of the disease or a contributing factor to the phenotype requires further investigation.

In fibroblasts with FBXL4 and CHCD10 mutations they are likely the outcome of mitochondrial and cellular distress resulting from the dysfunction of the given protein. In these cells the magnitude of the increase in both mitophagy and autophagy seemed to reflect the differences in disease severity. Hence it might be possible to use our INCell 1000 readout measuring mitophagic flux as a diagnostic biomarker of mitochondrial disease.

Table 4.2 Summary of the main findings

Patient	Mitophagy	Autophagy	OXPHOS defect	Membrane potential	mtDNA content	Mito fragmentation	Perinuclear nucleoid clustering	Lysosomal content
OPA1	↑	↔	N/A	↓	↓	**no**	yes	↓
MFN2	↑	↑	N/A	↓	qPCR to confirm	yes	**no**	N/A
DNM1LA	↑	↑	yes	↑	↓	elongated	yes	↓
DNM1LB	↑	↑	no	↑	↓	elongated	yes	N/A
FBXL4A	↑	↑	yes, (max res only)	↓	↓	elongated	yes	↑
FBXL4B	↑	↑	yes	↓	↓	yes	yes	↑
G58R	↑	↑	no	↓	↑	elongated	no	N/A
S59L	↑	↑	N/A	↑	↑	yes	**no**	N/A

4.6 Limitations of this study

In this study mitophagy is defined as co-localising mitochondria and autophagosomes, which is not an end point measurement in the degradation pathway. Therefore, I use a combination of lysosomal inhibitors and present mitophagy measured both at baseline and following inhibitor treatment side-by-side in order to infer (estimate) flux. However, unlike the mtDNA mutants described in chapter 3, in this chapter DNM1LA and OPA1 fibroblasts had lower lysosomal counts when compared to control cells. Therefore, additional methods (eg. protein turnover) should be used to confirm the rate of mitochondrial turnover.

Measuring mitochondrial DNA content using PicoGreen staining of mtDNA nucleoids was previously shown to correlate well with qPCR results (Uusimaa et al., 2014). Nonetheless, given that nucleoid abnormalities, such as size and organisation, were present in some of the fibroblasts investigated, mtDNA content results should be confirmed by qPCR analysis.

The oxygen consumption data is derived from a single run (n=1), although a minimum of five wells were used for each fibroblasts culture. Additional biological replicates are needed confirm the differences presented here prior to publication.

4.7 Future directions

Based on these results a new collaborative study emerged regarding the pathogenesis of CHCHD10 mutations between us and the Narendra group (NIH).

Chapter 5. Mitochondrial DNA depletion in POLG fibroblasts is rescued by dNTP supplementation

5.1 Introduction

Previously I described fibroblasts from patients with either qualitative changes in mitochondrial DNA due to the presence of point mutations (Chapter 3) or mitochondrial dysfunction as a result of nuclear DNA mutations in genes encoding for integral mitochondrial proteins (Chapter 4). In this chapter I will present a single patient with mitochondrial disease caused by a reduction in mtDNA secondary to mutations in the nuclear encoded catalytic subunit of mitochondrial DNA gamma polymerase, POLG.

Mitochondrial diseases as a result of tissue specific reduction of mitochondrial DNA copy number are referred to as mitochondrial DNA depletion syndromes, the first paediatric cases of which were described in 1991 (Moraes et al., 1991). Each mitochondrion contains multiple copies of their circular genome that are maintained and synthesised by the mitochondrial replisome. Although mtDNA replication is considered to be independent of the cell cycle as it is continuous throughout (Taanman et al., 2003), the rate of transcription increases prior to cell division (Chatre and Ricchetti, 2013). Despite the seemingly autonomous life cycle of the mitochondrial DNA, all enzymes necessary for its replication and repair are encoded by the nucleus.

Mitochondrial depletion syndrome (MDS) is an umbrella term for a constantly expanding group of human disorders that result from defects in mtDNA maintenance. Today, in the rapidly developing world of genome sequencing, mutations in numerous nuclear genes are associated with MDS (Table 5.1). Most of these appear to be either directly involved in the replication of the mitochondrial genome or

indirectly in mtDNA maintenance (Poulton et al., 2009; Spinazzola et al., 2009; Suomalainen and Isohanni, 2010).

Table 5.1 Genes and their functions implicated in mitochondrial DNA depletion syndromes

Gene	Protein	Function
Mitochondrial DNA replication		
TWNK/C10orf2/PEO1	TWINKLE	mtDNA helicase
POLG	POLG	Catalytic subunit of the mitochondrial DNA polymerase
POLG2	POLG2	POLG accessory subunit
TFAM	TFAM	Mitochondrial transcription factor A
Nucleotide metabolism		
RRM2B	P53R2	Constitutively expressed ribonucleotide reductases
DGUOK	dGK	Mitochondrial dioxyguanosine kinase
TK2	TK2	Mitochondrial thimidine kinase
SUCLA2	SUCLA2	Succinyl-CoA synthase α subunit
SUCLG2	SUCLG2	Succinyl-CoA synthase β subunit
SLC25A4	ANT1	Adenine nucleotide translocase type 1
Genes encoding proteins with unknown functions		
MPV17	MPV17	Mitochondrial inner membrane protein
FBXL4	FBXL4	Mitochondrial inner membrane protein

5.1.1 The mitochondrial replisome

The current models of mitochondrial DNA replication are reviewed in Section 1.1.5. Polymerase gamma (poly γ) is a key enzyme of the mitochondrial replisome (Figure 5.1 A) and the only known mitochondria specific polymerase (Ropp and Copeland, 1996). It is a holoenzyme that consists of a catalytic subunit with exonuclease activity encoded by the *POLG* gene, and the accessory subunit encoded by *POLG2* which enhances binding to DNA as well as processivity (Gray and Wong, 1992; Lee et al., 2009). Poly γ cooperates with the mitochondrial 5'-3' helicase TWINKLE, encoded by the *TWNK* gene, necessary for mtDNA replication (Milenkovic et al., 2013). Additionally, single stranded DNA binding protein 1 (SSBP1) interacts with both enzymes and supports their function (Chinnery and Hudson, 2013) (Figure 5.1 A).

Efficient mitochondrial DNA replication and maintenance requires a balanced supply of deoxynucleoside triphosphates (dNTPs), the building blocks of DNA. Deoxynucleotides are either synthesized *de novo* (Figure 5.2) in the cytosol or through the so called salvage pathway localised partially in the mitochondria and partially in the cytosol (Figure 5.1 B) (Lane and Fan, 2015). *De novo* nucleotide synthesis incorporates low molecular weight precursors into ribonucleoside diphosphates that are reduced to their corresponding deoxyribonucleoside diphosphates by ribonucleotide reductases (RNRs) (Figure 5.2) (Nordlund and Reichard, 2006). The *de novo* synthesis pathway is mainly active during S-phase and provides dNTPs for both the nuclear and mitochondrial genome replication in proliferating cells (Nordlund and Reichard, 2006). RNRs are regulated by the cell cycle and present at very low amounts in non-replicating cells (Hakansson et al., 2006).

Therefore, terminally differentiated or quiescent cells depend on the salvage pathway for a balanced supply of dNTPs that are produced from recycled deoxynucleosides. The recycled deoxynucleosides are phosphorylated by thymidine kinase 1 (TK1) and deoxycytidine kinase (dCK) in the cytosol and thymidine kinase 2 (TK2) and deoxyguanosine kinase (dGK) in the mitochondria (Figure 5.1 B). Mutations in both mitochondrial kinases (TK2 and dGK), but not the cytosolic ones have been linked to MDS (Brahimi et al., 2009; Saada et al., 2001).

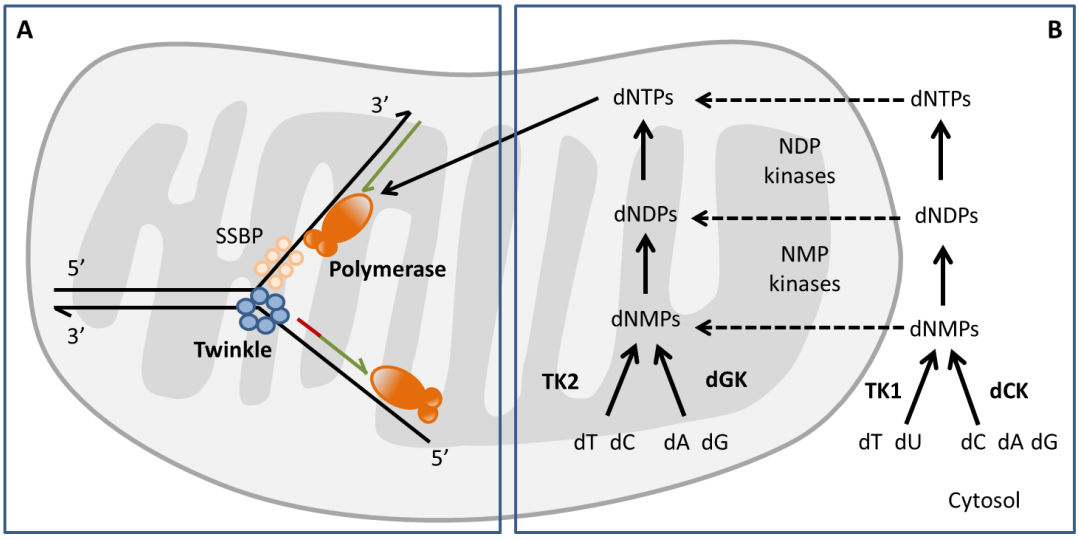

Figure 5.1 Mitochondrial DNA replication and nucleotide synthesis
(A) The mitochondrial replisome consists of the heterotrimeric mitochondria specific polymerase poly γ, the hexameric helicase Twinkle and the single-strand binding proteins (SSBP). The catalytic subunit of poly γ is encoded by the POLG gene and the accessory subunit that forms a homodimer is encoded by the POLG2 gene. (B) In the mitochondrial leg of the nucleotide salvage pathway pyrimidine deoxynucleosides are phosphorylated by thymidine kinase 2 (TK2) and purine nucleotides by deoxyguanosine kinase (dGK). The recycled deoxynucleosides are phosphorylated by thymidine kinase 1 (TK1) and deoxycytidine kinase (dCK) in the cytosol. Deoxynucleoside monophosphates are further phosphorylated by nucleoside monophosphate (NMP) and nucleoside diphosphate (NDP) kinases into deoxynucleoside triphophates (dNTPs) which can be incorporated into DNA.

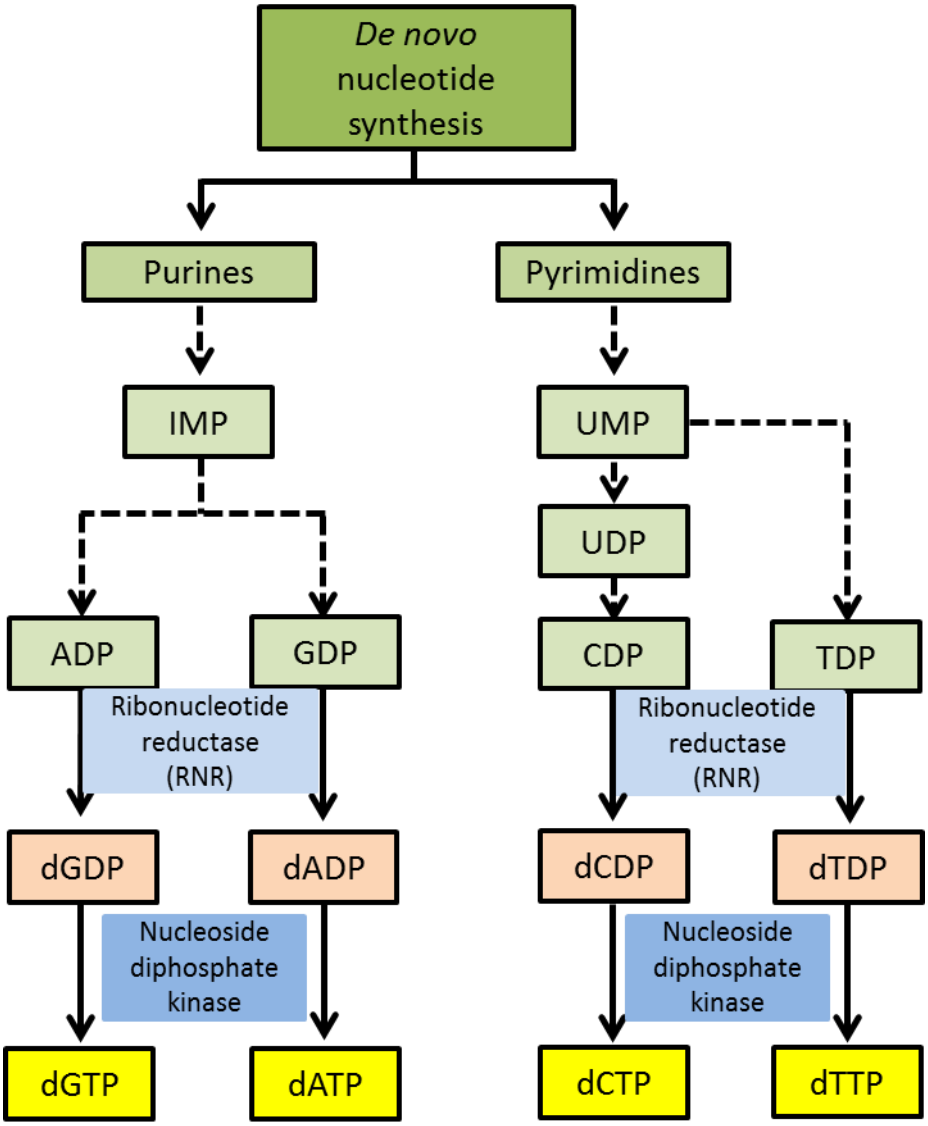

Figure 5.2 *De novo* nucleotide syntheses in the cytosol
De novo nucleotide syntheses incorporates low molecular weight precursors into ribonucleoside diphosphates that are reduced to their corresponding deoxyribonucleoside diphosphates by ribonucleotide reductases (RNRs). These are further phosphorylated into deoxyribonucleoside triphosphates by nucleoside diphosphate kinases. IMP= inosine monophosphate, UMP= Uridine monophosphate, A=adenosine, G=guanine, C=cytidine, T=thymidine, DP=diphosphate, TP=tiphosphate

5.1.2 The role of POLG in mitochondrial DNA depletion syndromes

Although the clinical phenotypes of MDS are broadly categorized into myopathic, encephalomyopathic and hepatocerebra (Spinazzola et al., 2009), clinical presentations are often heterogeneous and overlapping, as with most mitochondrial diseases. The most severe cases however are associated with mutations in POLG, which are also by far the most frequent mutations identified in mtDNA depletion. POLG mutations leading to mtDNA depletion are most commonly associated with Alpers syndrome. It is a neurogenetic developmental mitochondrial DNA depletion disorder characterized by multi-system disease with refractory seizures, neurodegeneration, and liver disease due to mtDNA depletion in brain, liver, muscle and other tissues. The number of POLG mutations reported in association with Alpers syndrome is over 100 (Tang et al., 2011).

Defects in POLG can lead to replication stalling and the introduction of point mutations during mtDNA synthesis (Ashley et al., 2008). Proteins encoded by the mitochondrial genome are key catalytic subunits of the electron transport chain; therefore defects in mitochondrial DNA replication are detrimental to oxidative phosphorylation and hence the entire organelle. The resulting mitochondrial dysfunction can lead to increased mitophagy which may drive mtDNA synthesis (Medeiros et al., 2018). This can lead to more replication stalling and further reduce replication fidelity thus exacerbate pre-existing dNTP deficiency (Nikkanen et al., 2016) resulting in a vicious circle (Figure 5.3).

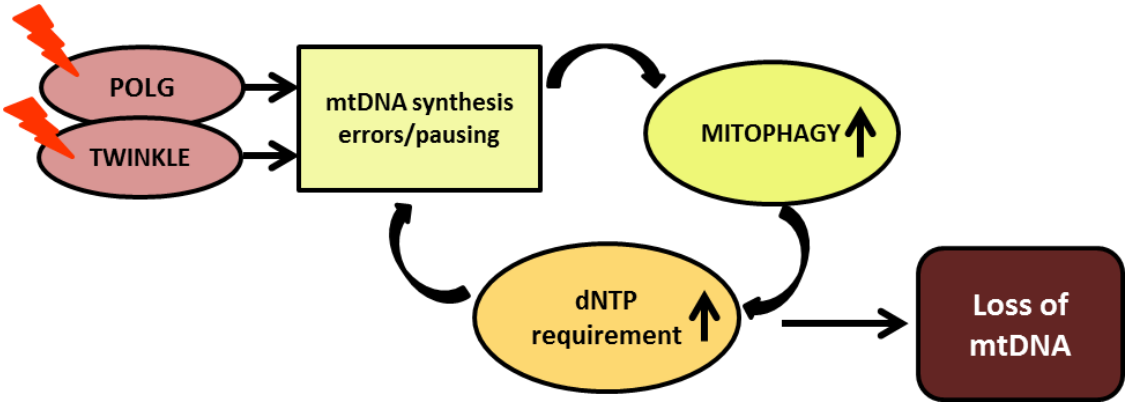

Figure 5.3 Increased mitophagy may contribute to mtDNA loss in MDS
Mutations in genes encoding proteins involved in mtDNA maintenance and replication result in increased mitophagy due to the enhanced presence of dysfunctional mitochondria with mtDNA errors. This heightened mitochondrial turnover increases dNTP requirements due to compensatory mtDNA replication which in turn results in more errors being incorporated. We postulate that this vicious circle contributes to the loss of mtDNA.

5.1.3 Nucleotide supplementation therapy as a potential treatment for MDS

The supplementation of nucleotides has long been under investigation in cellular as well as animal models for mutations in DGUOK and TK2 (Bulst et al., 2012; Garone et al., 2014; Munro et al., 2018; Taanman et al., 2003). These are two enzymes that carry out the initial phosphorylation of deoxypurines and deoxypyrimidines respectively during salvage nucleotide synthesis in the mitochondria (Figure 5.1 B). In MDS secondary to TK2 and DGUOK mutations mtDNA depletion is most likely triggered by substrate limitation (Taanman et al., 2003; Ashley et al., 2007). Supplementation of deoxypyrimidine monophosphates, also known as nucleoside bypass therapy has been implemented in about 18 patients as an experimental therapy for TK2 deficiency. Supplementation of nucleotides has also been reported to increase mitochondrial DNA copy numbers in POLG deficient myotubes (Bulst et al., 2012). Nonetheless, it has not been investigated further as a potential therapy.

5.1.4 Proband mutations and clinical presentation

For this experimental chapter fibroblasts were derived from a severely affected child exhibiting faltering growth and profound motor delay. The patient also presented with liver dysfunction and non-ketotic hypoglycaemia. DNA sequencing revealed three point mutations within the POLG gene (Figure 5.4). On one allele, two mutations were present, one in the exonuclease region (p.T251I) and one in the linker region (p.P587L). These two mutations tend to co-segregate in cis (Tang et al., 2011). The third mutation was found on the second allele in the polymerase domain (p.E1136K). Defects in mtDNA maintenance are difficult to study as mtDNA depletion is often only evident in the affected tissues and rarely present in patient derived fibroblasts. The patient presented here was chosen because the compound heterozygous mutations affecting both exonuclease and polymerase activity of POLG resulted in such a severe phenotype that mitochondrial DNA depletion is readily apparent even in fibroblasts.

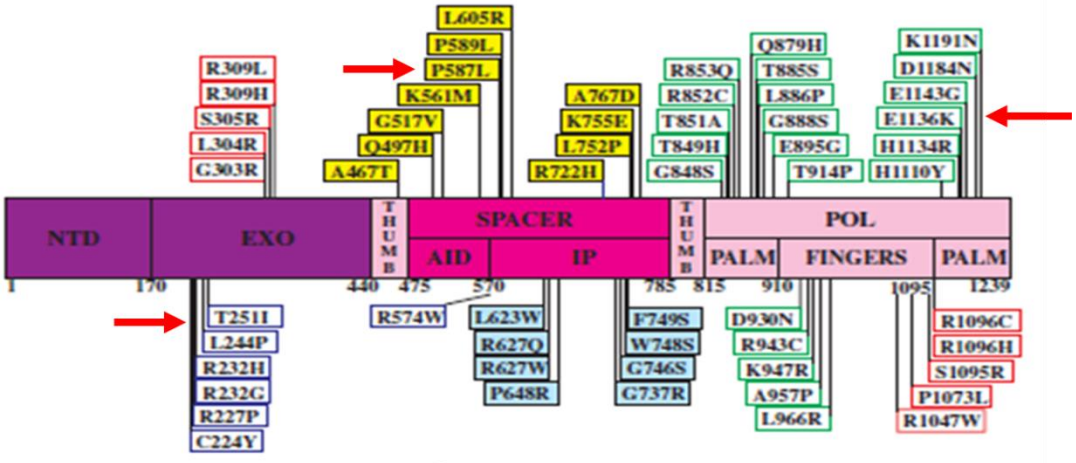

Figure 5.4 Structure of the polymerase γ catalytic subunit and its common mutations
The catalytic subunit of POLG consists of and N-terminal exonuclease domain and a C-terminal polymerase domain joined together by a so called linker or spacer region. The mutations harboured by our patient are indicated by red arrows.

5.2 Aims of chapter 5

I. To characterize fibroblasts derived from a patient with compound heterozygous POLG mutations resulting in severe mtDNA depletion

II. To evaluate whether nucleotide supplementation is efficient in alleviating mtDNA depletion in both replicating and quiescent fibroblast cultures

5.3 Materials and methods

5.3.1 Fibroblast cultures

Skin biopsy was obtained from a patient carrying compound heterozygous *POLG* mutations for diagnostic purposes at Arch Makarios III Hospital, 1474 Nicosia, Cyprus. Informed parental consent for research was subsequently obtained for work in our laboratory in accordance with ethical approval. Control fibroblasts were derived from a healthy consented adult (male, aged 21) whose fibroblasts were used in every high-throughput experiment as mitophagy in these cells were identified being closest to the mean value amongst 15 control cultures (Control 1). Additionally, control fibroblasts obtained from a child with parental consent undergoing skin biopsy for diagnostic karyotyping (male, aged 5) were used as a paediatric control (Control 2). Primary fibroblast cultures were established using standard techniques.

5.3.2 Nucleotides used for supplementation

Fibroblasts were supplemented with a combination of 2'-Deoxyadenosine-5'-monophosphate (dAMP), final concentration 200µM and 2'-Deoxyguanosine-5'-monophosphate (dGMP), final concentration 200µM (Sigma Aldrich).

5.3.3 Cell plating and experimental design

Fibroblast for high-content microscopy experiments were seeded into tissue culture treated 96-welled imaging plates (Cell Carrier). The aim was to evaluate the effect of nucleotide supplementation on both replicating and quiescent cultures. Cell cycling was inhibited by culturing the cells in standard medium supplemented with 1% FCS rather than 10%. Complete serum withdrawal was reported to inhibit cell cycling to the extent that only 0.5-1% of fibroblasts pass through S-phase (Taanman et al.,

2003). Fibroblasts were plated at a density of 500 cells/well for treatment in media containing 10% FCS, and 1000 cells/well for treatment in media with 1% serum (Figure 5.5 A). Cells were left to attach overnight following plating and media was changed the next day (d0) to either glucose (25mM) or low glucose (3mM) media supplemented with 10% FCS or glucose /low glucose media supplemented with 1% FCS. Fibroblasts were maintained in these conditions for three days prior to supplementation (Figure 5.5 B). Supplementation of fibroblasts with a combination of dAMP and dGMP was started on day three. Media and supplements were changed at day six and day eight. Lysosomal inhibitors E64 and Pepstatin A were also included in the media in the applicable treatment group on day eight. Plates were either fixed or prepared for live cell imaging on day nine.

For all other materials and methods please refer to Chapter 2.

5.3.4 Disclaimer

Fibroblasts for the supplementation experiments were plated and treatment was carried out with our 2016/2017 MSc Clinical Embryology student Natnita Mattawanon who was under my supervision in the lab.

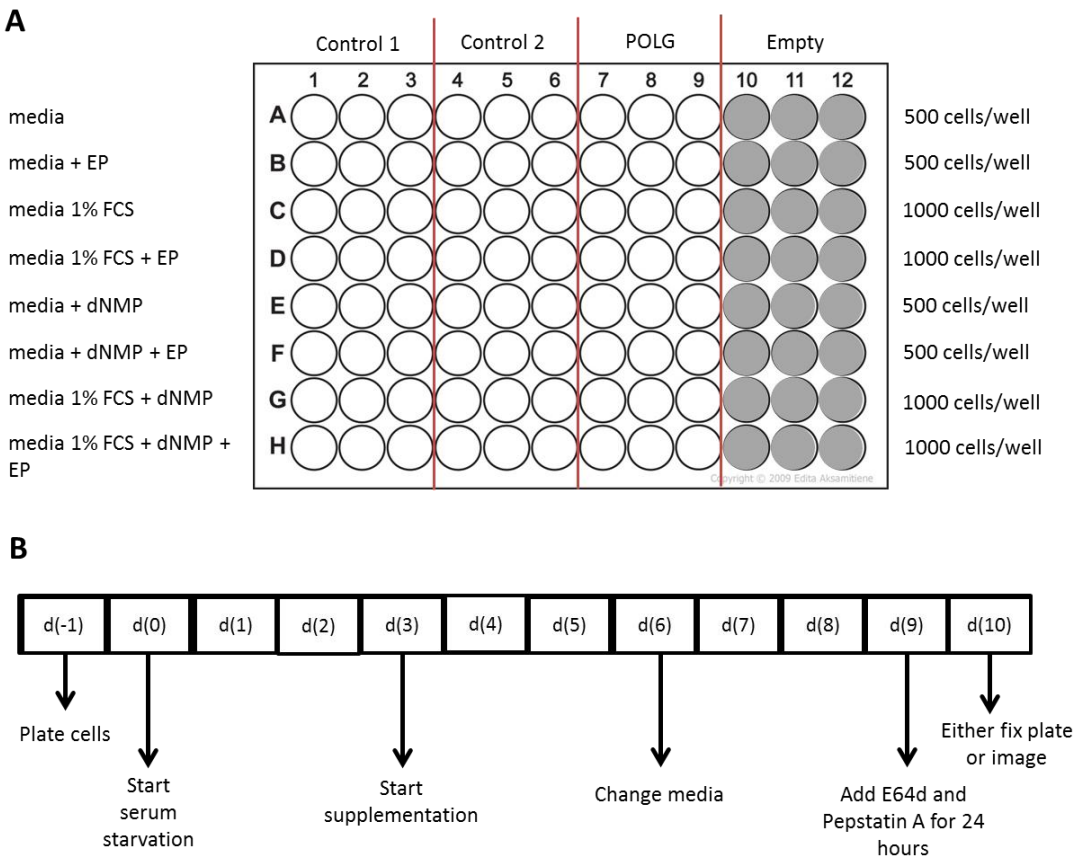

Figure 5.5 Cell plating and experimental design
(A) Schematic representation of plate layout and treatment groups. (B) Experimental timeline of POLG supplementation experiments.

5.4 Results

5.4.1 *POLG* mutant fibroblasts are depleted of mitochondrial DNA

Mitochondrial DNA content was assessed using PicoGreen staining as previously. Mitochondrial DNA content measured as the total area of mitochondrial DNA nucleoids was significantly reduced in POLG fibroblasts when compared to the two control cell cultures (Figure 5.6 A and B). The mean mtDNA content of POLG fibroblasts was 8.2% of control cells (control mean=50.51 and POLG mean =4.15). Concurrently, the percentage of Rho zero cells (those without any detectable mtDNA) was increased to approximately 35% in POLG cells while in control fibroblasts it remained close to zero (Figure 5.6 C). We are aware of no primary cultures from any other patient harbouring such a high proportion of rho zero cells.

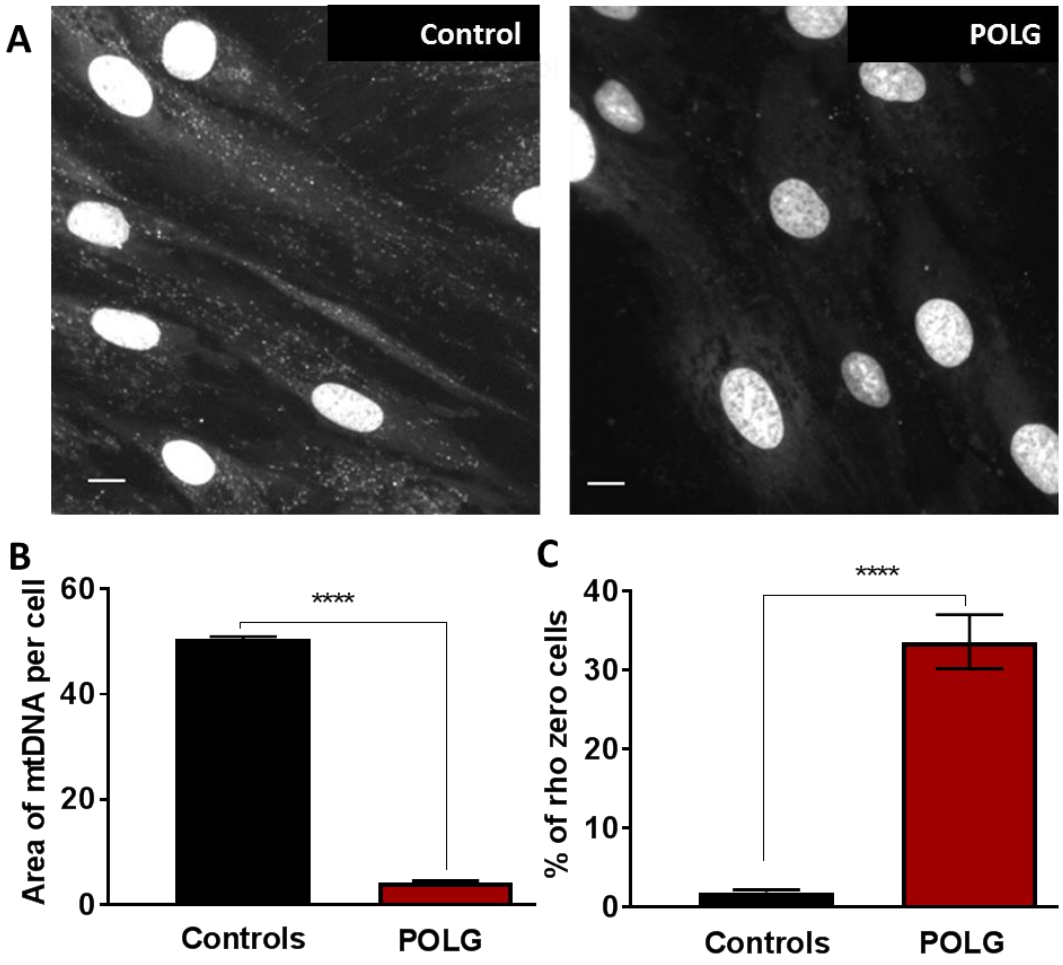

Figure 5.6 Mitochondrial DNA analysis of POLG fibroblasts using PicoGreen
(A) Representative images of control and POLG fibroblasts stained by the DNA specific dye PicoGreen. (B) Quantification of total mtDNA area. (C) Quantification of Rho zero cells (those without any detectable mtDNA) as the % of all cells analysed n=2, minimum of 736 cells analysed per condition, mean +/- 95% CI, **** p<0.0001, scale bar 10µM

5.4.2 Mitochondrial morphology and mitochondrial content in POLG fibroblasts

Mitochondrial content and morphology was assessed by labelling mitochondria with antibodies raised against the outer mitochondrial membrane protein TOM20. Compared to healthy control cells, which typically contain a well-balanced mixture of long and short mitochondria, mean mitochondrial length was significantly reduced in POLG fibroblasts (Figure 5.7 A and B). On the other hand, mitochondrial content assessed by measuring the total mitochondrial area within each cell was not different in control and POLG cell cultures (Figure 5.7 C).

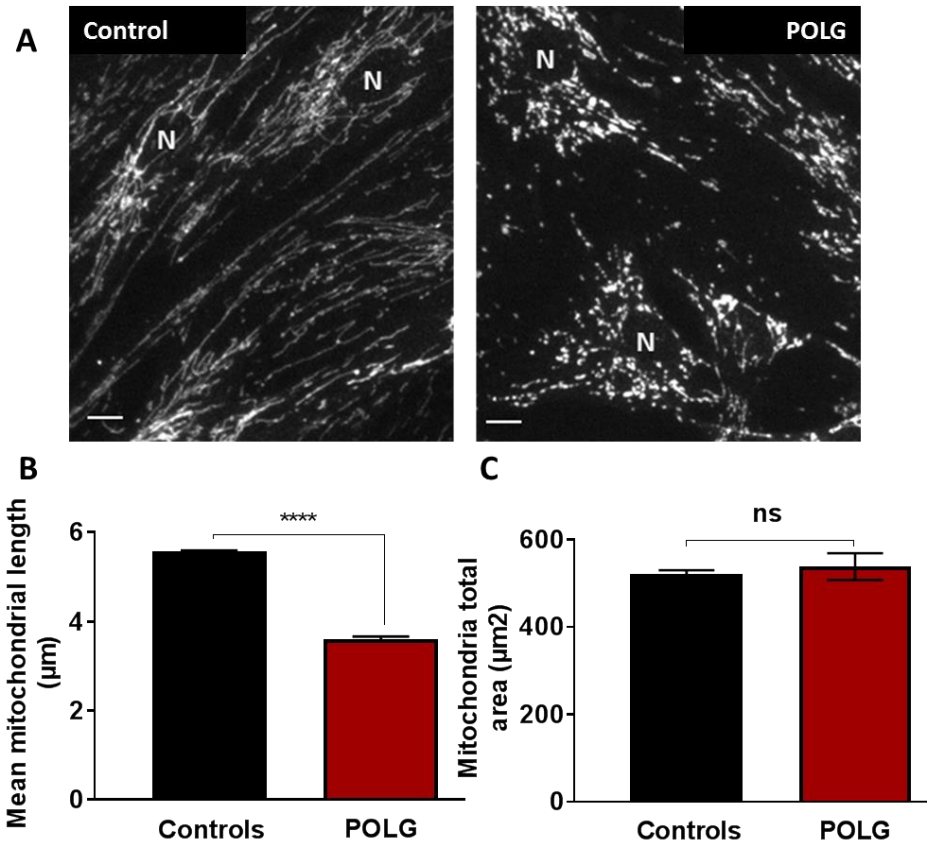

Figure 5.7 Mitochondrial content and morphology of POLG fibroblasts
(A) Representative images control and POLG fibroblasts stained against the outer mitochondrial membrane protein TOM20. (B) Mean mitochondrial length. (C) Mitochondrial content expressed as the total mitochondrial area per cell
**** p<0.0001, n=2, minimum of 651 cells analysed per condition, mean +/- 95% CI, scale bar 10µm

5.4.3 Bioenergetics of POLG fibroblasts

Western blot analysis of subunits of the mitochondrial electron transport chain revealed a reduction in the expression of these proteins in POLG fibroblasts compared to control cells (Figure 5.8). Cell lysates were analysed by BCA assay to estimate protein content. Each sample was loaded into the gel for electrophoresis at a concentration of ~ 100µg/ml. The OXPHOS antibody cocktail (Abcam) was used assess protein levels. It contains antibodies against the NDUFB8 subunit of complex I, SDHB subunit of complex II, UQCRC2 subunit of complex III, mtDNA encoded MTCO1 subunit of complex IV and the ATPA5 subunit of complex V. Protein expression of all subunits except for complex V were substantially reduced in POLG cells when compared to lysates from control cells.

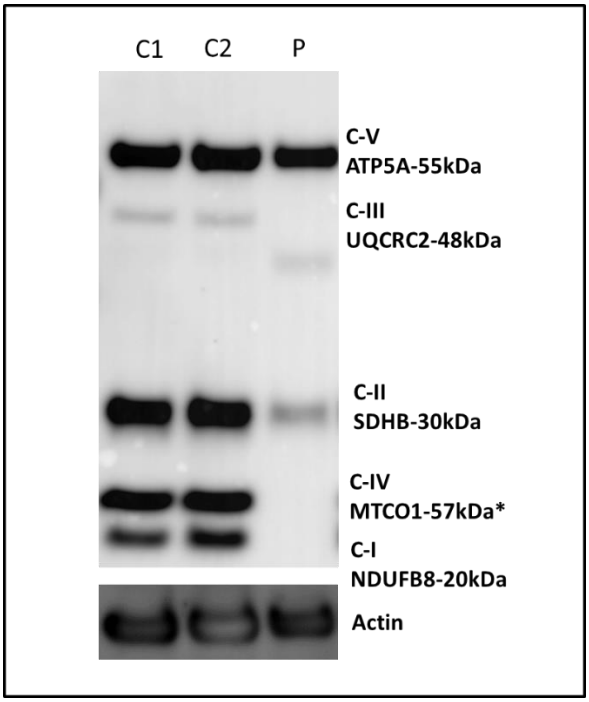

Figure 5.8 Protein expression of the electron transport chain subunits is reduced in POLG fibroblasts
*Highly hydrophobic mtDNA encoded protein. Real MW is 57kDa but migrates differently in different systems according to the manufacturer. n=2, representative image

Since the western blot analyses implied the almost complete absence of a functional electron transport chain POLG cells were subjected to the Mito Stress Test using the Seahorse platform, as previously. Oxygen consumption rate of POLG fibroblasts was very close to zero as opposed to control fibroblasts (Figure 5.9) Basal, maximal and ATP-linked respiration were calculated based OCR values measured following sequential injections of oligomycin, FCCP, and a mix of rotenone and antimycin A. All of these parameters were significantly reduced in POLG cells when compared to control fibroblasts (Figure 5.9 A and B). Simultaneously, the rate of extracellular acidification (ECAR) was increased in POLG fibroblast, compared to control cells (Figure 5.9 C).

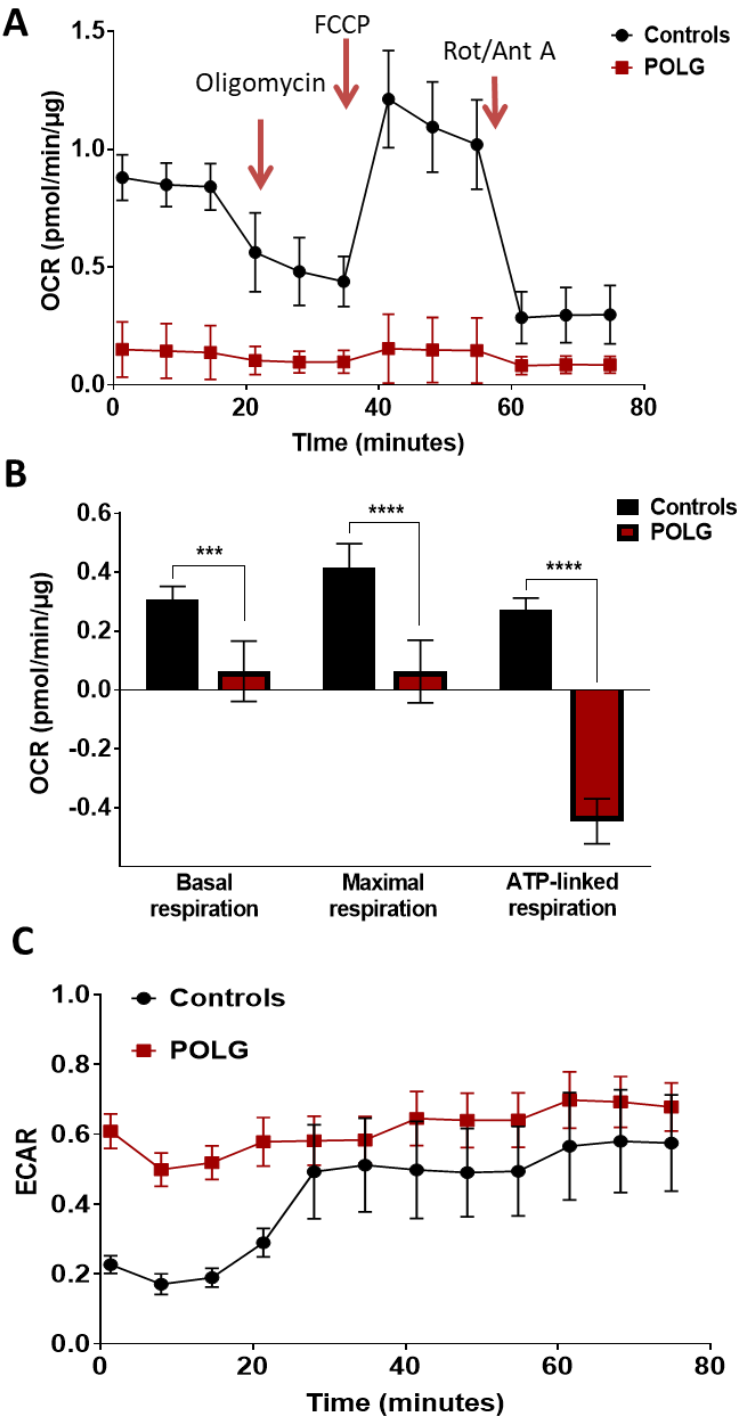

Figure 5.9 Oxygen consumption and extracellular acidification rates in POLG and control fibroblasts

(A) Kinetic graph of oxygen consumption rate measured every 18 minutes normalized to protein content, all injections indicated. Rot/Ant A = Rotenone and Antimycin A.
(B) Baseline, maximal and ATP linked respiration calculated from the results shown in graph A.
Mean +/- 95%CI from a single experiment based on at least 4 technical replicates, *=p<0.05, ****=p<0.0001

5.4.4 Glucose dependency of POLG fibroblasts

Fibroblasts are routinely maintained and assayed in DMEM high-glucose (25mM glucose) medium. Control 2 and POLG fibroblasts were cultured in 6-well plates in high glucose, low glucose (3mM) and glucose free galactose medium for 9 consecutive days to assess viability and growth of cells under variable glucose availability. The number of cells remaining in low glucose and galactose media after 9 days was expressed as the percentage of the number of cells remaining in high glucose after 9 days (Figure 5.10). Control fibroblasts grew the fastest in 3mM glucose medium as the percentage of cells remaining in culture after 9 days was 120.5% of the cells in 25mM glucose. Galactose reduced the growth of control cells by approximately 20%. The growth of POLG cells was reduced by approximately 20% in low glucose media as opposed to the increased growth seen for control fibroblasts. Furthermore, culture in galactose reduced the percentage of POLG cells by approximately 90%.

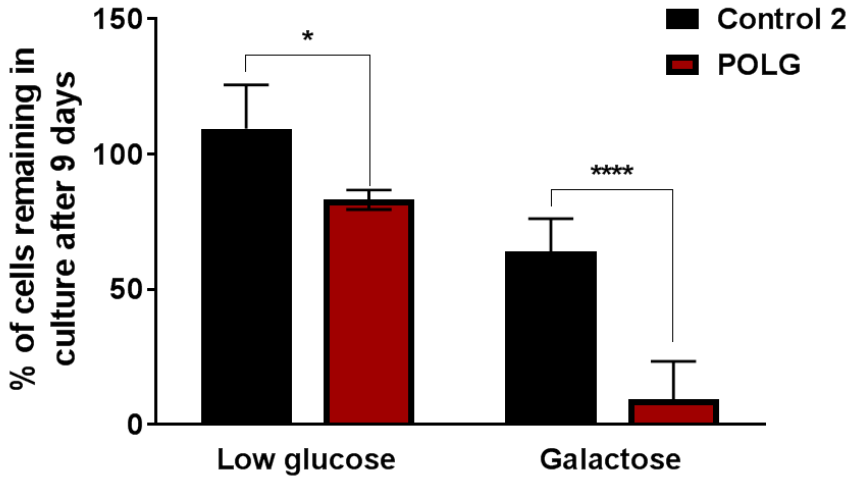

Figure 5.10 POLG fibroblast growth is heavily dependent on glucose availability
Number of cells remaining in culture after 9 days in low glucose (3mM glucose) or galactose (0mM glucose) medium, expressed as the percentage of cells grown at baseline (25mM glucose). n=1, mean +/- 95% CI, error bars are technical replicates ***=p<0.0001, *=p<0.05

5.4.5 Autophagy and mitophagy in POLG and control fibroblasts

Autophagy is characterized by the accumulation of LC3 positive punctae on double membraned phagophores that engulf cytosolic material and organelles destined for degradation by lysosomes. Autophagic activity, measured by counting the number of LC3 positive punctae within cells was increased in POLG fibroblasts compared to control cells both at baseline and at the presence of lysosomal inhibitors E64d and Pepstatin A (Figure 5.11 A). Mitophagy, measured as the number of LC3 punctae co-localising with mitochondria and expressed as the percentage of total mitochondrial area per cell, was also increased in patient cells although to a much lesser extent (Figure 5.11 B). This increase was only apparent in the presence of lysosomal inhibitors. Representative images of TOM20 and LC3 labelled control and patient fibroblasts are shown in Figure 5.12.

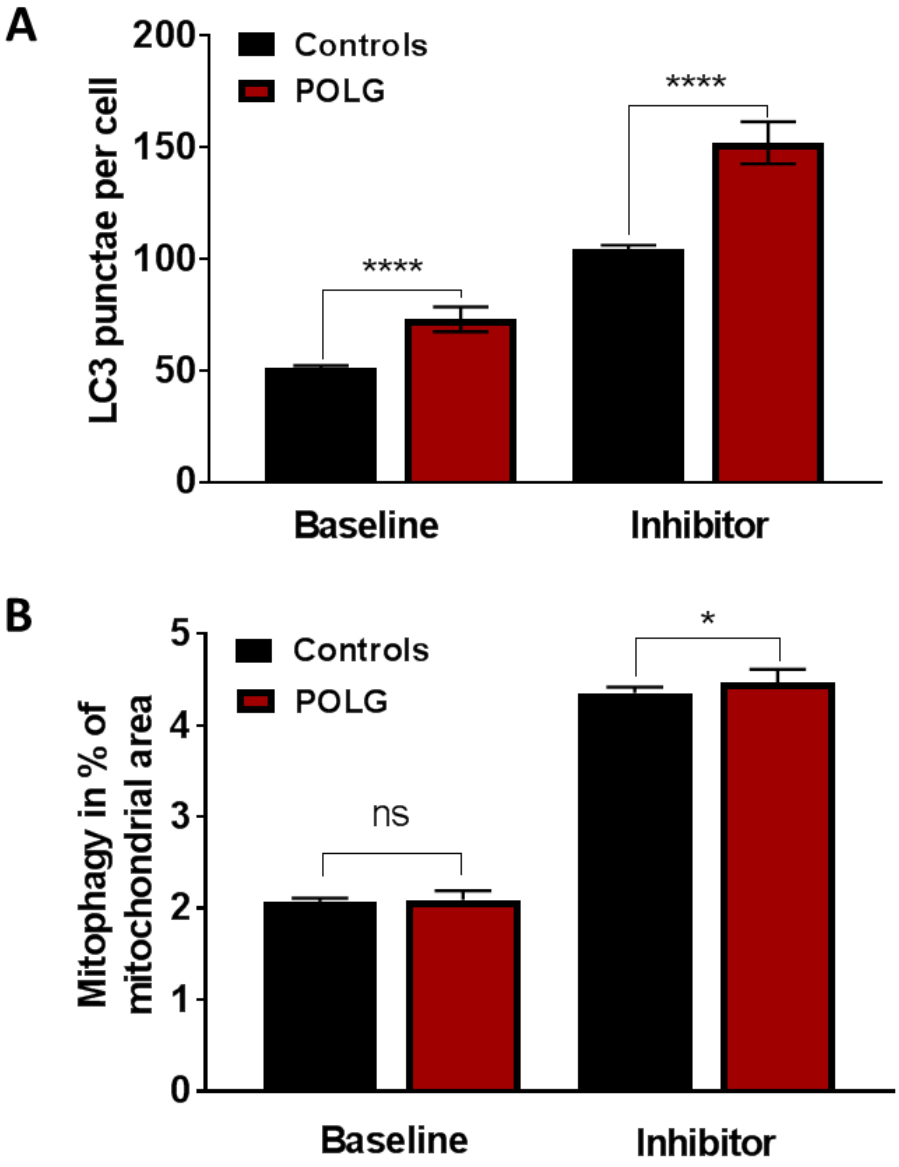

Figure 5.11 Autophagy and mitophagy in POLG and control fibroblasts
(A) Autophagy, measured by the number of LC3 positive punctae per cell (B) Mitophagy defined as the co-localisation of LC3 punctae with mitochondria. Lysosomal inhibitors are E64d and Pepstatin A.
* $p<0.05$; **** $p<0.0001$, n=2, minimum of 636 cells analysed per condition, Mean +/- 95% CI

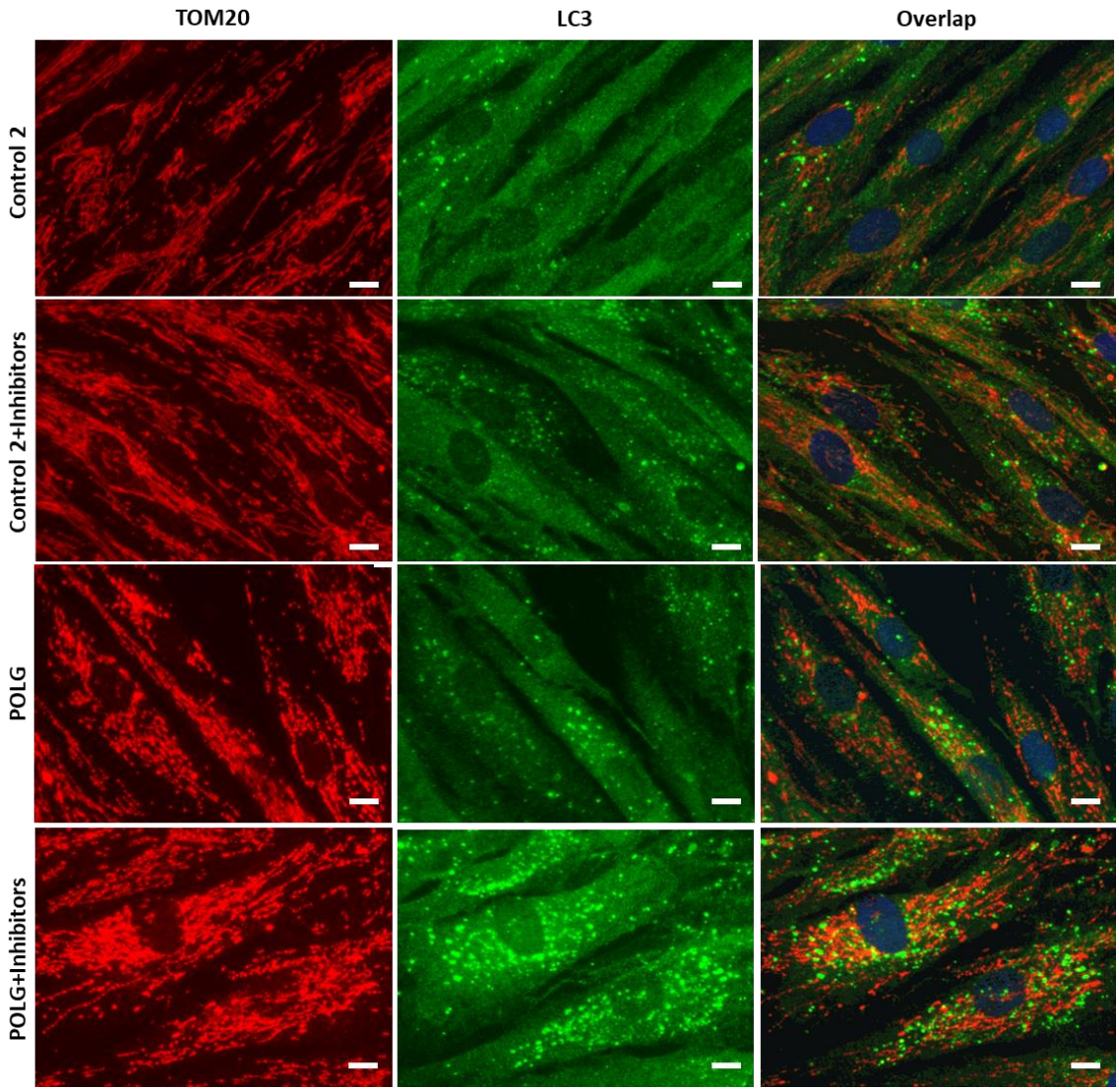

Figure 5.12 Representative images of Control 2 and POLG fibroblasts
Showing TOM20-labelled mitochondria and LC3-labelled autophagosomes cultured either at baseline or with the addition of lysosomal inhibitors E64d and Pepstatin A. Scale bar 10µm.

5.4.6 Nucleoside monophosphate supplementation alleviates mtDNA depletion in POLG fibroblasts

The aim of this study was to explore whether supplementing POLG fibroblasts with deoxynucleotide monophosphates could alleviate mtDNA depletion seen in these cells. Enrichment of culture media with exogenous dAMP and dGMP was shown to increase mtDNA copy number in *DGUOK* mutant cells (Taanman, et al., 2003) as well as in a zebrafish model of DGUOK deficiency (Munro et al., 2008). In this study, POLG fibroblasts were supplemented with a combination of dGMP and dAMP for 7 consecutive days. Treatment was carried out in standard growth medium as well as reduced serum culture medium (1% FCS). Treatment of POLG cells with a combination of dAMP and dGMP significantly increased mtDNA content in POLG mutant as well as control cells (Figure 5.13 A). A significant increase in mtDNA content upon dNMP treatment was achieved in media supplemented with 10% FCS, as well as in serum starved conditions compared to untreated cells. Nonetheless, the rescue effect was more prominent when cells were cultured in media supplemented with 1% FCS.

Concurrent to the increase in mtDNA content the percentage of Rho zero cells was also significantly reduced (Figure 5.13 B). Interestingly, the reduction of serum in the culture medium alone increased mtDNA content and significantly reduced the percentage of rho zero cells within the POLG fibroblast population (Figure 5.13). These observations are contradicting the effect of serum deprivation on DGUOK deficient fibroblasts where it rather exacerbates the loss of mtDNA (Taanman et al., 2003).

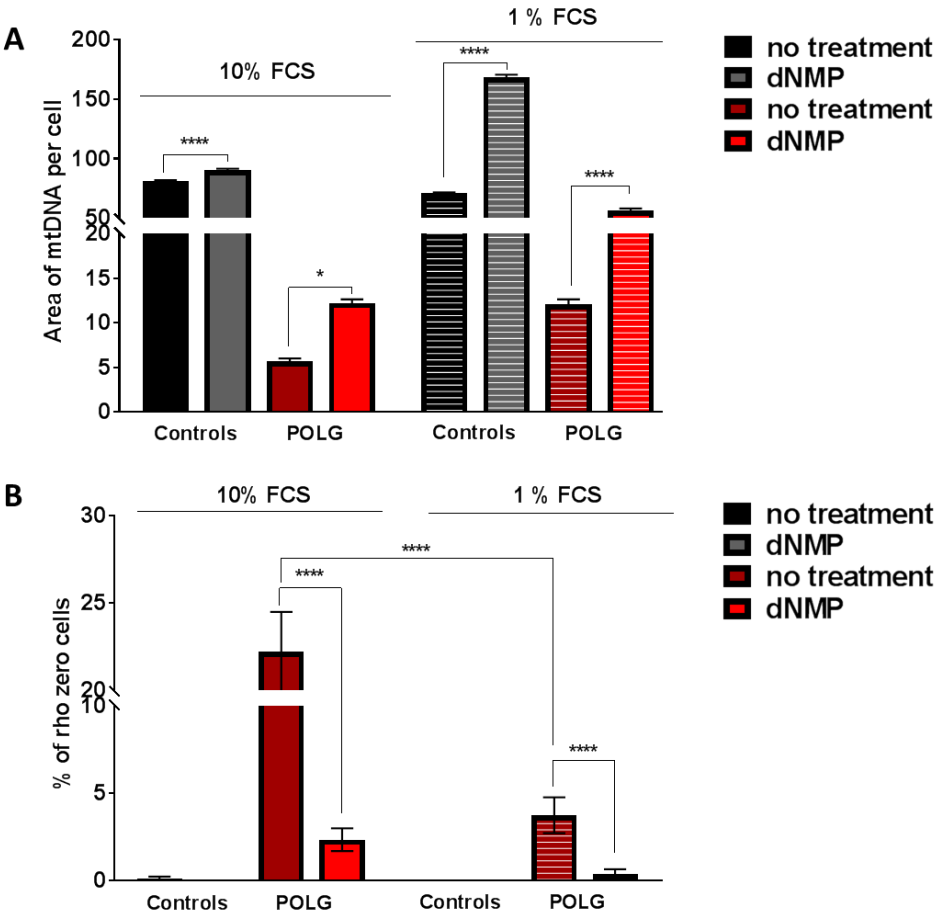

Figure 5.13 Nucleotide supplementation alleviates mtDNA depletion in POLG fibroblasts

(A) Mitochondrial content expressed as the total are of mtDNA nucleoids measured by PicoGreen staining (B) The percentage of rho zero cells, those with no mtDNA, in each condition

* $p<0.05$; **** $p<0.0001$, minimum of 329 cells analysed per condition, n=1, Mean +/- 95% CI

Additionally, we found that nucleotide supplementation reduces the levels of mitophagy in both control and patient derived cells when compared to their untreated counterparts (Figure 5.14 A). The number of LC3 punctae was also reduced in control cells following treatment when compared to untreated ones but it did not change on POLG fibroblasts (Figure 5.14 B).

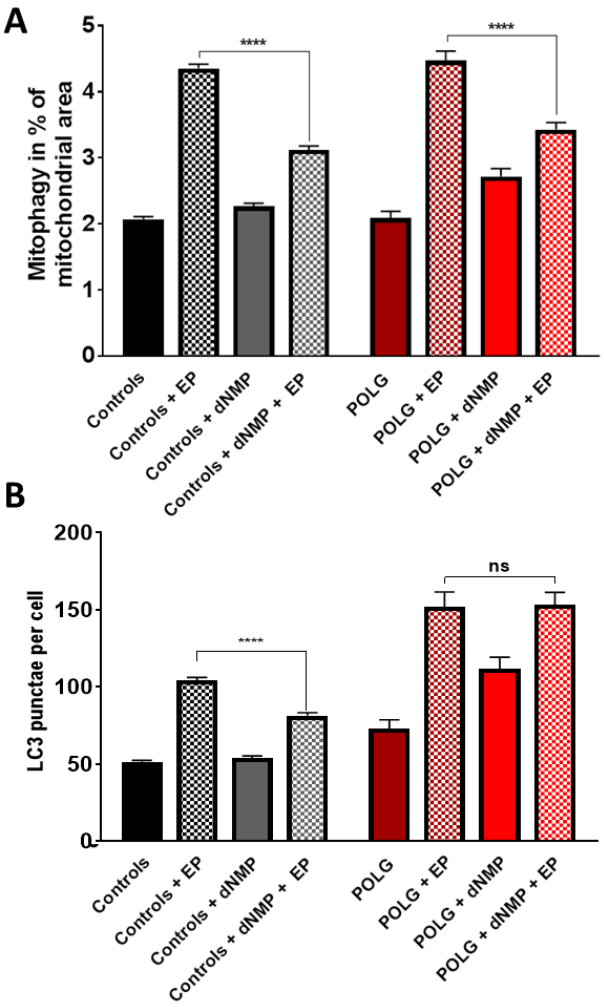

Figure 5.14 dNMP supplementation reduces mitophagy in control and POLG fibroblasts
n=2, minimum of 636 cells analysed per condition, Mean +/- 95% CI, * $p<0.05$; **** $p<0.0001$

5.5 Discussion

I characterised fibroblast cultures from one patient with profound mosaic mtDNA depletion and respiratory chain dysfunction due to mutations in both the polymerase and exonuclease domains of the mitochondrial polymerase subunit POLG. Mitophagy and autophagy were both increased in POLG patient fibroblasts when compared to control cells. Supplementing cells with dNMPs increased mtDNA content of POLG cells while reducing mitophagy. Despite the reduced amount of mtDNA in cultured cells mitochondrial content was comparable to control cells. Nevertheless, the functionality of the mitochondrial reticulum in POLG cells was extremely compromised. Western blot analysis of OXPHOS complex subunits revealed profound reduction of CI, CII, CIII and CIV subunits. In line with this finding, oxygen consumption of POLG fibroblasts was significantly lower than that of control ones. Additionally, they were close to non-viable when cultured in low glucose or glucose free galactose media. Mitochondrial DNA depletion syndromes are a devastating group of disorders with the majority of the cases being childhood onset and often fatal within the first years of life. It is a particularly difficult disease to study because depletion of patient mtDNA is tissue-specific, significant reduction in muscle is not reflected by mtDNA copy number in blood and is apparent in fibroblast cultures from only about 25% of patients. Most research relating to MDS utilises knock in/knock out animal models such as the deletor or mutator mice. However, the phenotypes of these animal models rarely resemble those seen in patients. Our patient had exceptionally severe mtDNA depletion manifest in his fibroblasts, providing a unique opportunity to study the relationship between dNTPs and mitophagy.

Supplementation of exogenous deoxynucleotides has largely been explored in cellular as well as animal models of *DGUOK* and *TK2* deficiency (Bulst et al., 2012; Garone et al., 2014; Munro et al., 2018; Taanman et al., 2003). In the disorders where supplementation efficiently rescued the phenotype, mtDNA depletion results from substrate limitation. Both dGK and TK2 are responsible for the first phosphorylation step of deoxynucleotide synthesis via the salvage pathway. The biochemical events leading to the reduction of mtDNA content in *POLG* deficient tissues are potentially more complicated and yet to be documented.

Nucleotide supplementation could benefit POLG deficient cells as a combination of erroneous mtDNA replication and hence increased mitophagy could increase dNTP demand in a viscous circle and eventually contribute to mtDNA depletion (Figure 5.3). Although POLG fibroblasts had a subtle but significant increase in mitophagy, autophagy levels were significantly above control values. Medeiros et al. (2018) has recently shown that increased autophagy drives mtDNA synthesis in starving yeast. We found that the supplementation of only two deoxynucleotides increased mtDNA content of POLG cells after only 7 days. Most published experiments on nucleotide supplementation utilise much longer time courses up to several weeks (Taanman et al., 2003).

DGUOK and TK2 supplementation experiments are routinely carried out in quiescent non-replicating cells. Quiescence is achieved by serum derivation that arrests the cell cycle. The reason behind this approach is that the dGK and TK2 are kinases of the salvage nucleotide synthesis pathway that supplies the bulk of the deoxynucleotide pools in non-replicating cells. In replicating cells the majority of DNA building blocks is produced via *de novo* synthesis. Serum deprivation aggravates mtDNA depletion in

DGUOK mutant fibroblasts (Taanman et al, 2003). In POLG cells it seems to do the opposite, as fibroblasts cultured in reduced serum medium (1% FCS) had less rho zero cells, while there was a substantial but non-significant increase in mtDNA content. This is sensible, considering that mitochondrial DNA synthesis is slower in non-diving cells as they are not required to double their volume prior to cell division.

In conclusion, supplementation of exogenous deoxynucleotides may prove to be an efficient therapy not only for MSD as a result of deficiencies in the nucleotide synthesis pathway but also for mutations affecting the mitochondrial replisome.

5.6 Limitations of this study

Mitochondrial DNA content measurements following supplementation are based on a single experiment as these results were aimed to provide preliminary data. These will be replicated multiple times prior to publication.

POLG fibroblasts were treated with a combination of purine dNMPs only rather than then the various combinations of purine and pyrimidine dNMPs. This will be addressed below.

5.7 Future directions

The results presented in this chapter served as preliminary data for a successful grant application to explore the therapeutic potential of nucleotide supplementation in a wider range of MDS mutations. In this study we will explore the effect of all combinations of dNMPs. Additionally, we will adapt an already described method (Haines et al., 2010) for measuring mtDNA synthesis in single cells using high-content imaging and will aim to combine this with an existing live cell mitophagy assay.

Chapter 6. Potential drug modulators of mitophagy

6.1 Introduction

The discovery and development of new drugs is a lengthy process that often takes 12-16 years from the first high-throughput screen to the approval and marketing of a single compound. Nevertheless, the success rate of new drugs proceeding from clinical trial to the market is typically less than 5% (Dahlin et al., 2015). Contemporary drug development takes a target-based approach, referred to as reverse pharmacology. As well as increasing our understanding of disease mechanism, advances in the field of biotechnology, molecular biology and medicinal chemistry have identified specific protein targets on which reverse pharmacology can be focused. Specific compounds that bind to this target with a high affinity can then be identified by high throughput screening. On the other hand, most drugs that have long been on the market were identified using the classical or so called forward pharmacology approach during which drug selection relies on phenotypic changes. The mode of action for these drugs was not well understood and their discovery was mostly serendipitous. The mechanism of action for most of these is relatively well described now; however, some remain poorly understood. For example, metformin is the most widely prescribed medication for type-2 diabetes that has been in use for nearly a century but its mode of action remains only partially understood. There also remain unexplored systemic affects that can be valuable for the treatment of other diseases. Therefore, one approach to reduce the time and cost of drug development in the time of ever increasing demand for novel medicines, especially in the field of rare diseases, is drug repurposing and repositioning. This involves the investigation of existing drugs or candidate drugs for an alternative application. A historical example

is Viagra, which is widely prescribed for erectile dysfunction; however, it was originally developed as an angina treatment but failed during clinical trial. Viagra was repurposed based on its side effects. Today, there are commercially available chemical libraries of FDA approved drugs and compounds that have been in phase I-III clinical trials. The sizes of these can range from a few hundred to many thousands. Given that there are no treatments available for mitochondrial disease, mitophagy is potentially a novel therapeutic target. In 2012, Park *et al*. screened two chemical libraries each containing 1200 drugs looking for chemical modulators of mitophagy using LC3 (GFP) and mitochondria (YFP) tagged HeLa cells. The investigators identified phenanthroline as a potent inducer of mitophagy, inducing DNM1L dependent fragmentation. However, this fragmentation is potentially excessive. Indeed, the vast majority of mitophagy inducing compounds identified to date are essentially toxins that induce mitochondrial turnover by inflicting damage to the organelle. These compounds and their mechanisms are summarized in Table 6.1.

The molecular mechanisms governing mitophagy are still poorly understood. Most of the current research set out to dissect these mechanisms uses many of the mitochondrial poisons listed in Table 6.1 to initiate mitophagy. For example, FCCP and CCCP are used to dissipate mitochondrial membrane potential and Antimycin A and Oligomycicn to impair mitochondrial respiration.

Table 6.1 Chemical modulators of mitophagy (modified from Georgakopoulos et al., 2017)

Pharmacological class	Mitophagy inducer	Mechanism of action
Protonophores (proton (H+) ionophores)	CCCP FCCC 2,4-dinitrophenol (DNP) BAM15	Collapse of ΔΨm induced by proton leak and thereby depletion of the electrochemical proton gradient.
K+ Ionophores	Valinomycin	Reversible dissipation of the ΔΨm by disturbing potassium (K+) homeostasis.
	Salinomycin	Hyperpolarisation by disturbing potassium (K+) homeostasis.
Respiratory complex inhibitors	Antimycin A	Dissipation of ΔΨm via complex III inhibition coupled with increased superoxide production.
	Oligomycin	Dissipation of ΔΨm via complex V inhibition coupled with increased superoxide production.
Parkinsonian toxins	Paraquat	Excessive complex I-dependent superoxide generation.
	Rotenone	Excessive ROS generation, promoting the externalization of cardiolipin.
	MPP+	Excessive ROS generation.
Iron chelators	Deferiprone (DFP)	Promotes mitophagy via iron depletion-dependent mechanism without causing a ΔΨm collapse.
	1,10'-phenanthroline (Phen)	Excessive mitochondrial fragmentation and collapse of ΔΨm
NAD+ precursor	Nicotinamide (NAM)	NAD+ accumulation and subsequent activation of SIRT1
PARP inhibitor	AZD2281 (olaparib)	NAD+ accumulation and subsequent activation of SIRT1

On the other hand, the basic molecular pathways governing autophagy are relatively well described owning to the breakthrough discovery of Atg proteins in yeast in 1993 (Tsukada and Oshumi, 1993) and subsequently their human homologues. Thereupon, there has been a rising interest in chemical modulators of autophagy as a potential treatment for various neurodegenerative diseases as well as cancer. Fleming et al. provides a comprehensive review of known drug modulators of autophagy that principally target the mTORC1 pathway (Figure 6.1) (Fleming et al., 2011).

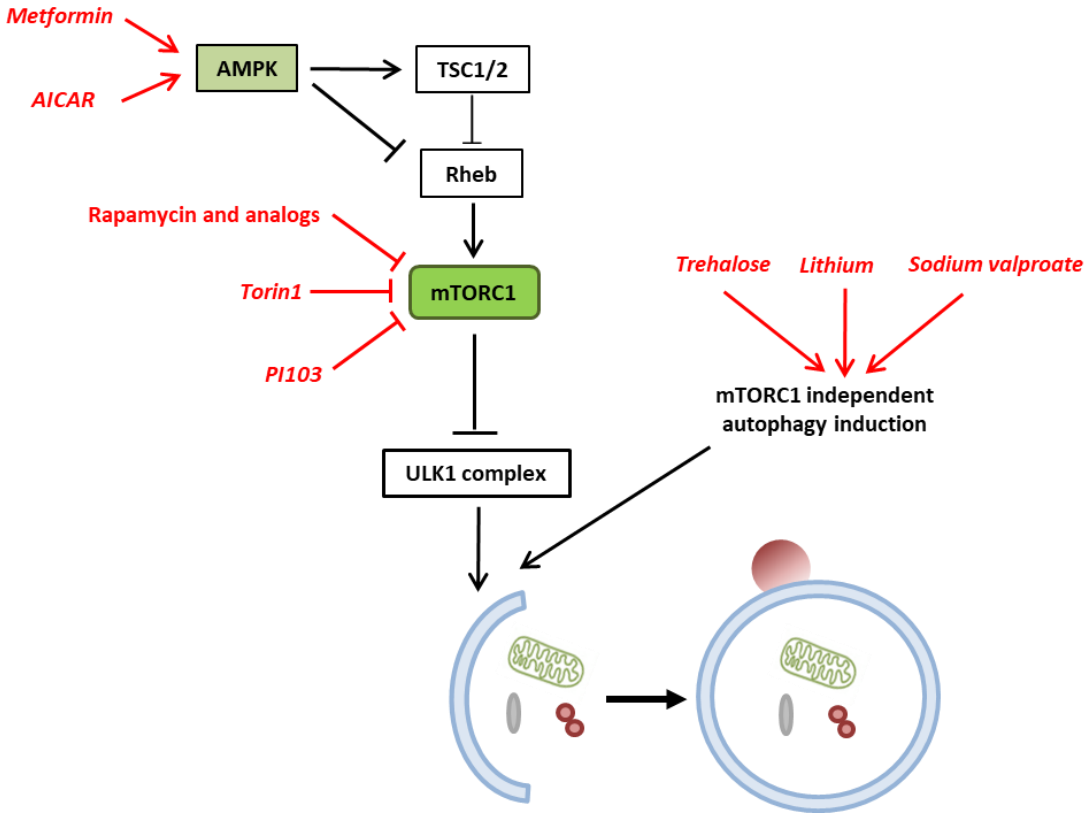

Figure 6.1 Chemical modulators of autophagy
A schematic representation of known chemical modulators of autophagy indicating their molecular targets. Most drugs exert their effect on mTORC1 or upstream regulators such as AMPK. However, there are a handful of drugs that induce mitophagy via mTORC1 independent pathways.
Modified from Fleming et al., 2011 and Dombi et al., 2017

Rapamycin, an inhibitor of the mTORC1 complex was shown to enhance survival and attenuate disease progression in both a mouse (Johnson et al., 2013) and a *Drosop*hila (Wang et al., 2016) model of Leigh disease.

Regardless, the regulation of mitochondria specific autophagy is much less understood and hence the information available on specific modulators of mitophagy is less comparable. In order for modulators of mitophagy to be considered as a potential therapy for heteroplasmic mitochondrial diseases in the future the drug candidates must target mitochondria enriched for pathogenic mutant mtDNA. In other terms, these drugs need to promote the turnover of damaged mitochondria rather than bulk/non-specific mitophagy. Hence, in this chapter I will investigate potential drug modulators of mitophagy and their effect on mutant load *in vitro* using heteroplasmic patient derived fibroblasts.

6.2 Aims

I. To identify selective drug modulators of mitophagy that can be implemented as potential novel therapies for mitochondrial disease.

6.3 Materials and methods

6.3.1 Patient and control fibroblasts used

Control fibroblasts were derived from consented healthy adults as described previously. Control 1 was derived from a 22 year old male corresponding to control 1 used in the previous chapters (male, 21 years old, median age and mean mitophagic activity within our control range). Control 2 was derived from a 52 year old healthy female. These cells were chosen to provide control fibroblasts that are closer to the age of the patients. Patient fibroblasts were derived from a male, aged 46 (Patient 1) and female, aged 42 (Patient 2) harbouring the m.3243A>G mtDNA mutation. The heteroplasmy levels of the mutation varied between the two patients (Patient1 ~40%; Patient 2 ~30%). All fibroblast lines were established and maintained as described previously (Section 2.2.1). A short clinical description of the patients is presented in Table 6.2.

Table 6.2 Short clinical description of the 3243 patients

Patient	mtDNA mutation	Heteroplasmy	Diagnosis	Clinical description
Patient 1	m.3243A>G	~40%	MELAS	Presented with myopathy in childhood. Developed diabetes and deafness in adult life. Died from encephalopathic episode at the age of 46 years.
Patient 2	m.3243A>G	~30%	MELAS	Presented with myopathy. Developed CPEO and hyperthyroidism later in life. Patient is still alive at the time of writing.

6.3.2 Experimental set up for high-content fluorescent microscopy

Fibroblasts were seeded into optically clear bottom imaging plates (96-well) at a density of 2500 cells per well (section 2.2.2) a day before commencing treatment. The next day media was changed on each well containing either vehicle or drug at various concentrations, see Table 6.3. Treatment lasted for 3 days. Most drug treatments followed a semi-log dose response curve ranging from 0.1 to 10µM. Drug stocks were made up as a 1000x concentration of the highest treatment concentration and further diluted in media. Plates were fixed, imaged and analysed as described in section 2.2.3. For metformin and AICAR experiments images were taken in 9 fields per well rather than 12 and one control and one patient culture was used rather than two each as in the subsequent experiments.

Table 6.3 Concentration range and solvent used for each compound screened

Drug	Solvent	Concentration range used (µM)
Metformin	dH_2O	0.5, 1, 5, 10, 50, 100, 500
AICAR	DMSO	1, 5, 10, 50, 100, 500, 1000
Duloxetine	Ethanol	0.1, 0.3, 1, 3, 10
Librium	dH_2O	0.1, 0.3, 1, 3, 10
mtDOX	DMSO	0.1, 0.3, 1, 3, 10
KH301	DMSO	0.1, 0.3, 1, 3, 10
KH401	DMSO	0.1, 0.3, 1, 3, 10
KH501	DMSO	0.1, 0.3, 1, 3, 10

6.3.3 Measuring mtDNA heteroplasmy of the m.3243A>G mtDNA mutation

Patient fibroblasts were seeded into T25 flasks at a density of 200,000 cells per flask for 3 day and 100,000 cells per flask for 7 day treatment. Fibroblasts were harvested by trypsinisation and DNA was extracted from whole cell lysates using the Illustra Nucleon BACC2 Genomic DNA Extraction Kit (GE Healthcare) following manufacturer's instructions. Levels of the m.3243A>G mtDNA mutation were detected by PCR amplification of DNA extracts followed by last cycle labelling and restriction digestion. All reaction volumes and cycle conditions are summarized in Table 6.4. PCR amplification was performed with primers at nucleotide position 3110-3129 light chain (5' CAA ATT CCT CCC TGT ACG AA 3') –MELAS1b and at nucleotide position 3433-3404 heavy chain (5' AGG GGC CTA CAA CGT TGG GCC CTT TGC GTA 3') – MELAS APAL using Kapa 2G Fast HS Ready Mix (Eurogentec). PCR fragments were subjected to last cycle labelling using MELAS 1bHEX fluorescent primer (HEX-CAA ATT CCT CCC TGT ACG AA 3' (3110-3129); Eurogentec) using Roche Taq Polymerase (Roche). The labelled PCR fragments were digested with Apa1 restriction enzyme. The PCR product has a length of 324bp. Digestion with ApaI produced a HEX tagged wild type fragment with a length of 307bp and an untagged fragment of 17bp. The m.3243A>G mutation introduces an additional ApaI cut site. Therefore digestion of PCR fragments amplified from mutant DNA produce a HEX tagged fragment of 132bp and two untagged fragments (17bp+174bp). DNA was analysed using the ABI3730 Genetic Analyser (Life Technologies – Applied Biosystems). Samples were prepared as described in Table 6.4. Fluorescent intensity peaks are produced corresponding to wild type and mutant digestion products. The ABI3730 sizes the undigested products as ~322bp, and the cut products as ~303bp and ~132bp because sizing is not accurate

on the ABI. Results were analysed using the GeneMapper® software, a representative output of which and the method of calculation is presented in Figure 6.2. Heteroplasmy levels were calculated the following way: mutant intensity/(mutant intensity + wild type intensity)x100 (Figure 6.2). Fluorescent intensities below 200 were excluded from the analysis.

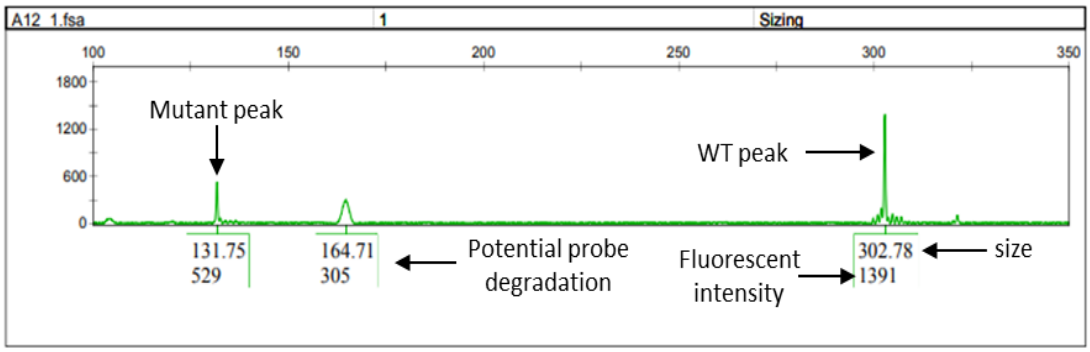

Mutant mtDNA		Wild type mtDNA		Total mtDNA	**Heteroplasmy %**
size	fluorescence	size	fluorescence	fluorescence	(mutant /total)*100
131.75	529	302.78	1391	1920	27.6

Figure 6.2 Representative output of the m.3243 heteroplasmy analysis
The top panel shows a representative results obtained from the ABI3730 DNA Analyser following analysis of the output using the GeneMapper® software.

6.3.4 Statistical analysis

All statistical analyses was performed using Graphpad Prism (version 7). Metformin and AICAR data was analysed based on cell-by-cell output values. Treatment conditions were compared to untreated cells using the non-parametric Kruskall-Wallis test with multiple comparisons as the data did not have normal distribution. Dose-response curves were analysed using non-linear regression to determine the EC50, the concentration that provokes a response half way between the basal (Bottom) response and the maximal (Top) response. Treatment conditions were compared to vehicle treated cells using Two-way ANOVA. Each data point in a dose-response curve comprises of 6 values. Each value is the mean of single-cell values per

well. Data from the two control cultures was merged as was the patient data. The n value represents the number of technical replicates (number of plates run).

Table 6.4 Reaction volumes and cycle conditions of each reaction used in 3243 heteroplasmy analysis

1st PCR amplification	
Reagent	Volume (µl)/reaction
dH_2O	8.8
Kapa2G Fast HS Ready Mix	10
MELAS1b (20µM stock)	0.1
MELAS2APAL (20µM stock)	0.1
DNA	1
Total reaction volume:	20µl
Cycle conditions: 94°C 5mins, (94°C 10s, 50°C 10s, 72°C 1s) x 30, 72°C 7mins, 15oC hold	
Last cycle labelling	
PCR product	15
MELAS1bHEX	1
Roche Taq Polymerase	0.1
Total reaction volume	16.1µl
Cycle conditions: 95°C 2min, 50°C 1min, 72°C 6min, 15oC hold.	
Restriction digestion	
Labelled PCR product	16.1
Buffer A	5
ApaI enzyme	1.5
dH_2O	27.4
Total reaction volume	50µl
Cycle conditions: Incubate at 25°C for 2 hours, followed by 65°C for 20mins	
Sample preparation for ABI	
Amplified, labelled and digested PCR product	1
Hi-Di Formamide	8.5
Liz-500 (G5) size standard:	0.5
Total reaction volume	10µl

6.4 Results

Previously, Alexander Hinks-Roberts (placement student) performed a high-throughput screen of the NCC1 drug library of 446 drugs in order to identify potential drug modulators of mitophagy. The screen utilised fibroblasts derived from two patients harbouring the heteroplasmic m.3243A>G mutation. One of the fibroblast cultures was same as the Patient 1 fibroblasts presented in this chapter. Cells were plated into 384 well plates and treated with the appropriate drug (1x) for 3 days either at low (0.5µM) or high (10µM) concentration. The staining and analysis procedure was the same as described in section 2.2.3 for detecting mitophagy. Plates were imaged at 40X at the Department of Neuroscience, University of Sheffield using an In Cell 6000 automated microscope (collaborator Heather Mortiboys). The list of top hits for both increasing and decreasing co-localisation of mitochondria and autophagosomes are presented in Supplementary Table 3. The drugs investigated in this chapter and their current applications are listed in Table 6.5.These are either mostly FDA approved medications that emerged as potential modulators of mitophagy from this preliminary screen, or were received from collaborators and are currently under development.

Table 6.5 Potential drug modulators of mitophagy

Drug	Target	Application	Crosses BBB*?
Compounds emerged from preliminary drug screen			
Metformin	AMP-dependant protein kinase (AMPK) activator, Complex I inhibitor	First-line medication for the treatment of type 2 diabetes	yes
AICAR	AMPK activator	Treat and protect against cardiac ischemic injury, preserve blood flow during surgery.	low permeability
Chlorodiazepoxide	benzodiazepine analogue	Used to treat anxiety, insomnia and withdrawal symptoms from alcohol and/or drug abuse.	yes
Duloxetine	serotonin and norepinephrine reuptake inhibitor in CNS	Major depressive disorder, generalized anxiety disorder, fibromyalgia and neuropathic pain.	yes
Compounds received from collaborators			
mtDoxorubicin	Mitochondria targeted form of doxorubicin		no
KH176, KH176m, KH176i	Redox signalling	Phase II clinical trial for MELAS completed.	yes

6.4.1 Activators of AMPK, metformin and AICAR

5' AMP-activated protein kinase or AMPK is a conserved master regulator of cellular energy metabolism. AMPK responds to an increase in the AMP/ATP ratio within cells and promotes catabolic pathways, such as autophagy, in order to generate ATP while inhibiting anabolic processes (Kahn et al., 2005). Induction of autophagy by AMPK proceeds via the inhibition of the mTORC1 complex and subsequent autophagosome formation (Table 6.1). Metformin is a widely prescribed orally administered treatment for type 2 diabetes that has been in use since the 1950s. It is currently the recommended treatment by the European Association for the Study of Diabetes. The detailed mechanism of action underlying the metabolic effects of metformin are still unclear, however, it was shown to suppress gluconeogenesis in the liver via the activation of AMPK (Cao et al., 2014). More recently, Hunter et al. (2018) reported that metformin acts via fructose-1,6-bisphosphatase-1 that is inhibited by AMP. Metformin was also shown to induce autophagy and this feature of the drug was attributed tumour-suppressive (Feng et al., 2014) as well as neuro-protective (Chiang et al., 2016; Porceddu et al., 2016) properties. The maximum daily dose of metformin is 2000mg and the plasma concentration is the highest within 1 hour of administration in humans ranging from 10 to 40μM (Higgins et al., 2012). High concentrations of metformin (~5mM) were also shown to decrease oxygen consumption of isolated hepatocytes via complex I inhibition (El-Mir et al., 2000). 5-aminoimidazole-4-carboxamide riboside (AICAR) is another AMPK agonist that mimics AMP within cells (Hardie and Frenguelli, 2007). It was first used in the 1980s during surgery in order to preserve blood flow to the heart. Since then AICAR has been administered to treat cardiac ischemia injury. It was also used as a performance

enhancer agent as AICAR promotes fatty acid oxidation and muscle remodelling and therefore was added to the Prohibited List of performance enhancer drugs in 2009. Control 1 and Patient 1 fibroblasts were treated with an increasing concentration of either metformin (Figure 6.3) or AICAR (Figure 6.4). Cells received a single treatment on day 0 and the plates were fixed on day 3. Staining for mitophagy analyses was performed as described previously. The mitophagy response following metformin treatment did not follow a conventional dose response curve. However, treatment with up to 50µM drug increased both mitophagy (Figure 6.3 A) and autophagy (Figure 6.3 B) in control as well as patient derived cells. Conversely, at the highest concentration (500µM) metformin had the opposite effect and significantly decreased both mitophagy and autophagy. An increase in mitophagy can indicate the onset of mitochondria induced apoptosis. Therefore cell numbers were estimated by counting the number of nuclei in each imaged field per treatment (Figure 6.3 C). This totalled to 27 fields per condition, across 3 well. The number of cells remaining in culture following treatment was expressed as a percentage of untreated cells. Metformin treatment did not drastically affect the number of control cells at any concentration as the values remained close to 100%. Viable cells in the patient group noticeably increased following metformin treatment. The highest number of cells remaining in culture following treatment was achieved at 1µM (147% of untreated cells) closely followed by 100µM (143% of untreated cells). The increase at all other concentrations was close to 130% except for the highest (500µM), which did not increase cell viability.

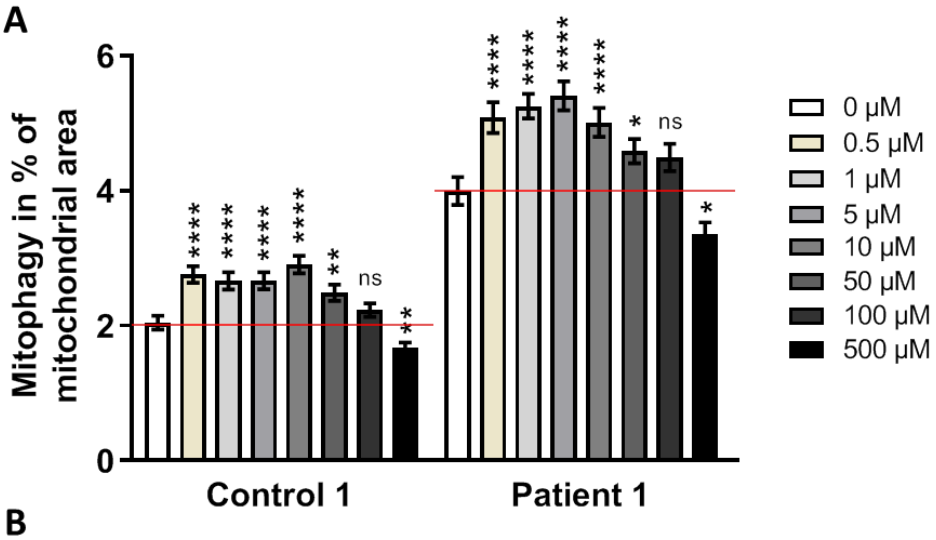

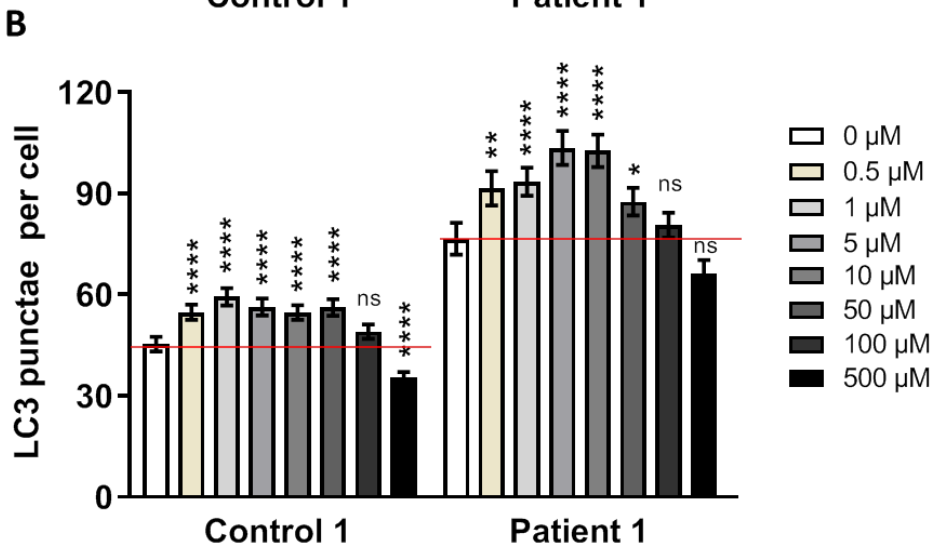

C

Viable cells expressed as the % of untreated cells		
	C1	**P1**
0.5µM	113	99
1µM	108	147
5µM	104	130
10µM	111	128
50µM	109	133
100µM	113	143
500µM	107	97

Figure 6.3 Metformin treatment of control and patient fibroblasts
Fibroblasts received a single treatment of metformin at various concentrations and plates were fixed after 3 days. (A) Mitophagy following metformin treatment (B) Autophagy following metformin treatment (C) Viable cells in each treatment condition expressed as the percentage of untreated cells
n=1, mean +/- 95% CI

AICAR treatment (Figure 6.4) of Control 1 and Patient 1 cells followed a very similar trend to metformin treated ones. Mitophagy increased in AICAR treated control cells up to 10µM and up to 50µM in patient derived fibroblasts (Figure 6.4 A). Autophagy followed the same pattern (Figure 6.4 B). Similarly to metformin treatment, AICAR treatment at the highest concentration (1000µM) significantly reduced both mitophagy and autophagy. The percentage of control cells remaining following AIACR treatment stayed remarkably close to 100% up to 500µM. However, 1000µM treatment reduced this to 60% in control cells and 51% in patient cells indicating a cytotoxic affect. The percentage patient fibroblasts remaining in culture after treatment gradually increased from 10µM treatment, peaking at 142% at 500µM.

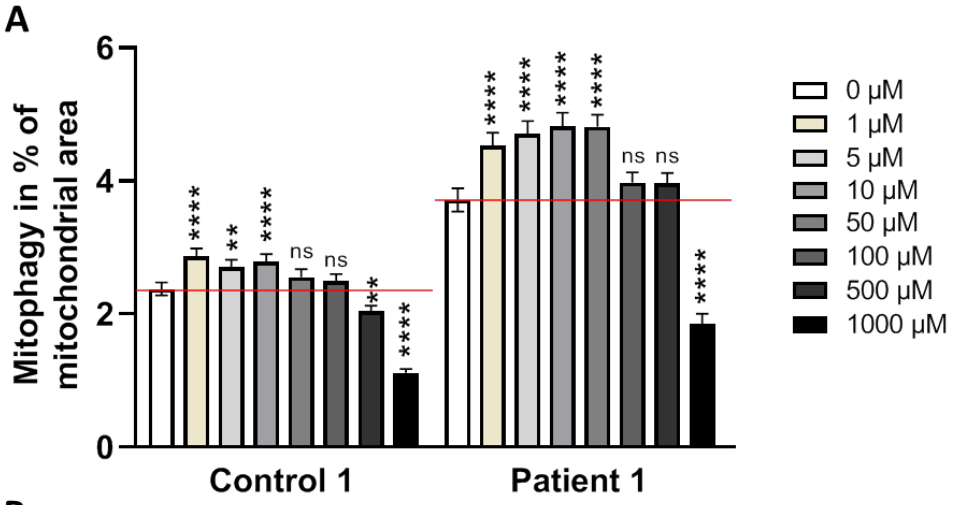

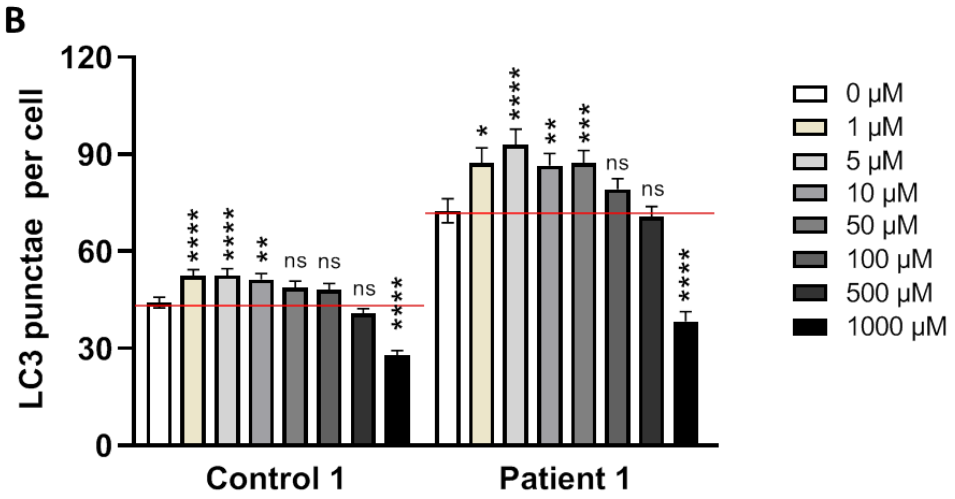

C

Viable cells expressed as the % of untreated cells		
	C1	**P1**
1µM	92	95
5µM	98	94
10µM	108	119
50µM	94	116
100µM	99	120
500µM	104	142
1000µM	60	51

Figure 6.4 AICAR treatment of control and patient fibroblasts
Fibroblasts received a single treatment of AICAR at various concentrations.
(A) Mitophagy following AICAR treatment, (B) Autophagy following AICAR treatment
(C) Viable cells remaining in culture in each treatment condition expressed as the percentage of untreated cells
n=1, mean +/- 95% CI

6.4.2 Chlordiazepoxide (Librium)

Chlordiazepoxide (trade name Librium) was patented in 1958 and was the first benzodiazepine to be made available for the treatment of anxiety in 1962 (López-Munoz et al., 2011). Librium is used to treat anxiety disorders and symptoms of drug and alcohol withdrawal. Chlordiazepoxide acts on a specific receptor site on the GABA-A receptor. The half-life of the drug following a single treatment in healthy individuals is 5-30 hours, but its active metabolite has a very long elimination time (Liljequist et al., 1979). The drug is highly soluble in lipids and binds to albumin therefore diffuses rapidly across the blood-brain barrier. This property of chlordiazepoxide makes it an attractive candidate drug for the treatment of mitochondrial disease as in many cases the CNS is affected.

A single-treatment with chlordiazepoxide increased mitophagy in both control and patient cells (Figure 6.5 A). The EC50 was determined at 0.06µM for control cells and at ~0.0002 for patient cells; however, this result was flagged as ambiguous, which means that the fitted curve did not quite lock in all of the values. Librium treatment did not elicit a dose dependent autophagy response in any of the cells (Figure 6.5 B). The treatment increased autophagy at low concentrations. The increase was only significant in patient cells at 0.3µM. Chlordiazepoxide treatment had no remarkable effect on cell numbers at any of the concentrations (Figure 6.5 C). Even the highest concentration (10µM) was well tolerated in both control and patient cells which indicates that the drug is not cytotoxic.

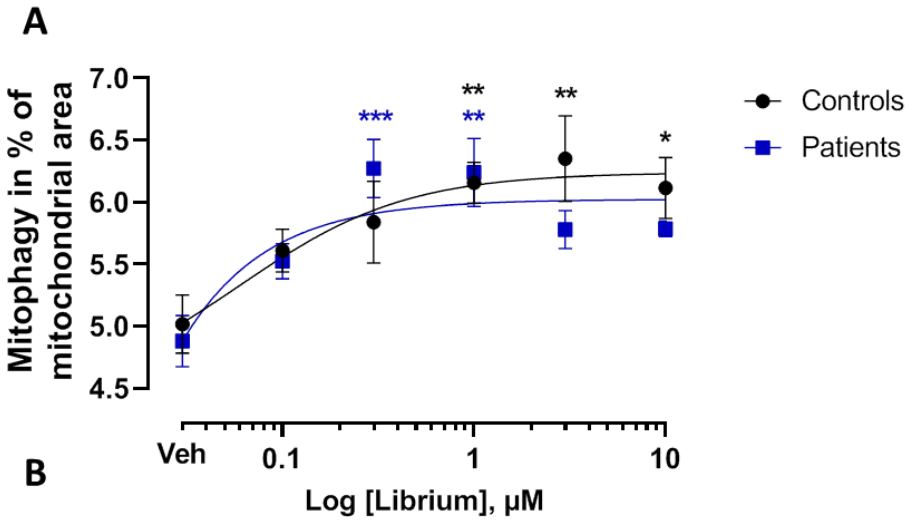

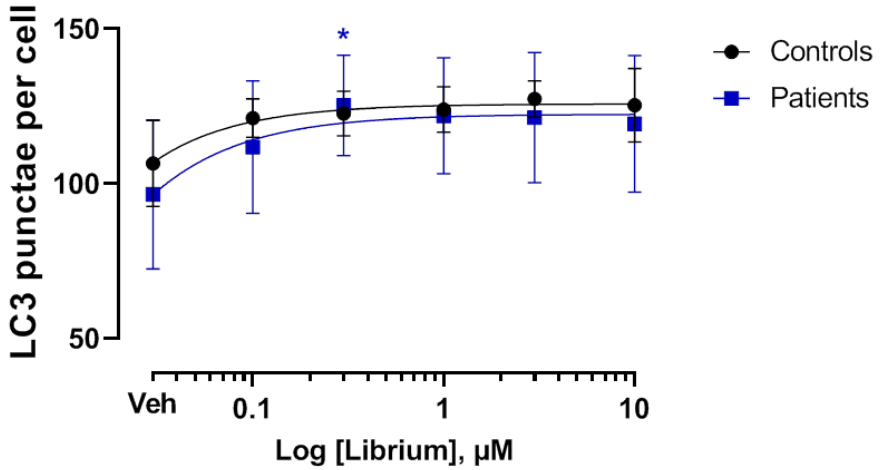

C

Viable cells expressed as the % of untreated cells		
	C (n=2)	**P (n=2)**
0.1µM	114	96
0.3µM	115	99
1µM	111	96
3µM	108	97
10µM	115	101

Figure 6.5 Chlordiazepoxide treatment of control and patient fibroblasts
Fibroblasts received a single dose of Chlordiazepoxide at various concentrations. (A) Mitophagy following Chlordiazepoxide treatment (B) Autophagy following Chlordiazepoxide treatment (C) Viable cells in each treatment condition expressed as the percentage of untreated cells
n=1, mean +/- 95 CI%

6.4.3 Duloxetine

Duloxetine (trade name Cymbalta) is a systemic drug treatment available as an oral capsule (20mg, 30mg & 60mg). It is currently approved in both the European Union (EU) and in the United States for the treatment of major depressive disorder (MDD), generalized anxiety disorder (GAD), diabetic peripheral neuropathic pain (DPNP) and chronic musculoskeletal pain. Duloxetine is also approved for the treatment of fibromyalgia in the US (approved June 2008) and for the treatment of moderate to severe stress urinary incontinence in women in the EU (Yentreve™ approved in August 2004). Duloxetine is a selective serotonin and norepinephrine reuptake inhibitor and is often prescribed for patients suffering from mitochondrial disease to manage neurogenic pain.

Duloxetine treatment did not exert a dose-response effect on either mitophagy or autophagy (Figure 6.6). However, at the highest concentration (10µM) Duloxetine did significantly increase mitophagy levels in both control and patient cells (Figure 6.6 A). Autophagy was also significantly increased at both 3µM and 10µM concentrations but not the lower ones (Figure 6.6 B). The number of control cells remaining in culture following treatment expressed as the percentage of vehicle treated control cells remarkably increased with Duloxetine treatment even at the lowest, 0.1µM concentration (115%) reaching a peak at 3µM (140%) (Figure 6.6 C). However, cell viability dropped to 83% following treatment with the highest drug concentration (10µM). Drug treatment up to 3µM did not have a major effect on patient cell viability but 10µM drug treatment did reduce the percentage of viable cells to 60%, indicating cytotoxicity.

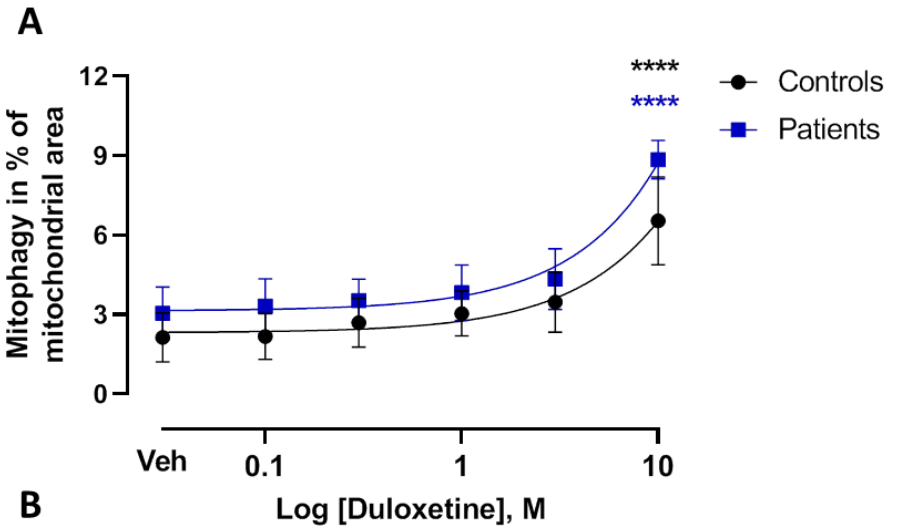

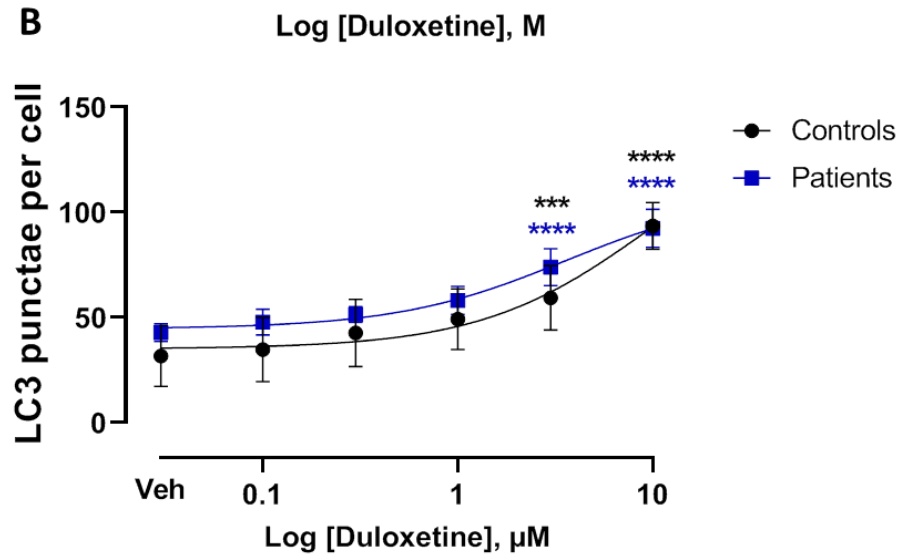

C

Viable cells expressed as the % of untreated cells		
	C (n=2)	**P (n=2)**
0.1µM	115	91
0.3µM	125	109
1µM	135	101
3µM	140	94
10µM	83	60

Figure 6.6 Duloxetine treatment of control and patient fibroblasts
Fibroblasts received three doses of Duloxetine (one per day)
(A) Mitophagy following Duloxetine treatment, (B) Autophagy following Duloxetine treatment, (C) Viable cells in each treatment condition expressed as the percentage of untreated cells
n=1, mean +/- 95% CI

6.4.4 Mitochondria targeted Doxorubicin (mtDox)

Doxorubicin (trade name Adriamycin) is a commonly used anti-cancer drug with long term adverse side effects. Acute dose-related cardiac complications occur but, in addition, patients may develop dilated cardiomyopathy even 10-15 years after the course of Doxorubicin treatment. Previous work on doxorubicin showed marked remodelling of mitochondrial morphology and mitochondrial nucleoid structure changes that could be relevant to cardiotoxicity (Ashley et al., 2008). We wished to determine whether this was accompanied by dysregulated mitophagy. In a preliminary study, Doxorubicin treatment of fibroblasts was a strong inducer of mitophagy and autophagy; however, it is extremely cytotoxic. A single treatment induces considerable cell death by day 3 even at a low (0.5µM) concentration and one additional treatment wipes out approximately 90% of the cells by day 7 (personal observations). In order to avoid the adverse side effects while preserving the anti-cancer properties of Doxorubicin Shana O. Kelly's group at the University of Toronto developed mitochondria targeted form of the drug (Chamberlain et al., 2013; Jean et al., 2014). Professor Kelly kindly provided our team with mtDox in order to test it in our mitophagy assay. Fibroblasts received a single treatment of increasing concentrations of mtDox and mitophagy was assayed following 3 days treatment as previously. Drug treatment significantly increased mitophagy in all cells at the highest concentration (10µM) (Figure 6.7 A). Non-linear regression analysis determined the EC50 to be 3.168 µM for patient cells. EC50 for control cells was ambiguous. Autophagic response to mtDox treatment was more dose-response like with a significant increase following treatment with 0.3µM, 1µM, 3µM and 10µM mtDox (Figure 6.7 B). EC50 was determined at 1.1µM for both control and patient cells.

Despite previous reports showing an advantage over Doxorubicin (Jean et al., 2014), mtDOX treatment appeared to be cytotoxic affecting control cells slightly more than patient ones (Figure 6.7 C).

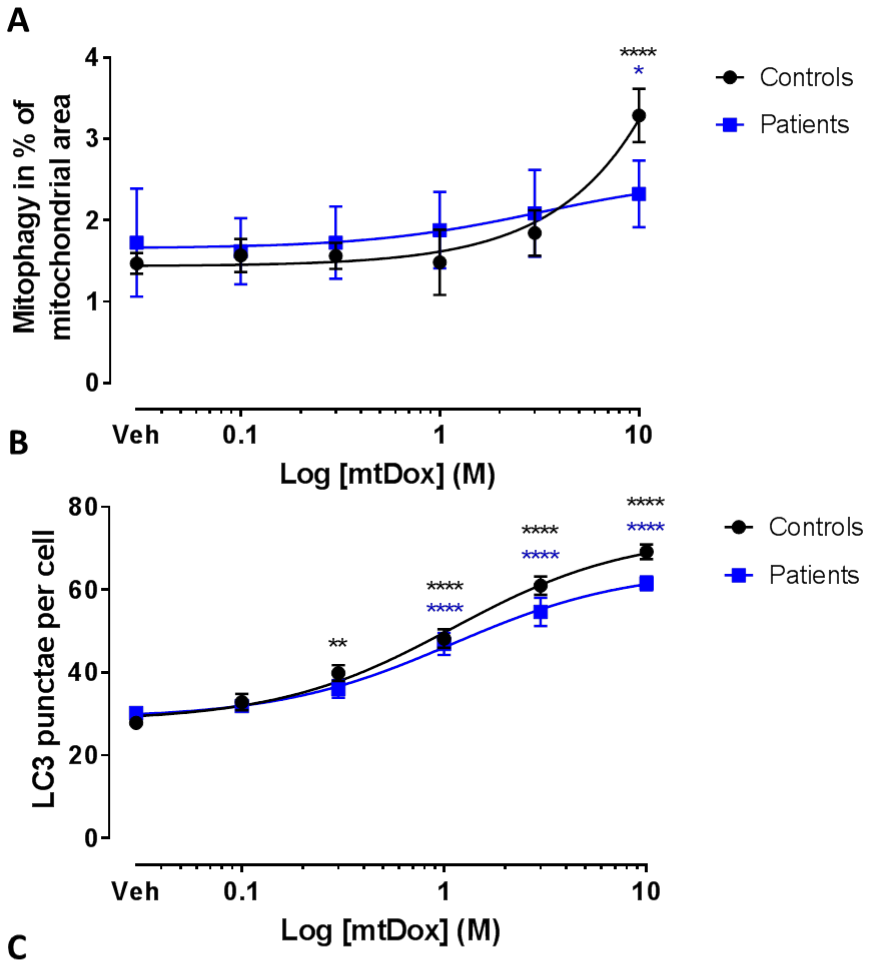

C

Viable cells expressed as the % of untreated cells		
	C (n=2)	**P (n=2)**
0.1µM	89	104
0.3µM	67	97
1µM	52	57
3µM	39	42
10µM	35	36

Figure 6.7 mtDox treatment of control and patient fibroblasts
(A) Mitophagy following mtDox treatment, (B) Autophagy following mtDox treatment, (C) Viable cells in each treatment condition expressed as the percentage of untreated cells
n=1, mean +/- 95% CI

6.4.5 KH176

Khondrion is a pharmaceutical company based in the Netherlands and specialises in drug development for the treatment of mitochondrial diseases. KH176 and its active metabolite KH176m are their most recent developments both intracellular agents targeting reactive oxygen species. KH176 is a derivative of Trolox, a water-soluble form of vitamin E with improved antioxidant properties (Beyrath et al., 2018). KH176 was selected from 226 compounds generated based on its potency and efficacy in scavenging cellular ROS and protecting cells from redox perturbations evaluated in patient-derived fibroblasts with complex I deficiency, as well as its oral bioavailability, penetrance of the blood-brain-barrier, solubility in water and chemical stability assayed *in vivo* in various animal models (Beyrath et al., 2018). When the therapeutic effects of KH176 were investigated *in vivo* in an animal model of complex I deficiency (*Nudfs4* -/- mice) KH176 treatment normalized lipid peroxidation, improved motor performance and reduced degeneration of ganglion cells in *Ndufs4* -/- animals (de Haas et al., 2017). The safety and tolerability of KH176 was assessed in a randomized, placebo controlled, double-blinded phase 1 study (Koene et al., 2017). We have received KH176, KH176m (active metabolite) and KH176i (inactive, negative control) all blinded. The compounds were shared with our team in order to asses any beneficial effect on patient fibroblasts in terms of mitophagy before KH176 entered phase-II clinical trial for mitochondrial m.3243A>G spectrum disorders. KH176 or KH176i (negative control) treatment had no effect on the mitophagic activity of either on control or patient cells (Figure 6.8 A and C). KH176m treatment, the more potent active metabolite of the drug however significantly increased mitophagy in both control and patient cells at the highest 10µM concentration (Figure 6.8 B).

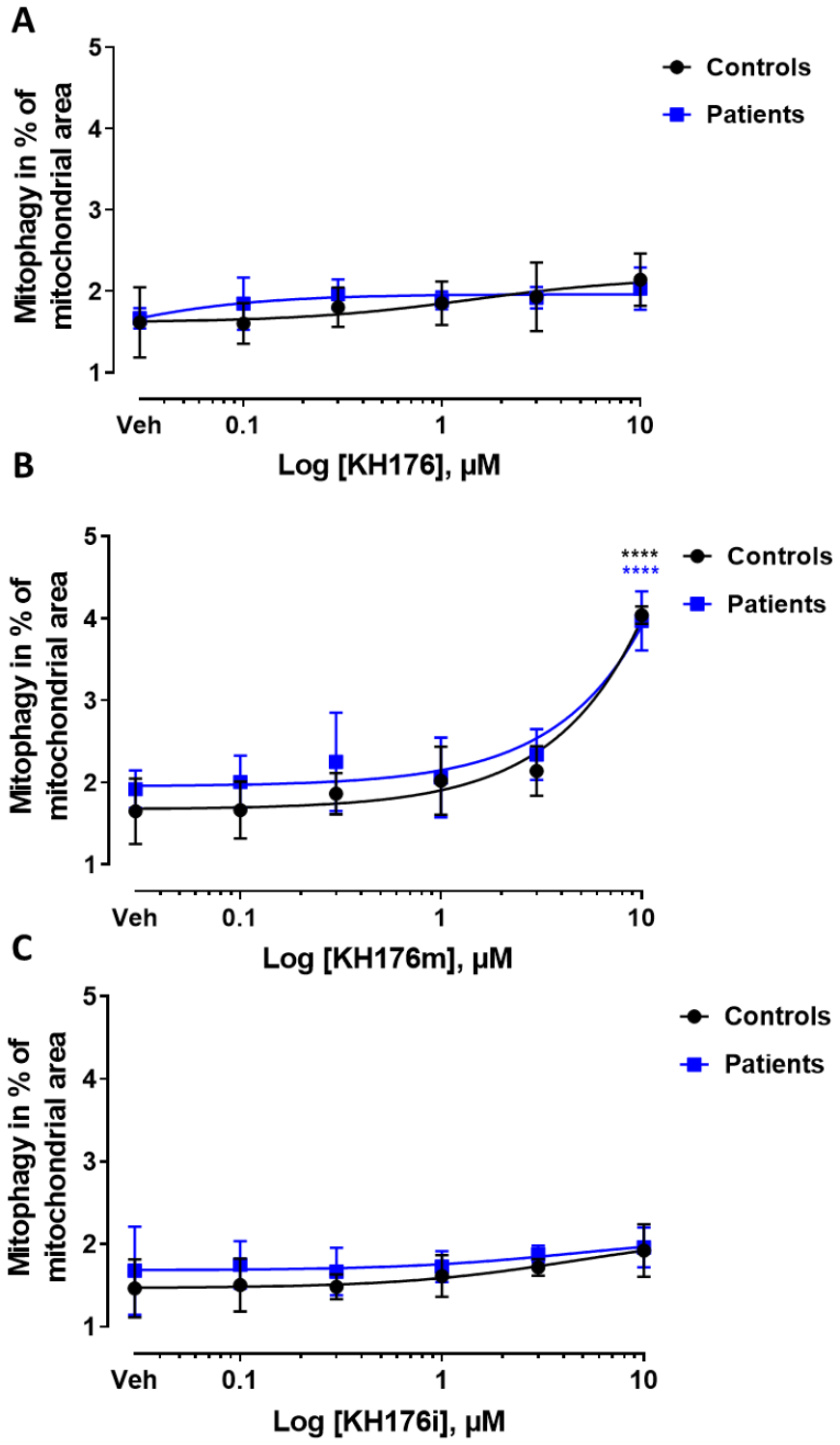

Figure 6.8 Mitophagy in KH drug treated control and patient fibroblasts
Fibroblasts received a single dose of either A: KH176, B: KH176m or C: KH176i at various concentrations and mitophagy was analysed after 3 days.
n=1, mean +/- 95% CI

KH176 and KH176i neither improved nor diminished the viable of either control or patient fibroblasts following 3 days treatment (Figure 6.9 A and C). The active metabolite KH176m on the other hand reduced the percentage of viable cell below 80% at the highest 10µM concentration (Figure 6.9 B).

A

Viable cells expressed as the % of untreated cells (KH176)		
	C (n=2)	**P (n=2)**
0.1µM	97	108
0.3µM	105	116
1µM	118	116
3µM	118	115
10µM	108	104

B

Viable cells expressed as the % of untreated cells (KH176m)		
	C (n=2)	**P (n=2)**
0.1µM	94	104
0.3µM	108	110
1µM	110	115
3µM	92	97
10µM	79	74

C

Viable cells expressed as the % of untreated cells (KH176i)		
	C (n=2)	**P (n=2)**
0.1µM	93	116
0.3µM	101	111
1µM	107	120
3µM	103	119
10µM	87	107

Figure 6.9 The number of viable cells expressed as the percentage of vehicle treated ones following KH drug treatment

6.4.6 3243 heteroplasmy in drug treated patient fibroblasts

The aim of this study was to identify selective drug modulators of mitophagy that are able to induce mitophagy while reducing the load of mutant mtDNA. Metformin, AICAR and Librium treatment of 3243 patient cells all induced increased mitophagy without adversely affecting cell viability. Indeed, metformin and AICAR treatment even increased the number of cells in culture up to a certain concertation (Figure 6.3 C and 6.4 C respectively). Although Duloxetine treatment did not induced a dose-response type response in fibroblasts it still increased mitophagy and only reduced cell-viability at the highest (10µM) concentration (Figure 6.6 C). Therefore, these drugs were selected to treat 3243 patient fibroblasts for 3 and 7 days. The levels of 3243 mutant DNA was measured after each treatment in order to determine whether these drugs are able to reduce heteroplasmy levels via the induction of mitophagy. Cells were treated with a single dose of each drug which are listed in Table 6.6. These doses were selected based on the mitophagic responses presented in the previous sections.

Table 6.6 Drugs and concentrations selected for heteroplasmy treatment

Drug	Concentration used
Metformin	5µM
AICAR	10µM
Librium	1µM
Duloxetine	5µM

Neither of the drug treatments had a significant effect on heterpoplasmy levels either after 3 or 7 days (Figure 6.10). Despite no significant changes which is likely due to the small number of technical replicates (n=2) AICAR treatment decreased the load of mutant by approximately 11% in Patient 1 fibroblasts (mean 88.5%) and by 20% in Patient 2 derived cells (mean 80%) after 7 days (Figure 6.10 B). Duloxetine treatment also reduced mutant load by approximately 16% in Patient 1 derived cells (mean 83.5) by day 7 however had no impact on the load of mutant in Patient 2 cells (Figure 6.10 D). Whereas, Librium treatment reduced the load of mutant in cells derived from Patient 2 by approximately 15% (mean 85.5) without affecting 3243 levels in patient 1 cells (Figure 6.10 C)

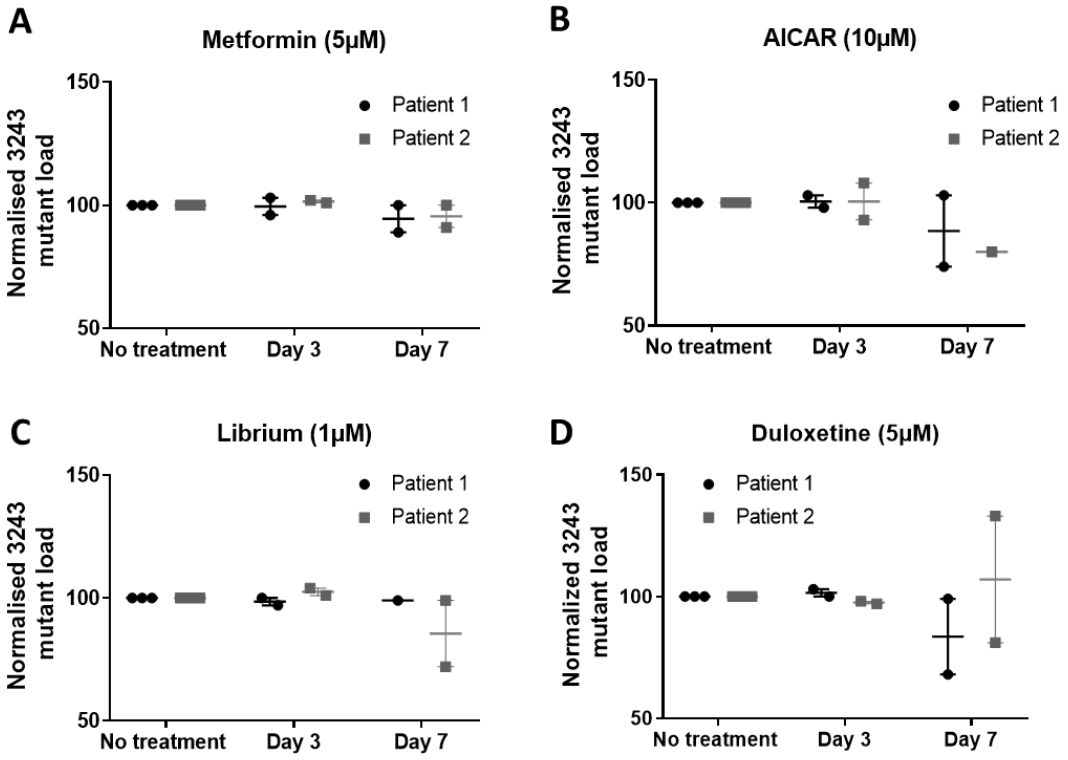

Figure 6.10 Heteroplasmy levels in 3243 patient cells following treatment with selected drugs
Normalized heteroplasmy levels measured following A: 5µM metformin treatment; B: 10µ AICAR treatment; C: 1µM Librium treatment; D: 5µM Duloxetine treatment Media was changed on d0 and d7 for all drugs, n=2

6.5 Discussion

Disease causing mutations in mtDNA primarily affect tissues with high energy demand such as muscle and neural tissue. Both of these tissues are post-mitotic which means that extensive mitochondrial dysfunction can lead to apoptosis and successive tissue degeneration. Therefore, preventing the accumulation of extensively damaged mitochondria is essential. Additionally, in heteroplasmic mitochondrial disease clinical severity is often influenced by the proportion of mutant mtDNA within cells, and mitophagy is the only currently known built-in mechanism within cells that recycles mitochondrial DNA. The aim of this chapter was to identify potential drug modulators of mitophagy that selectively target dysfunctional mitochondria and therefore may be used in the future for the treatment of mitochondrial disease. I have presented six compounds that significantly increased mitophagy. Mitochondria targeted doxorubicin and KH176m treatment only resulted in increased mitophagy at the highest concentration (10µM), which was also cytotoxic. Duloxetine increased mitophagy but more so autophagy while increasing control cell numbers but not patient ones.Chlorodiazepoxide increased mitophagy without affecting autophagy or cell viability. And finally, metformin and AICAR both increased mitophagy at clinically relevant concentrations (<100µM) while increasing cell viability of patient cells.

The investigation of mtDox was not taken further due its serious cytotoxic affect. Additionally, KH176m is a potent antioxidant and was expected to decrease mitophagy if beneficial to patient cells much like Idebenone, a related antioxidant compound did previously (Dombi et al., 2016). KH176 was developed using a complex

I deficient model and showed no improvement of 3243 patients in phase II clinical trial.

As previously mentioned, in a similar *in vitro* screen phenanthroline was identified as a potent mitophagy inducer (Park et al., 2012). When used in the mitophagy assay presented here, phenanthroline significantly induced mitophagy in both control and patient fibroblasts harbouring the heteroplasmic m.3243A>G mtDNA mutation (Diot et al., 2015). However, the treatment also considerably reduced mtDNA content within cells without affecting 3243 heteroplasmy levels. This suggests that phenanthroline induced mitophagy is poorly selective as it turns over both wild type and mutant mtDNA without exerting any specificity. The remaining four drugs identified here (chlorodiazepoxide, Duloxetine, AICAR, metformin) were used to treat 3243 patient cells for 3 and 7 days followed by the measurement of heteroplasmy levels. AICAR reduced heteroplasmy levels in both Patient 1 (~15%) and Patient 2 (~20%) fibroblasts, while duloxetine and chlorodiazepoxide reduced heteroplamy levels in either Patient 1 or Patient 2 derived fibroblasts respectively, but never both. However, none of these reached statistical significance.

Metformin and AICAR are both known autophagy inducers via the activation of AMPK. AMPK responds to an increase in AMP/ATP ratio and mediates starvation induced mitophagy, during which mitochondria was shown to hyperfuse and as a consequence are spared from degradation. Unlike AICAR, metformin did not influence heteroplamy levels; however it did have similarly beneficial effects on cell growth. Mitophagy that removes pathogenic mutants might improve cell growth. Metformin is an FDA approved compound and its use in humans is well-documented while AICAR is not a currently approved medication for any diseases. Additionally,

metformin is known to cross to blood-brain barrier (BBB) while AICAR was reported to have a low permeability. Many mitochondrial diseases are multi systemic and frequently involve the CNS, therefore BBB permeability is a desired quality when it comes to drug candidates as potential therapies. Although metformin treatment did not affect heteroplasmy levels it did increase cell viability, therefore, its potential therapeutic affects in patients might be worth exploring further.

Duloxetine and chlorodiazepoxide are both central nervous system acting drug used to treat anxiety and depression. The mitophagy response following chlorodiazepoxide treatment was the one that most resembled to a classical dose-response curve. Chlorodiazepoxide is a benzodiazepine analogue and recently TSPO, an OMM protein previously known as the peripheral benzodiazepine receptor, was shown to mediate ROS dependent mitophagy (Gatliff et al., 2014). It is plausible that the mitophagy inducing properties of chlorodiazepoxide are secondary to a receptor ligand interaction, such as TSPO. This motion is reinforced by the fact that unlike all the other drugs investigated, chlorodiazepoxide did not simultaneously increase autophagy.

Besides their potential therapeutic benefit for patients with mitochondrial disease, agents that selectively induce mitophagy without damaging the organelle would also serve as invaluable chemical probes to corroborate the core pathways of this process.

6.6 Limitations of this study

All dose response results are based on a single biological replicate, although one could argue that the use of four different cultures represent an n=4.

Heteroplasmy levels were stable following 3 days treatment and changes only started to become apparent after 7 days. However, none of these were statistically significant. A longer course of treatment would better determine whether these drugs are really effective in reducing 3243 heteroplasmy levels.

Standard cell culture glucose concentrations were used for this study which are much higher than physiological levels. At the outset of this project we used 3mM and 0mM media, in which mitophagy was generally more active. The rationale was that a mitophagic flux could be estimated by comparison with baseline (25mM glucose). Furthermore, these media have the advantage that they drive segregation of pathogenic mutant mtDNA such as m.3243A>G and we previously reported that segregation of these mutants could be used to assay mitophagy. I decided not to pursue this because m.3243A>G cells grow badly in zero glucose medium, especially those with high mutant load and I wanted to study mitophagy in viable cells.

Colocalisation of mitochondria and autophagosomes was the only method used to assess mitophagy. Neither mitophagic flux nor lysosomal numbers were assessed.

6.7 Future directions

Based on the results presented here AICAR, metformin, duloxetine and chlorodiazepoxide are promising candidates for their repurposing as treatments for certain mitochondrial diseases. Chlorodiazepoxide appears to have a specific effect

on mitophagy independent of autophagy. The other three increase both mitophagy and cell abundance, suggesting that mitochondrial quality may be improved. The beneficial effects of metformin and AICAR on cell viability should be confirmed on additional patient derived cells using prolonged treatment. Heteroplasmy measurements should also be repeated using additional 3243 cultures and more time points. All the experiments presented in this section were carried out in standard 25mM culture medium. The drug candidates should be tested on cells grown in more physiological (3-5mM) glucose conditions.

Chapter 7. General Discussion

7.1 General discussion

The work presented in this thesis aims to investigate mitophagy, the cell's own recycling mechanism that turns over redundant and dysfunctional mitochondria, in fibroblasts derived from patients with mitochondrial disease. I investigated mitophagy with a view that it might provide a potential therapeutic target in some cases of mitochondrial disease. This study provides an insight into mitochondrial quality control in a uniquely large cohort of patient derived fibroblasts with a variety of mtDNA and nDNA mutations.

7.2 Measuring mitophagy – High-throughput fluorescent imaging

Measuring mitophagy is challenging as it is a transient event that is complete in approximately 30-60 minutes (Lemasters et al., 2014). The vast majority of currently available methods are based on imaging (section 1.4) among which the most definitive one for the visualization of mitophagy is electron microscopy (EM). However, EM is time consuming, especially if one wants to make it quantitative. For that reason, one of the most commonly used methods to study mitophagy in mammalian cells is fluorescence microscopy for co-localization of mitochondria with autophagosomes or lysosomes as it allows the analyses of a large number of cells. The data presented in this thesis are based on co-localisation events between immunolabelled mitochondria and autophagsomes.

The main limitation of this approach is that it is not an end point measurement and it reflects but does not precisely measure the turnover rate of mitochondria. The use of lysosomal inhibitors is required from which mitophagic flux can be inferred. There are

multiple fluorescent constructs such as MitoQC, mt-Keima and Rosella (section 1.4) that are arguably better able to monitor the degradation of mitochondria in live cells, while MitoQC is also compatible with fixation. However, all of these systems require the stable transfection of the investigated cells. Therefore, their use was not feasible in this project as over 30 different fibroblast cultures were investigated, and fibroblasts are particularly difficult when it comes to transfection.

There are also several advantages to using this method. Both the imaging and the analyses part are blinded and therefore unbiased. The In Cell 1000 microscope is an automated system that captures images of the experimental plate in a set amount of fields, the position of which is defined by the software. This way, the inherent human bias towards capturing the prettiest looking cell is avoided. When developing the method (Diot et al., 2015), our group used the corresponding software package (In Cell Developer) to generate an in-house written protocol including several standard and custom measurements. Therefore, by the analyses of a single image stack extensive data are acquired on a large number of cells.

7.3 Does mitophagy contribute to mitochondrial disease pathology?

Even though mitophagy ensures the presence of a healthy and well-functioning mitochondrial pool, it is often overlooked when investigating mitochondrial disease. This is probably because navigating mitophagy is a minefield. Despite the tremendous progress made in the past years in identifying numerous signalling pathways that govern the turnover of mitochondria in vitro, their physiological significance is poorly understood. Most of the established pathways are based on cultured cell models in

which key proteins are over-expressed in immortalised cells treated with mitochondrial toxins. A decade ago, Parkin was identified as a mediator of CCCP induced mitophagy using HEK293 and HeLa cells (Narendra et al., 2008) establishing an important link between mitochondrial dysfunction and Parkinson's disease. The Parkin/PINK1 pathway soon became accepted as the canonical mitophagy pathway, although its relevance outside the model systems is debatable. The mechanisms governing mitophagy induced by physiological cellular stress are generally not well studied. Most recently, PINK1 was shown to be dispensable for basal mitophagy in vivo (McWilliams et al., 2018). It is important to dissect the differences between mitophagy pathways concerned with the degradation of damaged versus merely superfluous mitochondria. There is increasing evidence that dysfunctional mitophagy contributes to the progression of many diseases such as cancer, Parkinson's disease and inflammation (Springer et al.,2016).

Using fibroblasts cultures derived from patients with mitochondrial disease I have documented increased mitophagy in most cells regardless of whether they carried mtDNA or nDNA mutations. While mitophagy, as well as autophagy was increased in most of the fibroblast cultures investigated, the questions of whether either or both contribute to the pathology is unclear. A cellular mechanism that removes damage mitochondria is likely to be beneficial, particularly in the case of heteroplasmic mtDNA diseases. Hence, in Chapter 6 investigated drugs that emerged as potential modulators of mitophagy and identified compounds that increased mitophagy without affecting cell viability. Three of these resulted in a reduction of mutant load in m.3243G>A heteroplasmic cells, although this did not reach statistical significance.

Nonetheless we previously showed that mitophagy was increased in fibroblasts from patients with mtDNA depletion syndrome due to POLG and DGUOK mutations (unpublished data). We postulated that mitophagy might be excessive in these patients, causing nucleotide depletion that in itself causes polymerase stalling in a viscous circle (illustrated in Figure 5.3). In chapter 5 I investigated a severely depleted fibroblast culture in which mitophagy was barely increased, however dNTP supplementation alleviated mtDNA depletion while reducing mitophagy.

While I did not investigate the molecular mechanisms involved in dysregulated mitophagy in patient fibroblasts, it is likely to be different in different mitochondrial diseases and involve the combination of multiple pathways, some of which are potentially yet to be described. Mitochondrial fragmentation or mitochondrial depolarization does not seem to be essential as mitophagy was increased in two cultures harbouring mutant DNM1L and hyperpolarized mitochondria.

7.4 Can we target mitophagy in mitochondrial disease for therapy?

There is no cure for mitochondrial disease. Current treatment options mainly include vitamins and supplements that in some cases may confer symptomatic improvements. These are usually determined on an individual bases. Most of these supplements, such as riboflavin, Coenzyme Q10 (CoQ10) and related synthetic quinones are prescribed for their antioxidant capacity primarily in complex I deficiencies.

Targeting mitophagy in mitochondrial disease could offer a novel therapeutic target. However, this requires the identification of a drug or small molecule that induces

selective mitophagy as the currently known stimulators of this pathway, such as rapamycin, might cause more harm by the induction of non-selective bulk mitophagy as well as autophagy. In Chapter 6 I investigated three compounds, two which are FDA approved, that increased mitophagy without affecting cell viability and also decreased heteroplasmy levels in a very short period of time. While targeting mitophagy may not be a viable option for mitochondrial disease resulting from nDNA mutations it may benefit patients with mtDNA defects. In heteroplasmic disease selective degradation of mitochondria may drive heteroplasmy levels below the pathogenic threshold. Additionally, in homoplasmic mtDNA disease an increase in mtDNA content is a well-documented compensatory mechanism in non-symptomatic carriers (Giordano et al., 2014). Mitochondrial degradation and biogenesis are two opposing cellular mechanism that were shown to co-ordinately regulate each other (Medeiros et al., 2018). Therefore, one would think that stimulating mitophagy might be beneficial. On the contrary, when patient 11778B (chapter 3) who is homoplastic for the m.11778G>A mtDNA mutation was prescribed rapamycin, a mitophagy inducer that was previously shown to reduce heteroplasmy levels (Dai et al., 2009), his condition worsened. A milder inhibition of mitophagy might better benefit patients with homoplasmic disease by increasing the mitochondrial pool, although this proposition needs further investigation.

7.5 Can we change the paradigm? - Mitochondrial disease mechanism and pathogenesis

It is a long-standing paradigm that mitochondrial disease pathology is the result of a chronic reduction in cellular energy due to the insufficient supply of ATP. In line with

this, patients in whom mitochondrial diseases are suspected are investigated by a series of extensive laboratory testing and biochemical evaluation of tissue samples. In many cases OXPHOS dysfunction is not apparent. The affected tissues in mitochondrial disease are often said to be those with high energy demand, such as muscle, cardiac and neuronal, are the most commonly affected. While these tissues are indeed regularly affected, it is not always the case. The metabolic consequences of mitochondrial dysfunction are incompletely understood both at a cellular level and especially in the whole organism.

In this study I showed that dysregulation, not only of mitophagy but also of autophagy, seems to be a hallmark of mitochondrial diseases. An increase in general autophagy, which was apparent in most patient cultures investigated, points to a systemic dysfunction within these cells rather than an isolated mitochondrial defect. While in the case of mtDNA mutations that affect OXPHOS complex subunits it is perfectly reasonable to assume that the disease pathology stems from ETC dysfunction, in the case of other mutations (eg. Fission/fusion defects) oxidative phosphorylation defects are likely secondary. Therefore, potential treatments should be targeted accordingly. For example calcium signalling associated with the ER is a major component of the many functions that mitochondria fulfil within the cells. Despite this well-established relationship alterations in calcium signalling or ER-mitochondria connectivity are rarely, if ever investigated in mitochondrial disease pathology.

Chapter 8. References

Ajioka, R.S., Phillips, J.D., and Kushner, J.P. (2006). Biosynthesis of heme in mammals. Biochimica et Biophysica Acta (BBA) - Molecular Cell Research *1763*, 723-736.

Ajroud-Driss, S., Fecto, F., Ajroud, K., Lalani, I., Calvo, S.E., Mootha, V.K., Deng, H.X., Siddique, N., Tahmoush, A.J., Heiman-Patterson, T.D.*, et al.* (2015). Mutation in the novel nuclear-encoded mitochondrial protein CHCHD10 in a family with autosomal dominant mitochondrial myopathy. Neurogenetics *16*, 1-9.

Allen, G.F., Toth, R., James, J., and Ganley, I.G. (2013). Loss of iron triggers PINK1/Parkin-independent mitophagy. EMBO reports *14*, 1127-1135.

Almannai, M., Dai, H., El-Hattab, A.W., and Wong, L.J.C. (1993). FBXL4-Related Encephalomyopathic Mitochondrial DNA Depletion Syndrome. In GeneReviews((R)),

M.P. Adam, H.H. Ardinger, R.A. Pagon, S.E. Wallace, L.J.H. Bean, K. Stephens, and A. Amemiya, eds. (Seattle (WA): University of Washington, Seattle

Anderson, S., Bankier, A.T., Barrell, B.G., de Bruijn, M.H., Coulson, A.R., Drouin, J., Eperon, I.C., Nierlich, D.P., Roe, B.A., Sanger, F.*, et al.* (1981). Sequence and organization of the human mitochondrial genome. Nature *290*, 457-465.

Andersson, S.G., Zomorodipour, A., Andersson, J.O., Sicheritz-Ponten, T., Alsmark, U.C., Podowski, R.M., Naslund, A.K., Eriksson, A.S., Winkler, H.H., and Kurland, C.G. (1998). The genome sequence of Rickettsia prowazekii and the origin of mitochondria. Nature *396*, 133-140.

Aras, S., Bai, M., Lee, I., Springett, R., Huttemann, M., and Grossman, L.I. (2015). MNRR1 (formerly CHCHD2) is a bi-organellar regulator of mitochondrial metabolism. Mitochondrion *20*, 43-51.

Ashley, N., Adams, S., Slama, A., Zeviani, M., Suomalainen, A., Andreu, A.L., Naviaux, R.K., and Poulton, J. (2007). Defects in maintenance of mitochondrial DNA are associated with intramitochondrial nucleotide imbalances. Human molecular genetics *16*, 1400-1411.

Ashley, N., Harris, D., and Poulton, J. (2005). Detection of mitochondrial DNA depletion in living human cells using PicoGreen staining. Experimental cell research *303*, 432-446.

Ashrafian, H., Docherty, L., Leo, V., Towlson, C., Neilan, M., Steeples, V., Lygate, C.A., Hough, T., Townsend, S., Williams, D.*, et al.* (2010). A mutation in the mitochondrial fission gene Dnm1l leads to cardiomyopathy. PLoS genetics *6*, e1001000.

Auranen, M., Ylikallio, E., Shcherbii, M., Paetau, A., Kiuru-Enari, S., Toppila, J.P., and Tyynismaa, H. (2015). CHCHD10 variant p.(Gly66Val) causes axonal Charcot-Marie-Tooth disease. Neurology Genetics *1*, e1.

Bai, C., Sen, P., Hofmann, K., Ma, L., Goebl, M., Harper, J.W., and Elledge, S.J. (1996). SKP1 connects cell cycle regulators to the ubiquitin proteolysis machinery through a novel motif, the F-box. Cell *86*, 263-274.

Bannwarth, S., Ait-El-Mkadem, S., Chaussenot, A., Genin, E.C., Lacas-Gervais, S., Fragaki, K., Berg-Alonso, L., Kageyama, Y., Serre, V., Moore, D.G.*, et al.* (2014). A mitochondrial origin for frontotemporal dementia and amyotrophic lateral sclerosis through CHCHD10 involvement. Brain : a journal of neurology *137*, 2329-2345.

Baracca, A., Sgarbi, G., Mattiazzi, M., Casalena, G., Pagnotta, E., Valentino, M.L., Moggio, M., Lenaz, G., Carelli, V., and Solaini, G. (2007). Biochemical phenotypes associated with the mitochondrial ATP6 gene mutations at nt8993. Biochimica et biophysica acta *1767*, 913-919.

Baum, D.A., and Baum, B. (2014). An inside-out origin for the eukaryotic cell. BMC biology *12*, 76.

Bereiter-Hahn, J., and Voth, M. (1994). Dynamics of mitochondria in living cells: shape changes, dislocations, fusion, and fission of mitochondria. Microscopy research and technique *27*, 198-219.

Beyrath, J., Pellegrini, M., Renkema, H., Houben, L., Pecheritsyna, S., van Zandvoort, P., van den Broek, P., Bekel, A., Eftekhari, P., and Smeitink, J.A.M. (2018). KH176 Safeguards Mitochondrial Diseased Cells from Redox Stress-Induced Cell Death by Interacting with the Thioredoxin System/Peroxiredoxin Enzyme Machinery. Scientific reports *8*, 6577.

Blok, R.B., Gook, D.A., Thorburn, D.R., and Dahl, H.H. (1997). Skewed segregation of the mtDNA nt 8993 (T-->G) mutation in human oocytes. American journal of human genetics *60*, 1495-1501.

Bogenhagen, D.F. (2012). Mitochondrial DNA nucleoid structure. Biochimica et biophysica acta *1819*, 914-920.

Bogenhagen, D.F., Rousseau, D., and Burke, S. (2008). The layered structure of human mitochondrial DNA nucleoids. The Journal of biological chemistry *283*, 3665-3675.
Bonnen, P.E., Yarham, J.W., Besse, A., Wu, P., Faqeih, E.A., Al-Asmari, A.M., Saleh, M.A., Eyaid, W., Hadeel, A., He, L.*, et al.* (2013). Mutations in FBXL4 cause mitochondrial encephalopathy and a disorder of mitochondrial DNA maintenance. American journal of human genetics *93*, 471-481.

Bowmaker, M., Yang, M.Y., Yasukawa, T., Reyes, A., Jacobs, H.T., Huberman, J.A., and Holt, I.J. (2003). Mammalian mitochondrial DNA replicates bidirectionally from an initiation zone. The Journal of biological chemistry *278*, 50961-50969.

Braestrup, C., and Squires, R.F. (1977). Specific benzodiazepine receptors in rat brain characterized by high-affinity (3H)diazepam binding. Proceedings of the National Academy of Sciences of the United States of America *74*, 3805-3809.

Brand, M.D. (2010). The sites and topology of mitochondrial superoxide production. Experimental gerontology *45*, 466-472.

Brown, M.D., Trounce, I.A., Jun, A.S., Allen, J.C., and Wallace, D.C. (2000). Functional analysis of lymphoblast and cybrid mitochondria containing the 3460, 11778, or 14484 Leber's hereditary optic neuropathy mitochondrial DNA mutation. The Journal of biological chemistry *275*, 39831-39836.

Bulst, S., Holinski-Feder, E., Payne, B., Abicht, A., Krause, S., Lochmuller, H., Chinnery, P.F., Walter, M.C., and Horvath, R. (2012). In vitro supplementation with deoxynucleoside monophosphates rescues mitochondrial DNA depletion. Molecular genetics and metabolism *107*, 95-103.

Burrage, L.C., Tang, S., Wang, J., Donti, T.R., Walkiewicz, M., Luchak, J.M., Chen, L.C., Schmitt, E.S., Niu, Z., Erana, R.*, et al.* (2014). Mitochondrial myopathy, lactic acidosis, and sideroblastic anemia (MLASA) plus associated with a novel de novo mutation (m.8969G>A) in the mitochondrial encoded ATP6 gene. Molecular genetics and metabolism *113*, 207-212.

Burstein, S.R., Valsecchi, F., Kawamata, H., Bourens, M., Zeng, R., Zuberi, A., Milner, T.A., Cloonan, S.M., Lutz, C., Barrientos, A.*, et al.* (2018). In vitro and in vivo studies of the ALS-FTLD protein CHCHD10 reveal novel mitochondrial topology and protein interactions. Human molecular genetics *27*, 160-177.

Cai, H., Zhang, G., Chen, W., Zhang, B., Zhang, J., Chang, J., Tang, C., Qi, Y., and Yin, X. (2014). Metformin protects the myocardium against isoproterenol-induced injury in rats through alleviating endoplasmic reticulum stress. Die Pharmazie *69*, 64-69.
Calvo, S.E., Clauser, K.R., and Mootha, V.K. (2016). MitoCarta2.0: an updated inventory of mammalian mitochondrial proteins. Nucleic acids research *44*, D1251-1257.

Carroll, J., Fearnley, I.M., Skehel, J.M., Shannon, R.J., Hirst, J., and Walker, J.E. (2006). Bovine complex I is a complex of 45 different subunits. The Journal of biological chemistry *281*, 32724-32727.

Cenciarelli, C., Chiaur, D.S., Guardavaccaro, D., Parks, W., Vidal, M., and Pagano, M. (1999). Identification of a family of human F-box proteins. Current biology : CB *9*, 1177-1179.
Chamberlain, G.R., Tulumello, D.V., and Kelley, S.O. (2013). Targeted delivery of doxorubicin to mitochondria. ACS chemical biology *8*, 1389-1395.
Chan, E.Y. (2009). mTORC1 phosphorylates the ULK1-mAtg13-FIP200 autophagy regulatory complex. Science signaling *2*, pe51.

Chandel, N.S. (2014). Mitochondria as signaling organelles. BMC biology *12*, 34.

Chandel, N.S., McClintock, D.S., Feliciano, C.E., Wood, T.M., Melendez, J.A., Rodriguez, A.M., and Schumacker, P.T. (2000). Reactive oxygen species generated at mitochondrial complex III stabilize hypoxia-inducible factor-1alpha during hypoxia: a mechanism of O2 sensing. The Journal of biological chemistry *275*, 25130-25138.

Chao, Y.H., Robak, L.A., Xia, F., Koenig, M.K., Adesina, A., Bacino, C.A., Scaglia, F., Bellen, H.J., and Wangler, M.F. (2016). Missense variants in the middle domain of DNM1L in cases of infantile encephalopathy alter peroxisomes and mitochondria when assayed in Drosophila. Human molecular genetics *25*, 1846-1856.

Chatre, L., and Ricchetti, M. (2013). Large heterogeneity of mitochondrial DNA transcription and initiation of replication exposed by single-cell imaging. Journal of cell science *126*, 914-926.

Chen, H., and Chan, D.C. (2009). Mitochondrial dynamics--fusion, fission, movement, and mitophagy--in neurodegenerative diseases. Human molecular genetics *18*, R169-176.

Chen, H., Chomyn, A., and Chan, D.C. (2005). Disruption of fusion results in mitochondrial heterogeneity and dysfunction. The Journal of biological chemistry *280*, 26185-26192.

Chen, H., Detmer, S.A., Ewald, A.J., Griffin, E.E., Fraser, S.E., and Chan, D.C. (2003). Mitofusins Mfn1 and Mfn2 coordinately regulate mitochondrial fusion and are essential for embryonic development. The Journal of cell biology *160*, 189-200.
Chen, Z., Liu, L., Cheng, Q., Li, Y., Wu, H., Zhang, W., Wang, Y., Sehgal, S.A., Siraj, S., Wang, X*., et al.* (2017). Mitochondrial E3 ligase MARCH5 regulates FUNDC1 to fine-tune hypoxic mitophagy. EMBO reports *18*, 495-509.

Cheong, H., Lindsten, T., Wu, J., Lu, C., and Thompson, C.B. (2011). Ammonia-induced autophagy is independent of ULK1/ULK2 kinases. Proceedings of the National Academy of Sciences of the United States of America *108*, 11121-11126.

Chiang, M.C., Cheng, Y.C., Chen, S.J., Yen, C.H., and Huang, R.N. (2016). Metformin activation of AMPK-dependent pathways is neuroprotective in human neural stem cells against Amyloid-beta-induced mitochondrial dysfunction. Experimental cell research *347*, 322-331.

Chinnery, P.F. (2004). New approaches to the treatment of mitochondrial disorders. Reproductive biomedicine online *8*, 16-23.
Chinnery, P.F., Elliott, H.R., Hudson, G., Samuels, D.C., and Relton, C.L. (2012). Epigenetics, epidemiology and mitochondrial DNA diseases. International journal of epidemiology *41*, 177-187.

Chinnery, P.F., and Hudson, G. (2013). Mitochondrial genetics. British medical bulletin *106*, 135-159.

Chu, C.T., Ji, J., Dagda, R.K., Jiang, J.F., Tyurina, Y.Y., Kapralov, A.A., Tyurin, V.A., Yanamala, N., Shrivastava, I.H., Mohammadyani, D*., et al.* (2013). Cardiolipin externalization to the outer mitochondrial membrane acts as an elimination signal for mitophagy in neuronal cells. Nature cell biology *15*, 1197-1205.

Chu, C.T., Zhu, J., and Dagda, R. (2007). Beclin 1-independent pathway of damage-induced mitophagy and autophagic stress: implications for neurodegeneration and cell death. Autophagy *3*, 663-666.

Cipolat, S., Martins de Brito, O., Dal Zilio, B., and Scorrano, L. (2004). OPA1 requires mitofusin 1 to promote mitochondrial fusion. Proceedings of the National Academy of Sciences of the United States of America *101*, 15927-15932.

Clayton, D.A. (1982). Replication of animal mitochondrial DNA. Cell *28*, 693-705.
Copeland, W.C. (2012). Defects in mitochondrial DNA replication and human disease. Critical reviews in biochemistry and molecular biology *47*, 64-74.

Copeland, W.C. (2014). Defects of mitochondrial DNA replication. Journal of child neurology *29*, 1216-1224.

Coppola, M., Pizzigoni, A., Banfi, S., Bassi, M.T., Casari, G., and Incerti, B. (2000). Identification and characterization of YME1L1, a novel paraplegin-related gene. Genomics *66*, 48-54.

Cortes-Hernandez, P., Vazquez-Memije, M.E., and Garcia, J.J. (2007). ATP6 homoplasmic mutations inhibit and destabilize the human F1F0-ATP synthase without preventing enzyme assembly and oligomerization. The Journal of biological chemistry *282*, 1051-1058.

Costa, B., Pini, S., Gabelloni, P., Da Pozzo, E., Abelli, M., Lari, L., Preve, M., Lucacchini, A., Cassano, G.B., and Martini, C. (2009). The spontaneous Ala147Thr amino acid substitution within the translocator protein influences pregnenolone production in lymphomonocytes of healthy individuals. Endocrinology *150*, 5438-5445.

Csordás, G., Renken, C., Várnai, P., Walter, L., Weaver, D., Buttle, K.F., Balla, T., Mannella, C.A., and Hajnóczky, G. (2006). Structural and functional features and significance of the physical linkage between ER and mitochondria. The Journal of cell biology *174*, 915-921.

Dahlin, J.L., Inglese, J., and Walters, M.A. (2015). Mitigating risk in academic preclinical drug discovery. Nature reviews Drug discovery *14*, 279-294.

Dautant, A., Meier, T., Hahn, A., Tribouillard-Tanvier, D., di Rago, J.P., and Kucharczyk, R. (2018). ATP Synthase Diseases of Mitochondrial Genetic Origin. Frontiers in physiology *9*, 329.

de Brito, O.M., and Scorrano, L. (2008). Mitofusin 2 tethers endoplasmic reticulum to mitochondria. Nature *456*, 605-610.

de Castro, I.P., Martins, L.M., and Tufi, R. (2010). Mitochondrial quality control and neurological disease: an emerging connection. Expert reviews in molecular medicine *12*, e12.

de Haas, R., Das, D., Garanto, A., Renkema, H.G., Greupink, R., van den Broek, P., Pertijs, J., Collin, R.W.J., Willems, P., Beyrath, J.*, et al.* (2017). Therapeutic effects of the mitochondrial ROS-redox modulator KH176 in a mammalian model of Leigh Disease. Scientific reports *7*, 11733.

Del Dotto, V., Mishra, P., Vidoni, S., Fogazza, M., Maresca, A., Caporali, L., McCaffery, J.M., Cappelletti, M., Baruffini, E., Lenaers, G.*, et al.* (2017). OPA1 Isoforms in the Hierarchical Organization of Mitochondrial Functions. Cell reports *19*, 2557-2571.
Deluca, H.F., and Engstrom, G.W. (1961). Calcium uptake by rat kidney mitochondria. Proceedings of the National Academy of Sciences of the United States of America *47*, 1744-1750.

Dias, V., Junn, E., and Mouradian, M.M. (2013). The role of oxidative stress in Parkinson's disease. Journal of Parkinson's disease *3*, 461-491.

Ding, W.X., Ni, H.M., Li, M., Liao, Y., Chen, X., Stolz, D.B., Dorn, G.W., 2nd, and Yin, X.M. (2010). Nix is critical to two distinct phases of mitophagy, reactive oxygen species-mediated autophagy induction and Parkin-ubiquitin-p62-mediated mitochondrial priming. The Journal of biological chemistry *285*, 27879-27890.

Diot, A., Hinks-Roberts, A., Lodge, T., Liao, C., Dombi, E., Morten, K., Brady, S., Fratter, C., Carver, J., Muir, R.*, et al.* (2015). A novel quantitative assay of mitophagy: Combining high content fluorescence microscopy and mitochondrial DNA load to quantify mitophagy and identify novel pharmacological tools against pathogenic heteroplasmic mtDNA. Pharmacological research *100*, 24-35.

Dombi, E., Diot, A., Morten, K., Carver, J., Lodge, T., Fratter, C., Ng, Y.S., Liao, C., Muir, R., Blakely, E.L.*, et al.* (2016). The m.13051G>A mitochondrial DNA mutation results in variable neurology and activated mitophagy. Neurology *86*, 1921-1923.

Duchen, M.R. (2000). Mitochondria and calcium: from cell signalling to cell death. The Journal of physiology *529 Pt 1*, 57-68.
Dudkina, N.V., Kouril, R., Peters, K., Braun, H.P., and Boekema, E.J. (2010). Structure and function of mitochondrial supercomplexes. Biochimica et biophysica acta *1797*, 664-670.

El-Hattab, A.W., and Scaglia, F. (2013). Mitochondrial DNA depletion syndromes: review and updates of genetic basis, manifestations, and therapeutic options. Neurotherapeutics : the journal of the American Society for Experimental NeuroTherapeutics *10*, 186-198.

El-Mir, M.Y., Nogueira, V., Fontaine, E., Averet, N., Rigoulet, M., and Leverve, X. (2000). Dimethylbiguanide inhibits cell respiration via an indirect effect targeted on the respiratory chain complex I. The Journal of biological chemistry *275*, 223-228.
Elachouri, G., Vidoni, S., Zanna, C., Pattyn, A., Boukhaddaoui, H., Gaget, K., Yu-Wai-Man, P., Gasparre, G., Sarzi, E., Delettre, C.*, et al.* (2011). OPA1 links human mitochondrial genome maintenance to mtDNA replication and distribution. Genome research *21*, 12-20.

Fahrner, J.A., Liu, R., Perry, M.S., Klein, J., and Chan, D.C. (2016). A novel de novo dominant negative mutation in DNM1L impairs mitochondrial fission and presents as childhood epileptic encephalopathy. American journal of medical genetics Part A *170*, 2002-2011.

Falk, M.J., and Sondheimer, N. (2010). Mitochondrial genetic diseases. Current opinion in pediatrics *22*, 711-716.

Fassone, E., and Rahman, S. (2012). Complex I deficiency: clinical features, biochemistry and molecular genetics. Journal of medical genetics *49*, 578-590.
Fernandez-Moreira, D., Ugalde, C., Smeets, R., Rodenburg, R.J., Lopez-Laso, E., Ruiz-Falco, M.L., Briones, P., Martin, M.A., Smeitink, J.A., and Arenas, J. (2007). X-linked NDUFA1 gene mutations associated with mitochondrial encephalomyopathy. Annals of neurology *61*, 73-83.

Fernandez-Mosquera, L., Diogo, C.V., Yambire, K.F., Santos, G.L., Luna Sanchez, M., Benit, P., Rustin, P., Lopez, L.C., Milosevic, I., and Raimundo, N. (2017). Acute and chronic mitochondrial respiratory chain deficiency differentially regulate lysosomal biogenesis. Scientific reports *7*, 45076.

Filadi, R., Greotti, E., Turacchio, G., Luini, A., Pozzan, T., and Pizzo, P. (2017). On the role of Mitofusin 2 in endoplasmic reticulum-mitochondria tethering. Proceedings of the National Academy of Sciences of the United States of America *114*, E2266-e2267.
Fisher, R.P., Lisowsky, T., Parisi, M.A., and Clayton, D.A. (1992). DNA wrapping and bending by a mitochondrial high mobility group-like transcriptional activator protein. The Journal of biological chemistry *267*, 3358-3367.

Fleming, A., Noda, T., Yoshimori, T., and Rubinsztein, D.C. (2011). Chemical modulators of autophagy as biological probes and potential therapeutics. Nature chemical biology *7*, 9-17.
Floreani, M., Napoli, E., Martinuzzi, A., Pantano, G., De Riva, V., Trevisan, R., Bisetto, E., Valente, L., Carelli, V., and Dabbeni-Sala, F. (2005). Antioxidant defences in cybrids harboring mtDNA mutations associated with Leber's hereditary optic neuropathy. The FEBS journal *272*, 1124-1135.

Frank, M., Duvezin-Caubet, S., Koob, S., Occhipinti, A., Jagasia, R., Petcherski, A., Ruonala, M.O., Priault, M., Salin, B., and Reichert, A.S. (2012). Mitophagy is triggered by mild oxidative stress in a mitochondrial fission dependent manner. Biochimica et biophysica acta *1823*, 2297-2310.

Frederick, R.L., and Shaw, J.M. (2007). Moving mitochondria: establishing distribution of an essential organelle. Traffic (Copenhagen, Denmark) *8*, 1668-1675.

Friedman, J.R., Lackner, L.L., West, M., DiBenedetto, J.R., Nunnari, J., and Voeltz, G.K. (2011). ER tubules mark sites of mitochondrial division. Science (New York, NY) *334*, 358-362.

Gai, X., Ghezzi, D., Johnson, M.A., Biagosch, C.A., Shamseldin, H.E., Haack, T.B., Reyes, A., Tsukikawa, M., Sheldon, C.A., Srinivasan, S.*, et al.* (2013). Mutations in FBXL4, encoding a mitochondrial protein, cause early-onset mitochondrial encephalomyopathy. American journal of human genetics *93*, 482-495.

Gammoh, N., Florey, O., Overholtzer, M., and Jiang, X. (2013). Interaction between FIP200 and ATG16L1 distinguishes ULK1 complex-dependent and -independent autophagy. Nature structural & molecular biology *20*, 144-149.

Ganley, I.G., Lam du, H., Wang, J., Ding, X., Chen, S., and Jiang, X. (2009). ULK1.ATG13.FIP200 complex mediates mTOR signaling and is essential for autophagy. The Journal of biological chemistry *284*, 12297-12305.

Garone, C., Garcia-Diaz, B., Emmanuele, V., Lopez, L.C., Tadesse, S., Akman, H.O., Tanji, K., Quinzii, C.M., and Hirano, M. (2014). Deoxypyrimidine monophosphate bypass therapy for thymidine kinase 2 deficiency. EMBO molecular medicine *6*, 1016-1027.

Gatliff, J., East, D., Crosby, J., Abeti, R., Harvey, R., Craigen, W., Parker, P., and Campanella, M. (2014). TSPO interacts with VDAC1 and triggers a ROS-mediated inhibition of mitochondrial quality control. Autophagy *10*, 2279-2296.

Geisler, S., Holmstrom, K.M., Skujat, D., Fiesel, F.C., Rothfuss, O.C., Kahle, P.J., and Springer, W. (2010). PINK1/Parkin-mediated mitophagy is dependent on VDAC1 and p62/SQSTM1. Nature cell biology *12*, 119-131.

Genin, E.C., Bannwarth, S., Lespinasse, F., Ortega-Vila, B., Fragaki, K., Itoh, K., Villa, E., Lacas-Gervais, S., Jokela, M., Auranen, M.*, et al.* (2018). Loss of MICOS complex integrity and mitochondrial damage, but not TDP-43 mitochondrial localisation, are likely associated with severity of CHCHD10-related diseases. Neurobiology of disease *119*, 159-171.

Genin, E.C., Plutino, M., Bannwarth, S., Villa, E., Cisneros-Barroso, E., Roy, M., Ortega-Vila, B., Fragaki, K., Lespinasse, F., Pinero-Martos, E.*, et al.* (2016). CHCHD10 mutations promote loss of mitochondrial cristae junctions with impaired

mitochondrial genome maintenance and inhibition of apoptosis. EMBO molecular medicine *8*, 58-72.

Georgakopoulos, N.D., Wells, G., and Campanella, M. (2017). The pharmacological regulation of cellular mitophagy. Nature chemical biology *13*, 136-146.
Gerdes, F., Tatsuta, T., and Langer, T. (2012). Mitochondrial AAA proteases--towards a molecular understanding of membrane-bound proteolytic machines. Biochimica et biophysica acta *1823*, 49-55.

Gerhold, J.M., Cansiz-Arda, S., Lohmus, M., Engberg, O., Reyes, A., van Rennes, H., Sanz, A., Holt, I.J., Cooper, H.M., and Spelbrink, J.N. (2015). Human Mitochondrial DNA-Protein Complexes Attach to a Cholesterol-Rich Membrane Structure. Scientific reports *5*, 15292.

Giordano, C., Iommarini, L., Giordano, L., Maresca, A., Pisano, A., Valentino, M.L., Caporali, L., Liguori, R., Deceglie, S., Roberti, M.*, et al.* (2014). Efficient mitochondrial biogenesis drives incomplete penetrance in Leber's hereditary optic neuropathy. Brain : a journal of neurology *137*, 335-353.

Glynn, S.E. (2017). Multifunctional Mitochondrial AAA Proteases. Frontiers in molecular biosciences *4*, 34.

Gomes, L.C., Di Benedetto, G., and Scorrano, L. (2011). During autophagy mitochondria elongate, are spared from degradation and sustain cell viability. Nature cell biology *13*, 589-598.

Gorman, G.S., Schaefer, A.M., Ng, Y., Gomez, N., Blakely, E.L., Alston, C.L., Feeney, C., Horvath, R., Yu-Wai-Man, P., Chinnery, P.F.*, et al.* (2015). Prevalence of nuclear and mitochondrial DNA mutations related to adult mitochondrial disease. Annals of neurology *77*, 753-759.

Gray, H., and Wong, T.W. (1992). Purification and identification of subunit structure of the human mitochondrial DNA polymerase. The Journal of biological chemistry *267*, 5835-5841.

Gueven, N., Nadikudi, M., Daniel, A., and Chhetri, J. (2017). Targeting mitochondrial function to treat optic neuropathy. Mitochondrion *36*, 7-14.

Hakansson, P., Hofer, A., and Thelander, L. (2006). Regulation of mammalian ribonucleotide reduction and dNTP pools after DNA damage and in resting cells. The Journal of biological chemistry *281*, 7834-7841.

Hamon, M.P., Bulteau, A.L., and Friguet, B. (2015). Mitochondrial proteases and protein quality control in ageing and longevity. Ageing research reviews *23*, 56-66.
Hanada, T., Noda, N.N., Satomi, Y., Ichimura, Y., Fujioka, Y., Takao, T., Inagaki, F., and Ohsumi, Y. (2007). The Atg12-Atg5 conjugate has a novel E3-like activity for protein lipidation in autophagy. The Journal of biological chemistry *282*, 37298-37302.

Hara, T., Takamura, A., Kishi, C., Iemura, S., Natsume, T., Guan, J.L., and Mizushima, N. (2008). FIP200, a ULK-interacting protein, is required for autophagosome formation in mammalian cells. The Journal of cell biology *181*, 497-510.

Hardie, D.G., and Frenguelli, B.G. (2007). A neural protection racket: AMPK and the GABA(B) receptor. Neuron *53*, 159-162.

Higgins, J.W., Bedwell, D.W., and Zamek-Gliszczynski, M.J. (2012). Ablation of both organic cation transporter (OCT)1 and OCT2 alters metformin pharmacokinetics but has no effect on tissue drug exposure and pharmacodynamics. Drug metabolism and disposition: the biological fate of chemicals *40*, 1170-1177.

Holt, I.J., Lorimer, H.E., and Jacobs, H.T. (2000). Coupled leading- and lagging-strand synthesis of mammalian mitochondrial DNA. Cell *100*, 515-524.

Hoppins, S., and Nunnari, J. (2009). The molecular mechanism of mitochondrial fusion. Biochimica et biophysica acta *1793*, 20-26.

Hornig-Do, H.T., Tatsuta, T., Buckermann, A., Bust, M., Kollberg, G., Rotig, A., Hellmich, M., Nijtmans, L., and Wiesner, R.J. (2012). Nonsense mutations in the COX1 subunit impair the stability of respiratory chain complexes rather than their assembly. The EMBO journal *31*, 1293-1307.

Hosokawa, N., Hara, T., Kaizuka, T., Kishi, C., Takamura, A., Miura, Y., Iemura, S., Natsume, T., Takehana, K., Yamada, N.*, et al.* (2009). Nutrient-dependent mTORC1 association with the ULK1-Atg13-FIP200 complex required for autophagy. Molecular biology of the cell *20*, 1981-1991.

Howell, N., Oostra, R.J., Bolhuis, P.A., Spruijt, L., Clarke, L.A., Mackey, D.A., Preston, G., and Herrnstadt, C. (2003). Sequence analysis of the mitochondrial genomes from Dutch pedigrees with Leber hereditary optic neuropathy. American journal of human genetics *72*, 1460-1469.

Hu, C., Huang, Y., and Li, L. (2017). Drp1-Dependent Mitochondrial Fission Plays Critical Roles in Physiological and Pathological Progresses in Mammals. International journal of molecular sciences *18*.

Huang, X., Wu, B.P., Nguyen, D., Liu, Y.T., Marani, M., Hench, J., Benit, P., Kozjak-Pavlovic, V., Rustin, P., Frank, S.*, et al.* (2019). CHCHD2 accumulates in distressed mitochondria and facilitates oligomerization of CHCHD10. Human molecular genetics *28*, 349.

Huemer, M., Karall, D., Schossig, A., Abdenur, J.E., Al Jasmi, F., Biagosch, C., Distelmaier, F., Freisinger, P., Graham, B.H., Haack, T.B.*, et al.* (2015). Clinical, morphological, biochemical, imaging and outcome parameters in 21 individuals with mitochondrial maintenance defect related to FBXL4 mutations. Journal of inherited metabolic disease *38*, 905-914.

Iborra, F.J., Kimura, H., and Cook, P.R. (2004). The functional organization of mitochondrial genomes in human cells. BMC biology *2*, 9.
Ishihara, N., Eura, Y., and Mihara, K. (2004). Mitofusin 1 and 2 play distinct roles in mitochondrial fusion reactions via GTPase activity. Journal of cell science *117*, 6535-6546.

Ishihara, N., Fujita, Y., Oka, T., and Mihara, K. (2006). Regulation of mitochondrial morphology through proteolytic cleavage of OPA1. The EMBO journal *25*, 2966-2977.
Itakura, E., Kishi-Itakura, C., Koyama-Honda, I., and Mizushima, N. (2012). Structures containing Atg9A and the ULK1 complex independently target depolarized mitochondria at initial stages of Parkin-mediated mitophagy. Journal of cell science *125*, 1488-1499.

Jean, S.R., Tulumello, D.V., Riganti, C., Liyanage, S.U., Schimmer, A.D., and Kelley, S.O. (2015). Mitochondrial Targeting of Doxorubicin Eliminates Nuclear Effects Associated with Cardiotoxicity. ACS chemical biology *10*, 2007-2015.
Jeppesen, T.D., Duno, M., Risom, L., Wibrand, F., Rafiq, J., Krag, T., Jakobsen, J., Andersen, H., and Vissing, J. (2014). A novel de novo mutation of the mitochondrial tRNAlys gene mt.8340G>a associated with pure myopathy. Neuromuscular disorders : NMD *24*, 162-166.

Johnson, J.O., Glynn, S.M., Gibbs, J.R., Nalls, M.A., Sabatelli, M., Restagno, G., Drory, V.E., Chio, A., Rogaeva, E., and Traynor, B.J. (2014). Mutations in the CHCHD10 gene are a common cause of familial amyotrophic lateral sclerosis. Brain : a journal of neurology *137*, e311.

Johnson, S.C., Yanos, M.E., Kayser, E.B., Quintana, A., Sangesland, M., Castanza, A., Uhde, L., Hui, J., Wall, V.Z., Gagnidze, A*., et al.* (2013). mTOR inhibition alleviates mitochondrial disease in a mouse model of Leigh syndrome. Science (New York, NY) *342*, 1524-1528.

Jonckheere, A.I., Smeitink, J.A., and Rodenburg, R.J. (2012). Mitochondrial ATP synthase: architecture, function and pathology. Journal of inherited metabolic disease *35*, 211-225.

Jung, C.H., Jun, C.B., Ro, S.H., Kim, Y.M., Otto, N.M., Cao, J., Kundu, M., and Kim, D.H. (2009). ULK-Atg13-FIP200 complexes mediate mTOR signaling to the autophagy machinery. Molecular biology of the cell *20*, 1992-2003.

Kabeya, Y., Mizushima, N., Yamamoto, A., Oshitani-Okamoto, S., Ohsumi, Y., and Yoshimori, T. (2004). LC3, GABARAP and GATE16 localize to autophagosomal membrane depending on form-II formation. Journal of cell science *117*, 2805-2812.
Kageyama, Y., Zhang, Z., Roda, R., Fukaya, M., Wakabayashi, J., Wakabayashi, N., Kensler, T.W., Reddy, P.H., Iijima, M., and Sesaki, H. (2012). Mitochondrial division ensures the survival of postmitotic neurons by suppressing oxidative damage. The Journal of cell biology *197*, 535-551.

Kahn, B.B., Alquier, T., Carling, D., and Hardie, D.G. (2005). AMP-activated protein kinase: ancient energy gauge provides clues to modern understanding of metabolism. Cell metabolism *1*, 15-25.

Kamer, K.J., and Mootha, V.K. (2015). The molecular era of the mitochondrial calcium uniporter. Nature reviews Molecular cell biology *16*, 545-553.

Kane, M.S., Alban, J., Desquiret-Dumas, V., Gueguen, N., Ishak, L., Ferre, M., Amati-Bonneau, P., Procaccio, V., Bonneau, D., Lenaers, G.*, et al.* (2017). Autophagy controls the pathogenicity of OPA1 mutations in dominant optic atrophy. Journal of cellular and molecular medicine *21*, 2284-2297.

Kasamatsu, H., Grossman, L.I., Robberson, D.L., Watson, R., and Vinograd, J. (1974). The replication and structure of mitochondrial DNA in animal cells. Cold Spring Harbor symposia on quantitative biology *38*, 281-288.

Kasamatsu, H., Robberson, D.L., and Vinograd, J. (1971). A novel closed-circular mitochondrial DNA with properties of a replicating intermediate. Proceedings of the National Academy of Sciences of the United States of America *68*, 2252-2257.

Kase, E.T., Nikolic, N., Bakke, S.S., Bogen, K.K., Aas, V., Thoresen, G.H., and Rustan, A.C. (2013). Remodeling of oxidative energy metabolism by galactose improves glucose handling and metabolic switching in human skeletal muscle cells. PloS one *8*, e59972.

Katayama, H., Kogure, T., Mizushima, N., Yoshimori, T., and Miyawaki, A. (2011). A sensitive and quantitative technique for detecting autophagic events based on lysosomal delivery. Chemistry & biology *18*, 1042-1052.

Kaufman, B.A., Durisic, N., Mativetsky, J.M., Costantino, S., Hancock, M.A., Grutter, P., and Shoubridge, E.A. (2007). The mitochondrial transcription factor TFAM coordinates the assembly of multiple DNA molecules into nucleoid-like structures. Molecular biology of the cell *18*, 3225-3236.

Kipreos, E.T., and Pagano, M. (2000). The F-box protein family. Genome biology *1*, Reviews3002.

Kirichok, Y., Krapivinsky, G., and Clapham, D.E. (2004). The mitochondrial calcium uniporter is a highly selective ion channel. Nature *427*, 360-364.

Klionsky, D.J., Cregg, J.M., Dunn, W.A., Jr., Emr, S.D., Sakai, Y., Sandoval, I.V., Sibirny, A., Subramani, S., Thumm, M., Veenhuis, M.*, et al.* (2003). A unified nomenclature for yeast autophagy-related genes. Developmental cell *5*, 539-545.

Koene, S., Spaans, E., Van Bortel, L., Van Lancker, G., Delafontaine, B., Badilini, F., Beyrath, J., and Smeitink, J. (2017). KH176 under development for rare mitochondrial

disease: a first in man randomized controlled clinical trial in healthy male volunteers. Orphanet journal of rare diseases *12*, 163.

Kondapalli, C., Kazlauskaite, A., Zhang, N., Woodroof, H.I., Campbell, D.G., Gourlay, R., Burchell, L., Walden, H., Macartney, T.J., Deak, M.*, et al.* (2012). PINK1 is activated by mitochondrial membrane potential depolarization and stimulates Parkin E3 ligase activity by phosphorylating Serine 65. Open biology *2*, 120080.

Koopman, W.J., Willems, P.H., and Smeitink, J.A. (2012). Monogenic mitochondrial disorders. The New England journal of medicine *366*, 1132-1141.

Koppen, M., Metodiev, M.D., Casari, G., Rugarli, E.I., and Langer, T. (2007). Variable and tissue-specific subunit composition of mitochondrial m-AAA protease complexes linked to hereditary spastic paraplegia. Molecular and cellular biology *27*, 758-767.

Kukat, C., Davies, K.M., Wurm, C.A., Spahr, H., Bonekamp, N.A., Kuhl, I., Joos, F., Polosa, P.L., Park, C.B., Posse, V.*, et al.* (2015). Cross-strand binding of TFAM to a single mtDNA molecule forms the mitochondrial nucleoid. Proceedings of the National Academy of Sciences of the United States of America *112*, 11288-11293.
Kukat, C., Wurm, C.A., Spahr, H., Falkenberg, M., Larsson, N.G., and Jakobs, S. (2011). Super-resolution microscopy reveals that mammalian mitochondrial nucleoids have a uniform size and frequently contain a single copy of mtDNA. Proceedings of the National Academy of Sciences of the United States of America *108*, 13534-13539.

Kuroyanagi, H., Yan, J., Seki, N., Yamanouchi, Y., Suzuki, Y., Takano, T., Muramatsu, M., and Shirasawa, T. (1998). Human ULK1, a novel serine/threonine kinase related to UNC-51 kinase of Caenorhabditis elegans: cDNA cloning, expression, and chromosomal assignment. Genomics *51*, 76-85.

Lackner, L.L. (2014). Shaping the dynamic mitochondrial network. BMC biology *12*, 35.

Ladds, E., Whitney, A., Dombi, E., Hofer, M., Anand, G., Harrison, V., Fratter, C., Carver, J., Barbosa, I.A., Simpson, M.*, et al.* (2018). De novo DNM1L mutation associated with mitochondrial epilepsy syndrome with fever sensitivity. Neurology Genetics *4*, e258.

Lagouge, M., and Larsson, N.G. (2013). The role of mitochondrial DNA mutations and free radicals in disease and ageing. Journal of internal medicine *273*, 529-543.

Lake, N.J., Compton, A.G., Rahman, S., and Thorburn, D.R. (2016). Leigh syndrome: One disorder, more than 75 monogenic causes. Annals of neurology *79*, 190-203.

Lane, A.N., and Fan, T.W. (2015). Regulation of mammalian nucleotide metabolism and biosynthesis. Nucleic acids research *43*, 2466-2485.

Larsson, N.G., Wang, J., Wilhelmsson, H., Oldfors, A., Rustin, P., Lewandoski, M., Barsh, G.S., and Clayton, D.A. (1998). Mitochondrial transcription factor A is necessary for mtDNA maintenance and embryogenesis in mice. Nature genetics *18*, 231-236.

Lazarou, M., Sliter, D.A., Kane, L.A., Sarraf, S.A., Wang, C., Burman, J.L., Sideris, D.P., Fogel, A.I., and Youle, R.J. (2015). The ubiquitin kinase PINK1 recruits autophagy receptors to induce mitophagy. Nature *524*, 309-314.

Lee, H., Smith, S.B., and Yoon, Y. (2017). The short variant of the mitochondrial dynamin OPA1 maintains mitochondrial energetics and cristae structure. The Journal of biological chemistry *292*, 7115-7130.

Lee, J.E., Westrate, L.M., Wu, H., Page, C., and Voeltz, G.K. (2016). Multiple dynamin family members collaborate to drive mitochondrial division. Nature *540*, 139-143.

Lee, Y.S., Kennedy, W.D., and Yin, Y.W. (2009). Structural insight into processive human mitochondrial DNA synthesis and disease-related polymerase mutations. Cell *139*, 312-324.

Leger, M.M., Petru, M., Zarsky, V., Eme, L., Vlcek, C., Harding, T., Lang, B.F., Elias, M., Dolezal, P., and Roger, A.J. (2015). An ancestral bacterial division system is widespread in eukaryotic mitochondria. Proceedings of the National Academy of Sciences of the United States of America *112*, 10239-10246.

Legros, F., Malka, F., Frachon, P., Lombes, A., and Rojo, M. (2004). Organization and dynamics of human mitochondrial DNA. Journal of cell science *117*, 2653-2662.

Lemasters, J.J. (2014). Variants of mitochondrial autophagy: Types 1 and 2 mitophagy and micromitophagy (Type 3). Redox biology *2*, 749-754.

Leonhard, K., Herrmann, J.M., Stuart, R.A., Mannhaupt, G., Neupert, W., and Langer, T. (1996). AAA proteases with catalytic sites on opposite membrane surfaces comprise a proteolytic system for the ATP-dependent degradation of inner membrane proteins in mitochondria. The EMBO journal *15*, 4218-4229.

Lewis, S.C., Uchiyama, L.F., and Nunnari, J. (2016). ER-mitochondria contacts couple mtDNA synthesis with mitochondrial division in human cells. Science (New York, NY) *353*, aaf5549.

Li, F., Liu, J., Liu, N., Kuhn, L.A., Garavito, R.M., and Ferguson-Miller, S. (2016). Translocator Protein 18 kDa (TSPO): An Old Protein with New Functions? Biochemistry *55*, 2821-2831.

Li, F., Liu, J., Zheng, Y., Garavito, R.M., and Ferguson-Miller, S. (2015). Protein structure. Crystal structures of translocator protein (TSPO) and mutant mimic of a human polymorphism. Science (New York, NY) *347*, 555-558.

Liang, C., Ahmad, K., and Sue, C.M. (2014). The broadening spectrum of mitochondrial disease: shifts in the diagnostic paradigm. Biochimica et biophysica acta *1840*, 1360-1367.

Liao, C., Ashley, N., Diot, A., Morten, K., Phadwal, K., Williams, A., Fearnley, I., Rosser, L., Lowndes, J., Fratter, C.*, et al.* (2017). Dysregulated mitophagy and mitochondrial organization in optic atrophy due to OPA1 mutations. Neurology *88*, 131-142.
Lightowlers, R.N., Taylor, R.W., and Turnbull, D.M. (2015). Mutations causing mitochondrial disease: What is new and what challenges remain? Science (New York, NY) *349*, 1494-1499.

Liljequist, R., and Mattila, M.J. (1979). Acute effects of temazepam and nitrazepam on psychomotor skills and memory. Acta pharmacologica et toxicologica *44*, 364-369.

Lill, R. (2009). Function and biogenesis of iron–sulphur proteins. Nature *460*, 831.
Liu, L., Feng, D., Chen, G., Chen, M., Zheng, Q., Song, P., Ma, Q., Zhu, C., Wang, R., Qi, W.*, et al.* (2012). Mitochondrial outer-membrane protein FUNDC1 mediates hypoxia-induced mitophagy in mammalian cells. Nature cell biology *14*, 177-185.

Lopez-Fabuel, I., Le Douce, J., Logan, A., James, A.M., Bonvento, G., Murphy, M.P., Almeida, A., and Bolanos, J.P. (2016). Complex I assembly into supercomplexes determines differential mitochondrial ROS production in neurons and astrocytes. Proceedings of the National Academy of Sciences of the United States of America *113*, 13063-13068.

Lopez-Munoz, F., and Alamo, C. (2011). Neurobiological background for the development of new drugs in schizophrenia. Clinical neuropharmacology *34*, 111-126.
Loson, O.C., Song, Z., Chen, H., and Chan, D.C. (2013). Fis1, Mff, MiD49, and MiD51 mediate Drp1 recruitment in mitochondrial fission. Molecular biology of the cell *24*, 659-667.

Lott, M.T., Leipzig, J.N., Derbeneva, O., Xie, H.M., Chalkia, D., Sarmady, M., Procaccio, V., and Wallace, D.C. (2013). mtDNA Variation and Analysis Using Mitomap and Mitomaster. Current protocols in bioinformatics *44*, 1.23.21-26.

Lunt, S.Y., and Vander Heiden, M.G. (2011). Aerobic glycolysis: meeting the metabolic requirements of cell proliferation. Annual review of cell and developmental biology *27*, 441-464.
Luo, S., Valencia, C.A., Zhang, J., Lee, N.C., Slone, J., Gui, B., Wang, X., Li, Z., Dell, S., Brown, J.*, et al.* (2018). Biparental Inheritance of Mitochondrial DNA in Humans. Proceedings of the National Academy of Sciences of the United States of America *115*, 13039-13044.

Mackey, D.A., Oostra, R.J., Rosenberg, T., Nikoskelainen, E., Bronte-Stewart, J., Poulton, J., Harding, A.E., Govan, G., Bolhuis, P.A., and Norby, S. (1996). Primary pathogenic mtDNA mutations in multigeneration pedigrees with Leber hereditary optic neuropathy. American journal of human genetics *59*, 481-485.

MacVicar, T. (2013). Mitophagy. Essays in biochemistry *55*, 93-104.

Magri, S., Fracasso, V., Plumari, M., Alfei, E., Ghezzi, D., Gellera, C., Rusmini, P., Poletti, A., Di Bella, D., Elia, A.E*., et al.* (2018). Concurrent AFG3L2 and SPG7 mutations associated with syndromic parkinsonism and optic atrophy with aberrant OPA1 processing and mitochondrial network fragmentation. Human mutation *39*, 2060-2071.

Makela-Bengs, P., Suomalainen, A., Majander, A., Rapola, J., Kalimo, H., Nuutila, A., and Pihko, H. (1995). Correlation between the clinical symptoms and the proportion of mitochondrial DNA carrying the 8993 point mutation in the NARP syndrome. Pediatric research *37*, 634-639.

Manoharan, S., Guillemin, G.J., Abiramasundari, R.S., Essa, M.M., Akbar, M., and Akbar, M.D. (2016). The Role of Reactive Oxygen Species in the Pathogenesis of Alzheimer's Disease, Parkinson's Disease, and Huntington's Disease: A Mini Review. Oxidative medicine and cellular longevity *2016*, 8590578.

Manwaring, N., Jones, M.M., Wang, J.J., Rochtchina, E., Howard, C., Mitchell, P., and Sue, C.M. (2007). Population prevalence of the MELAS A3243G mutation. Mitochondrion *7*, 230-233.

Matsuda, N., Sato, S., Shiba, K., Okatsu, K., Saisho, K., Gautier, C.A., Sou, Y.S., Saiki, S., Kawajiri, S., Sato, F*., et al.* (2010). PINK1 stabilized by mitochondrial depolarization recruits Parkin to damaged mitochondria and activates latent Parkin for mitophagy. The Journal of cell biology *189*, 211-221.

Matsushima, Y., Goto, Y., and Kaguni, L.S. (2010). Mitochondrial Lon protease regulates mitochondrial DNA copy number and transcription by selective degradation of mitochondrial transcription factor A (TFAM). Proceedings of the National Academy of Sciences of the United States of America *107*, 18410-18415.

McKinney, E.A., and Oliveira, M.T. (2013). Replicating animal mitochondrial DNA. Genetics and molecular biology *36*, 308-315.

Mears, J.A., Lackner, L.L., Fang, S., Ingerman, E., Nunnari, J., and Hinshaw, J.E. (2011). Conformational changes in Dnm1 support a contractile mechanism for mitochondrial fission. Nature structural & molecular biology *18*, 20-26.

Medeiros, T.C., Thomas, R.L., Ghillebert, R., and Graef, M. (2018). Autophagy balances mtDNA synthesis and degradation by DNA polymerase POLG during starvation. The Journal of cell biology *217*, 1601-1611.

Melser, S., Chatelain, E.H., Lavie, J., Mahfouf, W., Jose, C., Obre, E., Goorden, S., Priault, M., Elgersma, Y., Rezvani, H.R*., et al.* (2013). Rheb regulates mitophagy induced by mitochondrial energetic status. Cell metabolism *17*, 719-730.

Mercer, C.A., Kaliappan, A., and Dennis, P.B. (2009). A novel, human Atg13 binding protein, Atg101, interacts with ULK1 and is essential for macroautophagy. Autophagy *5*, 649-662.

Milenkovic, V.M., Bader, S., Sudria-Lopez, D., Siebert, R., Brandl, C., Nothdurfter, C., Weber, B.H.F., Rupprecht, R., and Wetzel, C.H. (2018). Effects of genetic variants in the TSPO gene on protein structure and stability. PloS one *13*, e0195627.

Mishra, P., and Chan, D.C. (2014). Mitochondrial dynamics and inheritance during cell division, development and disease. Nature reviews Molecular cell biology *15*, 634-646.

Misiewicz, M., Dery, M.A., Foveau, B., Jodoin, J., Ruths, D., and LeBlanc, A.C. (2013). Identification of a novel endoplasmic reticulum stress response element regulated by XBP1. The Journal of biological chemistry *288*, 20378-20391.

Moraes, C.T., Zeviani, M., Schon, E.A., Hickman, R.O., Vlcek, B.W., and DiMauro, S. (1991). Mitochondrial DNA deletion in a girl with manifestations of Kearns-Sayre and Lowe syndromes: an example of phenotypic mimicry? American journal of medical genetics *41*, 301-305.

Morais, V.A., Haddad, D., Craessaerts, K., De Bock, P.J., Swerts, J., Vilain, S., Aerts, L., Overbergh, L., Grunewald, A., Seibler, P.*, et al.* (2014). PINK1 loss-of-function mutations affect mitochondrial complex I activity via NdufA10 ubiquinone uncoupling. Science (New York, NY) *344*, 203-207.

Morten, K.J., Poulton, J., and Sykes, B. (1995). Multiple independent occurrence of the 3243 mutation in mitochondrial tRNA(leuUUR) in patients with the MELAS phenotype. Human molecular genetics *4*, 1689-1691.

Munro, B., Horvath, R., and Muller, J.S. (2018). Nucleoside supplementation modulates mitochondrial DNA copy number in the dguok-/- zebrafish. Human molecular genetics.

Murakawa, T., Yamaguchi, O., Hashimoto, A., Hikoso, S., Takeda, T., Oka, T., Yasui, H., Ueda, H., Akazawa, Y., Nakayama, H.*, et al.* (2015). Bcl-2-like protein 13 is a mammalian Atg32 homologue that mediates mitophagy and mitochondrial fragmentation. Nature communications *6*, 7527.

Murphy, M.P. (2009). How mitochondria produce reactive oxygen species. The Biochemical journal *417*, 1-13.

Naon, D., Zaninello, M., Giacomello, M., Varanita, T., Grespi, F., Lakshminaranayan, S., Serafini, A., Semenzato, M., Herkenne, S., Hernandez-Alvarez, M.I.*, et al.* (2016). Critical reappraisal confirms that Mitofusin 2 is an endoplasmic reticulum-

mitochondria tether. Proceedings of the National Academy of Sciences of the United States of America *113*, 11249-11254.

Napier, I., Ponka, P., and Richardson, D.R. (2005). Iron trafficking in the mitochondrion: novel pathways revealed by disease. Blood *105*, 1867-1874.

Narendra, D., Kane, L.A., Hauser, D.N., Fearnley, I.M., and Youle, R.J. (2010). p62/SQSTM1 is required for Parkin-induced mitochondrial clustering but not mitophagy; VDAC1 is dispensable for both. Autophagy *6*, 1090-1106.

Narendra, D., Tanaka, A., Suen, D.F., and Youle, R.J. (2008). Parkin is recruited selectively to impaired mitochondria and promotes their autophagy. The Journal of cell biology *183*, 795-803.

Nemoto, S., Takeda, K., Yu, Z.X., Ferrans, V.J., and Finkel, T. (2000). Role for mitochondrial oxidants as regulators of cellular metabolism. Molecular and cellular biology *20*, 7311-7318.

Neuspiel, M., Schauss, A.C., Braschi, E., Zunino, R., Rippstein, P., Rachubinski, R.A., Andrade-Navarro, M.A., and McBride, H.M. (2008). Cargo-selected transport from the mitochondria to peroxisomes is mediated by vesicular carriers. Current biology : CB *18*, 102-108.

Nikkanen, J., Forsstrom, S., Euro, L., Paetau, I., Kohnz, R.A., Wang, L., Chilov, D., Viinamaki, J., Roivainen, A., Marjamaki, P.*, et al.* (2016). Mitochondrial DNA Replication Defects Disturb Cellular dNTP Pools and Remodel One-Carbon Metabolism. Cell metabolism *23*, 635-648.

Nishida, G., and Labbe, R.F. (1959). Heme biosynthesis on the incorporation of iron into protoporphyrin. Biochimica et biophysica acta *31*, 519-524.
Nordlund, P., and Reichard, P. (2006). Ribonucleotide reductases. Annual review of biochemistry *75*, 681-706.

Okatsu, K., Saisho, K., Shimanuki, M., Nakada, K., Shitara, H., Sou, Y.S., Kimura, M., Sato, S., Hattori, N., Komatsu, M.*, et al.* (2010). p62/SQSTM1 cooperates with Parkin for perinuclear clustering of depolarized mitochondria. Genes to cells : devoted to molecular & cellular mechanisms *15*, 887-900.

Olichon, A., Elachouri, G., Baricault, L., Delettre, C., Belenguer, P., and Lenaers, G. (2007). OPA1 alternate splicing uncouples an evolutionary conserved function in mitochondrial fusion from a vertebrate restricted function in apoptosis. Cell death and differentiation *14*, 682-692.

Olichon, A., Emorine, L.J., Descoins, E., Pelloquin, L., Brichese, L., Gas, N., Guillou, E., Delettre, C., Valette, A., Hamel, C.P.*, et al.* (2002). The human dynamin-related protein OPA1 is anchored to the mitochondrial inner membrane facing the inter-membrane space. FEBS letters *523*, 171-176.

Orsi, A., Razi, M., Dooley, H.C., Robinson, D., Weston, A.E., Collinson, L.M., and Tooze, S.A. (2012). Dynamic and transient interactions of Atg9 with autophagosomes, but not membrane integration, are required for autophagy. Molecular biology of the cell *23*, 1860-1873.

Otten, A.B.C., Sallevelt, S., Carling, P.J., Dreesen, J., Drusedau, M., Spierts, S., Paulussen, A.D.C., de Die-Smulders, C.E.M., Herbert, M., Chinnery, P.F.*, et al.* (2018). Mutation-specific effects in germline transmission of pathogenic mtDNA variants. Human reproduction (Oxford, England) *33*, 1331-1341.

Paillusson, S., Stoica, R., Gomez-Suaga, P., Lau, D.H.W., Mueller, S., Miller, T., and Miller, C.C.J. (2016). There's Something Wrong with my MAM; the ER-Mitochondria Axis and Neurodegenerative Diseases. Trends in neurosciences *39*, 146-157.

Palikaras, K., Lionaki, E., and Tavernarakis, N. (2015a). Balancing mitochondrial biogenesis and mitophagy to maintain energy metabolism homeostasis. Cell death and differentiation *22*, 1399-1401.

Palikaras, K., Lionaki, E., and Tavernarakis, N. (2015b). Coordination of mitophagy and mitochondrial biogenesis during ageing in C. elegans. Nature *521*, 525-528.

Parisi, M.A., Xu, B., and Clayton, D.A. (1993). A human mitochondrial transcriptional activator can functionally replace a yeast mitochondrial HMG-box protein both in vivo and in vitro. Molecular and cellular biology *13*, 1951-1961.

Park, S.J., Shin, J.H., Kim, E.S., Jo, Y.K., Kim, J.H., Hwang, J.J., Kim, J.C., and Cho, D.H. (2012). Mitochondrial fragmentation caused by phenanthroline promotes mitophagy. FEBS letters *586*, 4303-4310.

Petherick, K.J., Conway, O.J., Mpamhanga, C., Osborne, S.A., Kamal, A., Saxty, B., and Ganley, I.G. (2015). Pharmacological inhibition of ULK1 kinase blocks mammalian target of rapamycin (mTOR)-dependent autophagy. The Journal of biological chemistry *290*, 11376-11383.
Petroski, M.D., and Deshaies, R.J. (2005). Function and regulation of cullin-RING ubiquitin ligases. Nature reviews Molecular cell biology *6*, 9-20.

Picard, M., Zhang, J., Hancock, S., Derbeneva, O., Golhar, R., Golik, P., O'Hearn, S., Levy, S., Potluri, P., Lvova, M.*, et al.* (2014). Progressive increase in mtDNA 3243A>G heteroplasmy causes abrupt transcriptional reprogramming. Proceedings of the National Academy of Sciences of the United States of America *111*, E4033-4042.

Plecita-Hlavata, L., Lessard, M., Santorova, J., Bewersdorf, J., and Jezek, P. (2008). Mitochondrial oxidative phosphorylation and energetic status are reflected by morphology of mitochondrial network in INS-1E and HEP-G2 cells viewed by 4Pi microscopy. Biochimica et biophysica acta *1777*, 834-846.

Porceddu, P.F., Ishola, I.O., Contu, L., and Morelli, M. (2016). Metformin Prevented Dopaminergic Neurotoxicity Induced by 3,4-Methylenedioxymethamphetamine Administration. Neurotoxicity research *30*, 101-109.

Poulton, J., Hirano, M., Spinazzola, A., Arenas Hernandez, M., Jardel, C., Lombes, A., Czermin, B., Horvath, R., Taanman, J.W., Rotig, A.*, et al.* (2009). Collated mutations in mitochondrial DNA (mtDNA) depletion syndrome (excluding the mitochondrial gamma polymerase, POLG1). Biochimica et biophysica acta *1792*, 1109-1112.

Purandare, N., Somayajulu, M., Huttemann, M., Grossman, L.I., and Aras, S. (2018). The cellular stress proteins CHCHD10 and MNRR1 (CHCHD2): Partners in mitochondrial and nuclear function and dysfunction. The Journal of biological chemistry *293*, 6517-6529.

Rainbolt, T.K., Lebeau, J., Puchades, C., and Wiseman, R.L. (2016). Reciprocal Degradation of YME1L and OMA1 Adapts Mitochondrial Proteolytic Activity during Stress. Cell reports *14*, 2041-2049.

Rambold, A.S., Kostelecky, B., Elia, N., and Lippincott-Schwartz, J. (2011). Tubular network formation protects mitochondria from autophagosomal degradation during nutrient starvation. Proceedings of the National Academy of Sciences of the United States of America *108*, 10190-10195.

Rapizzi, E., Pinton, P., Szabadkai, G., Wieckowski, M.R., Vandecasteele, G., Baird, G., Tuft, R.A., Fogarty, K.E., and Rizzuto, R. (2002). Recombinant expression of the voltage-dependent anion channel enhances the transfer of Ca2+ microdomains to mitochondria. The Journal of cell biology *159*, 613-624.

Ravanan, P., Srikumar, I.F., and Talwar, P. (2017). Autophagy: The spotlight for cellular stress responses. Life sciences *188*, 53-67.

Reyes, A., Kazak, L., Wood, S.R., Yasukawa, T., Jacobs, H.T., and Holt, I.J. (2013). Mitochondrial DNA replication proceeds via a 'bootlace' mechanism involving the incorporation of processed transcripts. Nucleic acids research *41*, 5837-5850.
Richter, U., Lahtinen, T., Marttinen, P., Suomi, F., and Battersby, B.J. (2015). Quality control of mitochondrial protein synthesis is required for membrane integrity and cell fitness. The Journal of cell biology *211*, 373-389.

Rizzuto, R., De Stefani, D., Raffaello, A., and Mammucari, C. (2012). Mitochondria as sensors and regulators of calcium signalling. Nature reviews Molecular cell biology *13*, 566-578.

Rizzuto, R., Pinton, P., Carrington, W., Fay, F.S., Fogarty, K.E., Lifshitz, L.M., Tuft, R.A., and Pozzan, T. (1998). Close contacts with the endoplasmic reticulum as determinants of mitochondrial Ca2+ responses. Science (New York, NY) *280*, 1763-1766.

Ropp, P.A., and Copeland, W.C. (1996). Cloning and characterization of the human mitochondrial DNA polymerase, DNA polymerase gamma. Genomics *36*, 449-458.
Rosado, C.J., Mijaljica, D., Hatzinisiriou, I., Prescott, M., and Devenish, R.J. (2008). Rosella: a fluorescent pH-biosensor for reporting vacuolar turnover of cytosol and organelles in yeast. Autophagy *4*, 205-213.

Rouault, T.A. (2012). Biogenesis of iron-sulfur clusters in mammalian cells: new insights and relevance to human disease. Disease models & mechanisms *5*, 155-164.
Roufayel, R. (2016). Regulation of stressed-induced cell death by the Bcl-2 family of apoptotic proteins. Molecular membrane biology *33*, 89-99.

Rubino, E., Brusa, L., Zhang, M., Boschi, S., Govone, F., Vacca, A., Gai, A., Pinessi, L., Lopiano, L., Rogaeva, E.*, et al.* (2017). Genetic analysis of CHCHD2 and CHCHD10 in Italian patients with Parkinson's disease. Neurobiology of aging *53*, 193.e197-193.e198.

Russell, R.C., Tian, Y., Yuan, H., Park, H.W., Chang, Y.Y., Kim, J., Kim, H., Neufeld, T.P., Dillin, A., and Guan, K.L. (2013). ULK1 induces autophagy by phosphorylating Beclin-1 and activating VPS34 lipid kinase. Nature cell biology *15*, 741-750.

Sagan, L. (1967). On the origin of mitosing cells. Journal of theoretical biology *14*, 255-274.

Sallevelt, S., de Koning, B., Szklarczyk, R., Paulussen, A.D.C., de Die-Smulders, C.E.M., and Smeets, H.J.M. (2017). A comprehensive strategy for exome-based preconception carrier screening. Genetics in medicine : official journal of the American College of Medical Genetics *19*, 583-592.

Sallevelt, S.C., Dreesen, J.C., Drusedau, M., Spierts, S., Coonen, E., van Tienen, F.H., van Golde, R.J., de Coo, I.F., Geraedts, J.P., de Die-Smulders, C.E.*, et al.* (2013). Preimplantation genetic diagnosis in mitochondrial DNA disorders: challenge and success. Journal of medical genetics *50*, 125-132.
Sandoval, H., Thiagarajan, P., Dasgupta, S.K., Schumacher, A., Prchal, J.T., Chen, M., and Wang, J. (2008). Essential role for Nix in autophagic maturation of erythroid cells. Nature *454*, 232-235.

Scarpulla, R.C. (2011). Metabolic control of mitochondrial biogenesis through the PGC-1 family regulatory network. Biochimica et biophysica acta *1813*, 1269-1278.

Schaefer, A.M., McFarland, R., Blakely, E.L., He, L., Whittaker, R.G., Taylor, R.W., Chinnery, P.F., and Turnbull, D.M. (2008). Prevalence of mitochondrial DNA disease in adults. Annals of neurology *63*, 35-39.

Schagger, H. (2001). Respiratory chain supercomplexes. IUBMB life *52*, 119-128.

Schon, E.A., DiMauro, S., and Hirano, M. (2012). Human mitochondrial DNA: roles of inherited and somatic mutations. Nature reviews Genetics *13*, 878-890.

Schweers, R.L., Zhang, J., Randall, M.S., Loyd, M.R., Li, W., Dorsey, F.C., Kundu, M., Opferman, J.T., Cleveland, J.L., Miller, J.L.*, et al.* (2007). NIX is required for programmed mitochondrial clearance during reticulocyte maturation. Proceedings of the National Academy of Sciences of the United States of America *104*, 19500-19505.

Sgarbi, G., Baracca, A., Lenaz, G., Valentino, L.M., Carelli, V., and Solaini, G. (2006). Inefficient coupling between proton transport and ATP synthesis may be the pathogenic mechanism for NARP and Leigh syndrome resulting from the T8993G mutation in mtDNA. The Biochemical journal *395*, 493-500.

Shadel, G.S., and Horvath, T.L. (2015). Mitochondrial ROS signaling in organismal homeostasis. Cell *163*, 560-569.

Shirihai, O.S., Song, M., and Dorn, G.W., 2nd (2015). How mitochondrial dynamism orchestrates mitophagy. Circulation research *116*, 1835-1849.

Sicheritz-Ponten, T., Kurland, C.G., and Andersson, S.G. (1998). A phylogenetic analysis of the cytochrome b and cytochrome c oxidase I genes supports an origin of mitochondria from within the Rickettsiaceae. Biochimica et biophysica acta *1365*, 545-551.

Skowyra, D., Craig, K.L., Tyers, M., Elledge, S.J., and Harper, J.W. (1997). F-box proteins are receptors that recruit phosphorylated substrates to the SCF ubiquitin-ligase complex. Cell *91*, 209-219.

Smirnova, E., Griparic, L., Shurland, D.L., and van der Bliek, A.M. (2001). Dynamin-related protein Drp1 is required for mitochondrial division in mammalian cells. Molecular biology of the cell *12*, 2245-2256.

Sofou, K., De Coo, I.F., Isohanni, P., Ostergaard, E., Naess, K., De Meirleir, L., Tzoulis, C., Uusimaa, J., De Angst, I.B., Lonnqvist, T.*, et al.* (2014). A multicenter study on Leigh syndrome: disease course and predictors of survival. Orphanet journal of rare diseases *9*, 52.

Song, S., Wheeler, L.J., and Mathews, C.K. (2003). Deoxyribonucleotide pool imbalance stimulates deletions in HeLa cell mitochondrial DNA. The Journal of biological chemistry *278*, 43893-43896.

Sood, A., Jeyaraju, D.V., Prudent, J., Caron, A., Lemieux, P., McBride, H.M., Laplante, M., Toth, K., and Pellegrini, L. (2014). A Mitofusin-2-dependent inactivating cleavage of Opa1 links changes in mitochondria cristae and ER contacts in the postprandial liver. Proceedings of the National Academy of Sciences of the United States of America *111*, 16017-16022.

Soubannier, V., McLelland, G.L., Zunino, R., Braschi, E., Rippstein, P., Fon, E.A., and McBride, H.M. (2012a). A vesicular transport pathway shuttles cargo from mitochondria to lysosomes. Current biology : CB *22*, 135-141.

Soubannier, V., Rippstein, P., Kaufman, B.A., Shoubridge, E.A., and McBride, H.M. (2012b). Reconstitution of mitochondria derived vesicle formation demonstrates selective enrichment of oxidized cargo. PloS one *7*, e52830.

Spinazzola, A. (2011). Mitochondrial DNA mutations and depletion in pediatric medicine. Seminars in fetal & neonatal medicine *16*, 190-196.

Spinazzola, A., Invernizzi, F., Carrara, F., Lamantea, E., Donati, A., Dirocco, M., Giordano, I., Meznaric-Petrusa, M., Baruffini, E., Ferrero, I.*, et al.* (2009). Clinical and molecular features of mitochondrial DNA depletion syndromes. Journal of inherited metabolic disease *32*, 143-158.

Spinazzola, A., Viscomi, C., Fernandez-Vizarra, E., Carrara, F., D'Adamo, P., Calvo, S., Marsano, R.M., Donnini, C., Weiher, H., Strisciuglio, P.*, et al.* (2006). MPV17 encodes an inner mitochondrial membrane protein and is mutated in infantile hepatic mitochondrial DNA depletion. Nature genetics *38*, 570-575.

Stefanatos, R., and Sanz, A. (2018). The role of mitochondrial ROS in the aging brain. FEBS letters *592*, 743-758.

Stewart, J.B., and Chinnery, P.F. (2015). The dynamics of mitochondrial DNA heteroplasmy: implications for human health and disease. Nature reviews Genetics *16*, 530-542.

Stiburek, L., Cesnekova, J., Kostkova, O., Fornuskova, D., Vinsova, K., Wenchich, L., Houstek, J., and Zeman, J. (2012). YME1L controls the accumulation of respiratory chain subunits and is required for apoptotic resistance, cristae morphogenesis, and cell proliferation. Molecular biology of the cell *23*, 1010-1023.

Straub, I.R., Janer, A., Weraarpachai, W., Zinman, L., Robertson, J., Rogaeva, E., and Shoubridge, E.A. (2018). Loss of CHCHD10-CHCHD2 complexes required for respiration underlies the pathogenicity of a CHCHD10 mutation in ALS. Human molecular genetics *27*, 178-189.

Suomalainen, A., and Isohanni, P. (2010). Mitochondrial DNA depletion syndromes--many genes, common mechanisms. Neuromuscular disorders : NMD *20*, 429-437.

Suzuki, K., Kubota, Y., Sekito, T., and Ohsumi, Y. (2007). Hierarchy of Atg proteins in pre-autophagosomal structure organization. Genes to cells : devoted to molecular & cellular mechanisms *12*, 209-218.

Taanman, J.W., Muddle, J.R., and Muntau, A.C. (2003). Mitochondrial DNA depletion can be prevented by dGMP and dAMP supplementation in a resting culture of

deoxyguanosine kinase-deficient fibroblasts. Human molecular genetics *12*, 1839-1845.

Taddei, M.L., Giannoni, E., Raugei, G., Scacco, S., Sardanelli, A.M., Papa, S., and Chiarugi, P. (2012). Mitochondrial Oxidative Stress due to Complex I Dysfunction Promotes Fibroblast Activation and Melanoma Cell Invasiveness. Journal of signal transduction *2012*, 684592.

Tan, M.K., Lim, H.J., Bennett, E.J., Shi, Y., and Harper, J.W. (2013). Parallel SCF adaptor capture proteomics reveals a role for SCFFBXL17 in NRF2 activation via BACH1 repressor turnover. Molecular cell *52*, 9-24.

Tang, S., Wang, J., Lee, N.C., Milone, M., Halberg, M.C., Schmitt, E.S., Craigen, W.J., Zhang, W., and Wong, L.J. (2011). Mitochondrial DNA polymerase gamma mutations: an ever expanding molecular and clinical spectrum. Journal of medical genetics *48*, 669-681.

Taylor, E.B., and Rutter, J. (2011). Mitochondrial quality control by the ubiquitin-proteasome system. Biochemical Society transactions *39*, 1509-1513.

Thiselton, D.L., Alexander, C., Taanman, J.W., Brooks, S., Rosenberg, T., Eiberg, H., Andreasson, S., Van Regemorter, N., Munier, F.L., Moore, A.T.*, et al.* (2002). A comprehensive survey of mutations in the OPA1 gene in patients with autosomal dominant optic atrophy. Investigative ophthalmology & visual science *43*, 1715-1724.

Tsai, C.W., Wu, Y., Pao, P.C., Phillips, C.B., Williams, C., Miller, C., Ranaghan, M., and Tsai, M.F. (2017). Proteolytic control of the mitochondrial calcium uniporter complex. Proceedings of the National Academy of Sciences of the United States of America *114*, 4388-4393.

Tsukada, M., and Ohsumi, Y. (1993). Isolation and characterization of autophagy-defective mutants of Saccharomyces cerevisiae. FEBS letters *333*, 169-174.
Twig, G., Elorza, A., Molina, A.J., Mohamed, H., Wikstrom, J.D., Walzer, G., Stiles, L., Haigh, S.E., Katz, S., Las, G.*, et al.* (2008). Fission and selective fusion govern mitochondrial segregation and elimination by autophagy. The EMBO journal *27*, 433-446.

Twig, G., and Shirihai, O.S. (2011). The interplay between mitochondrial dynamics and mitophagy. Antioxidants & redox signaling *14*, 1939-1951.
Ugarte, N., Petropoulos, I., and Friguet, B. (2010). Oxidized mitochondrial protein degradation and repair in aging and oxidative stress. Antioxidants & redox signaling *13*, 539-549.

Uusimaa, J., Evans, J., Smith, C., Butterworth, A., Craig, K., Ashley, N., Liao, C., Carver, J., Diot, A., Macleod, L.*, et al.* (2014). Clinical, biochemical, cellular and molecular characterization of mitochondrial DNA depletion syndrome due to novel mutations in the MPV17 gene. European journal of human genetics : EJHG *22*, 184-191.

Vafai, S.B., and Mootha, V.K. (2012). Mitochondrial disorders as windows into an ancient organelle. Nature *491*, 374-383.

Van Rechem, C., Black, J.C., Abbas, T., Allen, A., Rinehart, C.A., Yuan, G.C., Dutta, A., and Whetstine, J.R. (2011). The SKP1-Cul1-F-box and leucine-rich repeat protein 4 (SCF-FbxL4) ubiquitin ligase regulates lysine demethylase 4A (KDM4A)/Jumonji domain-containing 2A (JMJD2A) protein. The Journal of biological chemistry *286*, 30462-30470.

Vilarinho, L., Barbot, C., Carrozzo, R., Calado, E., Tessa, A., Dionisi-Vici, C., Guimaraes, A., and Santorelli, F.M. (2001). Clinical and molecular findings in four new patients harbouring the mtDNA 8993T>C mutation. Journal of inherited metabolic disease *24*, 883-884.

Vinothkumar, K.R., Zhu, J., and Hirst, J. (2014). Architecture of mammalian respiratory complex I. Nature *515*, 80-84.

Wallace, D.C., and Chalkia, D. (2013). Mitochondrial DNA genetics and the heteroplasmy conundrum in evolution and disease. Cold Spring Harbor perspectives in biology *5*, a021220.

Wallace, D.C., Singh, G., Lott, M.T., Hodge, J.A., Schurr, T.G., Lezza, A.M., Elsas, L.J., 2nd, and Nikoskelainen, E.K. (1988). Mitochondrial DNA mutation associated with Leber's hereditary optic neuropathy. Science (New York, NY) *242*, 1427-1430.

Chapter 9. Appendices

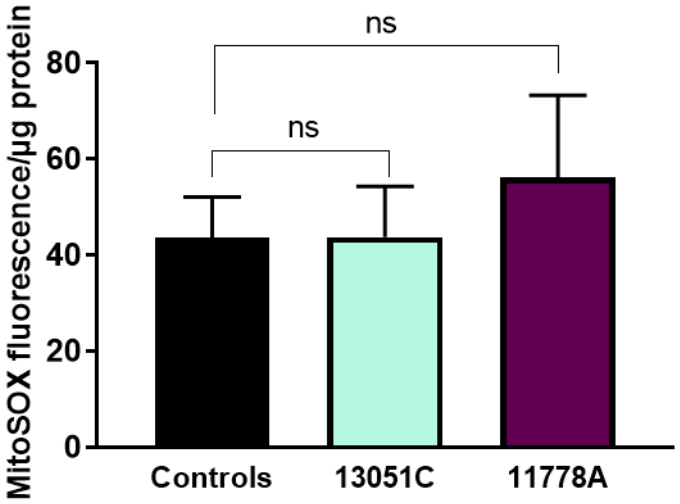

Supplementary figure 1. MitoSOX assay of superoxide measurement in complex I fibroblasts

Control, 13051C and 11778A fibroblasts were incubated with MitoSOX for 1 hour and fuoresence was measured using an Omega plate reader.

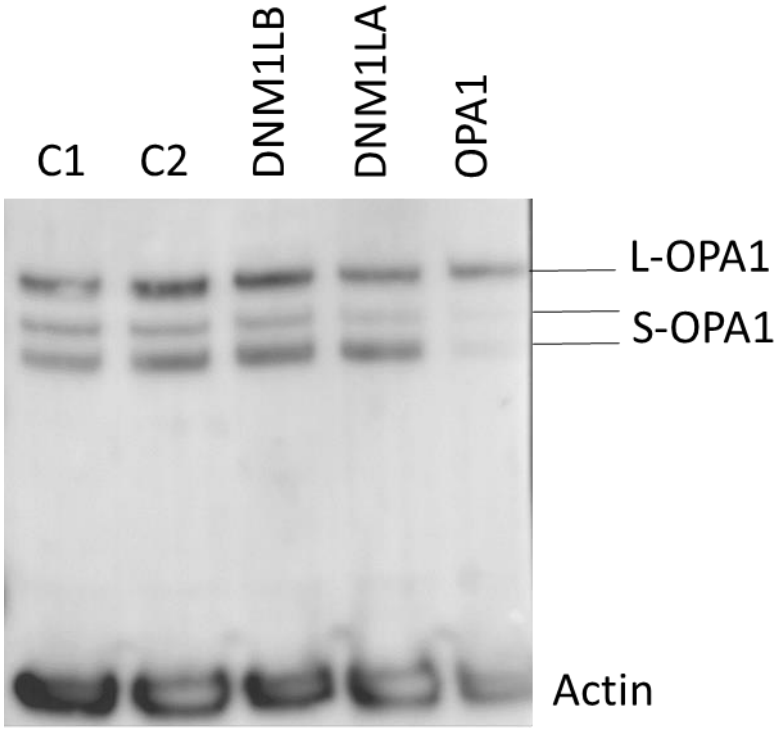

Supplementary figure 2. Western blot analysis of OPA1 protein expression on control, DNM1L and OPA1 fibroblasts

Supplementary table 1. Core protein subunits of ETC Complex I

Domain	Subunit	Genome
Hydrophilic arm	NDUFV1	nDNA (Chr 11)
	NDUFV2	nDNA (Chr 18)
	NDUFS1	nDNA (Chr 2)
	NDUFS2	nDNA (Chr 1)
	NDUFS3	nDNA (Chr 11)
	NDUFS7	nDNA (Chr 19)
	NDUFS8	nDNA (Chr 11)
Membrane arm	ND1	mtDNA
	ND2	mtDNA
	ND3	mtDNA
	ND4	mtDNA
	ND5	mtDNA
	ND6	mtDNA
	ND4L	mtDNA

Supplementary table 2. TSPO polymorphism in complex I patients

Patient identifier	TSPO genotype	Mitophagy
13051A	**GG**	↑
13051B	**AG**	↓
13051C	**GG**	↑
13051D	N/A	↑
11778A	**GG**	↑
11778B	**GG**	↑
11778C	N/A	↑
11778D	**AG**	↓

Supplementary table 3. Drug hits that emerged from the NCC1 library

Drug number	Drug name (if available)
INCREASE co-localisation	
9	10H-Phenothiazine, 2-chloro-10-[3-(4-methyl-1-piperazinyl)propyl- [CAS]
16	Isoquercitrin
66	vinorelbineÂ tartrate
69	HONOKIOL
131	Cisapride
163	Duloxetine
170	
172	ICARIIN
173	
176	RIFABUTIN
212	METHYLANDROSTENEDIOL
222	NITAZOXANIDE
224	
228	MILRINONE
229	OLMESARTAN MEDOXOMIL
232	Chlorpheniramine
234	
235	TRIMEBUTINE MALEATE
238	GR 89696
241	PILOCARPINE HYDROCHLORIDE
249	Naltrindole
262	
270	Piroxicam
293	Maprotiline hydrochloride
294	MOSAPRIDE CITRATE
322	VINDESINE SULFATE
324	CLOFAZIMINE
337	TOREMIFENE CITRATE
367	HOMOHARRINGTONINE
398	Lofexidine hydrochloride
438	Enrofloxacin
DECREASE co-localisation	
200	72-33-3 Mestranol D4
344	Metylperon
346	CCPA
348	DESOXIMETASONE
350	CHLORDIAZEPOXIDE
352	Thiophene, 5-bromo-2-(4-fluorophenyl)-3-[4-(methylsulfonyl)phenyl]- [CAS]